University of Strathclyde

Department of Mechanical & Aerospace Engineering

The effect of nanofibers for improving the dynamic and mechanical properties of composite laminates and their application as self-powered sensors

Cristobal García Pariente

A thesis presented in fulfilment of the requirements
for the degree of Doctor of Philosophy

2018

Declaration of author's rights

This thesis is the result of the author's original research. It has been composed by the author and has not been previously submitted for examination which has led to the award of a degree.

The copyright of this thesis belongs to the author under the terms of the United Kingdom Copyright Acts as qualified by the University of Strathclyde Regulation 3.50. Due acknowledgement must always be made of the use of any material contained in, or derived from, this thesis.

Cristobal García Pariente

November 18, 2018

Acknowledgements

The author would like to thank the following people for their support, without whose help this work would never have been possible.

First and foremost, I would like to extend my sincere gratitude and appreciation to my supervisor Dr Irina Trendafilova for her dedicated help, advice, inspiration, and continuous support, through my PhD. Irina is a wonderful person and a very good friend, who was always available to guide, help, and encourage through this thesis. I really appreciate her precious teaching and great confidence in myself.

My special words of thanks go to IMDEA Materials Institute for being an excellent research institute and provided me with all the infrastructures and materials necessary to carry out this research. A very special thank you goes to Dr Jose Sanchez, Dr Juan Pedro, Jose Luis Jimenez and Vanesa Martínez for their important help and support during the experimental tests in the laboratory. I would also like to thank all and each one of my colleagues, especially to Andrea, Miguel, Angel, Daniel, Jimena, Ivan, Hugo, Rudi, and Paco for making this period so enjoyable and for all the funny time spent together.

I would also like to thank Dr Roberto Guzman de Villoria for his help and support in this research collaboration between the University of Strathclyde, IMDEA Materials Institute and his research centre Foundation for the Research, Development and Application of Composite Materials (FIDAMC).

Last and most importantly, I would like to express my deep gratitude to my family for their dedication and support over so many years. It was not possible to carry out such this research without their constant support and encouragement. A very special thank goes to María, for her unwavering love and understanding during this research investigation that made the completion of the thesis possible.

Abstract

One of the main objectives of this thesis is to investigate the effect of the inclusion of nanofibers on the global dynamical and mechanical properties of composite laminates. For this aim, the natural frequencies, damping, interlaminar strength and impact response of pristine and nanomodified composites are determined experimentally and numerically using a finite element model. Experimental and numerical results showed a significant effect of the nanofibers on the mechanical and dynamic properties of the composites. Nanomodified composites demonstrated a consistent increase in the damping, interlaminar strength ad impact resistance. However, the variation in the natural frequencies was very small. This study expands the knowledge about the macro mechanical and dynamical properties of composites reinforced with nanofibers. Furthermore, it proposes finite element models to simulate with high accuracy the mechanical and vibratory behaviour of pristine and nanomodified composites. These findings are of great interest for the research community and for industry as composite laminates reinforced with nanofibers could be potentially used to improve the properties of the composite structures used in aircrafts, wind turbines and other civil structures.

The other major objective of the thesis is to investigate the potential applications of nanofibers as self-powered triboelectric sensors. The first triboelectric triboelectric sensor was invented in 2012 and it has become one of the most important innovations in the field of self-powered sensing technologies. As compared to traditional sensors, triboelectric sensors are self-powered and do not require and external power supply or battery to sense the mechanical stimulus. As a result, they are maintenance free and energy independent, which results in important cost-savings. In this work, the potential of two new classes of triboelectric sensors for monitoring of pressures and impacts is demonstrated. To carry out this investigation, the developed triboelectric sensors are subjected to controlled pressures and impacts using the techniques of dynamic mechanical analysis and drop weight impact tests, respectively. The experimental results proved that the sensors generated electric responses are affected by the magnitude of the mechanical

stimulus and their amplitude increases linearly under stronger pressures/impacts. Furthermore, the sensor electric responses show a large detection range, high sensitivity, good reproducibility, and fast response time, which is essential for the practical applications of the sensor. The main contributions of this study are the development of two novel triboelectric nanogenerators and active sensors based on polyvinyl fluoride nanofibers and their investigation for its potential use for monitoring of pressures and impacts. The results of this work successfully demonstrated that the developed triboelectric sensor measure dynamic pressures and impacts in real time, which has important applications in monitoring systems, vehicle safety, and touch screens. These findings are the utmost importance as the new developed sensors could be utilized as sustainable and maintenance free sensors with the advantages of easy fabrication and low-cost processing technology.

In conclusion, this thesis contributes to the knowledge about nanofibers in terms of their applications to improve material and structural properties of composite laminates and their use as two novel nanostructured sensors for detection and measurement of pressures and impacts.

List of Publications

Journal publications

- C. Garcia, and I. Trendafilova, Triboelectric sensor as a dual system for impact monitoring and prediction of the damage in composite structures, *Nano Energy*, **60** (2019) 527-535.

- C. Garcia, and I. Trendafilova, Real-time detection of small energy impacts using a triboelectric nanogenerator, *Sensor and Actuators A: Physical,* **291** (2019) 196-203.

- C. Garcia, I. Trendafilova, and J. Sanchez del Rio, Detection and measurement of impacts in composite structures using a self-powered triboelectric sensor, *Nano Energy*, **56** (2019) 443-453.

- C. Garcia, I. Trendafilova, and A. Zucchelli, The effect of Polycaprolactone Nanofibers on the Dynamic and Impact Behavior of Glass Fibre Reinforced Polymer Composites, *Composite Science,* **2** (2018) 43.

- C. Garcia, I. Trendafilova, R. Guzman de Villoria, and J. Sanchez del Rio, Self-powered pressure sensor based on the triboelectric effect and its analysis using dynamic mechanical analysis, *Nano Energy*, **50** (2018) 401-409.

- C. Garcia, J. Wilson, I. Trendafilova, and L. Yang, Vibratory behaviour of glass fibre reinforced polymer (GFRP) interleaved with nylon nanofibers, *Composite Structures,* **176** (2017) 923-932.

Peer reviewed conference papers

- C. Garcia, and I. Trendafilova, A self-powered triboelectric velocity sensor for impact detection in composite structures, *MATEC Web Conf.*, **211** (2018) 21004.

- C. Garcia, I. Trendafilova, and A. Zucchelli, Effect of polycaprolactone nanofibers on the vibratory behaviour and the damage resistance of composite laminates, *MATEC Web Conf.*, **211** (2018) 19003.

- P. Wolszczak, and C. Garcia, Assessment of the distribution of nanofibers in membranes based on microstructure photos, *J. Phys. Conf. Ser.*, 413 (2018) 012048.

- C. Garcia, I. Trendafilova, R. Guzman de Villoria, and J. Sanchez del Rio, Triboelectric nanogenerator as self-powered impact sensor, *MATEC Web Conf.*, **148** (2018) 14005.

- C. Garcia, I. Trendafilova, A. Zucchelli, and J. Contreras, The effect of nylon nanofibers on the dynamic behaviour and the delamination resistance of GFRP composites, *MATEC Web Conf.*, **148** (2018) 14001.

Chapters

- C. Garcia, and I. Trendafilova, Self-powered pressure sensor based on triboelectric nanogenerator, New trends in nanotechnology, material and environmental sciences, Akademiker-Verlag, (2018) 349-357.

- C. Garcia, and I. Trendafilova, Applications of nanofibers as reinforcement for composite laminates, Fiber-reinforced nanocomposites, *Elsevier*. (in preparation)

- C. Garcia, and I. Trendafilova, Development and applications of triboelectric sensors, Nanosensors for smart cities, *Elsevier*. (in preparation)

Contents

Chapter 1

Introduction

1.1 Motivation

This thesis is dedicated to the effect of nanofibers on the properties of composite laminated structures and their application as nanogenerators and self-powered sensors for measuring different quantities like pressure and impact characteristics.

The first part of the thesis considers the use of electrospun nanofibers as reinforcement for glass fibre epoxy composites. The impact of nanofibers on the composite laminate is minimum as the weight of the nanofibers is very light, but the mechanical and vibratory properties of the laminates can be significantly increased with respect to that of the pristine material. The major motivations of the first part for this research thesis are presented below:

i. Vibrations are one of the most important motions as most structures vibrate as a result of their use. Vibrations can be dangerous, and they are responsible for a considerable number of failures and accidents in aircrafts, bridges and other composite structures that fail because of large amplitude vibrations. For example, the propagation of the delamination and other cracks is faster in composite structures with large amplitude vibrations, which affects the integrity of aircrafts, wind turbines and other composite structures. Therefore, the control of the vibrations of composite structures is of critical importance for the purposes of safety and structural maintenance. One of the methods of suppressing vibrations in composite laminates is to increase the damping, which can be achieved by the introduction of nanofibers in the ply interfaces of the laminates [1]. This is of great interest for machines and structures in which vibrations are a source of problems. Motivated by the above, we have

investigated the effect of electrospun nanofibers on the vibratory behaviour of composite laminates.

ii.   The main weak point of the composite laminates is their poor interlaminar strength, which can result in invisible delamination failures. Due to the delamination, the performance of the composite structures used in aircrafts, wind turbines and other civil structures can be seriously affected and lose up to 60% of their strength and stiffness [2]. Recently, researchers have suggested an important number of methods to mitigate the delamination as matrix-toughening [3], optimum stacking sequence [4] and stitching with polymeric filaments [5]. Among the techniques that have been developed over the years to mitigate the delamination problem, the reinforcement with electrospun nanofibers [6-7] has proven to be one of the most effective thanks to the strong bonding between the nanofibers and the composite laminas, which results in a significant improvement of the mechanical properties of the composites. In the fourth chapter of the present thesis, we have demonstrated how the reinforcement with nylon nanofibers can be used to avoid the delamination failures in composite laminates.

iii. In those applications where the composite laminates are employed on outer sides of structures (e.g. airplanes, wind turbines, etc.), impacts are a main concern, and the delamination attributed to the impacts has been widely investigated. One of the methods to reduce the delamination and improving the resistance to impacts is the incorporation of nanofibers in the interlaminar regions of composite laminates [8]. This can be used to develop composite structures with higher resistance to impacts (e.g. bird strikes or hailstones), which is important for the health of the composite materials used in aircrafts, wind turbines and other civil structures. In the sixth chapter of this thesis, we have investigated the effect of polycaprolactone nanofibers on the impact response of glass fibre epoxy composite laminates.

The second part of the thesis investigates the applications of nanostructured triboelectric nanogenerators as self-powered active sensors. The first triboelectric nanogenerator was invented in 2012 and therefore, it is a rather new topic which needs a lot of research to demonstrate their important practical applications. As compared to traditional sensors, triboelectric nanogenerators are self-powered and do not require an external power supply or battery to sense the mechanical stimulus. Therefore, they can be used as sustainable and maintenance-free sensors able to work independently without any external power supply which results in important cost-savings. In the present thesis, the potential of triboelectric nanogenerators as self-powered sensors for pressures, impacts and velocities is demonstrated. The main motivations of this research are summarized below:

iv. Pressure sensors are required in thousands of everyday applications as touchscreens, touchpads, microphones and medical devices. According to their mechanism to convert the mechanical energy into electricity can be generally divided into the following categories: piezoelectric [9-10], capacitive [11], triboelectric [12-13], optical [14] and resistive sensors [15]. Among these approaches, the sensors based on the triboelectric effect have attracted the most attention because they are self-powered and do not need a battery or an external power supply to power the sensor. Therefore, they can be used as sustainable sensors able to work independently without any external power supply which results in important cost-savings. Furthermore, the fabrication of triboelectric sensors is simple and low-cost as does not require time-consuming and cost processing steps as annealing or electrical poling. In the sixth chapter of the thesis, we demonstrate a novel self-powered triboelectric sensor composed of polyvinylidene fluoride (PVDF) and polyvinyl pyrrolidone (PVP) nanofibers, which can be easily manufactured by electrospinning.

v. An impact sensor plays a critical role in vehicle safety, fast medical assistance of elderlies and structural health monitoring. For example, in the event of a car crash an impact sensor detect the collision to release an air-bag for the protection of the passengers. In the case of falls in the elderly, an

impact sensor can be used to inform about the accident and provide a fast-medical assistance.

Other practical examples could be detection of impacts in hail storms, where impacts are responsible for a considerable number of accidents in aircrafts, wind turbines and other civil infrastructures. Therefore, the sensing of impacts is the vital importance as impacts can seriously affect the health and safety of humans. In the chapter seven of the present study, we reported that a novel triboelectric sensor can be successfully used for the detection and measurement of impacts in real time.

vi. Composite structures as e.g. aircrafts, wind turbines or racing cars are frequently subjected to numerous impacts. For example, aircrafts may collide with birds during take-off and landing or get damaged due to the impact of hailstones. These impacts harm the integrity of the composite laminates used in their structures which results in delamination and other failures which are usually very difficult to detect by visual inspections. Hence, the detection and quantification of impacts is of vital importance for monitoring the health state of composite structures. Recently, triboelectric sensors have been demonstrated to detect touches, pressures, vibrations and other mechanical motions with the advantages of being self-powered, maintenance-free and easy to fabricate. However, there is no research focusing on the potential of triboelectric sensors to monitor the impacts applied to composite structures. In the chapter eight and nine of the present thesis, a self-powered triboelectric triboelectric sensor is developed to measure strong energy impacts applied to structures made of composite materials. This could be particularly beneficial for the detection of bird strikes, hailstones and other high energy impacts in aircraft composite structures.

1.2 Scope, objectives and contributions

Research on the mechanical and dynamic behaviour of composites reinforced with electrospun nanofibers is still far from being completed, therefore, we have

investigated the mechanical and dynamical properties of nanomodified composites. The main objectives of the first part of this thesis, which investigates the influence of nanofibers on the mechanical and dynamical properties of composite laminates are summarized below:

i. Study of the effect of nylon nanofibers on the vibratory properties of glass fibre reinforced polymer composites. To address this study, composite beams reinforced with and without nylon nanofibers are subjected to free vibration tests with the aim to assess the influence of nylon nanofibers on the natural frequencies and damping ratio.

ii. Development of a simple finite element model to simulate with high accuracy the vibration properties of nanomodified composites. For this purpose, the natural frequencies and damping ratio of pristine and nanomodified composites are simulated using transient analysis in ANSYS workbench.

iii. Study of the potential of nylon nanofibers to reduce the susceptibility of delamination in composite laminates. To carry out this investigation, the interlaminar shear strength of glass fibre epoxy composites reinforced with and without nylon nanofibers is determined experimentally using the international standard D2344.

iv. Analysis of the delamination behaviour of pristine and nanomodified composites using cohesive zone modelling in ANSYS workbench. For this aim, the experimental force-displacement curves are simulated with the aim to compare the delamination response of pristine and nanomodified composites.

v. Investigation of the effect of polycaprolactone nanofibers in the impact response of glass fibre reinforced polymer composites using a finite element model. The main idea of this investigation is to demonstrate if the addition of polycaprolactone nanofibers can be used to develop composite laminates with higher resistance to impacts (e.g. bird strikes or hailstones), which is

important for the health of the composite materials used in aircrafts, wind turbines and other civil structures.

The topic of the second part of the thesis relates to the applications of nanostructured triboelectric nanogenerators as self-powered active sensors. Recently, various approaches have been developed and applied for detection and measurement of pressures and impacts in environment as per example piezoelectric sensors [16, 17], capacitive sensors [18], optical sensors [19], acoustic sensors [20], and resistive sensors [21]. However, most of these technologies require an external power supply or battery to sense the mechanical stimulus which the disadvantages of no self-powered operation, limited life-time and maintenance cost. In the present thesis, an environmentally friendly and self-powered technology based on a triboelectric nanogenerator is developed for the measurement of pressures and impacts. The main objectives of this research work are detailed below:

vi.   This research investigates the potential applications of a novel triboelectric nanogenerator based on polyvinyl fluoride (PVDF) and polyvinyl pyrrolidone (PVP) nanofibers as self-powered pressure sensor. To address this study, the technique of dynamic mechanical analyzer (DMA) is used to apply controlled pressures to the triboelectric nanogenerator and a commercial oscilloscope is utilized to measure the resultant electric signals of the nanogenerator.

vii.   This research also investigates the ability of the developed PVDF-based triboelectric nanogenerator to detect and quantify impacts applied to composite structures. To carry out this investigation, composite plates are subjected to various impacts in the energy range between 2 J and 30 J using a drop-weight impact machine. Then, the electric responses of the triboelectric sensor adhered to the composites are measured in the form of voltage and current. The idea is to study the changes in the resultant electric signals due to the variations in the impact energy.

viii.   In the present thesis, we investigate the development of a novel triboelectric nanogenerator prepared by a membrane of polyvinylidene fluoride (PVDF)

nanofibers and an ultra-thin layer of polypropylene (PP). Furthermore, our research studies analyse the potential applications of the developed TENG as self-powered impact sensor. For this aim, the triboelectric sensor is impacted at various energies using a free-falling ball dropped from five different heights. The idea is study if the electric responses of the nanogenerator are affected by the magnitude of the impacts.

ix. This investigation also demonstrates the potential of the developed PVDF-based triboelectric sensor for monitoring impacts in composite structures like e.g. aircrafts. For this study, composite plates equipped with a triboelectric sensor are subjected to various impacts using a drop-weight impact machine with velocities ranging from 4.6 to 11.6 km/h. Then, the sensor electric responses are measured in form of voltage and current using a commercial oscilloscope and digital multimeter respectively. The idea is to investigate if the amplitude of the voltage and current signals is affected by the velocity of the impacts.

1.3 Thesis outline

The thesis is made of two major parts: Chapters 3-5 are dedicated to the first part which considers the influence of nanofibers on the mechanic and dynamic properties of composite laminates. Chapters 6-9 are dedicated to the second part, which relates to the applications of nanostructured triboelectric nanogenerators as self-powered active sensors. The thesis is structured as follows:

Chapter 2 is a critical review of the research topic and provides and overview of the previous research on the field. Initially, the chapter introduces the use of electrospun nanofibers as reinforcement for composite laminates. Therefore, the scientific results reported of the field of nanomodified composites are analysed with the aim to study the effect of nanofibers on the mechanical and dynamical properties of composite laminates. Finally, the

most relevant scientific results reported on the field of triboelectric nanogenerators are presented and analysed with the aim to demonstrate the potential applications of triboelectric nanogenerators as self-powered sensors for pressures and impacts. As compared to traditional sensors, triboelectric nanogenerators do not require an external power supply or battery to sense the mechanical stimulus.

Chapter 3 investigates how nanofibers affect the vibration behaviour of the composite laminates. In this chapter, we concentrate on the effect of nylon nanofibers as these are particularly suitable to improve the properties of the laminates because of their excellent properties. The reinforcement with nanofibers is beneficial for purpose of reducing the vibration amplitude of composite structures, which limit the propagation of cracks and other irreversible damages.

Chapter 4 analyses the effect of nylon nanofibers on the delamination behaviour of glass fibre epoxy composites. This is of great interest for the industry as composite laminates reinforced with nylon nanofibers could be potentially used to prevent the delamination failures in aircrafts, wind turbines and other civil structures.

Chapter 5 examines the impact behaviour of glass fibre epoxy composites reinforced with and without polycaprolactone nanofibers. This is of critical importance as composites reinforced with polycaprolactone nanofibers could be potentially used to develop composite structures with higher resistance to impacts (e.g. bird strikes or hailstones), which is important for the health of the composite mats used in aircrafts, wind turbines and other civil structures.

Chapter 6 suggests a novel triboelectric nanogenerator prepared by PVDF and PVP fibers and tests its application as self-powered sensor, which detects and follows the pressure changes in real time. This is the utmost importance

as pressure sensors are required in thousands of everyday applications as touchscreens, touchpads, microphones and medical devices.

Chapter 7 presents a novel triboelectric nanogenerator based on polyvinylidene fluoride nanofibers and a thin film of polypropylene, which can be successfully used for real-time detection of small energy impacts. The sensing of impacts is the vital importance as impacts plays a critical role in vehicle safety, fast medical assistance of elderlies and structural health monitoring.

Chapter 8 introduces a new approach to detect and measure the energy of the impacts in composite structures using a self-powered triboelectric sensor. The findings of this work demonstrate that triboelectric sensors can be used for real-time detection of impacts in composite structures as aircrafts, wind turbines or bridges, which has important applications for the detection of bird strikes, hailstones and other high energy impacts in aircrafts and civil structures.

Chapter 9 introduces a new approach to detect and measure the velocity of the impacts applied to composite structures using a self-powered triboelectric sensor. The detection and quantification of impacts is of vital importance for monitoring the health state of composite structures such as aircrafts or wind turbines.

Chapter 10 presents the most important conclusions and provides the recommendations for further research.

References

[1]   C. Garcia, I. Trendafilova, A. Zucchelli, J. Contreras, The effect of nylon nanofibers on the dynamic behaviour and the delamination resistance of GFRP composites, Matec Web Conf., 148 (2018) 14001.

[2]   G. Minak, R. Palazzetti, I. Trendafilova, and A. Zucchelli, Localization of a delamination and estimation of its length in a composite laminate beam by the VSHM and pattern recognition methods, Mech Mater., 46 (2010) 387-394.

[3]   M. Hojo, S. Matsuda, M. Tanaka, S. Ochiai, A. Murakami, Mode I delamination fatigue properties of interlayer-toughened CF/epoxy laminates, Compos Sci Technol., 66 (2005) 665-675.

[4]   E. Fuoss, P. Straznicky, C. Poon, Effects of stacking sequence on the impact resistance in composite laminates – part 1: parameter study, Compos Struct., 41 (1998) 67-77.

[5]   T. Yang, C. Wang, J. Zhang, Toughening and self-healing of epoxy matrix laminates using mendable polymer stitching, Compos Sci Technol., 72 (2012) 1396-1401.

[6]   G. Li, P. Li, Y. Yu, X. Jia, S. Zhang, X. Yang, S. Ryu, Novel carbon fiber/epoxy composite toughened by electrospun polysulfone nanofibers, Mater Lett., 62 (2008) 511-4.

[7]   S. Hamer, H. Leibovich, A. Green, R. Intrater, R. Avrahammi, E. Zussman, A. Siegmann, D. Sherman, Mode I interlaminar fracture toughness on Nylon 66 nanofibre mat interleaved carbon/epoxy laminates, Polym Compos., 32 (2011) 1781-9.

[8]   R. Palazzetti, A. Zucchelli and I. Trendafilova, The self-reinforcing effect of Nylon 6,6 nano-fibres on CFRP laminates subjected to low velocity impact, J Compos Struct., 106 (2013) 661-72.

[9]   J.H. Lee, H.J. Yoon, T.Y. Kim, M.K. Gupta, J.H. Lee, W. Seung, H. Ryu, S.W. Kim, Micropatterned P(VDF-TrFE) film-based piezoelectric nanogenerators for highly sensitive self-powered pressure sensors, Adv Funct Mater., 25 (2015) 3203-3209.

[10]   J. Chun, K.Y. Lee, C.Y. Kang, M.W. Kim, S.W. Kim, J.M. Baik, Embossed hollow hemisphere-based piezoelectric nanogenerator and highly response pressure sensor, Adv Funct Mater., 24 (2014) 2038-2043.

[11]   D. Lipomi, M. Vosgueritchian, K. Tee, S. Hellstrom, J. Lee, C.H. Fox, Z. Bao, Skin-like pressure and strain sensors based on transparent elastic films of carbon nanotubes, Nat Nanotechnol., 6 (2011) 788-792.

[12]   L. Lin, Y. Xie, S. Wang, W. Wu, S. Niu, X. Wen, Z.L. Wang, Triboelectric active sensor array for self-powered static and dynamic pressure detection and tactile imaging, ACS Nano, 7 (2013) 8266-8274.

[13]   X.D. Wang, H.L. Zhang, L. Dong, X. Han, W.M. Du, J.Y. Zhai, C.F. Pan, Z.L. Wang, Self-powered high-resolution and pressure-sensitive triboelectric sensor matrix for real-time tactile mapping, Adv Mater., 28 (2016) 2896-2903.

[14]   J.S. Heo, J.H. Chung, J.J. Lee, Tactile sensor arrays using fiber Bragg grating sensors, Sens. Actuators A Phys. 126 (2006) 312-327.

[15]   J. Park, Y. Lee, J. Hong, M. Ha, Y.D. Jung, H. Lim, S.Y. Kim, and H. Ko, Giant tunnelling piezoresistance of composite elastomers with interlocked microdome arrays for ultrasensitive and multimodal electronic skins, ACS Nano, 8 (2014) 4689-4697.

[16]   W.Z. Wu, X.N. Wen, Z.L. Wang, Taxel-addressable matrix of vertical-nanowire piezotronic transistors for active and adaptive tactile imaging, Science, 340 (2013) 952-957.

[17]   J. Chun, N.R. Kang, J.Y. Kim, M.S. Noh, C.Y. Kang, D. Choi, S.W. Kim, Z.L. Wang, J.M. Baik, Highly anisotropic power generation in piezoelectric

hemispheres composed stretchable composite film for self-powered motion sensor, Nano Energy, 11 (2015) 1-10.

[18]   G. Schwartz, B. Tee, J. Mei, A. Appleton, D.H. Kim, H.L. Wang, Z. Bao, Flexible polymer transistors with high pressure sensitivity for application in electronic skin and health monitoring, Nat Commum., 4 (2013) 1859.

[19]   D. Liang, B. Culshaw, Fibre optic silicon impact sensor for application to smart skins, Electron. Lett. 29 (1993) 529-530.

[20]   X. Deng, Q. Wang, and V. Giurgiutiu, Structural health monitoring using active sensors and wavelet transforms. In: 6th Annual International Symposium on Smart Structures and Materials, 1-5 March 1999, Newport Beach, California, USA.

[21]   T. Yamada, Y. Hayamizu, Y. Yamamoto, Y. Yomogida, A. Izadi-Najafabadi, D.N. Futaba, K. Hata, A stretchable carbon nanotube strain sensor for human-motion detection, Nat Nanotechnol., 6 (2011) 296-301.

Chapter 2

Literature review

2.1 Applications of nanofibers as reinforcement for composite laminates

In the last years, the scientific community showed a considerable interest on the potential of electrospun nanofibers as reinforcement for composite laminates. For example, the authors of [1-3] demonstrated that the incorporation of nanofibers in the interlaminar regions of composite laminates can be used as a potential approach to mitigate the delamination. Other practical uses of interleaving with nanofibers is to increase the resistance to impacts [4, 5] or avoid the propagation of cracks [6]. Thus, the incorporation of electrospun nanofibers into the interfaces of composite laminates possesses a great potential to improve the mechanical and dynamic properties of composite laminates.

Nanofibers fabricated by electrospinning are considered as a promising candidate for composite reinforcement due to the following aspects:

- The high porosity of the nanostructured membranes allows the resin flow easily through them, which makes a solid bonding between the nanofibers and the epoxy resin.
- The membranes of interconnected nanofibers can be easily dispersed in the interlaminar regions of the composite laminates, which is the critical importance to improve the material properties of the laminates.
- The weight of the membranes of nanofibers is very light (just a few grams per square meter), which makes a negligible impact on the overall weight of the laminates.
- The very high surface area to volume ratio of the nanofibers enhances the load transfers between the matrix and the fibres.

- The dimensions of the composites are not affected by the incorporation of nanofibers due to the small size of the nanofibers.
- The addition of nanofibers in the interlaminar regions of the laminates can increase significantly some mechanical and dynamical properties of the composites.

In this review, the use of electrospun nanofibers as reinforcement for composite laminates is reviewed and discussed. Therefore, the scientific results reported of the field of nanomodified composites are analysed with the aim to study the effect of nanofibers on the mechanical and dynamical properties of composite laminates.

2.1.1 Effect of nanofibers on the vibratory behaviour

It is well known that the propagation of delamination and other failures in composite laminates is strongly affected by the vibratory of the composite laminates. Therefore, vibrations are responsible for a considerable number of accidents in aircrafts, bridges and other composite structures that fail (are destroyed) due to large amplitude vibrations. One of the methods to reduce the vibrations and avoid the propagation of cracks is to increase the damping of the composite laminates which can be achieved by the incorporation of electrospun nanofibers into the interlaminar regions of composite laminates. Thus, it is of vital importance to investigate the effect of electrospun nanofibers on the vibratory behaviour of composite mats.

Recently, several papers have investigated the effect of nanofibers on the natural frequencies of composite laminates. For example, Shiuh-Chuan Her et al. [7] analysed the natural frequencies on composites reinforced with and without carbon nanotubes. This work reports that the natural frequencies of epoxy composites increase a 7% due to the addition of carbon nanotubes. G. Balaganesan et al. [8] analysed the natural frequencies on pristine and clay nano-modified composites. The results reveal that natural frequencies of glass fibre composites can be increased up

to 12% due to the addition of clay nanofibers. Other authors as [9, 10] observed very small changes in the natural frequencies due to the incorporation of carbon nanofibers and nanotubes in composites. In general, it can be said that the change of the natural frequencies attributed to the reinforcement with nanofibers depends on the content and type of nanofibers interleaved.

Alternatively, other authors incorporated nanofibers on the interlaminar regions of composite laminates with the aim to increase the damping ratio. For example, Jihua Gou et al. [9] and Naser Kordani et al. [10] reported a 200% and 108% increase of the damping ratio of composite laminates interleaved with carbon nanotubes with respect to the damping of pristine composites. K.T.B. Padal et al. [11] showed that the damping ratio of epoxy composites reinforced with jute nanofibers is a 70% higher as compared to the damping ratio of the virgin panels. In summary, the vast majority of the published studies demonstrate that there is a significant increase of damping ratio due to the incorporation of nanofibers in the composite laminates. This can be attributed to the fact that nanofibers improve the load transference between the fibres and the epoxy resin, giving the nano modified composites a higher damping ratio. Thus, the interleaving with nanofibers is an effective method to increase the damping ratio and to reduce the vibration amplitudes of the structures.

Although some authors have studied the vibration behaviour of nanomodified composites mainly based on experimental method [7-11], there are only a few attempts to model the vibratory behaviour of nanomodified composites using finite element analysis [12, 13]. Special attention deserves the works of Rafiee and Moghadam [12] which attempt to develop a multi-scale finite element method to simulate the vibration behaviour of polymers reinforced with and without carbon nanotubes. Their results show a considerable growth of the natural frequencies due to the addition of carbon nanotubes. Other authors as Ribeiro [13] suggested a finite element model (FEM) to simulate the first three vibration modes of carbon nanotubes. In conclusion, it can be said that there are only a couple studies that

investigate numerically the effect of nanofibers on the vibration behaviour of composite laminates.

In the last years, the dynamic properties of composite materials reinforced with carbon nanofibers and nanotubes have been widely studied. However, only one study has investigated the vibratory behaviour of composites reinforced with electrospun nanofibers. Table 2.1 presents a summary of the results from these this study dealing with the vibratory behaviour of composite laminates reinforced with electrospun nanofibers. In [14], R. Palazzetti et al. found that the damping of carbon fibre composite panels reinforced with nylon nanofibers is about 60% higher than the damping of pristine panels. Additionally, the first natural frequency of the glass fibre epoxy composites shows a very small increment due to the incorporation of nylon nanofibers. To date, the vibratory behaviour of composite laminates reinforced with electrospun nanofibers has been poorly investigated. Therefore, there is an urgent need to explore the effect of electrospun nanofibers on the natural frequencies and damping ratio of composite laminates.

Reference	Laminate	Nanofiber	Amount	Variation
[14]	Carbon fibre	PA	25 µm	+ 60%

Table 2.1 Effect of electrospun nanofibers on the damping ratio

2.1.2 Effect of nanofibers on the delamination behaviour

In this section, the influence of polymer nanofibers on the delamination behaviour of composite laminates is analysed. To address this, it is explored the influence of electrospun nanofibers on three material properties which are related to delamination: (i) Mode I energy release, (ii) Mode II energy release rate and (iii) Interlaminar shear strength.

The Mode I and II energy release rates are the most common and effective approach to investigate delamination behaviour of composite laminates [1-3].

Therefore, most of the studies on the field of nanomodified composites have analysed the delamination behaviour of pristine and nanomodified composites using this approach. The main differences between both experimental tests is the way of applying the load. The load is applied in normal and parallel direction to the plane of the crack in Mode I and Mode II, respectively.

Alternatively, the interlaminar shear strength can also be used to analyse the delamination behaviour of composite laminates. In this test, the load is applied to a very short beam which generates dominant shear stress on the interlaminar region, where the nanofibers are laid. The composite specimens used in the test are very small which reduces considerably the material expenses and saves experimental time.

(i)   Effect of nanofibers on the mode I energy release rate

In this section, the influence of polymer nanofibers on the mode I energy release rate of composite laminates is analysed. To address this task, the scientific results reported on the field of composites reinforced with polymeric nanofibers are analysed with the aim to understand the effect of nanofibers on the energy release rates of the composites.

The mode I critical energy release rates for composite specimens reinforced with and without nanofibers are determined by the international standard ASTM D5528 [15]. During the tests, the force and displacement curves of the composite specimens are recorded with the aim to calculate the critical and propagation energy release rates of the pristine and nanomodified composites.

Table 2.2 presents the results from ten publications of the field of study. The table indicates that eight papers (80% of the total) show that the addition of nanofibers into the laminates cause a significant increment of the energy release rates in the range between 13% and 158% [16-23]. In the other two papers (20% of the

total), the incorporation of nanofibers results in a reduction of the mode I energy releases rates [24, 25]. As a result, the papers indicate that the presence of nanofibers in the ply interfaces of the laminates generally increase the energy release rate. Therefore, the interleaving with electrospun nanofibers is an effective method to prevent the delamination failures in composite laminates. The mode I toughness of the composite laminates reinforced with nanofibers is strongly influenced by these factors: manufacturing process of the nanocomposite, mechanical properties of nanofibers, number of nanofibers, and class of fabric. The changes in mode I toughness from +158 % to -27 % can be explained by the fact that the fabrication procedure, types of nanofibers, amount of nanofibers and type of fabrics used in the preparation of these nanomodified composites are completely different.

Reference	Laminate	Nanofiber	Amount	Variation
[16]	Carbon fibre	PSF	1 %	+ 158%
[17]	Carbon fibre	PA	1.8 g/m^2	+ 137%
[18]	Carbon fibre	Phenoxy	70 µm	+ 98%
[19]	Glass fibre	SBS	22 g/m^2	+ 90%
[20]	Glass fibre	PCL	15 g/m^2	+ 50%
[21]	Carbon fibre	PVDF	30 µm	+ 44%
[22]	Carbon fibre	PA	70 µm	+ 23%
[23]	Carbon fibre	PVB	4.5 g/m^2	+ 13%
[24]	Glass fibre	TEOS	NA	- 12%
[25]	Carbon fibre	PVA	7.1 g/m^2	- 27%

Table 2.2 Effect of electrospun nanofibers on the mode I energy release rate

The literature indicates that several types of nanofibers have been used to enhance the mode I energy release rates of composite laminates. For example, the authors of [17, 22] utilized nylon nanofibers to increase the energy release rates of carbon fibre epoxy composites. On the other hand, other researchers used other type of nanofibers to reinforce the composite laminates as polysulfone [16], phenoxy [18], styrene butadiene styrene [19], polycaprolactone [20], polyvinylidene fluoride [21] or polyvinyl butyral [23]. Additionally, it is important to mention that all studies found on the literature used a very small amount of nanofibers (below 22 g/m^2) to improve the mode I energy release rates of the composite laminates.

The increment of the energy release rate of the composite laminates has been attributed to various mechanisms discovered by the authors. For example, T. Brugo et al. [17] indicates that the incorporation of nylon nanofibers in the interlaminar regions of carbon fibre composites increase in a 137% the mode I energy release rate. This behaviour is explained by the fact that nanofibers block the propagation of the crack along the ply interfaces. Therefore, the crack is forced to follow another longer and tortuous path, which results in an increment of the energy required to propagate the crack. S. Heijden et al. [19] reports that the energy release rate of carbon fibre epoxy composites reinforced with styrene butadiene nanofibers is a 90% higher as compared to the energy release rate of the pristine specimens. This important increment of the energy release rate is attributed to the presence of significant bridging phenomena between the nanofibers and the composite laminas, which makes the nanofibers act as bridges to link the two adjacent composite plies. S. Alessi et al. [22] shows that carbon fibre epoxy composites reinforced with thin membranes of nylon nanofibers possess a 23% higher energy release rate with respect to neat specimens. This behaviour is due to the strong adhesion between the nanofibers and the epoxy resin, which results in higher energy release rates for the nanomodified samples. In general, it can be said that various reinforcing mechanisms has been reported in the literature with the aim to explain the increment of the energy release rates in the nanomodified composites.

On the other hand, other authors utilized a finite element model (FEM) to investigate the influence of nanofibers on the energy release rates in opening mode. For example, H. Saghafi et al. [21] simulated numerically the fracture behaviour of composites reinforced with thin and thick membranes of polyvinyl fluoride nanofibers. The results suggested that the interleaving with thin and thick membranes of nanofibers leads to 42% and 98% enhancement of the mode I energy release rate, respectively. G. Giuliese et al. [26] developed a cohesive zone model (CZM) to model the fracture response of composites reinforced with different configurations of nylon nanofibers. The results demonstrated that the opening mode energy release rates are strongly affected by the morphology of the nanofibers.

In summary, the vast majority of results reported on the literature demonstrates that the incorporation of a very small amount of nanofibers in the ply interfaces of glass and carbon fibre epoxy laminates can be used to enhance significantly the mode I energy release rate.

(ii)   Effect of nanofibers on the mode II energy release rate

The aim of this paragraph is to explain how the addition of polymer nanofibers can be used to improve the mode II energy release rate of the composite laminates. Therefore, some research results published on the topic of nanomodified composites are presented and reviewed with the aim to understand the effect of nanofibers on the energy release rates of the composites.

Most of the studies found on the literature use the international standard ASTM D7905 [27] to determinate the mode II energy release rate of the pristine and nanomodified composites. During the experiment, the force and displacement curves of the pre-delaminated composite beams are recorded with the purpose to calculate the critical energy release rate in sliding mode.

Table 2.3 summarizes the experimental results from ten publications in the scientific field. The table shows that nine of the papers (90% of the total) reported a clear increment (above the 20%) of the sliding mode energy releases rates when the nanofibers are interleaved in the composite laminates [18-20, 23, 28-31]. On the other hand, the other paper (10% of the total) show that the addition of nanofibers involves a small decrement of the mode II energy release rate [23]. Therefore, most of the papers indicate that the reinforcement with electrospun nanofibers increases the energy release rate. Hence, it is demonstrated that the interleaving with electrospun nanofibers is an effective method to prevent the delamination failures in composite laminates.

Reference	Laminate	Nanofiber	Amount	Variation
[28]	Glass fibre	PA	25 g/m^2	+ 109%
[19]	Glass fibre	SBS	22 g/m^2	+ 100%
[20]	Glass fibre	PCL	15 g/m^2	+ 81%
[29]	Carbon fibre	PVDF	5 %	+ 57%
[23]	Carbon fibre	PAI	4.1 g/m^2	+ 56%
[30]	Glass fibre	TEOS	2.5 g/m^2	+ 56%
[18]	Carbon fibre	Phenoxy	70 μm	+ 31%
[31]	Carbon fibre	Silk	5%	+ 30%
[23]	Carbon fibre	PES	3.6 g/m^2	+ 20%
[23]	Carbon fibre	PVB	4.3 g/m^2	- 8%

Table 2.3 Effect of electrospun nanofibers on the mode II energy release rate

Table 2.3 indicates the nanofibers which have been previously employed to improve the mode II energy release rate of the composite laminates. Furthermore, the table also includes the amount of nanofibers interleaved in the specimen and the type of composite laminate. H. Saghafi et al. [28] analysed the influence of nylon nanofibers on the interlaminar properties of unidirectional glass fibre epoxy composites. The results show that the addition of a minimum amount of nylon nanofibers in the composite interfaces increase the mode II energy release rate by 109%. K. Magniez et al. [29] demonstrated that the mode II energy release rate of carbon fibre composite epoxy reinforced with polyvinyl fluoride nanofibers is a 57% higher as compared to the neat panels. It is worthy to note that the weight fraction of the nanofibers in the nanomodified composites is very small (5%). G. Beckermann et al. [23] investigates the mode II energy release rate of polyvinyl butyral nanomodified and pristine composites. The results indicate that the incorporation of polyvinyl butyral nanofibers in the interfaces of carbon fibre epoxy composites decrease an 8% the energy release rate with respect to the neat panel. In general, most of the studies prove that the incorporation of electrospun nanofibers can be used to enhance the mode II energy release rate of composite laminates.

Similar results are found on [26, 32], where the authors investigated numerically the effect of nanofibers on the energy release rates of pristine and nanomodified composites. In [32], the authors developed a cohesive zone model to

simulate the fracture behaviour of composites modified with nylon nanofibers. The results show that the addition of nylon nanofibers in the interlaminar regions of carbon composite laminates increased an 11% the energy release rate in sliding mode. Other studies as [26] used a cohesive zone model to simulate the fracture response of composites reinforced with different configurations of nylon nanofibers. The results demonstrated that the energy release rates are strongly affected by the morphology of the nanofibers.

In conclusion, most of the studies indicate that a very small amount of nanofibers induce a generous increment of the mode II energy release rates of the composite laminates. The increment of the energy release rate in the composite specimens is attributed to the same reinforcing mechanisms presented in the section above. In [19, 20], the critical energy release rate is increased because of the modification of the crack path during the delamination process. In other words, the nanofibers hinder the propagation of the crack along the ply interfaces, and the crack is forced to follow another longer and harder path. In [28], the energy release rate is increased thanks to the presence of significant bridging phenomena between the nanofibers and the two adjacent composite plies, which induces an increment of the residual interlaminar fracture toughness. In [18], the authors attributed the compatibility between the epoxy resin and the polymer nanofibers as one of the main reasons to explain the increment of the energy release rate in the nanomodified composites.

(iii)   Effect of nanofibers on the interlaminar shear strength

In this section, the effect of electrospun nanofibers on the interlaminar shear strength of composite laminates is considered. For this aim, the ISO 14130 [33] and the ASTM D2344 [34] international standards are used to determinate the bending behaviour of the pristine and the nanomodified composites. During the bending tests, the load is applied to a very short composite beam to generate shear stresses on the interlaminar regions where nanofibers are interleaved.

Table 2.4 summarises the results found on the literature. In [30], it is shown that the incorporation of tetra ethyl orthosilicate into the interlaminar regions of glass fibre epoxy composites results in an increment of the interlaminar shear strength of 105%. In [35], our research group demonstrated that the interlaminar shear strength of unidirectional glass fibre epoxy composites increased a 27% due to the addition of nylon nanofibers. Other studies as [37] showed small increments of 11% due to the presence of polyacrylonitrile nanofibers in carbon fibre composites.

Reference	Laminate	Nanofiber	Amount	Variation
[30]	Glass fibre	TEOS	2.5 g/m^2	+ 105%
[35]	Glass fibre	PA	25 g/m^2	+ 27%
[36]	Glass fibre	TPU	N/A	+ 18%
[37]	Carbon fibre	PAN	N/A	+ 11%
[18]	Carbon fibre	Phenoxy	70 µm	+ 0%

Table 2.4 Effect of electrospun nanofibers on the interlaminar shear strength

In summary, most of the papers show that the interleaving with nanofibers has a positive effect on the composite laminates. This can be explained because the electrospun nanofibers enhance the transference of load from the epoxy to the fibres, reducing the stress concentrations on the interlaminar regions [37].

As stated above, many authors have extensively investigated how the incorporation of electrospun nanofibers into the ply interfaces of composite laminates can be used to mitigate the delamination. For example, the papers published by [1, 2] demonstrated that the addition of electrospun nanofibers in composite laminates can be used to increase the mode I energy release rate. Similar results are reported by [3], indicating that mode II energy release rate of composite laminates can be increased considerably due to the incorporation of electrospun nanofibers. Up to now, most of the publications about the delamination behaviour of nanomodified composites have investigated about the influence of electrospun nanofibers on the mode I and II energy release rates [1-3, 16-25, 28-31]. However,

only a few studies focus on the influence of electrospun nanofibers on the interlaminar shear strength of glass fibre epoxy composites [35-37].

2.1.3 Effect of nanofibers on the impact behaviour

Aircrafts, wind turbines and other structures made of composite laminates are frequently subjected to impacts. For example, aircrafts may collide with birds during take-off and landing or being damaged due to the impact of hailstones. These impacts damage the integrity of the composite laminates used in the structures, which results in delamination and other irreversible damages. One of the ways to prevent the delamination cones formed by the impacts is the incorporation of electrospun nanofibers in the interlaminar regions of composite laminates. In this section, the effect of electrospun nanofibers on the area damaged in composites by low velocity impacts is analysed.

Table 2.5 summarises the results from some publications found on the literature. From the table, it can be observed that most of the papers (80% of the total) reported an important reduction of the area damaged when nanofibers are interleaved in the composites [20, 38-40] and only one of the papers (20% of the total) showed that the addition of nanofibers causes an increment of the area damaged because of low velocity impact [41]. Therefore, many of the publications demonstrated that the incorporation of nanofibers in the interfaces of laminates is an effective method to reduce the area damaged because of low velocity impacts.

Reference	Laminate	Nanofiber	Amount	Variation
[38]	Glass fibre	PA+PCL	30 µm	- 59%
[20]	Glass fibre	PCL	15 g/m^2	- 50%
[39]	Carbon fibre	PA	1.7 g/m^2	- 46%
[40]	Glass fibre	PCL	30 µm	- 26%
[41]	Glass fibre	TEOS	8.2 g/m^2	+ 9%

Table 2.5 Effect of electrospun nanofibers on the area damaged by impact

Recently, several papers have investigated the effect of electrospun nanofibers on the impact response of composite laminates. For example, P. Akangah et al. [39] compared the impact response of carbon fibre laminates reinforced with and without nylon nanofibers. The results reveal that the area damaged because of low velocity impacts decreases considerably (up to 46%) because of the presence of nylon nanofibers. H. Saghafi et al. [38] demonstrated that the incorporation of a mixture of polycaprolactone and nylon nanofibers into the interlaminar regions of glass fibre epoxy composites reduce a 59% the area damaged because of the impact. The reinforcement mechanism is attributed to the fact that the nanofibers are linked with the two adjacent composite laminates, which avoids the delamination cones. Other authors as [42, 43] suggested that the interleaving with polyvinylidene fluoride and polyacrylonitrile nanofibers is not a good choice for toughening the epoxy and enhancing the impact response of glass fibre composites.

Additionally, other researchers have investigated the impact response of pristine and nanomodified composites using finite element analysis. For example, the authors of [44] investigated the impact behaviour of polymers interleaved with and without carbon nanotubes using a multi-scale finite element model. The results of this work revealed a considerable increase of the impact resistance of the carbon nanomodified polymers as compared to the pristine panels. In our paper [45], we developed a cohesive zone model to simulate the impact response of composites reinforced with and without polycaprolactone nanofibers. The results of our work show that the polycaprolactone nanomodified laminates are a 40% less damaged by the impacts as compared to the pristine specimens.

In general, most of the studies show that there is a significant reduction of the delamination due to the incorporation of electrospun nanofibers in the ply interfaces of composite laminates. Thus, it is demonstrated that the addition of electrospun nanofibers is an effective method to enhance the impact response of structures made of composite laminates.

Up to date, most of the studies have investigated the effect of electrospun nanofibers on the fracture toughness in opening and sliding mode [1-3], on the tensile strength [46, 47], and the compression strength after impact [48]. However, there are still very few works to report about the effect of electrospun nanofibers on the impact behaviour of composite laminates.

On the other hand, only a few authors have simulated the impact behaviour of nanomodified composites using finite element analysis. For example, the authors of [44] investigated the impact behaviour of polymers interleaved with and without carbon nanotubes using a multi-scale finite element model. The results of this work show an improvement of the impact resistance of the carbon nanomodified polymers as compared to the pristine panels. Therefore, there are very few attempts to simulate numerically the influence of nanofibers on the impact behaviour of composite laminates.

2.1.4 Conclusions

In this section, the use of electrospun nanofibers as reinforcement for composite laminates is reviewed and discussed. The vast majority of the papers found in literature show that the incorporation of nanofibers in laminates can bring significant benefits from the mechanical and dynamical points of view. The impact of nanofibers on a laminate is minimum as the weight of the nanofibers is very light, but the mechanical and dynamical properties of the composites can be significantly increased compared with that of the pristine material. Research on the mechanical and dynamic behaviour of composites reinforced with nanofibers is still far to be completed; therefore, we investigate the mechanical and dynamical properties of nanomodified composites.

2.2 Applications of nanofibers as triboelectric nanogenerators and sensors

This part of the literature review reports some recent progress in the application of triboelectric nanogenerators as self-powered sensors. Initially, we introduce the working mechanism and basic principles of triboelectric nanogenerators. After that, the scientific results reported of the field of triboelectric nanogenerators are analysed with the aim to demonstrate the potential of triboelectric nanogenerators as self-powered sensors.

Nanogenerator is a device that converts environmental energy (e.g. wind energy, thermal energy or water energy) into electricity. According to its operating principle, a nanogenerator can be generally classified into the following categories: piezoelectric [49, 50], triboelectric [51, 52] and pyroelectric [53] nanogenerators. Among them, the piezoelectric and triboelectric nanogenerators can convert mechanical energy into electricity and pyroelectric nanogenerators can be used to harvest thermal energy from a time-dependent temperature fluctuation. Among the various kinds of nanogenerators, triboelectric nanogenerators have recently attracted considerable attention among the research community because of their high energy conversion efficiency, self-powered mechanism, low-cost and easy fabrication.

In the last years, triboelectric nanogenerators (TENGs) have been extensively reported for its potential applications in the field of energy harvesting [54-58], which is of great value especially for powering mobile electronics by the harvesting of green energy. On the other hand, the electric signals generated from the nanogenerator are proportional to the magnitude and frequency of the mechanical stimulus and can be used as self-powered active sensors to measure multiple mechanical stimulus as pressures [59-61], vibrations [62, 63], human body motions [64, 65], environmental changes [66-68] and more. Hence, one of the main applications of triboelectric nanogenerators is to serve as sustainable sensor able to work independently without any external power supply.

2.2.1 Operation principle of the nanogenenerators

The working principle of triboelectric nanogenerators is based on the contact electrification and electrostatic induction [69, 70]. The contact electrification occurs when two materials with different electron affinities are brought into contact with each other, which induce positive and negative charges in the surfaces of the contacted mats. The amount of charge transferred between the two materials is related to the area of the materials in contact and their differences in electron affinities [71]. The electrostatic induction takes places when the two materials with opposite and equivalent triboelectric charges are separated, which result in a dipolar moment and a strong potential difference.

Fig. 2.1 shows a schematic description of the mechanism of generation of electricity, which is commonly known as vertical contact separation mode. At the original state, there is not contact between the two triboelectric materials of the nanogenerator, which results in no potential difference between the two electrodes (Fig. 2.1 (a)). Under a pressing force, the two frictional materials are brought into contact which each other, which generate net negative charges on the surface of the electronegative mat and net positive charges on the surface of the electronegative positive mat (Fig. 2.1 (b)). This is attributed to a natural phenomenon entitled contact electrification in which a material becomes electrically charged after it gets into contact with a material with different polarity. Since the triboelectric charges are generated on the surface of the triboelectric materials, charges with opposite signs coincide at almost the same plane in the contact state, which results in no electric potential difference between the top and bottom plate of the triboelectric nanogenerator. Subsequently, upon releasing of the pressing force, the two frictional materials are separated, and the relative position of the positive and negative triboelectric charges will change in the TENG device, which will create a potential drop between the top and bottom plate of the triboelectric nanogenerator (Fig. 2.1 (c)). As a result, the free electrons in one electrode will be driven to flow to the other electrode through an external load with the aim to reach the electrostatic equilibrium in a process known as electrostatic induction. In this way, the mechanical energy

39

applied to the nanogenerator is converted into electricity by the conjunction of the physical processes of contact electrification and electrostatic induction.
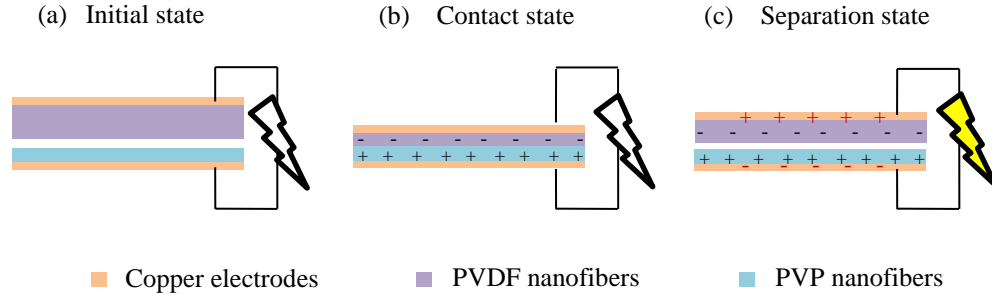
Fig. 2.1: Schematic diagram of the working mechanism of the nanogenerator: (a) Configuration of the nanogenerator in the original state. (b) Nanogenerator configuration during the pressure and (c) after the pressure.

2.2.2 Output performance enhancement of the nanogenerators

It is well known that there are numerous ways to increase the electric responses of a triboelectric nanogenerator. The aim of this paragraph is to present and discuss the different methods used to enhance the performance of TENGs. The voltage outputs of a triboelectric nanogenerator can be given by:

$$V = \frac{\sigma d}{\varepsilon_o} \qquad (1)$$

Where σ is the density of triboelectric charges, d is the distance between the frictional layers and ε_0 is an electric constant denominated vacuum permittivity. Therefore, the voltage output of a TENG can be increased due to the increment of two parameters: the density of triboelectric charges and the separation between the oppositely charged surfaces.

The first way to enhance the performance of the TENG is the selection of two triboelectric materials with strong tendency to lose and gain triboelectric charges during the frictional process. Table 2.6 represents the triboelectric series which is a general classification of the materials according to its ability to lose and gain

triboelectric charges. The materials at the top of the series show a strong tendency to gain electrons and become negative charged while the materials at the bottom easily lose electrons and become positively charged. As a result, the materials at the top of the list gain triboelectric charges, when they are in contact with materials from the bottom table. The further away the materials are from each other on the series, the more triboelectric charges are exchanged, which results in an increment of the triboelectric effect. Thus, the selection of the right triboelectric materials plays a critical role on the generation of triboelectric charges and electric responses of the nanogenerator. In general, the material choices for fabricating TENGs are huge as all materials present in our lives presents triboelectrification effect and can be candidates for fabricating a TENG.

The second approach to achieve high electric responses is through the modification of the surface morphology of the frictional material. The surface morphologies of the TENG can be modified by physical and chemical techniques which can be used to create nanofibers or surfaces with different topographies such as strips, cubes, and pyramids. The electric responses of the triboelectric nanogenerator are strongly affected by the contact surfaces between the frictional materials. Therefore, an increment of the contact area of the frictional materials is an effective way to increase the electric responses of the triboelectric nanogenerators.

The third way to improve the performance of a triboelectric nanogenerator is by optimizing the structural design of the nanogenerator. The periodic contacts and separations of the frictional materials from the triboelectric nanogenerator are of critical importance for enhancing the generation of electricity. To achieve this, TENGs with different structural designs as the spacer structure [72], arch-shaped structure [73] or spring-supported structure [74] have been developed with the aim to increase the contact and separations between the frictional materials and maximize the electric responses of the nanogenerators. Thus, it can be said that the structural design plays a very important role in the enhancement of the TENG output performance.

	Polytetrafluoroethylene
	Polytrifluorochlorethylene
	Polyvinylidene fluoride (PVDF)
	Polyvinyl chloride
	Polyimide
Negative ↑	Polypropylene
	Polyethylene
	Polystyrene
	Polyvinyl chloride
	Polychloroether
	Polyacrilonitrile
	Natural rubber
	Polychlorobutadiene
	Polyvinylbutiral
	Polyurethane
	Polyisobutylene
	Polyester
	Polyvinyl alcohol
	Polymethyl methacrylate
	Silver
	Copper
	Wood
Positive ↓	Steel
	Cotton
	Paper
	Aluminium
	Silk
	Wool
	Polyamide 66
	Polyamide 11
	Polyvinylpirrolidone (PVP)
	Polyformaldehide

Table 2.6 Triboelectric charges for some commonly triboelectric materials.

In general, it can be concluded that there are different approaches to improve the performance of the TENGs. In this regard, the ability of the materials to exchange triboelectric charges, the area of contact between the frictional materials and the structural design of the triboelectric nanogenerator are of critical importance to enhance the electric responses of the devices. These are the reasons why we used triboelectric materials which are on the far ends of the triboelectric series and have a large contact surface to fabricate the triboelectric nanogenerators.

2.2.3 Applications as self-powered active sensors

A triboelectric nanogenerator is a device that converts mechanical energy as produced by small scale physical action into electricity [75]. The amplitude and frequency of the output signal of the nanogenerator is dependent on the magnitude of the mechanical stimuli. As a result, the mechanical stimuli (e.g. pressure, vibration, impact, etc) could be measured by analysing the generated electric output signals. The focus of this review is to analyse the applications of triboelectric nanogenerators as self-powered active sensors for pressures [76-79], impacts [86-88] and velocities [96-98]. The main advantage of active sensors is that they do not need an external power source or battery to drive the device.

(i)   Self-powered pressure sensors

As stated above, the electric response of a TENG is strongly affected by the pressure of the mechanical stimuli. As a result, the first straightforward application for TENGs would be monitoring of external pressure applied on the TENG, which have many potential applications in thousands of everyday applications as touchscreens, medical devices, health monitoring, and so on.

In the last years, TENGs has been widely reported for their potential applications as self-powered pressure sensors. F.R. Fan et al. [76] was the first one to demonstrate the practical applications of triboelectric nanogenerators as high sensitivity self-powered pressure sensors. For the purpose, the authors measured the electric responses of a PDMS based triboelectric nanogenerator due to gentle pressures induced by a water droplet (3.6 Pa) and the falling of a piece of feather (0.4 Pa). The results proven that the nanogenerators were sensitive to the small pressures applied by the water droplet and the feather and showed electric responses of approximately 0.3 V. Furthermore, this paper also analysed the effect of the frictional materials contact area on the electric responses of the nanogenerator. For the purpose, the researchers fabricated four types of triboelectric nanogenerators with

different types of polymer micropatterned arrays: film, lines, cubes and pyramids. The results showed that the devices patterned with geometric features (lines, cubes and pyramids) showed from five to ten times larger electric responses than the film patterned nanogenerator, under the same mechanical pressure. This behaviour is attributed to the larger contact area of the devices with patterned geometric features, which improve the generation of triboelectric charges in the triboelectric nanogenerator.

K.Y. Lee et al. [77] developed a triboelectric nanogenerator which consists of a polymeric sheet of polytetrafluoroethylene (PTFE) and a metal film of copper patterned with hemispheres. In the design of the TENG, polytetrafluorethylene and copper were chosen as frictional materials to form the TENG due to their strong ability to gain and lose triboelectric charges, respectively. The hemispheres-array structure of the copper film was introduced in the nanogenerator with the aim to increase the area of contact between the frictional mats, which would help to increase the electric response of the TENG. Furthermore, the paper demonstrated the potential applications of the developed triboelectric nanogenerator as self-powered sensor. For the purpose, a commercial mechanical motor was used to apply controlled pressing forces to the nanogenerator. The results showed that the voltage outputs increase from 6 V to 25 V as the pressing forces increases between 1 N and 50 N. This behaviour can be explained by the increment of the contact area under stronger compressive forces, which increases the generation of triboelectric charges. In conclusion, the authors of [77] developed a self-powered pressure sensor using a triboelectric nanogenerator, which can measure a large range of pressing forces between 1 N and 50 N.

G. Zhu et al. [78] invented an ultrasensitive self-powered pressure sensor using a fluorinated ethylene propylene based triboelectric nanogenerator. The layer of fluorinated ethylene propylene (FEP) is chosen thanks to its high ability to gain triboelectric charges, which is caused by their large amount of fluorine on the material. From the results, it can be observed that the voltage output increases under stronger pressures and finally saturates at 50 V, when the contact pressure

approaches 10 kPa. Furthermore, the graph shows that the sensor is very sensitive to pressures in the low-pressure region (< 150 Pa). However, the sensitivity decreased significantly in the pressure region between 150 Pa and 10000 Pa. In the author's opinion, this is a very normal phenomenon for any pressure sensor as the linear relationship between the electric response and the pressing force can only hold within a certain range of pressing force. In summary, the paper successfully demonstrated that a FEP-based triboelectric nanogenerator can be used to measure pressures in a wide measurement range between 0 and 10 kPa.

B. Yu et al. [79] reported a new class of self-powered pressure sensor using a triboelectric nanogenerator made of nanofibers. Polyvinylidene fluoride (PVDF) and poly(3-hydroxybutyrate-co-3-hydro-xyvalerate) (PHBV) nanofibers were chosen as frictional materials to form the TENG because both materials are located at both ends of the triboelectric series. The polymer nanofibers are prepared by electrospinning because it is a simple and economic way to produce membranes with a dense population of triboelectric nanofibers [80]. Furthermore, the high contact surface of the nanostructured membranes will improve the generation of the triboelectric charges, which is beneficial to increase the electric responses of the nanogenerator. From the results, it can be observed that the voltage outputs of the triboelectric nanogenerator increased from 240 V to 550 V in the pressure range between 0 MPa and 25 MPa. A similar behaviour is observed for the current outputs of the nanogenerator which increased from 20 µA to 45 µA when the pressures are increased in the same pressure range. In conclusion, it can be said that the nanostructured triboelectric nanogenerator demonstrated an excellent performance to measure pressures in a wide measurement range between 0 and 25 MPa.

(ii)   Self-powered impact sensors

An impact sensor plays a critical role in vehicle safety, fast medical assistance of elderlies and structural health monitoring. For example, in the event of a car crash an impact sensor detect the collision to release an air-bag for the protection of the passengers. In the case of falls in the elderly, an impact sensor can be used to inform

about the accident and provide fast-medical assistance. Other practical examples could be detection of impacts in hail storms, where impacts are responsible for a considerable number of accidents in aircrafts, wind turbines and other civil infrastructures. Therefore, the detection of impacts is of vital importance as impacts can seriously affect the health and safety of humans.

In the last years, only a few works reported for the potential applications of triboelectric nanogenerators as self-powered impact sensors [86-88]. K. Dai et al. [93] developed a new class of PDMS-based triboelectric nanogenerator with the aim to test its application as self-powered acceleration sensor. Performance test on this high g acceleration sensor is carried out by the machete hammer test, which is the most widely used high acceleration test. The results from the experiment indicate that the voltage and the current outputs increase proportionally from 10 V (5 μA) to 100 V (17.5 μA) as the impact acceleration increases in the range between 2600 - 16000 g. Furthermore, the voltage and current outputs show a high sensitivity of 1.8 mV/g in a very large measurement range up to 16000 g. It is also important to mention that a clear linear relationship between the acceleration of the impacts and the electric outputs of the triboelectric nanogenerator is observed with a high Pearson coefficient of 0.999, which is beneficial for practical applications of the sensor. In summary, this paper introduces a new self-powered triboelectric sensor for strong impact detection which can be potentially used for detection and measurements of high acceleration impacts in military equipments and vehicle safety (e.g. car crash or detonation of missiles).

C. Xiang et al. [88] invented an original self-powered acceleration sensor for detection of impacts using a triboelectric nanogenerator. In the design of the TENG, a film of polydimethylsiloxane (PDMS) and polyethylene (PET) are chosen as negative and positive frictional triboelectric materials due to their distinct electronic affinities. Furthermore, the contact surface of PDMS film is increased by the incorporation of pyramids with the aim to increase the generation of triboelectric charges and electric responses of the nanogenerator. With the aim to the test the performance of the TENG as self-powered acceleration sensor, a shaker is used to

apply vibrations with different accelerations in the range from 1.44 m/s^2 to 5.69 m/s^2. The experimental results indicate that the voltage outputs are strongly influenced by the acceleration and a linear increase between 1.5 mV and 7.5 mV is observed as the acceleration of the impact raises from 1.44 m/s^2 to 5.69 m/s^2. Furthermore, the voltage output shows high reproducibility, linearity and sensitivity in the experimental measurement range between 1.44 m/s^2 to 5.69 m/s^2. In summary, it can be said that the developed triboelectric nanogenerator could be potentially used for a wide spectrum of applications as national defence, vehicle safety, military equipments and so on.

The author of this thesis [87] invented a novel nanostructured triboelectric generator composed of polyvinyl fluoride (PVDF) and polyvinyl pyrrolidone (PVP) nanofibers and suggested and evaluated its potential for application as impact sensor for the detection and quantification of small energy impacts. PVDF and PVP nanofibers are chosen to design the triboelectric nanogenerator because both materials are situated at both ends of the triboelectric series, which induces a strong polarity difference that enhances the generation of triboelectric charges. The experimental test used to evaluate the sensitivity of the triboelectric nanogenerator to impacts is carried out by a simple impact test, in which a free-falling ball is dropped on the nanogenerator at various energy impacts. The results show that increasing the energy of the impact from 0.02 to 0.2 J leads to increase of the voltage output of the triboelectric nanogenerator from 4 V to 24 V. Furthermore, the relation between the voltage output and the energy of the impact is approximately linear, which suggests the possible application of the developed TENG as an impact measurement sensor, as this simplifies the analysis of the sensor electric responses. This work demonstrates that a novel triboelectric nanogenerator based on electrospun nanofibers can be successfully used for the detection and quantification of small energy impacts in the energy range between 20 to 200 millijoules.

B. Zhang et al. [86] proposed a triboelectric nanogenerator based on the interaction between a mercury droplet and a membrane of polyvinyl fluoride nanofibers. The mercury droplet and the membranes of polyvinyl fluoride nanofibers

are purposely chosen because of their strong tendency to lose and gain triboelectric charges, respectively. More importantly, a membrane of polymeric nanofibers is utilized to enhance the effective contact area and improve the output performance of the TENG. To verify the effect of the impact height on the nanogenerator electric responses, a free-falling ball impact test is used to evaluate the sensitivity of the sensor to impacts at different heights in the range between 10 and 100 cm. The results show that the voltage outputs of the triboelectric nanogenerator increase from 1.8 V to 10 V as the impact height increases from 10 cm and 100 cm. Furthermore, a strong linear relationship between the height of the impacts and voltage outputs can be observed for the entire measurement range, which is positive for the practical applicability of the device. In summary, it can be said that the developed triboelectric nanogenerator showed an excellent performance to detect and evaluate the impacts applied by the free-falling ball.

(iii)   Self-powered velocity sensors

Velocity measurements are essential in many modern industrial applications in automation, transportation, robotics, etc. Recently, TENGs has been widely reported for their potential applications as self-powered velocity sensors. For example, Q. Jing et al. [94] proposed a self-powered velocity sensor based on a Kapton-based TENG which can detect various rotational velocities in the range 100-500 rpm. To fabricate the triboelectric nanogenerator, Kapton is used as electronegative material due to their high tendency to steal electrons and generating triboelectric charges during the frictional process. The experimental results reveal that the voltage outputs increase gradually from 10 V to 30 V as the rotational speeds raise from 100 rpm to 500 rpm. Moreover, the electric responses show an excellent reproducibility for repetitions of the same rotatory velocities, which is of critical importance for the practical applications of the sensor. The results of this work demonstrate the applications of triboelectric nanogenerators to develop velocity sensors for multiple industrial applications.

Other authors as Y. Xi et al. [95] developed a freestanding triboelectric nanogenerator which consist of a layer fluorinated ethylene propylene (FEP) and investigated its applications as self-powered wind sensor. To address this task, an industrial ventilator is used to apply wind on the triboelectric nanogenerator at six different speeds. The results show that the current output increase from 0.45 to 1.8 μA, when the wind speed is increased between 5 m s^{-1} and 13 m s^{-1}. Moreover, it can be observed that the output current signals were varied with the wind speeds almost linearly. This excellent linear relationship indicates that the triboelectric nanogenerator could be practically used for measuring the magnitude of wind speeds, which can have significant potential applications as self-powered wind-speed sensor.

Recently, several papers have investigated the applications of triboelectric sensors as self-powered active sensors for velocities [96-98]. However, there are no previous studies to report about the potential of triboelectric sensors for detection and measurement of impact velocities in composite structures.

2.2.4 Conclusions

In this section, the applications of triboelectric nanogenerators as self-powered active sensors are revised and discussed. As compared to traditional sensors, triboelectric nanogenerators do not require an external power supply or battery to sense the mechanical stimulus with the advantages of self-powered operation, environmentally friendly and maintenance-free. In this review, we introduce the working mechanism and basic principles of these devices. Furthermore, the scientific results reported of the field of triboelectric nanogenerators are presented, discussed and analysed with the aim to demonstrate the potential of triboelectric nanogenerators as self-powered sensors for pressures, impacts and velocities.

References

[1]   H. Saghafi, A. Zucchelli, R. Palazzetti, G. Minak, The effect of interleaved composite nanofibrous mats on delamination behaviour of polymeric composite materials, Compos Struct., 109 (2014) 41-47.

[2]   S. Heijden, L. Daelemans, B. Schoenmaker, I. Baere, H. Rahier, W. Paepegem, K. Clerck, Interminar toughening of resin transfer transfer moulded glass fibre epoxy laminates by polycaprolactone electrospun nanofibers, Compos Sci Technol., 104 (2014) 66-73.

[3]   L. Liu, Z. Huang, G. Xu, Y. Liang and G. Dong, Mode II interlaminar delamination of composite laminates incorporating with polymer ultrathin fibers, Polym Compos., 3 (2008) 285-92.

[4]   B. Beylergil, M. Tanoglu and E. Aktas, Enhancement of interlaminar fracture toughness of carbon fiber epoxy-composites using polyamide-6,6 electrospun nanofibers, J Appl Polym Sci, 134 (2017) 45244.

[5]   E. Ozden-Yenigun, K. Bilge, E. Sunbuloglu, E. Bozdag, M. Papila, High strain rate response of nanofiber interlayered structural composites, Compos Struct., 168 (2017) 47-55.

[6]   C. Garcia, J. Wilson, I. Trendafilova and L. Yang, Vibratory behaviour of glass reinforced polymer (GFRP) interleaved with nylon nanofibers, Compos Struct., 176 (2017) 923-923.

[7]   S.C. Her and C.Y. Lai, Dynamic behaviour of nanocomposites reinforced with multi-walled carbon nanotubes (MWCNTs), J Mater., 6 (2013) 2274-84.

[8]   G. Balaganesan and R. Velmurugan, Vibration and energy dissipation of nano composite laminates for below ballistic impact loading, Latin Am J Solids Struct., 12 (2015) 2259-80.

[9]   J. Gou, S. O'Braint, H. Gu and G. Song, Damping augmentation of nano composites using carbon nanofiber paper, J Nanomater., 2006 (2006) 32803.

[10] N. Kordani, A. Fereidoon and M. Ashoori, Damping augmentation of nano composites using carbon nanotube/epoxy, J Struct Dyn., 3 (2011) 1605-15.

[11] K.T.B. Padal, K. Ramji, V.V.S. Prased, Damping behaviour of Jute nano fibre reinforced composites, Int. J. Emerg. Technol. Adv. Eng., 4 (2014) 753-9.

[12] A. Fereidoon, R. Rafiee and R. Maleki Moghadam, Modal analysis of carbon nanotube reinforced polymer using multi-scale finite element method, J Mech Compos Mater., 49 (2013) 325-32.

[13] P. Ribeiro, O. Thomas, Nonlinear modes of vibration and internal resonances in nonlocal beams, J Comput Nonlinear Dyn., 12 (2017) 031017.

[14] R. Palazzetti, A. Zucchelli and I. Trendafilova, The self-reinforcing effect of Nylon 6,6 nano-fibres on CFRP laminates subjected to low velocity impact, J Compos Struct., 106 (2013) 661-72.

[15] ASTM D5528, Standard test method for mode I interlaminar fracture toughness of unidirectional fibre-reinforced polymer matrix composites, Annual Book of ASTM Standards (2014).

[16] G. Li, P. Li, C. Zhang, Y. Yu, H. Zhang, S. Zhang, X. Jia, X. Yang, Z. Xue, S. Ryu, Inhomogeneous toughening of carbon fiber/epoxy composite using electrospun polysulfone nanofibrous membranes by in situ phase separation. Compos Sci Technol., 68 (2008) 987-94.

[17] T. Brugo, G. Minak, A. Zucchelli, H. Saghafi, M. Fotouhi, An investigation on the fatigue based delamination of woven carbon-epoxy composite laminates reinforced with polyamide nanofibers, Proc Eng., 109 (2015) 65-72.

[18] K. Magniez, T. Chaffraix, B. Fox, Toughening of a carbon-fibre composite using electrospun poly(hydroxyether of bisphenol A) nanofibrous membranes through inverse phase separation and inter-domain etherification, Materials, 4 (2011) 1967-84.

[19]   S. Heijden, L. Daelemans, K. Bruycker, R. Simal, I. Baere, W. Paepegem, H. Rahier and K. Clerck, Novel composite materials with tunable delamination resistance using functionalizable electrospun SBS fibers, Compos Struct., 159 (2017) 12-20.

[20]   L. Daelemans, S. Heijden, I. Baere, H. Rahier, W. Paepegem and K. Clerck, Damage resistant composites using electrospun nanofibers: a multiscale analysis of the toughening, ACS Appl Mater Interfaces, 8 (2016) 11806-18.

[21]   H. Saghafi, S. Ghaffarian, T. Brugo, G. Minak, A. Zucchelli, H.A. Saghafi, The effect of nanofibrous membrane thickness on fracture behaviour of modified composite laminates – a numerical and experimental study, Compos Part B, 101 (2016) 116-23.

[22]   S. Alessi, M. Filippo, C. Dispenza, M. Focarete, C. Gualandi, R. Palazzetti, G. Pitarresi, and A. Zucchelli, Effect of nylon 6,6 nanofibrous mats on thermal properties and delamination behaviour of high performance CFRP laminates, Polym Compos, 36 (2015) 1303-13.

[23]   G. Beckermann and K. Pickering, Mode I and Mode II interlaminar fracture toughness of composite laminates interleaved with electrospun nanofiber veils, Compos Part A: Appl Sci Manuf., 72 (2015) 11-21.

[24]   A. Kelkar, R. Mohan, R. Bolick and S. Shendokar, Effect of nanoparticles and nanofibers on Mode I fracture toughness of fiber glass reinforced polymeric matrix composites, Mater Sci Eng B, 168 (2010) 85-9.

[25]   B. Beylergil, M. Tanoglu and E. Aktas, Modification of carbon fibre/epoxy composites by polyvinyl alcohol (PVA) based electrospun nanofibers, Adv Compos Lett., 25 (2016) 69-76.

[26]   G. Giuliese, R. Palazzetti, F. Moroni, A. Zucchelli, A. Pirondi, Cohesive zone modelling of delamination response of a composite laminate with interleaved nylon 6,6 nanofibres, Compos Part B, 78 (2015) 384-392.

[27]   ASTM D7905, Standard test method for determination of the mode II interlaminar fracture toughness of unidirectional fibre-reinforced polymer matrix composites, Annual Book of ASTM Standards (2014).

[28]   H. Saghafi, R. Palazzetti, A. Zucchelli, G. Minak, Influence of electrospun nanofibers on the interlaminar properties of unidirectional epoxy resin/glass fibre composite laminates, J Reinf Plast Compos, 34 (2015) 907-14.

[29]   K. Magniez, C. Lavigne, B.L. Fox, The effects of molecular weight and poly-morphism on the fracture and thermomechanical properties of a carbon-fibre composite modified by electrospun poly(vinylidene fluoride) membrane, Polymer, 51 (2010) 2585-96.

[30]   Y. Zhao, T. Xu, X. Ma, M. Xi, D. Salem and H. Fong, Hybrid multi-scale epoxy composites containing conventional glass microfibers and electrospun glass nanofibers with improved mechanical properties, J Appl Polym Sci., 132 (2015) 42731.

[31]   C.V. Manh, H.J. Choi, Enhancement of interlaminar fracture toughness of carbon fibre/epoxy composites using silk fibroin electrospun nanofibers, Polymer-Plastics Technol Eng., 55 (2016) 1048-1056.

[32]   F. Moroni, R. Palazzetti, A. Zucchelli, A. Pirondi, A numerical investigation on the interlaminar strength of nanomodified composite interfaces, Compos Part B, 55 (2013) 635-641.

[33]   ISO 1410, Fibre-reinforced plastic composites: Determination of apparent interlaminar shear strength by short-beam method, European Standard (1998).

[34]   ASTM D2344 2344M, Standard test method for short-beam strength of polymer matrix composite materials and their laminates, Annual Book of ASTM Standards (2018).

[35] C. Garcia, I. Trendafilova, A. Zucchelli, J. Contreras, The effect of nylon nanofibers on the dynamic behaviour and the delamination resistance of GFRP composites, Matec Web Conf., 148 (2018) 14001.

[36] L. Liu, Z. Huang, C. He, X. Han, Mechanical performance of laminated composites incorporated with nanofibrous membranes, Mater Sci Eng. A, 435-436 (2006) 309-17.

[37] K. Molnar, E. Kostakova, L. Meszaros, The effect of needleless electrospun nanofibrous interleaves on mechanical properties of carbon fabrics/epoxy laminates, Express Polym Lett., 8 (2014) 62-72.

[38] H. Saghafi, Mechanical behaviour of flat and curved laminates interleaved by electrospun nanofibers, PhD thesis, University of Bologne, Italy, 2013.

[39] P. Akangah, S. Lingaiah, K. Shivakumar, Effect of nylon 6,6 nano-fiber interleaving on impact damage resistance of epoxy/carbon fiber composite laminates, Compos Struct., 92 (2010) 1432-9.

[40] H. Saghafi, T. Brugo, G. Minak, A. Zucchelli, Improvement the impact damage resistance of composite materials by interleaving Polycaprolactone nanofibers, Eng Solid Mech., 3 (2015) 21-26.

[41] E. Kimbro, A.D. Kelkar, Development of energy absorbing laminated fiberglass composites using electrospun glass nanofibers. In Proceedings of the ASME International Mechanical Engineering Congress and Exposition, Denver, Colorado, USA, 8 (2011) 539-545.

[42] H. Saghafi, R. Palazzetti, A. Zucchelli and G. Minak, Impact response of glass/epoxy laminate interleaved with nanofibrous mats, Eng Solid Mech., 1 (2013) 85-90.

[43] H. Saghafi, R. Palazzetti, G. Minak, A. Zucchelli, Effect of PAN nanofiber interleaving on impact damage resistance of GFRP laminates. In Proceedings of the 6th International Conference on Nanomaterials: Research and Application, Brno, Czech Republic, 5–7 November 2014.

[44] R. Rafiee, R.M. Moghadam, Simulation of impact and post-impact behaviour of carbon nanotube reinforced polymer using multi-scale finite element modelling, J Comput Mater Sci., 63 (2012) 261-8.

[45] C. Garcia, I. Trendafilova and A. Zucchelli, The effect of polycaprolactone nanofibers on the dynamic and impact behaviour of glass fibre reinforced polymer composites, J Compos Sci., 2 (2018) 43.

[46] B. Schoenmaker, S. Heijden, I. Baere, W. Paepegem, K. Clerck, Effect of electrospun polyamide 6 nanofibres on the mechanical properties of a glass fibre/epoxy composite, Polym Testing, 32 (2013) 1495-501.

[47] N. Phong, M. Gabr, K. Okubo, B. Chuong and T. Fujii, Improvement in the mechanical performances of carbon fiber/epoxy composite with addition of nano-(Polyvinyl alcohol) fibers, Compos Struct., 99 (2013) 380-7.

[48] P. Akangah and K. Shivakumar, Impact damage resistance and tolerance of polymer nanofiber interleaved composite laminates. In Proceedings of the 53rd International Conference of Structures, Structural Dynamics and Materials Conference, Honolulu, Hawaii, USA, 23-26 April 2012.

[49] M.S. Salmanpour, Z.S. Khodaei, M.H. Ferri Aliabadi, Impact damage localisation with piezoelectric sensors under operation and environmental conditions, Sensors, 17 (2017) 1178.

[50] A. Dixit, S. Bhalla, Prognosis of fatigue and impact induced damage in concrete using embedded piezo-transducers, Sens. Actuator A-Phys., 274 (2018) 116-131.

[51] K. Xia, H. Zhang, Z. Zhu and Z. Xu, Folding triboelectric nanogenerator on paper based on conductive ink and teflon tape, Sens. Actuator A-Phys., 272 (2018) 28-32.

[52] S. Qi, H. Guo, J. Chen, J. Fu, C. Hu, M. Yu, Z.L. Wang, Magnetorheological elastomers enabled high-sensitive self-powered tribo-sensor for magnetic field detection, Nanoscale, 10 (2018) 4745-4752.

[53]   Y. Yang, W. Guo, K.C. Pradel, G. Zhu, Y. Zhou, Y. Zhang, Y. Hu, L. Lin, Z.L. Wang, Pyroelectric nanogenerators for harvesting thermoelectric energy, Nano Lett., 12 (2012) 2833-2838.

[54]   L. Pan, J. Wang, P. Wang, R. Gao, Y. Wang, X. Zhang, J. Zou, Z.L. Wang, Liquid-FEP-based U-tube triboelectric nanogenerator for harvesting water-wave energy, Nano Res., 11 (2018) 4062-4073.

[55]   T.X. Xiao, T. Jiang, J.X. Zhu, X. Liang, L. Xu, J.J. Shao, C.L. Zhang, J. Wang, Z.L. Wang, Silicone-based triboelectric nanogenerator for water wave energy harvesting, ACS Appl Mater Interfaces, 10 (2018) 3616-3623.

[56]   T. Jiang, L. Zhang, X. Chen, C.B. Han, W. Tang, C. Zhang, L. Xu, Z.L. Wang, Structural optimization of triboelectric nanogenerator for harvesting water wave energy, ACS Nano, 9 (2015) 12562-12572.

[57]   R. Zhang, J. Ortegren, M. Hummelgard, M. Olsen, H. Andersson, H. Olin, Harvesting triboelectricity from the human body using non-electrode triboelectric nanogenerators, Nano Energy, 45 (2018) 298-303.

[58]   S. Li, W. Peng, J. Wang, L. Lin, Y. Zi, G. Zhang, Z.L. Wang, All-elastomer-based triboelectric nanogenerator as a keyboard cover to harvest typing energy, ACS Nano, 10 (2016) 7973-7981.

[59]   C. Garcia, I. Trendafilova, R. Guzman de Villoria, J. Sanchez del Rio, Self-powered pressure sensor based on the triboelectric effect and its analysis using dynamic mechanical analysis, Nano Energy, 50 (2018) 401-409.

[60]   L. Dhakar, S. Gudla, X. Shan, Z. Wang, F.E.H. Tay, C.H. Heng, C. Lee, Large scale triboelectric nanogenerator and self-powered pressure sensor array using low cost roll-to-roll UV embossing, Sci. Rep., 6 (2016) 22253.

[61]   K. Parida, V. Bhavanasi, V. Kumar, R. Bendi and P.S. Lee, Self-powered pressure sensor for ultra-wide range pressure detection, Nano Res., 10 (2017) 3557-3570.

[62]   Q. Liang, Z. Zhanga, Xiaoqin Y., Y. Gu, Y. Zhao, G. Zhang, S. Lu, Q. Liao, Y. Zhang, Functional triboelectric generator as self-powered vibration sensor with contact mode and non-contact mode, Nano Energy, 14 (2015) 209-216.

[63]   S. Wang, S. Niu, J. Yang, L. Lin, Z.L. Wang, Quantitative measurements of vibration amplitude using a contact-mode freestanding triboelectric nanogenerator, ACS Nano, 8 (2014) 12004-12013.

[64]   W. Song, B. Gan, T. Jiang, Y. Zhang, A. Yu, H. Yuan, N. Chen, C. Sun, Z.L. Wang, Nanopillar arrayed triboelectric nanogenerator as a self-powered sensitive sensor for a sleep monitoring system, ACS Nano, 10 (2016) 8097-8103.

[65]   L. Jin, J. Tao, R. Bao, L. Sun, C. Pan, Self-powered real-time movement monitoring sensor using triboelectric nanogenerator technology, Sci Rep., 7 (2017) 10521.

[66]   Z.H. Lin, G. Zhu, Y.S. Zhou, Y. Yang, P. Bai, J. Chen, Z.L. Wang, A self-powered triboelectric nanosensor for mercury ion detection, Angew. Chem. Int. Ed., 52 (2013) 5065-5069.

[67]   Y. Su, G. Xie, S. Wang, H. Tai, Q. Zhang, H. Du, H. Zhang, X. Du, Y. Jiang, Novel high-performance self-powered humidity detection enabled by triboelectric effect, Sens. Actuator B-Chem., 251 (2017) 144-152.

[68]   S. Cui, Y. Zheng, T. Zhang, D. Wang, F. Zhou, W. Liu, Self-powered ammonia nanosensor based on the integration of the gas sensor and triboelectric nanogenerator, Nano Energy, 49 (2018) 31-39.

[69]   A. Yu, L. Chen, X. Chen, A. Zhang, F. Fan, Y. Zhan, Z.L. Wang, Triboelectric sensor as self-powered signal reader for scanning probe surface topography imaging, Nanotechnology, 26 (2015) 165501.

[70]   M.F. Lin, J. Xiong, J. Wang, K. Parida, P.S. Lee, Core-shell nanofiber mats for tactile pressure sensor and nanogenerator applications, Nano Energy, 44 (2018) 248-255.

[71] W. Li, J. Sun, M. Chen, Triboelectric nanogenerator using nano-Ag ink as electrode material, Nano Energy, 3 (2014) 95-101.

[72] G. Zhu, C.F. Pan, W.X. Guo, C.Y. Chen, Y.S. Zhou, R.M. Yu and Z.L. Wang, Triboelectric-generator-driven pulse electrodeposition for micropatterning, Nano Lett., 12 (2012) 4960-4965.

[73] S.H. Wang, L. Lin and Z.L. Wang, Nanoscale triboelectric-effect-enabled energy conversion for sustainably powering portable electronics, Nano Lett., 12 (2012) 6339-6346.

[74] G. Zhu, Z.H. Lin, Q.S. Jing, P. Bai, C.F. Pan, Y. Yang, Y.S. Zhou, Z.L. Wang, Toward large-scale energy harvesting by a nanoparticle-enhanced triboelectric nanogenerator, Nano Lett., 13 (2013) 847-853.

[75] Y. Yang, L. Lin, Y. Zhang, Q. Jing, T.C. Hou, Z.L. Wang, Self-powered magnetic sensor based on a triboelectric nanogenerator, ACS Nano, 6 (2012) 10378-10383.

[76] F.R. Fun, L. Lin, G. Zhu, W. Wu, R. Zhang, and Z.L. Wang, Transparent triboelectric nanogenerators and self-powered pressure sensors based on micropatterned plastic films, Nano Lett., 12 (2012) 3109-3114.

[77] K.Y. Lee, H.J. Yoon, T. Jiang, X. Wen, W. Seung, S.W. Kim, Z.L. Wang, Fully packaged self-powered triboelectric pressure sensor using hemispheres-array, Adv. Energy Mater., 6 (2016) 1502566.

[78] G. Zhu, W.Q. Yang, T. Zhang, Q. Jing, J. Chen, Y.S. Zhou, P. Bai, Z.L. Wang, Self-powered, ultrasensitive, flexible tactile sensors based on contact electrification, Nano Lett., 14 (2014) 3208-3213.

[79] B. Yu, H. Yu, H. Wang, Q. Zhang and M. Zhu, High-power triboelectric nanogenerator prepared from electrospun mats with spongy parenchyma-like structure, Nano Energy, 34 (2017) 69-75.

[80]   F. Zhang, B. Li, J. Zheng, C. Xu, Facile fabrication of micro-nano structured triboelectric nanogenerator with high electric output, Nanoscale Res. Lett., 10 (2015) 298.

[81]   F. Fan, Z.Q. Tian, Z.L. Wang, Flexible triboelectric generator!, Nano Energy, 1 (2012) 328-334.

[82]   X. Zhang, J. Brugger, B. Kim, A silk-fibroin-based transparent triboelectric generator suitable for autonomous sensor network, Nano Energy, 20 (2016) 37-47.

[83]   Y. Zheng, L. Zheng, M. Yuan, Z. Wang, L. Zhang, Y. Qin, T. Jing, An electrospun nanowire-based triboelectric nanogenerator and its application in a fully self-powered UV detector, Nanoscale, 6 (2014) 7842.

[84]   B.U. Ye, B. Kim, J. Ryu, J.Y. Lee, J.M. Baik, K. Hong, Electrospun ion gel nanofibers for flexible triboelectric nanogenerator: electrochemical effect on output power, Nanoscale, 7 (2015) 16189.

[85]   Y. Hao, Y. Bin, H. Tao, W. Cheng, W. Hongzhi, Z. Meifang, Preparation and optimization of polyvinylidene fluoride (PVDF) triboelectric nanogenerator via electrospinning, in Proceedings to the 15th International Conference on Nanotechnology, Rome, Italy, 27-30 July 2015, pp. 1485-1488.

[86]   B. Zhang, L. Zhang, W. Deng, L. Jin, F. Chun, H. Pan, B. Gu, H. Zhang, Z. Lv, W. Yang, Z.L. Wang, Self-powered acceleration sensor based on liquid metal triboelectric nanogenerator for vibration monitoring, ACS Nano, 11 (2017) 7440-7446.

[87]   C. Garcia, I. Trendafilova, R. Guzman de Villoria, J. Sanchez del Rio, Triboelectric nanogenerator as self-powered impact sensor, in Proceedings to the International Conference on Engineering Vibration, Sofia, Bulgaria, 4-7 September 2017; MATEC Web. Conf., 2018, 148, 14005.

[88] C. Xiang, C. Liu, C. Hao, Z. Wang, L. Che, X. Zhou, A self-powered acceleration sensor with flexible materials based on triboelectric effect, Nano Energy, 31 (2014) 469-477.

[89] J. Lin, B. Ding, J. Yu and Y. Hsieh, Direct fabrication of highly nanoporous polysterene fibers via electrospinning, ACS Appl Mater Interfaces, 2 (2010) 521-528.

[90] S. Piperno, L. Lozzi, R. Rastelli, M. Passacantado, S. Santucci, PMMA nanofibers production by electrospinning, Appl Surf Sci., 252 (2006) 5583-86.

[91] T. Huang, M. Lu, H. Yu, Q. Zhang, H. Wang, M. Zhu, Enhanced power output of a triboelectric nanogenerator composed of electrospun nanofiber mats doped with graphene oxide, Sci. Rep., 5 (2015) 13942.

[92] S. Cheon, H. Kang, H. Kim, Y. Son, J.Y. Lee, H. Shin, S. Kim and J.H. Cho, High-performance triboelectric nanogenerators based on electrospun polyvinylidene fluoride-silver nanowire composite nanofibers, Adv Funct Mater., 28 (2018) 1703778.

[93] K. Dai, X. Wang, F. Yi, C. Jiang, R. Li and Z. You, Triboelectric nanogenerators as self-powered acceleration under high-g impact, Nano Energy, 45 (2018) 84-93.

[94] Q. Jing, G. Zhu, W. Wu, P. Bai, Y. Xie, R. P.S. Han, Z.L. Wang, Self-powered triboelectric velocity sensor for dual-mode sensing of rectified linear and rotatory motions, Nano Energy, 10 (2014) 305-312.

[95] Y. Xi, H. Guo, Y. Zi, X. Li, J. Wang, J. Deng, S. Li, C. Hu, X. Cao, Z.L. Wang, Multifunctional TENG for blue energy scavenging and self-powered wind-speed sensor, Adv. Energy Mater., 7 (2017) 1602397.

[96] H. Yong, J. Chung, D. Choi, D. Jung, M. Cho, S. Lee, Highly reliable wind-rolling triboelectric nanogenerator operating in a wide wind speed range, Sci Rep., 6 (2016) 33977.

[97]   Y. Su, G. Zhu, W. Yang, J. Yang, J. Chen, Q. Jing, Z. Wu, Y. Jiang, Z.L. Wang, Triboelectric sensor for self-powered tracking of object motion inside tubing, ACS Nano, 8 (2014) 3843-3850.

[98]   Y.S. Zhou, G. Zhu, S. Niu, Y. Liu, P. Bai, Q. Jing, Z.L. Wang, Nanometer Resolution Self-Powered Static and Dynamic Motion Sensor Based on Micro-Grated Triboelectrification, Adv Mater., 26 (2014) 1719-1724.

[99]   P.K. Sarkar, S. Maji, G.S. Kumar, K.C. Sahoo, D. Mandal and S. Acharya, Triboelectric generator composed of bulk poly(vinylidene fluoride) and polyethylene polymers for mechanical energy conversion, RSC Adv., 2016, 6, 910-917.

[100]   C. Garcia, I. Trendafilova, A self-powered triboelectric velocity sensor for impact detection in composite structures, in Proceedings to the 14th International Conference on Vibration Engineering and Technology of Machinery, Lisbon, Portugal, 10-13 September 2017; MATEC Web. Conf., 2018, 211, 21004.

Chapter 3

The effect of Nylon nanofibers on the vibratory properties of Glass Fibre Composites

Vibrations affect the working condition and health of the composite structures used in aerospace, automotive and civil engineering. One of the methods to mitigate the vibrations is the incorporation of electrospun nanofibers in the interfaces of composite mats. Thus, it is important to study how nanofibers affect the vibration behaviour of the composite structures. In this chapter, we concentrate on the effect of nanofibers as these do not change the size and the weight of the structure, but on the other hand they do have an effect of the vibratory characteristics of the whole structure. Nylon nanofibers are particularly suitable to improve the properties of the laminates because of their excellent properties which include high heat resistance, good adhesion with epoxy resin and excellent mechanical characteristics. The aim of this chapter is to study the effect of nylon nanofibers on the vibratory behaviour of glass fibre reinforced polymer composites. For this purpose, the natural frequencies and damping ratio of composite beams with and without nylon nanofibers are determined by a free vibration test. The results show that the incorporation of nylon nanofibers increase the damping significantly, however it does not affect the natural frequencies. Therefore, this chapter demonstrates a new strategy to suppress vibrations in composite structures by the interleaving of nylon nanofibers. Furthermore, a three-dimensional finite element model is developed to analyse the vibratory behaviour of pristine and nanomodified composites. To address this study, the natural frequencies of composite beams with and without nylon nanofibers are simulated using modal and transient analysis in ANSYS Workbench. The natural frequencies extracted from the modal analysis do not agree with the frequencies measured experimentally. However, the natural

frequencies calculated using transient analysis show a very good agreement with the available experimental data. Thus, transient analysis is suggested to simulate the vibration behaviour of the pristine and nylon nanomodified composites. Eventually this chapter also proposes a simple finite element model based on transient analysis to simulate with high accuracy the vibratory behaviour of pristine and nanocomposites.

3.1 Introduction

Composite laminates reinforced with polymeric electrospun nanofibers are attracting increasing attention among the scientific community due to their superior material properties [1-5]. It is well known that the incorporation of electrospun nanofibers into the interfaces of composite laminates can drastically change/improve some material properties. For example, the inclusion of polycaprolactone nanofibers in the interfaces of composite laminates can be used to increase the mode I fracture toughness up to 50% [6]. The introduction of tetraethyl orthosilicate electrospun nanofibers in the epoxy resin of glass fiber composites was found to enhance the interlaminar shear strength up to 15% [7]. Core-shell polyamide nanofibers can be used to prepare flame-retardant polymer nanofibers [8], which can be potentially used to develop composite laminates with enhanced flame retardancy. Thus, electrospun nanofibers offer great potential to improve some structural properties of composite mats [9,10].

In the last years, the dynamic properties of composite laminates have been widely studied because of their applications in delamination detection [11] and structural health monitoring [12]. However, there is still very little research on the effect of nanofibers on the dynamic and vibratory properties of composites reinforced with electrospun nanofibers. For example, the authors of [13] investigated the effect of nylon nanofibers on the damping ratio of carbon fibre epoxy composites. The results showed that the addition of nylon nanofibers caused an

increment of 60% in the damping ratio. Similar results are reported on [14], where the damping of carbon fibre epoxy composites is strongly affected due to the incorporation of carbon nanotubes. To date, the vibratory behaviour of composite laminates reinforced with electrospun nanofibers has been poorly investigated. Therefore, there is an urgent need to explore the effect of electrospun nanofibers on the vibratory behaviour of composite laminates.

Vibrations are responsible for a considerable number of failures and accidents in aircrafts, bridges and other composite structures that fail because of large amplitude vibrations. For example, the propagation of the delamination and other cracks is faster in composite structures with large amplitude vibrations, which affects the integrity of aircrafts, wind turbines and other composite structures. Therefore, the control of the vibrations of the composite structures is the critical importance for the purposes of safety and structural maintenance. One of the methods of suppressing vibrations in composite laminates is to increase the damping, which can be achieved by the introduction of nanofibers in the ply interfaces of the laminates. This is of great interest for machines and structures in which vibrations are a source of problems. Therefore, it is the vital importance to investigate the effect of electrospun nanofibers on the damping of composite mats.

In this chapter, the influence of nylon nanofibers on the vibratory properties of glass fibre reinforced polymer composites is considered. For that purpose, composite beams without nanofibers (known as pristine) and with nylon nanofibers (known as nano) are subjected to free vibration tests. Subsequently, the vibration signals of the pristine and nano composites are acquired through a commercial accelerometer. The signals are further analysed to evaluate the natural frequencies and the damping ratio of the two types of specimens. The main goal is to assess the influence of nylon nanofibers on the natural frequencies and damping ratio of the glass fibre epoxy composite beams. To the best of our knowledge, this work is the first attempt to study the vibratory behaviour of glass fibre epoxy composites reinforced with nylon nanofibers.

Although some authors have studied the vibration behaviour of nanomodified composites mainly based on experimental method [15, 16], there are only a few attempts to model the vibratory behaviour of nanomodified composites using finite element analysis. Special attention deserves the works of Rafiee and Moghadam [17] which attempt to develop a multi-scale finite element method to simulate the vibration behaviour of polymers reinforced with and without carbon nanotubes. Their results show a considerable growth of the natural frequencies due to the addition of carbon nanotubes. Other authors as Ribeiro [18] suggested a finite element model (FEM) to simulate the first three vibration modes of carbon nanotubes. Therefore, there are only a couple studies that investigate numerically the effect of nanofibers on the vibration behaviour of composite laminates.

Historically, most structural vibration models are performed by modal analysis and they assume linearity of the structure and the material. Modal analysis can provide an acceptable approximation for most cases of homogeneous materials. However, composites and especially nanomodified ones are characterized by a well-expressed nonlinear behaviour due to their heterogeneous nature [19-21]. As a result, neglecting their inherent nonlinear behaviour can potentially lead to serious miscalculations in the modelling and the estimation of their properties. Thus, this study suggests a new finite element model based on transient analysis, which considers the complex nonlinear behaviour of the laminates.

In the second part of the chapter, a new finite element model based on transient analysis is suggested to simulate the vibrational behaviour of pristine and nanocomposites. For this aim, the natural frequencies and damping ratio of composite beams with and without nylon nanofibers are simulated using transient analysis. The results obtained from the numerical simulations show a good agreement with the experimental data available. Thus, transient analysis is recommended as a simulation tool to model the vibration properties of pristine and nanocomposites.

Furthermore, the thesis investigates numerically the influence of nylon nanofibers on the vibration behaviour of glass fibre epoxy composites. To address this, the natural frequencies and damping of composite beams without nanofibers and with nylon nanofibers are compared. The results are in good agreement with the experiments and reveal that the addition of nylon nanofibers in glass fibre epoxy composites do not affect the natural frequencies. However, a strong increase of the damping ratio can be clearly seen due to the incorporation of nylon nanofibers.

The main contributions of the chapter are threefold: Firstly, the chapter expands the knowledge about the influence of nylon nanofibers on the natural frequencies and damping of glass fibre epoxy composites. Secondly, the chapter demonstrates that the interleaving with nylon nanofibers increase the damping of the composite laminates. This can be beneficial for purposes of reducing the amplitude of the vibrations, which have important applications for composite structures in which vibrations are a source of problems. Lastly, the chapter demonstrates that a simple finite element model based on transient analysis can be used to simulate with high accuracy the vibratory behaviour of pristine and nanomodified composites.

The rest of the chapter is organised as follows: The second section is devoted to the fabrication of pristine and nylon nanomodified composites. The third section explains the free vibration test used to assess the natural frequencies and damping of the composite beams. The fourth section introduces the finite element model used to simulate the pristine and nylon nanocomposites. The fifth section presents, analyses and discusses the results obtained from the experimental and numerical tests. Eventually the paper ends with some conclusions about the finite element model and the vibratory properties of nanomodified of glass fibre epoxy composites.

3.2 Fabrication of glass fibre composites with and without nylon nanofibers

This section describes the fabrication of the glass fibre/epoxy composites reinforced with and without nylon nanofibers. Figure 3.1 (a) illustrates the composite lay-up of the pristine and nanomodified composites used in this study. Pristine composites (without nylon nanofibers) were manufactured by hand lay-up of ten layers of unidirectional glass fibre epoxy prepreg, as detailed in Figure 3.1 (a). The composite specimens are prepared with dimensions of 168 mm×32 mm×3 mm and stacking sequence $[0,90,0,90,0]_s$. After the lay-up, the composite beams are cured using a vacuum bag in an autoclave at 150° for about one hour, as indicated in the supplier's specifications. The heating rate employed in the curing was 2 °C/min and the pressure was 6.4 bars.
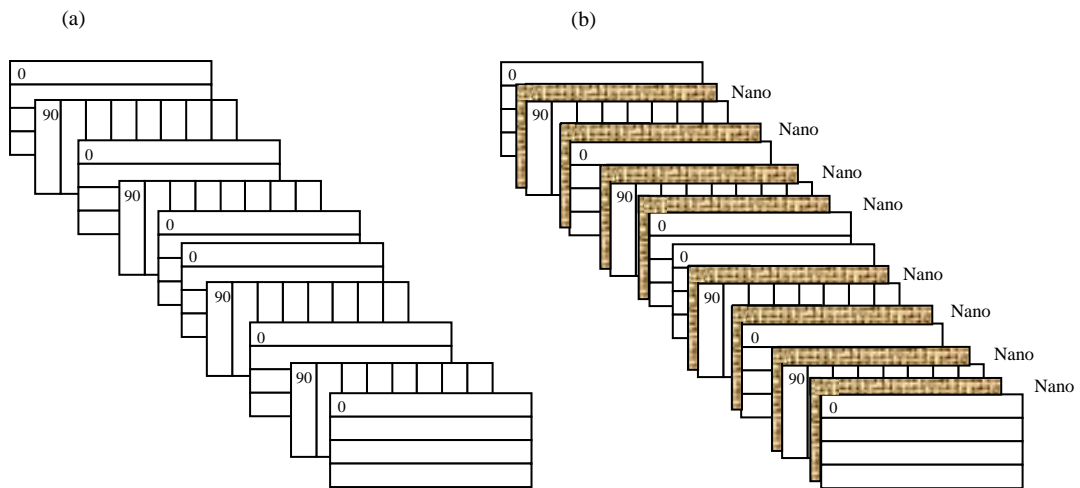
Figure 3.1 Composite lay-up of the (a) pristine and (b) nano modified composites.

The nano composites (with nylon nanofibers) are also manufactured by hand lay-up with identical composite prepregs, number of layers, dimensions, ply orientations, and curing process as the pristine composites. However, eight layers of nylon nanofibers are interleaved at each of the composite interfaces (excluding the central one), as shown in Figure 3.1 (b). The layers of nanofibers are located at each interface excluding the central one because the sample beams are tested in clamped-clamped configuration, and therefore the impact induces primarily flexural-type of loads, which induces bending stresses and strains that become negligible in the mid-composite interface. Consequently, it was considered unnecessary to interleave the

less-stressed middle composite interface. It is also important to mention that the weight fraction of nylon nanofibers in the nanomodified composites is very small (less than 1%). Therefore, the effect of the nanofibers on the thickness and weight of the composites laminates is negligible.

The layers of nylon nanofibers are prepared by the electrospinning technique [22]. This procedure was chosen because is an easy and low-cost technology to prepare nanofibers with a wide variety of morphologies [23]. For the preparation of the nylon nanofibers, nylon in the form of pellets and a solvent mixture of formic acid and Chloroform were used. The first step in the preparation of the nanofibers was to dissolve the polymer nylon in a solution of formic acid and chloroform (50:50 v/v) at a concentration of 14% w/v. Secondly, the polymer solution was transferred to an electrospinning apparatus for producing nanofibers. Finally, the electrospinning of nanofibers was carried out using the following conditions: applied voltage 23 kV, feed rate 0.3 mL/h per needle, needle-tip to collector distance 10 cm, room temperature, relative humidity of 40%. Finally, a very thin membrane of nylon nanofibers with a thickness of 25 µm is obtained.
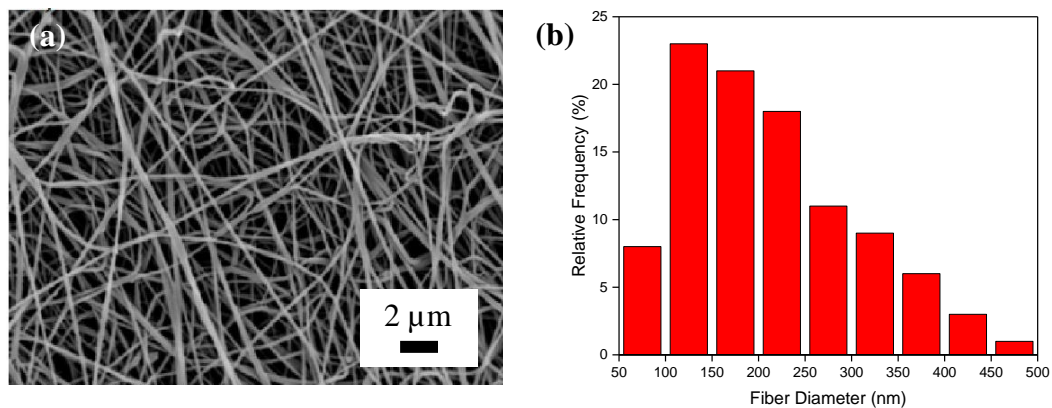
Figure 3.2 Scanning electron microscope (SEM) image of the nanostructured membranes of nylon (a) and fibre diameter distribution of nylon nanofibers (b).

The scanning electron microscope (SEM) image of the electrospun nanofibers [24] is given in figure 3.2 (a) and the fibre diameter distribution is presented in figure 3.2 (b). The SEM image shows a dense population of nylon nanofibers which are free of defects and shows random orientations. The diameter of the nanofibers was

measured on the basis of the SEM image using image-processing software Image J 1.45s. The fibre diameter distribution was determined by measuring the diameter of 100 fibres of the nanostructured membrane. The nanofibers mean diameter of nylon was measured to be ~200 nm. The diameter has a heavy tailed distribution which is skewed to the right thus indicating that the diameter is somewhere between 100 and 250 nm with a probability of about 65% (see figure 3.2 (b)).

The nanofibers are kept under vacuum over Diphosphorus pentoxide at room temperature overnight to remove residual solvents before being hand-interleaved into the laminate during the lay-up. The procedure to evacuate air from the nanofibrous material with the aim to enable a good resin infiltration into the nanofibrous material is the vacuum treatment. The vacuum treatment to evacuate air is carried out during the curing. It is also important to note that the content of nylon nanofibers in all the nanomodified composites is the same. This can be explained by the fact that the concentration of the chemical solutions and processing parameters used to prepare the membranes of interconnected nylon nanofibers is the same.

3.3 Vibration Testing

The aim of this section is to describe the vibration tests used to obtain the natural frequencies and the damping ratio of the pristine and nanomodified composites.

A free vibration test is used to obtain the vibration response of the pristine and nanomodified composites. A schematic description of the experimental procedure is given in Figure 3.3 and can be divided into three steps. First, composite beams of 168 mm long, 32 mm wide and 3 mm thick are fixed at both ends using a test rig. It should be noted that all the measurements were taken on the same test rig to ensure the same clamped-clamped boundary conditions for all the tests. Second, an external excitation (sharp impact) is applied to the middle of the composite beam using a modal hammer. Third, the vibration signals of the composite specimens are recorded for 0.5 s at a sampling rate of 5 kHz using a commercial accelerometer (RT-440

portable analyzer, SKF, Gotemburgo, Sweden). It is worthy to note that the accelerometer was strictly placed in the same position for all experiments (60 mm from the left support and mounted on the top surface of the composite beam as shown in Figure 3.3). Furthermore, the procedure was repeated ten times to obtain a multiple number of realizations for each specimen.
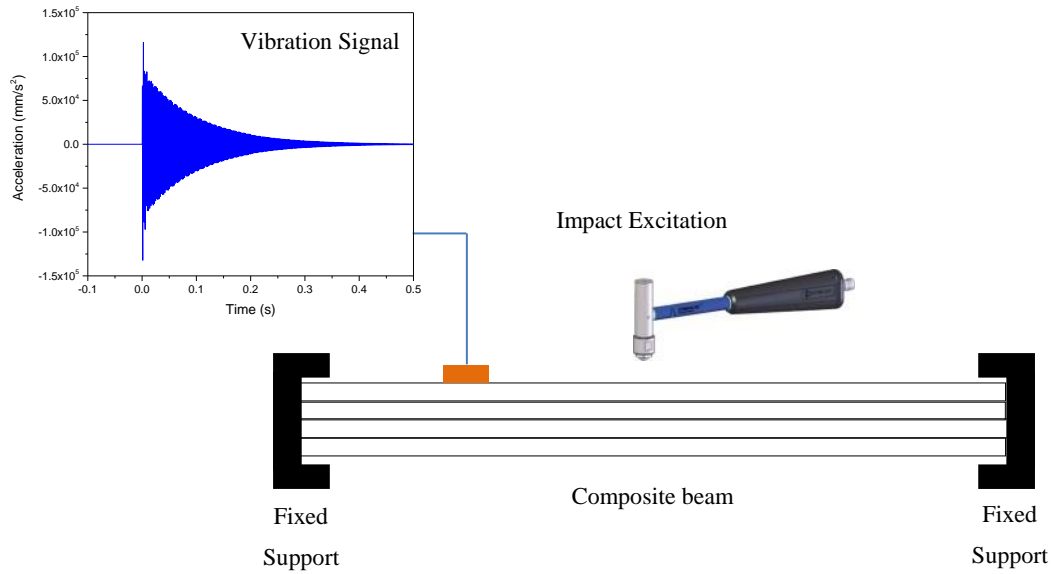
Figure 3.3 Schematic representation of the free vibration test used to obtain the vibration signals of the pristine and nanomodified composites.

The free vibration responses of the pristine and nanomodified composites are used to obtain the natural frequencies and the damping ratio. The first five natural frequencies of the composite beams were determined applying the Fast Fourier Transform [25, 26] on the recorded free vibration signals. The distinct peaks in the resulting spectrum are assumed to indicate the natural frequencies.

Additionally, the damping ratio of the composite specimens was also calculated using the time domain of the free decay acceleration signal by the Logarithm Decrement method [27, 28]. For the purpose, two peaks of the free decay acceleration signal are used to calculate the logarithmic decrement δ using equation (2).

$$\delta = \frac{1}{n} \ln\left(\frac{y_0}{y_n}\right) \qquad (2)$$

Where y_0 is the acceleration of the first peak and y_n was the acceleration of the second peak, taken n waves later. Subsequently, the damping ratio ζ was calculated from the logarithmic decrement using equation (3).

$$\zeta = \frac{1}{\sqrt{1 + \left(\frac{2\pi}{\delta}\right)^2}} \qquad (3)$$

The free vibration test was repeated ten times to obtain a multiple number of realizations for each specimen. The standard deviation for the natural frequencies from the ten measurements are practically zero, the values of the peaks did not change. Furthermore, ten specimens made of glass fibre epoxy composite identical in size, number of layers and stacking sequence are tested. Five of these are pristine (non-interleaved) and the other five are nylon modified. The standard deviation across the samples is a bit bigger but it is still less than 2%. So, the experimental results obtained in this experiment are rather stable and can be considered reliable/credible.

3.4 Finite Element Modelling

The finite element model used to simulate the geometry of the pristine and nanomodified composite laminates is developed using the software ANSYS Composite Prep-post. The layers of the composite laminates are modelled one by one including the ply thickness, stacking orientations, materials and other heterogeneous features for each of the layers. The vibration properties of the composites with and without nylon nanofibers are determined by modal and transient analysis in ANSYS Workbench. The free vibratory response was excited applying a short-time impulse force of ten Newtons for 0.1seconds.

The element type used in the finite element model is Shell 181. This is a four-noded element with six degrees of freedom at each node: translations in the x, y and z directions, and rotations about the x, y and z axes. This element was selected among a wide variety of elements due to its high accuracy and minimum computations time. Further information about the characteristics of the element Shell 181 can be found on the reference [29].

Abbreviation	Magnitude	Units
E_1	44	GPa
$E_2 = E_3$	11	GPa
$G_{12} = G_{13}$	4.5	GPa
G_{23}	0.5	GPa
υ_{23}	0.28	Dimensionless
$\upsilon_{13} = \upsilon_{12}$	0.1	Dimensionless
Φ	2000	Kg m^{-3}

Table 3.1 Material constants used to simulate the layers of the composite ply

The pristine composite beams are modelled using the same materials, dimensions, number of layers and ply orientations as those of the experimentally manufactured composite beams (see section 3.2). The material constants used to simulate the unidirectional layers of glass fibre and epoxy resin (known as composite ply) are given in Table 3.1, where E is the young modulus, G is the shear modulus, v is the poison's ratio and ρ is the density of the material [24].

Abbreviation	Magnitude	Units
$E_1 = E_2 = E_3$	3.6	GPa
$G_{12} = G_{13} = G_{23}$	1.6	GPa
$\upsilon_{12} = \upsilon_{13} = \upsilon_{23}$	0.35	Dimensionless
Φ	1160.0	Kg m^{-3}

Table 3.2 Material constants used to simulate the layers of the nano ply

The nanomodified composite beams are simulated using the same materials, dimensions, number of layers, and ply orientations as the pristine composite model however eight layers made of nylon nanofibers and epoxy resin are modelled into the

composite interfaces. These layers are allocated in all ply interfaces of the composite laminates excluding the middle interface. The material properties of uniform and continuous layers of nylon nanofibers and epoxy resin are calculated according to the rule of mixture as indicated in references [30-31]. Based on the estimations of [32, 33], it is assumed that the fractional volume of epoxy resin and nylon nanofibers in the interlaminar regions of the nanomodified composites is 80% and 20%, respectively. For the estimation of the properties, the properties of the interlaminar regions are calculated using the properties of nylon and epoxy resin, which are provided by the materials supplier. The interlaminar properties used to simulate the ply interfaces based on nylon nanofibers and epoxy resin (known as nano ply) are shown in the Table 3.2.

3.4.1 Model Refinement

The criteria employed to select the number of elements of the mesh is the convergence [34]. According to this criterion, the convergence is achieved, when the natural frequencies of the composite laminates do not change with the increase of the number of elements. Thus, it is considered that the number of the elements is appropriated when the values of the first five natural frequencies remain constants with the increase of the number of elements.

Figure 3.4 displays the first five natural frequencies as a function of the number of elements. A considerable change in the natural frequencies is observed when the number of elements increases from 88 to 936. On the other hand, the natural frequencies do not change when the number of elements varies between 936 and 1547. On the basis of these results, it can be said that the natural frequencies remain constants as the number of elements increases from 936 to 1547. Therefore, 936 elements are selected for all the numerical simulations with the aim to achieve high accuracy for minimum computations time.
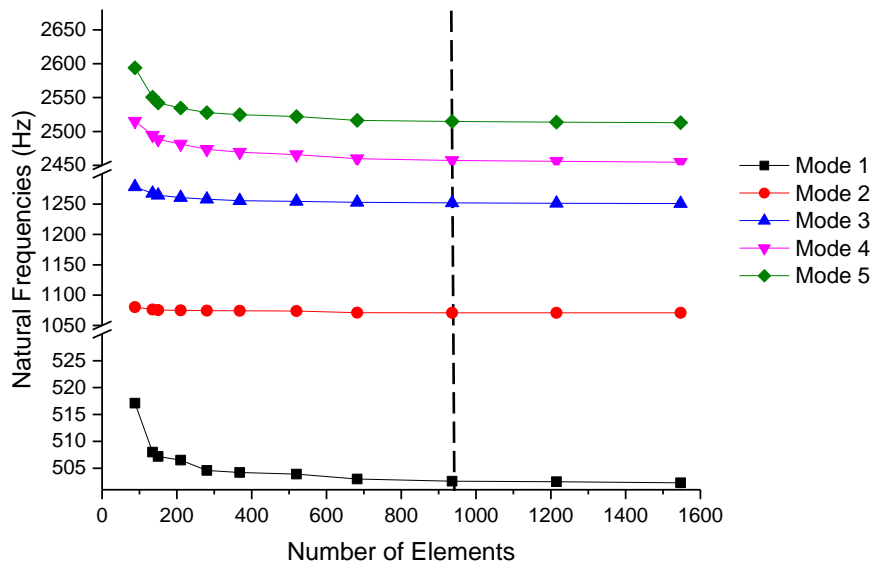
Figure 3.4 Natural frequencies as a function of the number of elements.

The results from the Figure 3.4 also show that the changes of the natural frequencies are not the same for the different modes. A considerable change in the natural frequencies is observed for the Modes 1, 4 and 5. Meanwhile, the changes of the natural frequencies for the Modes 2 and 3 are quite small. Therefore, it can be said that some modes are more sensitive to fluctuate with the variations of the element size. In general, it can be observed that the changes in all the natural frequencies are negligible after 936 elements. Thus, a mesh with 936 elements is used to simulate the vibratory behaviour of pristine and nanomodified composites as shown in Figure 3.5.
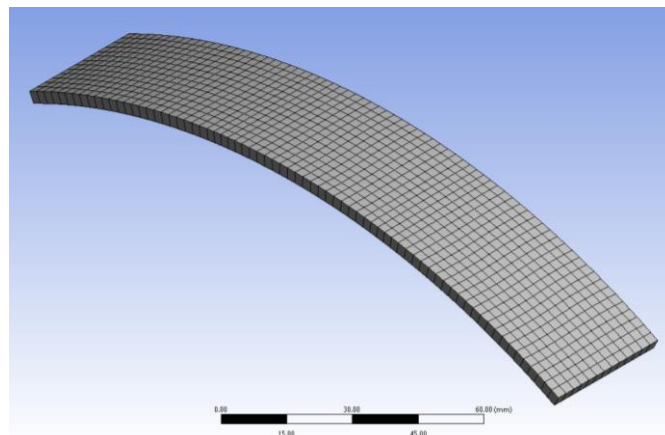
Figure 3.5 Image of the mesh with 936 elements used to simulate the composites.

74

3.4.2 Model Verification

To carry out this investigation, the natural frequencies of pristine and nanomodified composites are simulated numerically using a modal and transient analysis. In general, modal analysis based on the assumption that the behaviour of the composite specimens is linear, while transient analysis assumes that the behaviour of the composite beams is nonlinear.
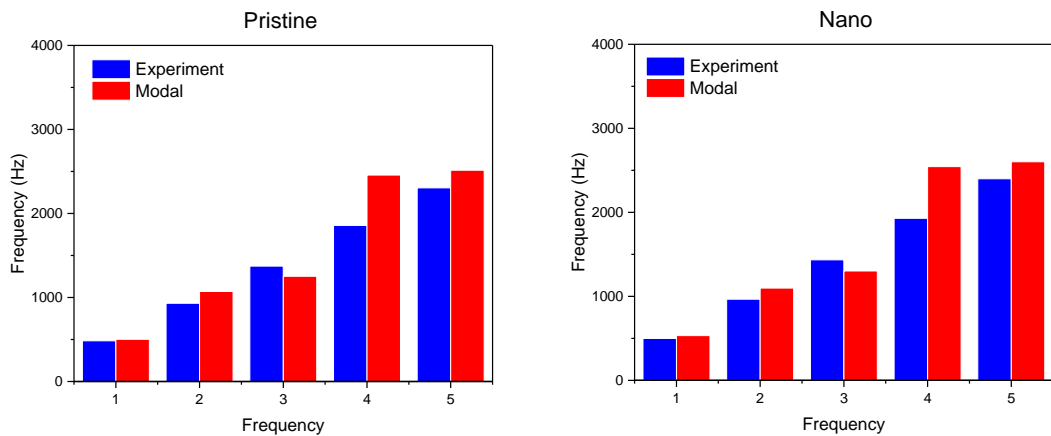
Figure 3.6 Comparison between the natural frequencies obtained experimentally and numerically using modal analysis.

To verify the results of the finite element model, the natural frequencies calculated using the numerical simulations are compared with the natural frequencies measured experimentally. The idea is to evaluate the differences between the simulated values and the experimental ones. Figure 3.6 displays the natural frequencies measured experimentally and numerically using modal analysis for the pristine and nanomodified composites. From the graph, it can be observed that some natural frequencies extracted from the modal numerical analysis are very different to the experimental results. These differences can be explained by the well-defined nonlinear behaviour of the composite beams, which is attributed to the multiple layers and anisotropic structure of the laminates. Therefore, modal analysis is not

suggested to simulate the vibratory properties of the pristine and nanomodified composites.

Tables 3.3 and 3.4 show the natural frequencies obtained experimentally and numerically using modal analysis and the corresponding percentage errors. The results given in the table show that the first natural frequency is the most precise one, while the average value of the percentage of error for the other frequencies are about 13 %. Therefore, it is concluded that the natural frequencies obtained numerically in the simulation do not have a good agreement with the experimental ones. Accordingly, modal analysis is not suggested as a simulation tool for the natural frequencies of the pristine and nanomodified composites. As stated above, modal analysis is not appropriate for these types of composites due to the material heterogeneous structure, which is attributed to their material discontinuous nature in terms of being made of multiple layers, nanostructured regions and anisotropic unidirectional layers of glass fibre/epoxy and nanofibers.

Frequencies	Experimental (Hz)	Modal (Hz)	Percentage Error (%)
f_1	484.5	502.6	3.6
f_2	930.9	1071.0	13.1
f_3	1373.8	1252.0	9.7
f_4	1857.5	2457.2	24.4
f_5	2303.8	2514.7	8.4

Table 3.3 Comparison between modal and experimental frequencies for pristine composite.

Frequencies	Experimental (Hz)	Modal (Hz)	Percentage Error (%)
f_1	498.8	533.3	6.5
f_2	965.9	1098.5	12.1
f_3	1434.8	1301.5	10.2
f_4	1929.0	2543.8	24.2
f_5	2399.3	2601.5	7.8

Table 3.4 Comparison between modal and experimental frequencies for nano composite.

In general, modal analysis provides an acceptable approximation to calculate the natural frequencies on most occasions however composite specimens are characterized by a well-defined non-linear behaviour and modal analysis is not suitable to analyse the dynamical behaviour of these composites.

Figure 3.7 also shows the first five natural frequencies obtained experimentally and numerically using transient analysis for the pristine and nanomodified composites. The natural frequencies calculated numerically by the transient analysis are in good agreement with the experimentally obtained ones. Therefore, it can be said that transient analysis gives a much better agreement with the experimentally measured natural frequencies as compared to the modal analysis. These differences are due to the nature of the analysis; modal analysis assumed a linear behaviour for the composite beams while transient analysis assumed a nonlinear behaviour. Accordingly, transient analysis is suggested to simulate the free vibratory behaviour of the pristine and nylon interleaved composites.
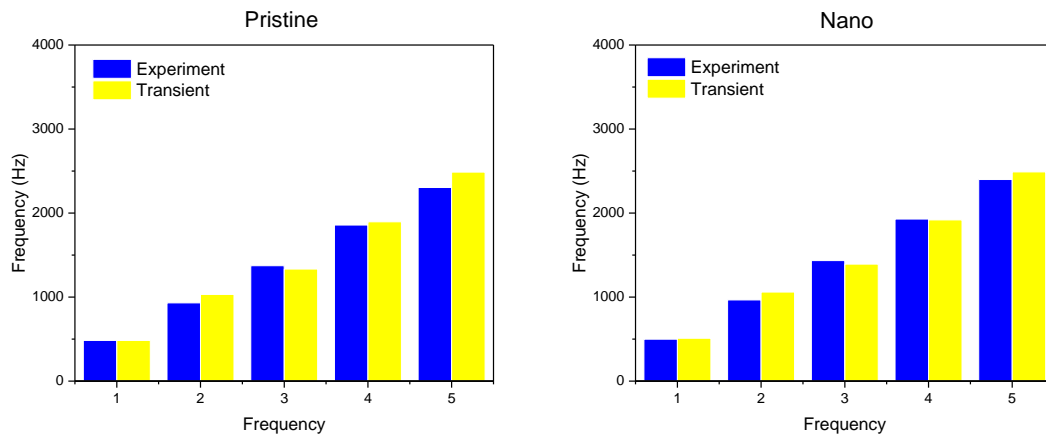
Figure 3.7 Comparison between the natural frequencies obtained experimentally and numerically using transient analysis.

In conclusion, this study proves that using transient vibration analysis rather than modal analysis results in more precise prediction of the vibratory behaviour of pristine and nanomodified composites. This can be attributed to the multiple layers and anisotropic structure of the composite specimens, which results in a well-defined

nonlinear behaviour. Thus, transient analysis is suggested to simulate the vibratory properties of glass fibre epoxy composites with and without nylon nanofibers.

3.5 Results and Discussion

This section analyses the effect of nylon nanofibers on the natural frequencies and damping of glass fibre epoxy composite laminates. The section is divided in two parts. The first part is devoted to the effect of nylon nanofibers on the natural frequencies, while the second part investigates the effect of the same nanofibers on the damping ratio.

3.5.1 Effect of nylon nanofibers on the natural frequencies

The effect of nylon nanofibers on the natural frequencies of the composite laminates is analysed experimentally in this section. To address this problem, the natural frequencies of the composite beams without nanofibers are compared to the natural frequencies of composite beams with nylon nanofibers.

Mode	Pristine (Hz)	Nylon (Hz)	Variation (%)
1	484.5	498.8	2.9
2	930.9	965.9	3.6
3	1373.8	1434.8	4.2
4	1857.5	1929.0	3.7
5	2303.8	2399.3	4.0

Table 3.5 Experimental variation of the natural frequencies due to nylon nanofibers

Table 3.5 presents the first five natural frequencies of the composite beams with and without nylon nanofibers. Moreover, the table also includes the variation of the natural frequencies caused by the incorporation of the nylon nanofibers. The change

of the natural frequencies is pretty small and within the range of the experimental and measurement error but since it is consistent one might assume that it is caused by the introduction of the nanofibers. Whether this is caused by the thickness change or the change of another property like e.g. the stiffness, it is not clear. It must be pointed out that the thickness change is miniscule in the nano range, so it is unlikely to cause frequency change, through the change of the mass or its distribution.

To evaluate the effect of nylon nanofibers on the natural frequencies of glass fibre epoxy composites, the natural frequencies of the composite beams without nanofibers (known as pristine) and with nanofibers (known as nano) are compared. The variation of the natural frequencies due to the incorporation of nylon nanofibers is calculated using the equation (4):

$$Variation \ (\%) = \left(\frac{f_{nano} - f_{pristine}}{f_{pristine}} \right) \times 100 \qquad (4)$$

Where f_{nano} are the natural frequencies associated to the nanomodified composites and f_{virgin} are the natural frequencies of the pristine beams. The natural frequencies of the composites interleaved with nylon nanofibers show a slight variation respect to the pristine specimens. Table 3.5 indicates that the presence of nylon nanofibers in the glass fiber composites varies the natural frequencies in the range between 2.9% and 4.0%. Thus, the variations in all the natural frequencies are rather small and inconclusive as these changes are lower than 5% (region of experimental measurement error).

These findings are in line with other results reported in the literature. For example, Shiuh-Chuan Her et al. [35] analysed the natural frequencies on composites reinforced with carbon nanotubes. This work reports up to 7% increase of the natural frequencies of epoxy composites due to the addition of carbon nanotubes. The same paper also indicates that the variation of natural frequencies depends on the content of carbon nanotubes. G. Balaganesan et al. [36] analysed the natural frequencies on pristine and clay nano-modified composites. The results reveal that natural frequencies of glass fibre composites can be increased up to 12% due to the addition of clay nanofibers. Other authors as [37] observed very small changes in the natural

frequencies due to the incorporation of carbon nanofibers in composites. In general, it can be said that the change of the natural frequencies depends on the content and type of nanofibers interleaved. In one of our research publications [38], we investigated the influence of polycaprolactone nanofibers on the natural frequencies of glass fibre epoxy composites. The results revealed that the first five natural frequencies of the glass fibre epoxy composites are barely affected by the interleaving of polycaprolactone nanofibers as the miniscule changes of the natural frequencies below 5% are in the range of the experimental and measurement error.

In this particular case, the changes on the natural frequencies as a result of the interleaving with nylon nanofibers are negligible (less than 5%). The very little changes in the frequencies can be by explained by the fact that the changes on the composite stiffness and mass due to the incorporation of nanofibers are very small. As shown in equation (5), the natural frequencies are directly proportional to the stiffness k and inversely proportional to the mass m.

$$f_n = \frac{1}{2\pi}\sqrt{\frac{k}{m}} \qquad (5)$$

The stiffness of nylon nanofibers is lower than the stiffness of glass fibres, thus it is expected that these nanofibers will not improve the overall composite stiffness. Furthermore, the interleaving with nylon nanofibers does not change the mass of the specimens. Therefore, it can be concluded that the natural frequencies of nanomodified composites will be very much the same as the natural frequencies of the pristine composites.

Mode	Pristine (Hz)	Nylon (Hz)	Variation (%)
1	484	510	5.0
2	1032	1060	2.6
3	1334	1392	4.2
4	1896	1918	1.1
5	2488	2490	0.1

Table 3.6 Numerical variation of the natural frequencies due to nylon nanofibers

Furthermore, the effect of nylon nanofibers on the natural frequencies of glass fibre epoxy composites is investigated numerically. For this aim, the numerical natural frequencies of glass fibre epoxy composites with and without nylon nanofibers are simulated using transient analysis.

The natural frequencies for the pristine and nanomodified composites are shown in Table 3.6. The results show that the natural frequencies of the pristine and nanomodified composites are almost the same. The small changes of the natural frequencies can be attributed to the small influence of nylon nanofibers in the global stiffness and mass of the composites. The stiffness of nylon nanofibers is much smaller than the stiffness of glass fibres, thus it is expected that these nanofibers will not improve the overall stiffness. Furthermore, the changes in mass due to the incorporation of nylon nanofibers are minuscule. Therefore, it can be concluded that the natural frequencies of the nanomodified composites are very much the same as the natural frequencies of the pristine composites.

The variations of the five natural frequencies due to the incorporation of nylon nanofibers are in the range from 0.1% to 5.0% (see table 3.6). Thus, the addition of nylon nanofibers in the glass fibre composites has a small impact on the natural frequencies. In general, the changes of the first five natural frequencies are rather small and inconclusive as these changes are within the region of the precision of the experiments. Thus, the numerical results show a negligible increase in all frequency modes due to the addition of nylon nanofibers.

In conclusion, it can be said that the changes of the natural frequencies depend on the properties of the nanofiber interleaved. For these practical cases, the effect of the nylon nanofibers on the natural frequencies is miniscule and inconclusive as these variations are in the region of experimental and measurement error.

3.5.2 Effect of nylon nanofibers on the damping ratio

The damping ratio is a measure of the amount of energy which a material can dissipate. Therefore, materials with a higher damping ratio are expected to dissipate more energy. This is beneficial as high damping materials can be used to reduce the vibration amplitudes in structures and alleviate the effect of resonances.

In this section, the effect of nylon nanofibers on the damping ratio of glass fibre composite laminates is analysed. To address this, the damping ratio of composite laminates with and without nylon nanofibers is compared. Table 3.7 compares the damping ratio of the pristine and nanomodified composites. Furthermore, the table also includes the variation of damping caused by the reinforcement with nylon nanofibers. The results show that the damping of the nanomodified modified composites is higher respect to the damping of the pristine panels. As a result, the interleaving with nylon nanofibers increase the damping ratio of the glass fibre epoxy composites in a 36 %.

	Pristine (dimensionless)	Nano (dimensionless)	Variation (%)
Nylon	0.0121	0.0165	36

Table 3.7 Effect of nylon and polycaprolactone nanofibers on the damping

Our results are in good agreement with other results published previously. For example, the authors of [13] found that the damping of carbon fibre composite panels reinforced with nylon nanofibers is about 60% higher than the damping of pristine panels. Other studies conducted by Jihua Gou et al. [37] and Naser Kordani et al. [14] reported a 200% and 108% increase of the damping ratio of composite laminates interleaved with carbon nanotubes with respect to the damping of pristine composites. The authors of [15] showed that the damping ratio of epoxy composites reinforced with jute nanofibers is a 70% higher as compared to the damping ratio of the virgin panels. In [38], we investigated the effect of polycaprolactone nanofibers on the damping ratio of glass fibre epoxy composites. The results show that the

damping ratio is increased a 6% due to the incorporation of polycaprolactone nanofibers on the interlaminar regions of the composites. In general, it can be said that the incorporation of nanofibers in composites increases the damping because the nanofibers are able to dissipate energy, giving the nano modified composite a higher damping ratio.

According to our results, the addition of nylon nanofibers in the interlaminar regions of glass fibre composites increases the damping ratio considerably. The increase of the damping can be explained by the fact that nanomodified composites have larger interface area as compared to the pristine composites. Therefore, the increase of the area of the interfaces is expected to increase the energy which is dissipated.

Furthermore, we investigate numerically the damping ratio of pristine composites (without nanofibers) and nanomodified composites (with nylon nanofibers). For the purpose, the damping of glass fibre epoxy composites with and without nylon nanofibers is simulated using transient analysis.

	Pristine (dimensionless)	Nano (dimensionless)	Variation (%)
Damping	0.0035	0.0046	31

Table 3.8 Effect of nylon nanofibers on the damping ratio

The damping ratio of the composite laminates with and without nylon nanofibers is shown in Table 3.8. The table shows that the damping of the pristine increase from 0.0035 to 0.0046 due to the incorporation of nylon nanofibers in the glass fibre epoxy composites. The increase of the damping ratio can be explained by the fact that the incorporation of nanofibers in the composite specimens increases the interface area between the epoxy resin and the fibres. Therefore, the nanomodified composites are able to dissipate more energy as compared to the pristine specimens.

To analyse the effect of nylon nanofibers on the damping of glass fibre epoxy composites, the damping ratio of the composite beams without nanofibers (known as pristine) and with nanofibers (known as nano) are compared. For this aim, the variations of damping caused by the addition of nylon nanofibers are studied through equation (6).

$$Variation\ (\%) = \left(\frac{\zeta_{nano} - \zeta_{pristine}}{\zeta_{pristine}}\right) \times 100 \qquad (6)$$

Where ζ_{nano} is the damping of the nanomodified composites and $\zeta_{pristine}$ is the damping of the pristine specimens. The increment of the damping ratio because of the incorporation of nylon nanofibers corresponds to a 31% (see table 6.3). Thus, the addition of nylon nanofibers in the glass fibre composites causes a strong increment on the damping ratio.

The results from the numerical simulations agree with the experimental observations in the sense that both results show a significant increase of 31% and 36% of the damping, respectively. Therefore, it can be concluded qualitatively that the incorporation of nylon nanofibers in the interfaces of glass fibre composites lead to a significant increase of the damping ratio. This is beneficial as high damping materials can be used to reduce the vibration amplitudes in structures and to alleviate the effect of resonances.

As a conclusion, it can be said that the interleaving with electrospun nanofibers causes a significant increase in the damping. The individual effect depends of course on the type of nanofiber used, but so far, most of studies report a significant increase in the damping as result of nanofibers. In this study, it is demonstrated that the reinforcement with nylon nanofibers increase the damping ratio of glass fibre composites in a 36 %. This can be potentially used to reduce the amplitude of the vibrations of composite structures such as aircrafts, wind turbines, or bridges, which is important to avoid the propagation of the cracks.

3.6 Conclusions

Vibrations are one of the most important motions as aircrafts, wind turbines, bridges and other composite structures vibrate while being in use. Thus, it is very important to analyse the influence of nylon nanofibers on the natural frequencies and damping of glass fibre epoxy composites, as these characteristics are rather important for the purposes of designing structures. In this chapter, we have investigated experimentally and numerically the vibration properties of composites reinforced with and without nylon nanofibers.

Based on the experimental and the numerical results, the following conclusions about the vibratory behaviour of pristine and nanomodified glass fibre epoxy composites can be drawn.

Nylon nanofibers did not affect the natural frequencies of the nylon nanomodified specimens. The frequencies underwent very small changes which can be considered within the range of the noise and the numerical errors. Thus, in terms of natural frequencies the vibratory behaviour of the nanomodified specimens is the same as the behaviour of the pristine ones. On the other hand, the natural frequencies of the nanomodified laminates are not supposed to change as the stiffness and mass of the composite specimens do not undergone significant changes due to the interleaving with nylon nanofibers.

The damping ratio considerably increased due to the incorporation of nylon nanofibers according to both the experiments and the numerical modelling. The experimental results showed an increment of 36% in the damping ratio of the nanomodified specimens while the numerical simulations reported a 31% increase. This can be explained by the larger interface area between the nanofibers and the epoxy matrix, which is expected to improve the dissipation of energy. From these results it is concluded that the nylon nanomodified composite materials dissipate much more energy than pristine ones. This can be potentially used for purposes of

reduction of the vibration amplitudes, which limit the propagation of cracks and other irreversible damages.

The small variations of the natural frequencies in the nanomodified composites combined with the damping increase can be used for designing structures from the nanomodified material which will retain the working frequency range of the original structure (made of the pristine composite) while increasing the damping. This can be beneficial for purposes of reducing the vibration amplitude and alleviating the effect of resonance.

In conclusion, this study contributes to and furthers the knowledge about the effect of nylon nanofibers on the global dynamic behaviour of glass fibre epoxy composites in two aspects. It suggests a simple finite element model to simulate the vibratory properties of pristine and nanomodified composites with a good accuracy. It also establishes some general trends in the dynamic behaviour of nylon modified composites as compared to the pristine composites. These can be potentially used to improve the dynamic/vibratory properties of aircrafts, wind turbines and other composite structures by the interleaving with nylon nanofibers.

References

[1]   A. Fereidoon, F. Memarian, Z. Ehsani, Effect of CNT on the delamination resistance of composites, J Fullerenes Nanotubes Carbon Nanostruct., 21 (2013) 712-724.

[2]   H. Saghafi, R. Palazzetti, A. Zucchelli, G. Minak, Influence of electrospun nanofibers on the interlaminar properties of unidirectional epoxy resin/glass fiber composite laminates, J Reinf Plast Compos., 34 (2015) 907-914.

[3]   K. Molnár, E. Koštáková, L. Mészáros, The effect of needleless electrospun nanofibrous interleaves on mechanical properties of carbon fabrics/epoxy laminates, J Express Polym Lett., 8 (2013) 62-72.

[4]   R. Palazzetti, Flexural behaviour of carbon and glass fiber composite laminates reinforced with Nylon 6,6 electrospun nanofibers, J Compos Mater., 49 (2014) 3407-3413.

[5]   B. Tyson, S. Asce, R. Al-Rub, Z. Grasley, Carbon nanotubes and carbon nanofibers for enhancing the mechanical properties of nanocomposite cementitious materials, J Mater Civ Eng., 23 (2015) 1028-1035.

[6]   L. Daelemans, S. Heijden, I. Baere, H. Rahier, W. Paepegem and K. Clerck, Damage resistant composites using electrospun nanofibers: a multiscale analysis of the toughening, ACS Appl Mater Interfaces, 8 (2016) 11806-18.

[7]   D.K. Shinde, A.D. Kelkar, Effect of TEOS electrospun nanofiber modified resin on interlaminar shear strength of glass fibre/epoxy composites, Int J Mater Metal Eng., 8 (2014) 54-59.

[8]   L. Xiao, L. Xu, Y. Yang, S. Zhang, Y. Huang, C.W. Bielawsky, J. Geng, Core-shell structured polyamide 66 nanofibers with enhanced flame retardancy, ACS Omega, 2 (2017) 2665-2671.

[9]   R. Palazzetti, A. Zucchelli, Electrospun nanofibers as reinforcement for composite laminates materials - A review, Compos Struct., 182 (2017) 711-27.

[10]   S. Jiang, Y. Chen, G. Duan, C. Mei, A. Greiner, S. Agarwal, Electrospun nanofiber reinforced composites: A review, Polym Chem., 9 (2018) 2685-720.

[11]   D. Garcia, R. Palazzetti, I. Trendafilova, C. Fiorini, A. Zucchelli, Vibration based delamination diagnosis and modelling for composite laminates plates, Compos Struct., 130 (2015) 155-162.

[12]   D. Garcia, D. Tcherniak, I. Trendafilova, Damage assessment for wind turbine blades based on a multivariate statistical approach, J Phys Conf Ser., 1 (2015) 628.

[13] R. Palazzetti, A. Zucchelli and I. Trendafilova, The self-reinforcing effect of Nylon 6,6 nano-fibres on CFRP laminates subjected to low velocity impact, J Compos Struct., 106 (2013) 661-72.

[14] N. Kordani, A. Fereidoon and M. Ashoori, Damping augmentation of nanocomposites using carbon nanotube/epoxy, J Struct Dynamics, 3 (2011) 1605-1615.

[15] K.T.B Padal, K. Ramji, VVS Prasad, Damping behaviour of jute nano fibre reinforced composites, Int J Emerg Techno Adv Eng., 4 (2014)753-759.

[16] D. Garcia, I. Trendafilova, Daniel J. Inman, A study on the vibration-based self-monitoring capabilities of nano-enriched composite laminated beams, Smart Mater Struct., 25 (2016) 045011.

[17] A. Fereidoon, R. Rafiee and R. Maleki Moghadam, Modal analysis of carbon nanotube reinforced   polymer using multi-scale finite element method, J Mech Compos Mater., 49 (2013) 325-332.

[18] P. Ribeiro, O. Thomas, Nonlinear modes of vibration and internal resonances in nonlocal beams, J Comput Nonlinear Dyn., 12 (2017) 031017.

[19] D. Garcia, R. Palazzetti, I. Trendafilova, C. Fiorioni, A. Zucchelli, Vibration-based delamination diagnosis and modelling for composite laminates plates, Compos Struct., 130 (2015) 155-162.

[20] D. Maio, A. Carri, F. Magi, I. Sever. Detection of nonlinear behaviour of composite components before and after endurance trials. Journal Nonlinear Dyn., 2 (2014) 83-95.

[21] M. Hammami, A. Mahi, C. Karra, M. Haddar, Nonlinear behaviour of glass fibre reinforced composites with delamination, J Compos., 92 (2016) 350-359.

[22]   L.V. Schueren, B. Schoenmaker, O.I. Kalaoglu, K. Clerck, An alternative solvent system for the steady state electrospinning of polycaprolactone, Eur Polym J., 47 (2011) 1256-1263.

[23]   B. Silva, J. Alberto, M. Greque, Production of polymeric nanofibers with different conditions of the electrospinning process, Materia, 22 (2017) 11847.

[24]   H. Saghafi, Mechanical behaviour of flat and curved laminates interleaved by electrospun nanofibers, PhD thesis, University of Bologne, Italy, 2013.

[25]   N. Rahman, An efficient method for frequency calculation of an audio signal, Presidency, 2 (2013) 41-45.

[26]   M.J. Casiano, Extracting damping ratio from dynamic data and numerical simulations. In proceedings of the Marshal Space Flight Center, Huntsville, Alabama, USA (2016) 2.

[27]   L.B. Magalas and T. Malinowski, Measurement Techniques of the Logarithmic Decrement, J Solid State Phenom., 89 (2013) 247-260.

[28]   H. Mevada and Dipal Patel, Experimental determination of structural damping of different materials. In proceedings of the 12th International Conference on Vibration Problems (ICOVP), 144 (2016) 110-115.

[29]   M. Kathryn, J.M. Thompson, ANSYS Mechanical APDL for finite element analysis, Butterworth-Heinemann, (2017) 107-122.

[30]   P. Zhu, Z.X. Lei, K.M. Liew, Static and free vibration analyses of carbon nanotube-reinforced composite plates using finite element method with first order shear deformation plate theory, Compos Struct., 94 (2012) 1450-1460.

[31]   M.H. Yas, N. Samadi, Free vibrations and buckling analysis of carbon nanotube-reinforced composite Timoshenko beams on elastic foundation, Int J Press Vessels Pip., 98 (2012) 119-128.

[32] F. Moroni, R. Palazzetti, A. Zucchelli, A. Pirondi, A numerical investigation on the interlaminar strength of nanomodified composite interfaces, Compos Part B, 55 (2013) 635-641.

[33] R. Palazzetti, A. Zucchelli, C. Gualandi, M.L. Focarete, L. Donati, G. Minak, and S. Ramakrishna, Influence of electrospun nylon 6,6 nanofibrous mats on the interlaminar properties of Gr-epoxy composite laminates, Compos Struct., 94 (2012) 571-579.

[34] K. Alnefaie, Finite element modelling of composite plates with internal delamination, Compos Struct., 90 (2009) 21-27.

[35] S. Her, C. Lai, Dynamic behaviour of nanocomposites reinforced with multi-walled carbon nanotubes (MWCNTs), J Mater., 6 (2013) 2274-2284.

[36] G. Balaganesan and R. Velmurugan, Vibration and energy dissipation of nanocomposite laminates for below ballistic impact loading, Latin Am J Solids Struct., 12 (2015) 2259-2280.

[37] J. Gou, S. O'Braint, H. Gu and G. Song, Damping augmentation of nanocomposites using carbon nanofiber paper, J Nanomater., 2006 (2006) 32803.

[38] C. Garcia, I. Trendafilova and A. Zucchelli, The effect of polycaprolactone nanofibers on the dynamic and impact behaviour of glass fibre reinforced polymer composites, J Compos Sci., 2 (2018) 43.

Chapter 4

The effect of Nylon nanofibers on the delamination behaviour of Glass Fibre Composites

The main weak point of the composite laminates is their poor interlaminar strength, which can result in delamination. One of the techniques to prevent the delamination is the incorporation of electrospun nanofibers in the interlaminar regions of the composite laminates. The aim of the present chapter is to investigate experimentally and numerically how nylon nanofibers can be used to prevent the delamination failures of glass fibre epoxy composites. To address this study, the interlaminar shear strength of composite beams with and without nylon nanofibers is determined experimentally by the short beam method [14]. The results show that the interlaminar strength of the glass fibre epoxy composites increases quite substantially from 50.2 MPa to 63.81 MPa due to the incorporation of nylon nanofibers. Therefore, nylon modified glass fibre epoxy composites are less susceptible to delamination than pristine specimens. Furthermore, the chapter proposes a three-dimensional finite element model to simulate the delamination behaviour of pristine and nanomodified composites. For the purpose, the interlaminar shear strength of composite beams with and without nylon nanofibers is simulated using cohesive zone modelling in Ansys Workbench. The numerical results are in good agreement with the experimental ones and confirm that the interlaminar shear strength of pristine and nanomodified composites increases quite notably from 51.5 MPa to 63.1 MPa. The findings of this chapter are of great interest for the industry as composite laminates reinforced with nylon nanofibers could be potentially used to prevent the delamination failures in aircrafts, wind turbines and other civil structures.

4.1 Introduction

Structures made of composite laminates are extensively used in aircrafts, wind turbines and other industrial applications due to their high strength-to-weight ratio and stiffness. On the other hand, the laminates used are susceptible to delamination failures, which are barely visible from the outside and may seriously affect to the performance of the structures. As consequence of the delamination, the composite structures used in aircrafts, wind turbines and other civil structures can lose up to 60% of their strength and stiffness and still remains visible unchanged [1]. Thus, it is of critical importance to prevent the delamination in composite laminates.

Recently, researchers have suggested an important number of methods to prevent the delamination as matrix-toughening [2, 3], optimum stacking sequence [4], reinforcement with nanofibers [5, 6] and stitching with polymeric filaments [7]. Among these techniques, the incorporation of electrospun nanofibers in the interlaminar regions of composite laminates is attracting a wide interest from the research community. The main advantage of the interleaving with electrospun nanofibers is that the strong bonding between the nanofibers and the composite laminas, makes a significant improvement of the mechanical properties of the composites.

Nylon nanofibers prepared by electrospinning are particularly suitable to improve the interlaminar properties of the laminates due to their excellent mechanical properties as compared to other electrospun polymers nanofibers and good adhesion with epoxy resin. Moreover, the high melting temperature of nylon allows the nanofibers to maintain their morphology during the curing process of the laminate, which is necessary for the bridging reinforcing mechanism. However, these enhancements which nylon nanofibers are expected to bring in composite laminates still have to be tested and proven.

In the last ten years, many authors have investigated experimentally how the incorporation of electrospun nanofibers into the ply interfaces of composite laminates can be used to mitigate the delamination. For example, the paper published by [8] demonstrated that the addition of phenoxy nanofibers in carbon fibre laminates increase the mode I energy release rate by a 325%. Similar results are reported by [9], indicating that mode II energy release rate of composite interleaved with nylon nanofibers is a 400% higher as compared to the pristine ones. Up to now, most of the publications have investigated about the influence of electrospun nanofibers on the mode I and II energy release rates [10-13]. However, only a few studies focused on the influence of electrospun nanofibers on the interlaminar shear strength of glass fibre epoxy composites.

Additionally, other authors have studied the delamination behaviour of pristine and nanomodified composites using finite element analysis. For example, H. Saghafi et al. [15] developed a cohesive zone model (CZM) to simulate numerically the fracture behaviour of composites reinforced with thin and thick membranes of polyvinyl fluoride nanofibers. The results of this work suggested that the interleaving with thin and thick membranes of nanofibers leads to 42% and 98% enhancement of the mode I energy release rate, respectively. G. Giuliese et al. [16] proposed a cohesive zone model to model the fracture response of composites reinforced with different configurations of nylon nanofibers. The results demonstrated that the opening mode energy release rates are strongly affected by the morphology of the nanofibers. F. Moroni et al. [17] suggested a cohesive zone model to simulate the fracture behaviour of composites modified with nylon nanofibers. The results show that the addition of nylon nanofibers in the interlaminar regions of carbon composite laminates increased an 11% the energy release rate in sliding mode.

The delamination failures of composite laminates are commonly simulated with a cohesive zone model. The simulation introduces the fracture by adopting softening relationships between the traction and separations of the cohesive elements and a critical fracture energy that is required to break apart the interface surfaces [18]. Different cohesive laws are defined in the literature for a better representation

of the fracture phenomena. The bilinear traction separation laws are normally used to simulate a brittle fracture, while the exponential cohesive laws are typically used to model a ductile fracture. In our simulations, the bi-linear traction separation law is used to simulate the delamination behaviour of the pristine and nanomodified composites because the experimental force/displacement curves present a predominantly brittle fracture.

In this chapter, the effect of nylon nanofibers on the delamination behaviour of glass fibre epoxy composites is considered. To address this study, fracture load and interlaminar shear strength of composite laminates with and without nylon nanofibers are determined using the international standard ASTM D2344 [14]. The experimental results indicate that the fracture load for the pristine and nanomodified composites is 1301.6 N and 1862.5 N, respectively. Therefore, the interlaminar shear strength is increased from 50.2 MPa to 63.8 MPa due to the incorporation of nylon nanofibers. As a result, it can be concluded that nylon nanomodified glass fibre epoxy composites are less susceptible to delamination failures as compared to the pristine panels.

Furthermore, the chapter introduces a finite element model to simulate the delamination behaviour of pristine and nylon nanomodified composites. For the purpose, the interlaminar shear strength of the composite beams with and without nylon nanofibers are simulated using cohesive zone modelling in Ansys Workbench. The numerical results are in good agreement with experimental results and indicate that the interlaminar shear strength of the pristine and nanomodified composites is 51.5 MPa and 63.1 MPa, respectively. Thus, the developed cohesive zone model is recommended as a simulation tool to model the delamination behaviour of pristine and nanomodified composites.

The most important finding of this chapter is to demonstrate experimentally and numerically that the interleaving with nylon nanofibers could be used to bring down the susceptibility of delamination in composite structures. This is of utmost importance for the aeronautic industry as composite structures with high interlaminar

strength are desired to avoid the delamination failures of the composite structures. Additionally, the chapter demonstrates that a cohesive element model can be used successfully to simulate with high accuracy the delamination behaviour of pristine and nylon nanomodified composites.

The rest of the chapter is organized as follows: Section 2 gives a brief overview of the fabrication of the composite beams with and without nylon nanofibers. The short beam method utilized to determine experimentally the interlaminar shear strength of the composite specimens is introduced in Section 3. The cohesive zone model used to simulate the pristine and nylon nanomodified composites is presented in Section 4. The fifth section presents, discusses and analyses the results obtained from the experimental and numerical testing. In the last section, some conclusions are offered.

4.2 Preparation of the composite beams

The aim of this section is to explain the preparation of the composite beams used to determinate the apparent interlaminar shear strength of the glass fibre/epoxy composites interleaved with and without nylon nanofibers. The composite specimens made of pristine and nylon nanomodified composites are prepared in accordance with the ASTM D2344 standard. As suggested by the standard guidelines, the dimensions of the pristine and nanomodified composite beams are 18 mm long, 6 mm wide and 3.2 mm thick.

Composites without nylon nanofibers (known as pristine) consist of ten layers of unidirectional glass fibre/epoxy prepreg. The staking sequence of the laminates is $[0,90,0,90,0]_s$ for a total of ten layers. After the pile up, the panels are cured in autoclave using the following curing conditions: a high temperature of 150 °C for one hour, a heating rate of 2 °C/min and a pressure of 6.4 bars. Eventually, seven specimens of composite beams with the following dimensions (18 mm long, 6 mm

wide and 3.2 mm thick) are cut from a large composite lamina by using a wire cutting saw.

Composites with nylon nanofibers (in this chapter referred to as nano) are also manufactured with the same mats, number of composite layers, dimensions, ply orientations and curing process as the pristine composites. However, eight layers of nylon nanofibers are located at each of the composite interfaces (excluding the central one). The dimensions of the seven nanomodified composite beams are the same ones as the pristine beams. The layers of interconnected nylon nanofibers are prepared using the technique of electrospinning. This procedure is selected because it is a simple and economic approach to prepare a wide variety of polymer nanofibers. Further information about the preparation of nylon nanofibers via electrospinning can be found on [19].

4.3 Experimental study

Due to the poor interlaminar properties of the composite laminates, delamination is the most frequent and dangerous failure mode of the composite structures [20]. The presence of delamination may arise during the manufacturing process (e.g. by insufficient wet of the fibres) or during the service (e.g. bird strikes or impacts with hailstorms). An important material property used to assess the susceptibility to delamination of composite laminates is the interlaminar shear strength.

The analysis of the interlaminar shear strength for the pristine and nylon nanomodified composites is performed in accordance with the international standard ASTM D2344 [14]. Figure 4.1 shows a schematic description of the three-point bending test used to measure the interlaminar shear strength of the composite specimens. Initially, the composite beams are aligned equidistant to the two side supports of the bending machine (Instron 5966) as indicated by the standard. The two side supports are free to rotate, allowing free lateral motion of the specimen. Subsequently, the composite beams are loaded in the centre of the beam by the

loading nose of the testing machine at a constant crosshead rate of 1.0 mm/min. The load is increased until the composite specimen breaks with the aim to obtain the force-displacement curves of the composite specimens.
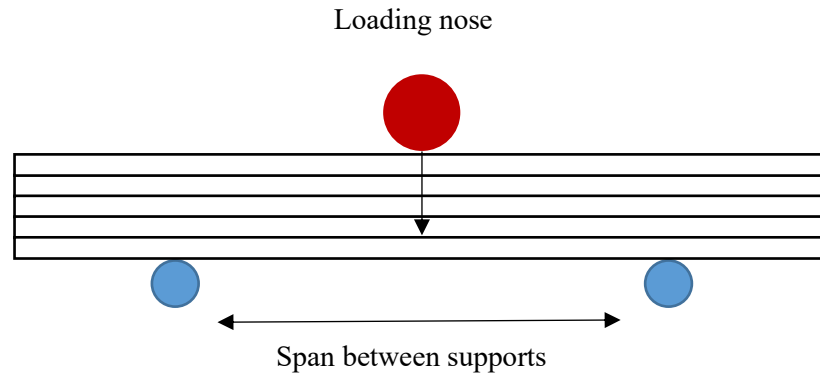

Figure 4.1 Schematic description of the three-point bending test used to measure the interlaminar shear strength

A force-displacement curve is obtained for each composite specimen. As the flexure load increases, the deflection of the composite specimen is increased linearly until a maximum load is achieved. At this point, the applied force drops dramatically which indicates that the composite specimens have failed. The apparent interlaminar shear strength of the composite beams is calculated for each specimen based on the equation 7, where F is the fracture load, b is the composite width and h is the composite thickness.

$$\tau = \frac{3}{4} \times \frac{F}{bh} \qquad (7)$$

During the experiment, seven composite specimens of each configuration (pristine and nano) are tested with the aim to verify the reproducibility of the results.

4.4 Numerical study

In this section, the cohesive zone model (CZM) used to simulate the delamination behaviour of the composite beams with and without nylon nanofibers is introduced. The simulations are performed using cohesive zone modelling in the commercial software Ansys Workbench. The pristine and the nanomodified composite beams are modelled with the same dimensions, number of layers and ply orientations as the experimentally manufactured composite beams.

The composite laminas of unidirectional glass fibre/epoxy layers are simulated using the element type Solid 185 and the material properties are given in table 3.1, where E is the young modulus, G is the shear modulus, v is the poison's ratio and ρ is the density of the material [21]. The composite interfaces of the pristine and the nylon nanomodified composite are modelled using cohesive elements.
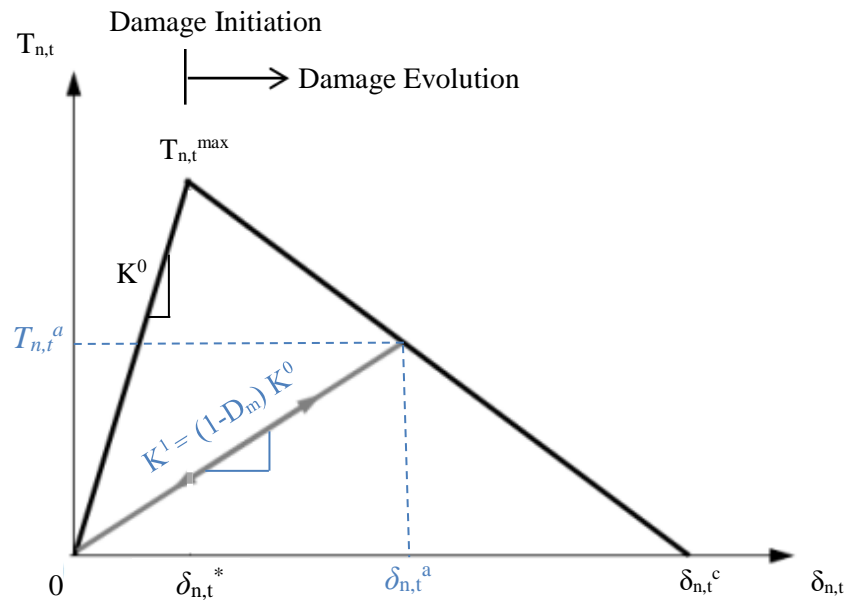

Figure 4.2 Schematic of the bi-linear traction separation law used to simulate the interfaces.

The bi-linear traction separation law used to simulate the delamination behaviour of the pristine and nanomodified composites is presented in figure 4.2 [22]. This cohesive law is chosen because it fits reasonably well to a predominantly brittle fracture, for which the force/displacement curve presents an initial maximum peak followed by and exponential-like decay. In the triangular figure, $T_{n,t}$ represents

the traction of the cohesive element, $\delta_{n,t}$ is the displacement of the cohesive element and K^0 is the initial stiffness of the cohesive element, which determinates the slope of the force-displacement curve before force drop and the beginning of crack propagation. When the displacement of the cohesive element is $\delta_{n,t}^a$, the stiffness and traction of the element are reduced to K^1 and $T_{n,t}^a$. Therefore, it can be said that when a certain level of displacement is reached, the stiffness and the traction of the cohesive elements are progressively reduced until complete separation is obtained.

The composite interfaces of the pristine and nanomodified composites are modelled using cohesive elements given in table 4.1, where $T_{n,t}^{max}$ are the maximum normal and tangential traction respectively, $\delta_{n,t}^c$ denotes the normal and the tangential displacement at the completion of the debonding, and the parameter α is the ratio between the displacement at which the linearity changes (δ^*) and the critical displacement (δ^c), which can be used to calculate the normal and tangential stiffness $K^0_{n,t}$ of the cohesive element using equation 8.

$$K_{n,t}^0 = \frac{T_{n,t}^{max}}{\alpha \, \delta_{n,t}^c} \qquad (8)$$

The subscripts "n" and "t" stand for the normal and tangential states and the superscript "c" indicates the critical displacement, at which complete separation is achieved.

Parameter	Abbreviation	Pristine	Nano	Units
Maximum normal traction	T_n^{max}	45	73	MPa
Normal displacement at debonding	δ_n^c	0.00005	0.00004	m
Maximum tangential traction	T_t^{max}	45	49	MPa
Tangential displacement at debonding	δ_t^c	0.00005	0.00009	m
Ratio	α	0.11	0.05	

Table 4.1 Cohesive zone parameters used to simulate the ply interfaces in the pristine and nanomodified composite.

Since the maximum traction (T^{max}), displacement at debonding (δ^c), and cohesive stiffness (K^0) cannot be determined by experimental tests, these values are determined through a comparison of the experimental and numerical force-

displacement curves, allowing for an estimation of the unknown material properties for the cohesive zone model. The first parameter to be identified in the cohesive zone model is the initial stiffness K^0 determined by progressively increasing its value until the elastic part of the numerical and experimental force-displacement curves coincide. Once the stiffness is established, a value of the maximum traction (T^{max}) is determined by progressively increasing T^{max} until no deviation from the linearity is left before the fracture peak. Finally, the other cohesive parameters (e.g. displacement at debonding (δ^c) and ratio) are identified by trial-and-error process in order to reproduce as closely as possible the data in the non-linear region of the experimental force-displacement curve.

4.4.1 Model Verification

To verify and validate the results obtained in the cohesive element model, the finite element results are compared with the experimental data available. Table 4.2 indicates the interlaminar shear strength measured experimentally and numerically for the pristine and nanomodified laminates. From the table, it can be appreciated that the numerical results show the same trend as the reported experimental results and the interlaminar strength increases for the nanomodified samples. Furthermore, it should be noted that the interlaminar strength measured experimentally is in very good agreement with the interlaminar strength calculated in the numerical simulations, which comes to further validate the results of the numerical simulations.

Sample	Experimental	Numerical
Pristine	50.2 MPa	51.5 MPa
Nano	63.8 MPa	63.1 MPa

Table 4.2 Comparison between experimental and numerical interlaminar shear strength in pristine and nanomodified composites.

4.5 Results and Discussion

In this chapter, the delamination behaviour of the nylon nanomodified specimens as compared to the pristine ones is examined. Initially, the international standard ASTM D 2344 [14] is performed to measure the interlaminar shear strength of the pristine and nanomodified composites. Subsequently, the delamination behaviour of the pristine and nanomodified composites is simulated using cohesive zone modelling via ANSYS Workbench 17.2. The following paragraphs present, analyses and discusses the results obtained in the experiments and numerical simulations.
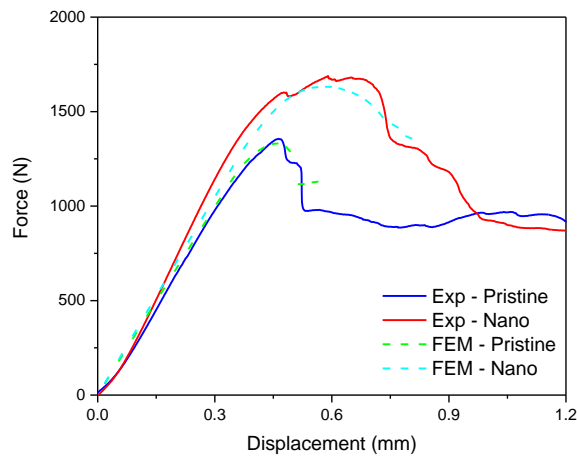

Figure 4.3 Force-displacement curves of pristine (a) and nanomodified (b) composites.

Figure 4.3 illustrates the experimental and numerical experimental force-displacement curves obtained for the composite laminates reinforced with and without nylon nanofibers. From the figure, it can be clearly seen that the fracture load of the pristine composites is approximately 1300 N and the fracture load of the nylon nanomodified composites is around 1700 N. Thus, the load required to initiate fracture in the nanomodified composites is a 23 % higher as compared to the pristine panels. Additionally, the figure shows that the numerical curves for the pristine and nanomodified composites are in very good agreement with the experimental ones, where the force-displacement curves presents an initial maximum peak followed by an exponential-like decay. It is worth to note that the failure mode for the composites with and without nylon nanofibers is multiple shear. Therefore, the cracks appear in the interlaminar regions of the pristine and the nanomodified laminates.

Figure 4.4 shows the seven force-displacement curves obtained for the pristine and nylon nanomodified composites. The curves show good repeatability for the seven specimens of pristine and nylon nanomodified specimens. Therefore, the average values and standard deviations for the fracture loads of pristine and nanomodified composites are 1302 ± 101 N and 1683 ± 63 N, respectively. Thus, the relatively low deviations confirm the good repeatability of the experimental results.
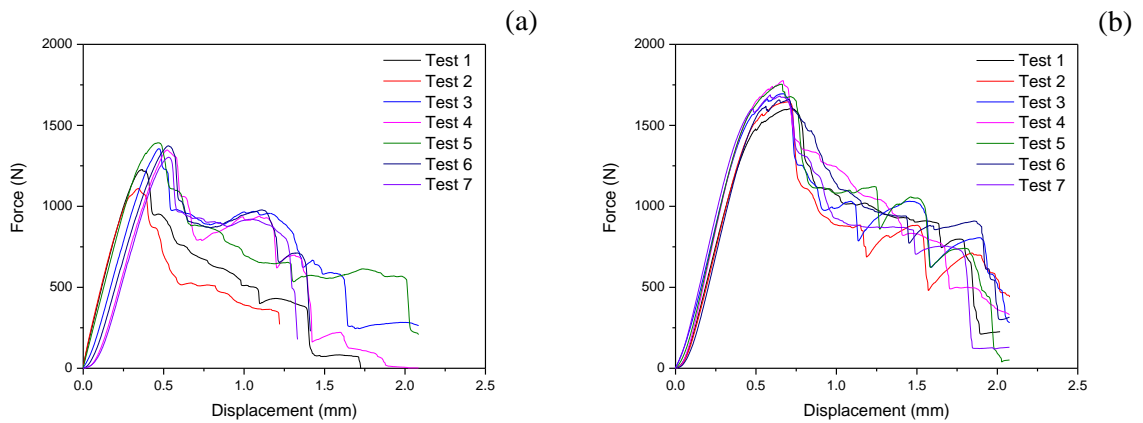

Figure 4.4 Repeatability of the force-displacement curves for the pristine (a) and nylon nanomodified (b) composites.

Table 4.3 shows the average interlaminar shear strength for the seven pristine and nanomodified composites. The experiments showed that the interlaminar strength for the pristine composite specimens is 50.2 ± 4.0 MPa. However, this value increased to 63.8 ± 2.5 MPa for the nylon nanomodified composite specimens. This can be explained by the fact that the nylon nanofibers stitch the different laminas of the composite (bridging mechanism) [23]. Thus, nanofibrous mats act as bridges between the different laminas of the laminate due to their good adhesion with the epoxy resin.

	Pristine	Nano	Units
Experiments	50.2 ± 4.0	63.8 ± 2.5	MPa
Simulations	51.5	63.1	MPa

Table 4.3 Interlaminar strength for the composites with and without nylon nanofibers

To evaluate the effect of nylon nanofibers on the delamination behaviour of glass fibre epoxy composites, the variation of the interlaminar shear strength due to the incorporation of nanofibers is calculated using equation 9:

$$\% \, Variation = \left(\frac{\tau_{nano} - \tau_{pristine}}{\tau_{pristine}} \right) \times 100 \qquad (9)$$

Where τ_{nano} is the interlaminar strength of the nanocomposites and $\tau_{pristine}$ is the interlaminar strength of the pristine composites. The variation of the interlaminar shear strength in glass fibre epoxy composites caused by the inclusion of nylon nanofibers is 21 %. Therefore, composites reinforced with nylon nanofibers are less susceptible to delamination than pristine panels.

Similar results have been reported in the literature. Liu et al. [24] reported that the interlaminar shear strength of glass fiber composites is increased a 18% due to the incorporation of thermoplastic polyurethane nanofibers. Zhao et al. [25] demonstrated that the incorporation of tetra ethyl orthosilicate electrospun nanofibers in the ply interfaces of glass fiber composites enhanced the interlaminar shear strength up to 105%. Other studies as [26, 27] also reported increments of 11% and 10% in the interlaminar strength of carbon fiber composites because of the inclusion of nanofibers of polyacrylonitrile and nylon, respectively. According to these results, it can be concluded that the interleaving with electrospun nanofibers has a significant impact on the interlaminar strength.

The numerical interlaminar shear strengths as per table 4.3 are 51.5 MPa and 63.1 MPa for the pristine and the nanomodified laminates respectively. The CZM results given show that the presence of nylon nanofibers in the composites increases the interlaminar shear strength with 18.4 %. According to these results, it can be concluded that the incorporation of nanofibers has a significant impact on the interlaminar strength. As indicated by [26], the increase in interlaminar strength is attributed to the ability to dissipate energy of the nanofibers as they transfer load toward the fibers, reducing stress concentrations.

In summary, this section investigates how the addition of nylon nanofibers changes the interlaminar shear strength of glass fiber composites. The findings of this study suggest that composites reinforced with nylon nanofibers possess higher interlaminar shear strength as compared to pristine composites. This discovery is of utmost importance as it demonstrates that the incorporation of nylon nanofibers into the ply interfaces of composite laminates can be used to bring down the likelihood of delamination.

4.6 Conclusions

The idea of this chapter is to analyse the effect of nylon nanofibers on the delamination behaviour of glass fibre epoxy composites. This is done experimentally and also by a simulation model. For the purpose membranes of interconnected nylon nanofibers are interleaved into the interlaminar regions of glass fibre epoxy composite laminates with the aim to prevent delamination. To verify the effect of nylon nanofibers on the delamination behaviour of glass fibre epoxy composites, the interlaminar shear strength of the pristine and nanomodified composites is determined experimentally by a short beam method and numerically using a cohesive zone model. Based on the experimental and numerical results, the following conclusion can be drawn:

The experimental results indicate that fracture load of the pristine composites is 1302 N, while the fracture load of the nanomodified composites is 1683 N. Therefore, the nanomodified composites require a 22 % more load to initiate the fracture as compared to the pristine specimens. Thus, the interleaving with electrospun nanofibers could be used to develop composite laminates with less susceptibility to fracture. Additionally, the experiments show that the interlaminar strength of the composite laminates increase from 50.2 MPa to 63.8 MPa due to the reinforcement with nylon nanofibers. This significant increment in the interlaminar strength can be explained by the presence of significant bridging phenomena

between the nanofibers and the composite laminates. Hence, composite laminates interleaved with nylon nanofibers are less prone to delamination than the pristine ones.

Furthermore, the delamination behaviours of pristine and nanomodified laminates are tested numerically using a finite element model. Both the experiments and the finite element modelling confirmed the increase of the interlaminar strength as a result of the modification with nylon nanofibers. The increase obtained numerically was 18% which agrees well with the 21% increase from the experimental study. Thus, one can conclude that nylon nanofibers can be used for improving the delamination resistance of glass fibre epoxy laminates.

For the future, the authors plan to continue the investigation of interleaving with nanofibers for the purposes of delamination prevention and restriction. In this line an investigation of the effect of nanofibers on the delamination caused by low velocity impacts in pristine and nanomodified laminates. This will be done experimentally and numerically while in the same time the FEM investigation will be done to bring more understanding about the impact behaviour of nanomodified glass fibre epoxy laminates.

References

[1]   G. Minak, R. Palazzetti, I. Trendafilova and A. Zucchelli, Localization of a delamination and estimation of its length in a composite laminate beam by the VSHM and pattern recognition methods, Mech Compos Mater., 46 (2010) 387-394.

[2]   S. Yadav, V. Kumar, S. Verma, Fracture toughness behaviour of carbon fibre epoxy composite with Kevlar reinforced interleave, Mater Sci Eng B, 132 (2006) 108-12.

[3]   D. Wong, L. Lin, P. McGrail, T. Peijs, P. Hogg, Improved fracture toughness of carbon fibre/epoxy composite laminates using dissolvable thermoplastic fibres, Compos Part A, 41 (2010) 759-67.

[4]   E. Fuoss, P. Straznicky, C. Poon, Effects of stacking sequence on the impact resistance in composite laminates - part: parameter study, Compos Struct., 41 (1998) 67-77.

[5]   T. Brugo, R. Palazzetti, The effect of thickness of Nylon 6,6 nanofibrous mat on Modes I-II fracture mechanics of UD and woven composite laminates, Compos Struct, 154 (2016) 172-8.

[6]   L. Daelemans, S. Heijden, I. Baere, H. Rahier, W. Paepegem, K. Clerck, Nanofiber bridging as a toughening mechanism in carbon/epoxy composite laminates interleaved with electrospun polyamide nanofibrous veils, Compos Sci Technol., 117 (2015) 244-56.

[7]   T. Yang, C. Wang, J. Zhang, Toughening and self-healing of epoxy matrix laminates using mendable polymer stitching, Compos Sci Technol., 72 (2012) 1396-1401.

[8]   H. Zhang, A. Bharti, Z. Li, S. Du, E. Bilotti, T. Peijs, Localized of carbon/ epoxy laminates using dissolvable thermoplastic interleaves and electrospun fibres, Compos Part A: Appl Sci Manuf., 79 (2015) 116-26.

[9]   L. Daelemans, S. Heijden, L. Baere, H. Rahier, W. Paepegem, K. Clerck, Using aligned nanofibers for identifying the toughening micromechanisms in nanofiber interleaved laminates, Compos Sci Technol., 124 (2016) 17-26.

[10]   L. Liu, Y. Liang, G. Xu, H. Zhang, Z. Huang, Mode I interlaminar fracture of composite laminates incorporating with ultrathin fibrous sheets, J Reinf Plast Compos., 27 (2008) 1147-62.

[11]   J. Zhang, T. Yang, T. Lin, C. Wang, Phase morphology of nanofiber interlayers: critical factor for toughening carbon/epoxy composites, Compos Sci Technol., 72 (2012) 256-262.

[12] K. Shivakumar, S. Lingaiah, H. Chen, P. Akangah and G. Swaminathan, L. Russell, Polymer nanofabric interleaved composite laminates, AIAA J., 47 (2009) 1723-9.

[13] R. Palazzetti, X. Yan, A. Zucchelli, Influence of geometrical features of electrospun nylon 6,6 interleave in the CFRP laminates mechanical properties. Polym Compos., 35 (2014) 137-50.

[14] ASTM D2344 2344M, Standard test method for short-beam strength of polymer matrix composite materials and their laminates, Annual Book of ASTM Standards (2000).

[15] H. Saghafi, S. Ghaffarian, T. Brugo, G. Minak, A. Zucchelli, H.A. Saghafi, The effect of nanofibrous membrane thickness on fracture behaviour of modified composite laminates – a numerical and experimental study, Compos Part B, 101 (2016) 116-23.

[16] G. Giuliese, R. Palazzetti, F. Moroni, A. Zucchelli, A. Pirondi, Cohesive zone modelling of delamination response of a composite laminate with interleaved nylon 6,6 nanofibres, Compos Part B, 78 (2015) 384-392.

[17] F. Moroni, R. Palazzetti, A. Zucchelli, A. Pirondi, A numerical investigation on the interlaminar strength of nanomodified composite interfaces, Compos Part B, 55 (2013) 635-641.

[18] K.C. Gopalakrishnan, R.R. Kumar, S.A. Lal, Cohesive zone modelling of coupled buckling – Debond growth in metallic honeycomb sandwich structure, J Sand Struct Mater., 14 (6) 679-693.

[19] C. Garcia, J. Wilson, I. Trendafilova and L. Yang, Vibratory behaviour of glass reinforced polymer (GFRP) interleaved with nylon nanofibers, Compos Struct., 176 (2017) 923-923.

[20] W. Ding, Delamination analysis of composite laminates, PhD thesis, University of Toronto, Canada, 1999.

[21]   H. Saghafi, Mechanical behaviour of flat and curved laminates interleaved by electrospun nanofibers, PhD thesis, University of Bologne, Italy, 2013.

[22]   G. Alfano, M.A. Crisfield, Finite element interface models for the delamination analysis of laminated composites: Mechanical and computational issues, Int J Numer Methods Eng., 50 (2001) 1701-1736.

[23]   L. Daelemans, S. Heijden, I. Baere, H. Rahier, W. Paepegem and K. Clerck, Damage resistant composites using electrospun nanofibers: a multiscale analysis of the toughening, ACS Appl Mater Interfaces, 8 (2016) 11806-18.

[24]   L. Liu, Z. Huang, C. He, X. Han, Mechanical performance of laminated composites incorporated with nanofibrous membranes, Mater Sci Eng. A, 435-436 (2006) 309-17.

[25]   Y. Zhao, T. Xu, X. Ma, M. Xi, D. Salem and H. Fong, Hybrid multi-scale epoxy composites containing conventional glass microfibers and electrospun glass nanofibers with improved mechanical properties, J Appl Polym Sci., 132 (2015) 42731.

[26]   K. Molnar, E. Kostakova, L. Meszaros, The effect of needleless electrospun nanofibrous interleaves on mechanical properties of carbon fabrics/epoxy laminates, Express Polym Lett., 8 (2014) 62-72.

[27]   B. Beylergil, M. Tanoglu and E. Aktas, Enhancement of interlaminar fracture toughness of carbon fiber epoxy-composites using polyamide-6,6 electrospun nanofibers, J Appl Polym Sci, 134 (2017) 45244.

Chapter 5

The effect of Polycaprolactone Nanofibers on the impact behaviour of Glass Fibre Composites

In this chapter, the impact behaviour of glass fibre epoxy composites interleaved with and without polycaprolactone nanofibers is examined. For this aim, pristine and nanomodified composite beams are impacted at 24 J and 36 J using a drop weight impact machine. The experimental results show that the interleaving of GFRC with polycaprolactone nanofibers can significantly decrease the area damaged by impact. Additionally, a finite element model is proposed to simulate the impact behaviour of composite laminates with and without polycaprolactone nanofibers. The numerical results show a good agreement with available experimental data and prove that composites reinforced with polycaprolactone nanofibers experience less damage when subjected to the same impact as the pristine composites. The findings of this chapter reveal that the incorporation of polycaprolactone nanofibers in glass fibre composite mats can be successfully used for reducing the delamination and improving the impact resistance of structures made of composite mats as aircrafts.

5.1 Introduction

The interleaving with nanofibers has attracted considerable attention in the composite community because it can improve the mechanical and physical properties of traditional fibre reinforced composites [1, 2]. For example, Hamed Saghafi et al. [3] investigate the effect of nylon nanofibers on the interlaminar properties of glass fiber/epoxy laminates. The results reveal that the addition of nylon nanofibers increased 62% and 109% the mode I and mode II energy releases rates respectively. Other works as [4] reported that the maximum stress of carbon fibre composites is

significantly enhanced (with an increment of 35%) due to the incorporation of nylon polymer nanofibers into the composite laminates. Up to date, most of the studies have investigated the effect of electrospun nanofibers on the fracture toughness in opening and sliding mode [5, 6], on the interlaminar shear strength [7], on the tensile strength [8], and the compression strength after impact [9]. However, there are still very few works to report about the effect of electrospun nanofibers on the impact behaviour of composite laminates.

On the other hand, only a few authors have simulated the impact behaviour of nanomodified composites using finite element analysis. For example, the authors of [10] investigated the impact behaviour of polymers interleaved with and without carbon nanotubes using a multi-scale finite element model. The results of this work show an improvement of the impact resistance of the carbon nanomodified polymers as compared to the pristine panels. Therefore, there are very few attempts to simulate numerically the influence of nanofibers on the impact behaviour of composite laminates.

Recently, various kinds of polymeric nanofibers have been used for improving the mechanical properties of composite laminates such as polysulfone [11], polyvinylidene fluoride [12], polyvinyl alcohol [13], phenoxy [14], and nylon [15]. Polycaprolactone nanofibers are also a good choice for improving the properties due to their high compatibility and strong adhesion with epoxy resin. Furthermore, there are no numerical studies to investigate the influence of polycaprolactone nanofibers on the impact response of glass fibre epoxy composites.

In this chapter, the effect of polycaprolactone nanofibers in the impact response of glass fibre composites is analysed. For this purpose, a finite element model is used to evaluate the impact behavior of composites with and without polycaprolactone nanofibers. The numerical results obtained are compared to the experimental results published by [16] and they show quite good agreement regarding the impact damaged area of the pristine and the nano modified specimens. Both the experimental and the numerical results show that the incorporation of

110

polycaprolactone nanofibers in the composite interfaces significantly enhances the impact damage resistance of the glass fiber composites. On the basis of these results it can be concluded that composites reinforced with polycaprolactone nanofibers are less prone to impact damage than the pristine composites.

The main contribution of this chapter is to demonstrate that the addition of polycaprolactone nanofibers can be used to develop composite structures with higher resistance to impacts (e.g. hailstones), which is important for the health of the composite mats used in aircrafts, wind turbines and other civil structures. Furthermore, a finite element model is developed for the first time to simulate the impact response of composites interleaved with polycaprolactone nanofibers.

The rest of the chapter is organized as follow: The next paragraph (section 2) provides an overview of the preparation of the specimens interleaved with and without polycaprolactone nanofibers. The third section introduces the impact test utilized to analyze the impact response of the pristine and nanomodified specimens. The fourth section introduces and verifies the numerical model used to simulate the impact response of the composites with and without polycaprolactone nanofibers. Section 5 present and discusses in detail the results from the experimental and numerical simulations. Eventually the chapter ends with some conclusions about the finite element model and the impact properties of nanomodified of glass fibre epoxy composites.

5.2 Fabrication of glass fibre epoxy composites with and without polycaprolactone nanofibers

This section describes the fabrication of the glass fiber/epoxy composites reinforced with and without polycaprolactone nanofibers. Figure 5.1 illustrates the composite lay-up of the pristine and nanomodified composites used in this study. Pristine composites (without polycaprolactone nanofibers) were fabricated by hand

lay-up of eight layers of unidirectional glass fiber epoxy prepreg, as detailed in Figure 5.1 (a). The composite specimens are prepared with dimensions of 168 mm $\times$ 100 mm $\times$ 3.1 mm and stacking sequence $[0,90,0,90]_s$. After the lay-up, the composite beams are cured using a vacuum bag in an autoclave at 150° for about one hour, as indicated in the supplier's specifications. The weight fractions of the glass fiber and epoxy resin are 78.6% and 21.4%, respectively, for the pristine composites.

The nano composites (with polycaprolactone nanofibers) are also manufactured by hand lay-up with identical composite prepregs, number of layers, dimensions, ply orientations, and curing process as the pristine composites. However, six layers of polycaprolactone nanofibers are interleaved at each of the composite interfaces (excluding the central one), as shown in Figure 5.1 (b). It is also important to mention that the effect of the nanofibers on the final thickness of the composites is negligible (less than 1%). Additionally, the difference in weight for the pristine and nanomodified composites due to the incorporation of polycaprolactone nanofibers is also negligible. Therefore, the weight fraction of polycaprolactone nanofibers in the nanomodified composites is very small (less than 1%).
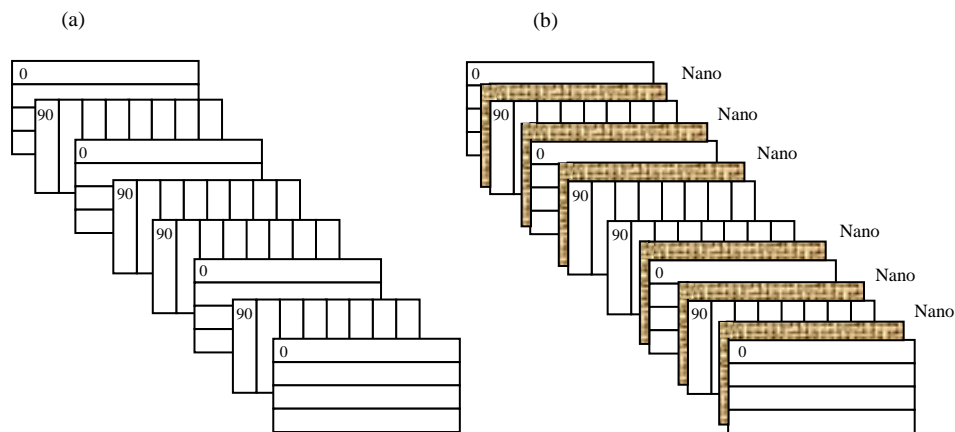

Figure 5.1. Composite lay-up of the (a) pristine and (b) nanomodified composites.

The layers of polycaprolactone nanofibers were prepared by the electrospinning technique [17]. This procedure was chosen because is an easy and low-cost technology to prepare polycaprolactone nanofibers with a wide variety of

morphologies. For the preparation of the nanofibers, polycaprolactone pellets are dissolved in a solvent mixture of formic acid and acetic acid (60/40) at 15% w/v. Subsequently, the chemical solution is transferred to a syringe to be spun using the following operational conditions: a high voltage of 23 kV, a feed rate of 0.9 mL/h, and a needle tip-collector distance of 15 cm. As a result, an ultrathin layer of interconnected polycaprolactone nanofibers is obtained, as depicted in Figure 5.2. The scanning electron microscope (SEM) image is adapted from [16] and shows a dense array of polycaprolactone nanofibers distributed randomly in the membrane. The diameter of the polycaprolactone nanofibers is 275 nm, with a standard deviation of 75 nm.
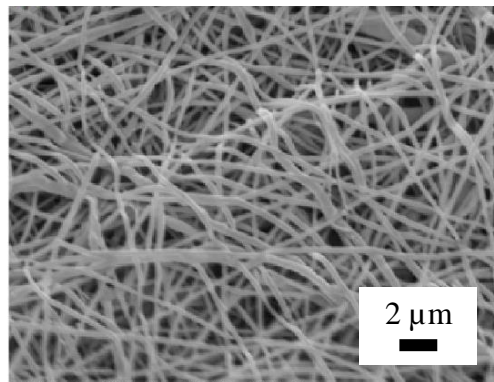

Figure 5.2. Scanning electron microscope (SEM) image of polycaprolactone nanofibers as spun, adapted from figure in [16].

5.3 Impact tests

Low velocity impact tests were conducted in a drop-weight impact machine equipped with a piezoelectric sensor on the tip of impactor for measuring the impact force and a laser device to determinate the position of the impact. A detailed description of the impact machine can be found in [18]. The impactor consists of a hemispherical head with a diameter of 12.7 mm and a weight of 1.22 kg. The composite beams are placed in a clamping fixture equipped with four rubber pins and impacted at controlled energies of 24 J and 36 J. During the impacts, an electromagnetic braking

system is used with the aim to avoid multiple collisions. Each impact was repeated three times for the pristine and nanomodified configurations.

The reason why the impact tests are performed on composite beams with smaller size than the conventional impact specimens are because of the increased preparation time for the nanomodified composites. I would like to point out that the preparation of one only membrane of nanofibers using a conventional electrospinning machine (not an industrial equipment) takes about 4-5 hours. Therefore, eight working days are needed to prepare one composite plate reinforced with eight membranes of nanofibers. Furthermore, it is also worth noting that the impact response of composite specimens is mainly affected by the sample thickness of the composite beams, which is constant for the pristine and nanomodified specimens, and not for the length and width of the composite beams.

5.4 Finite element modelling for impact behaviour of composite laminates beams

This paragraph presents the finite element model used to simulate the impact response of the composite beams with and without polycaprolactone nanofibers. For this aim, composite beams with the same characteristics of the manufactured composite specimens are modelled using ANSYS composite PrepPost. The pristine and the nanomodified composite beams are modelled with the same dimensions (168 mm × 100 mm × 3.1 mm), number of layers and ply orientations as the beams manufactured experimentally. The unidirectional glass fibre/epoxy layers are simulated using Solid 185 type elements and the material constants which are indicated in table 5.1. The composite interfaces made of epoxy resin in the pristine composite and polycaprolactone nanofibers in the nano composite are modelled using cohesive elements.

Constant	Definition	Value	Unit
E_x	Young's Modulus X direction	45	GPa
E_y	Young's Modulus Y direction	10	GPa
E_z	Young's Modulus Z direction	10	GPa
υ_{xy}	Poisson's Ratio XY	0.3	Dimensionless
υ_{yz}	Poisson's Ratio YZ	0.4	Dimensionless
υ_{xz}	Poisson's Ratio XZ	0.3	Dimensionless
G_{xy}	Shear Modulus XY	5	GPa
G_{yz}	Shear Modulus YZ	3.8	GPa
G_{xz}	Shear Modulus XZ	5	GPa

Table 5.1 Material constants used to simulate the layers of unidirectional glass fibre epoxy plies supplied by ANSYS Workbench Engineering Data.

Figure 4.2 represents the cohesive zone model used to simulate the initiation and the evolution of damage in the pristine and the nano-modified laminates. The cohesive model is based on the bilinear model proposed by Alfano and Crisfield [19]. From the figure, it can be deducted that the stiffness of the cohesive elements (K^0) is constant under small element displacements ($<\delta_{n,t}^*$). However, the stiffness of the cohesive elements (K^1) decreases progressively, when the level of displacement is above $\delta_{n,t}^*$. The figure also shows that the initiation of the damage is defined by the displacement at maximum cohesive traction ($\delta_{n,t}^*$), therefore for small displacements below $\delta_{n,t}^*$ it is considered that there is no delamination/damage. As the material is non-damaged, the stiffness is constant and equal to the original stiffness of the material. When the displacement of the elements is above $\delta_{n,t}^*$, the damage progresses with the increase of the displacement $\delta_{n,t}$ and accordingly the stiffness goes down with a factor of ($1-D_m$) as indicated in the equation shown in Figure 4.2.

The relation between the traction ($T_{n,t}$) and the displacement ($\delta_{n,t}$) of the cohesive elements can be defined using the following equation (10).

$$\frac{T_{n,t}}{\delta_{n,t}} = (1 - D_m)K_{n,t} \qquad (10)$$

Where $K_{n,t}$ represents the initial stiffness of the cohesive element and ($1- D_m$) is a factor reduction of the stiffness due to the damage. The subscripts "n" and "t" refer to the normal and the tangential states. When the composites are undamaged, the

damage parameter (D_m) is 0 and the value of the stiffness is equal to the original stiffness. When the composites are damaged, the D_m is between the two values 0 to 1 and the stiffness goes down as indicated in equation (10). Therefore, the level of damage is defined by the reduction of the stiffness. The value of $D_m = 1$ corresponds to complete debonding which corresponds to the critical displacement $\delta_{n,t}^c$.

The corresponding cohesive parameters used to simulate the delamination between the composite interfaces for the pristine and the nano-modified composites are indicated in Table 5.2. The parameter alpha is defined as the ratio of $\delta_{n,t}^*$ to $\delta_{n,t}^c$ (see Figure 4.2) and can be used to calculate $\delta_{n,t}^*$. This is of the utmost importance as the area under the triangle 0, $\delta_{n,t}^*$, $T_{n,t}^{max}$ on Figure 4.2 corresponds to the energy needed to initiate delamination and the area under the triangle $\delta_{n,t}^*$, $\delta_{n,t}^c$, $T_{n,t}^{max}$ is associated with the energy for the damage propagation. The non-dimensional weighting parameter (betha) assigns different weights to the tangential and normal displacements, where we have assumed that the tangential and normal displacement contributes to the delamination (mixed mode debonding).

Parameter	Abbreviation	Pristine	Nano	Units
Maximum normal traction	T_n^{max}	5	2.8	MPa
Normal displacement at debonding	δ_n^c	0.00027	0.00035	m
Maximum tangential traction	T_t^{max}	5	2.8	MPa
Tangential displacement at debonding	δ_t^c	0.00027	0.00035	m
Ratio	α	0.02	0.015	Dl
Non-dimensional parameter	β	1	1	Dl

Table 5.2 Cohesive zone parameters used to simulate the ply interfaces made of epoxy resin (pristine) and polycaprolactone nanofibers (nano).

Since the maximum traction (T_{max}), displacement at debonding (δ_c), and ratio of δ^* and δ_c (α) cannot be determined by experimental tests, these values are determined through a comparison of the experimental results with the numerical simulations of the same tests, allowing for an estimation of the unknown material properties for the cohesive zone model. By definition, the area under the triangle (see Figure 4.2) corresponds to the critical interlaminar fracture energy for the glass fiber

composites. Therefore, the numerical critical fracture energy for the pristine and nano composites is 675 J/m^2 and 490 J/m^2, respectively. These results are in the range of other composite laminates with similar characteristics.

The damage initiation law used in the numerical simulations is based on the Puck failure criteria [20]. According to this criterion, damage initiation is related to a certain value of stiffness reduction. In this study, the Puck criterion was used for modelling the interface delamination for the four failure modes of damage initiation related to the fibers and the matrix. These four modes are Tensile Fiber Failure Mode, Compressive Fiber Failure Mode, Tensile Matrix Failure Mode, and Compressive Matrix Failure Mode.

The damage evolution law utilized in the numerical simulations is based on the instant stiffness reduction. The stiffness reduction is used to define how the composite interfaces are degraded because of the damage. Accordingly, this stiffness reduction can vary between 0 and 1, where 0 indicates no reduction in the stiffness and 1 is associated with complete stiffness loss. In this study, we have assumed that there is an 80% reduction of stiffness reduction due to the delamination/damage for the four modes of damage.

5.4.1 Experimental Model Verification

To verify the results obtained using the finite element model and to validate the model, the finite element results are compared with the experimental results obtained in the paper of Saghafi et al. [16]. It is important to note that the composite beams manufactured experimentally are the same size and subjected to the same impacts as in the model. The numerical and the experimental results are presented in Table 5.3. The table represents the damaged area on the laminated beams with and without polycaprolactone nanofibers as a result of the impact with energies of 24 J and 36 J. From the table, it can be seen that the numerical results show the same trend as the reported experimental results and the delaminated area decreases for the nano

modified samples for both cases of impact. Furthermore, it should be noted that the experimentally measured damaged area is in very good agreement with the damaged area obtained in the numerical simulations, which comes to further validate the results of the numerical simulations.

Energy	Sample	Experimental [16]	Numerical
24 J	Pristine	0.000170 m^2	0.000175 m^2
	Nano	0.000125 m^2	0.000126 m^2
36 J	Pristine	0.000260 m^2	0.000275 m^2
	Nano	0.000197 m^2	0.000196 m^2

Table 5.3 Area damaged (mm^2) in pristine and nano modified composites due to the 24 J and 36 J energy impacts.

5.5 Results and Discussion

The aim of this section is to analyze the effect of polycaprolactone nanofibers on the impact damage resistance of glass fiber composite laminates. For this study, the finite element model introduced in Section 5.4 is used to simulate the damage caused by impacts with energies of 24 J and 36 J in the pristine and nano modified composite beams. It is important to note that the force-displacement curves shown in Fig. 5.3 represent the impact excitation of the composite specimens, which is taken from the studies of Saghafi et al. [16] where the same composite beams (made of the same number of layers, same materials and same size) are subjected to the same impact loadings.

The composite beams are subjected to impacts using energies of 24 J and 36 J, as detailed in Figure 5.3. The figure shows that the experimental and numerical force-displacement curves for the same energy impacts are very close to each other. Therefore, it can be concluded that the total impact energy used in the experiments and numerical simulations is the same. From the figure, the peak forces and displacements for the 24 and 36 J energy impacts can be clearly observed. Therefore, according to our simulations, the peak force increases from 3795 to 4821 N when the

energy of the impact varies between 24 and 36 J. The mechanical impacts are located at the centre of the specimen and each impact is applied at the same location for each test. The composite beams are fixed using clamp-clamp boundary conditions. Therefore, the composite specimens are clamped using fixed supports at both ends of the composite beams.
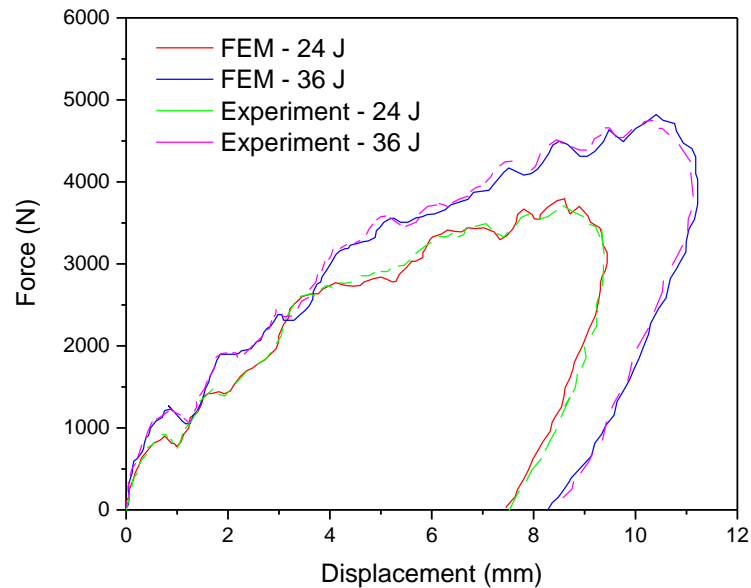

Figure 5.3 Comparison between the experimental and numerical force-displacement curves for the energy impacts at 24 J and 36 J.

The results obtained in the drop weight impact test are shown in Figure 5.4. The composite specimens reinforced with polycaprolactone nanofibers and the pristine ones are subjected to controlled energy impacts at 24 J and 36 J. As seen in the pictures, the area damaged because of the low velocity impacts is smaller for the nanomodified composites. From the figure, it can be clearly seen that the area damaged as a consequence of the 24 J impact is 170 mm^2 and 125 mm^2 for the pristine and nanomodified composites, respectively. The same trend of reduction of the damaged area is observed for the energy impact at 36 J, where the nanomodified composite shows a significant reduction (24 %) with respect to the pristine beams of the delaminated area due to the impact. The reduction of the damaged area is attributed to the fact that polycaprolactone nanofibers absorb energy during the impact, which is beneficial to dissipate the energy of the impact.
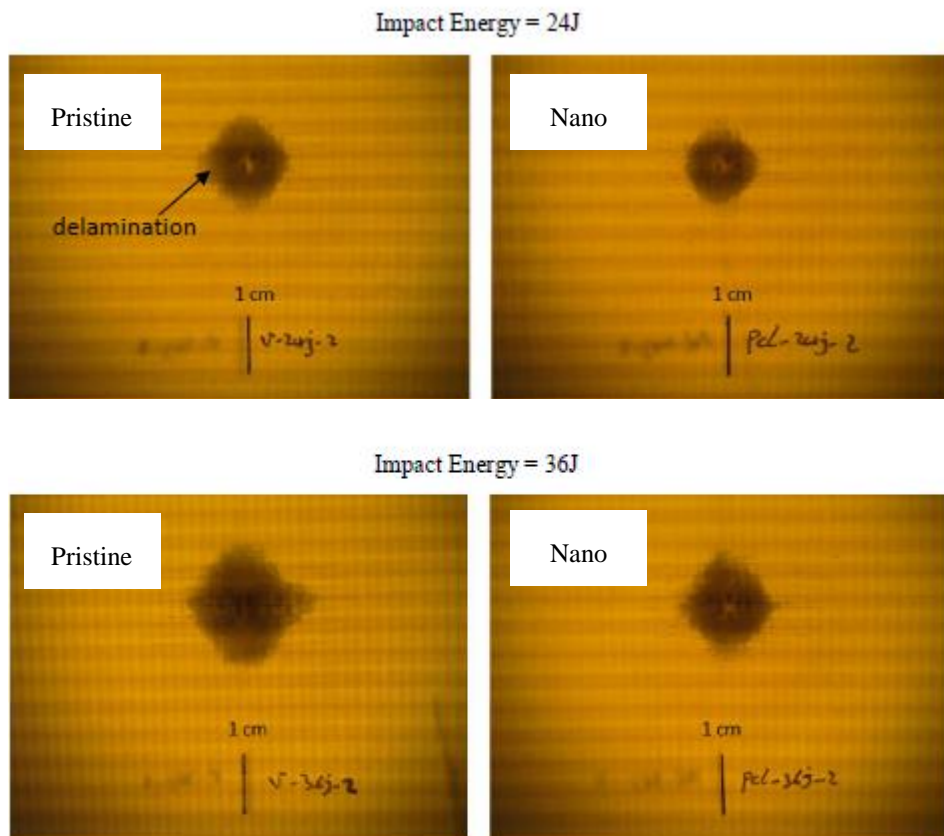
Figure 5.4 Results obtained in the drop-weight impact test. Area damaged after the energy impact at 24 J and 36 J for the pristine and nano composites [16].
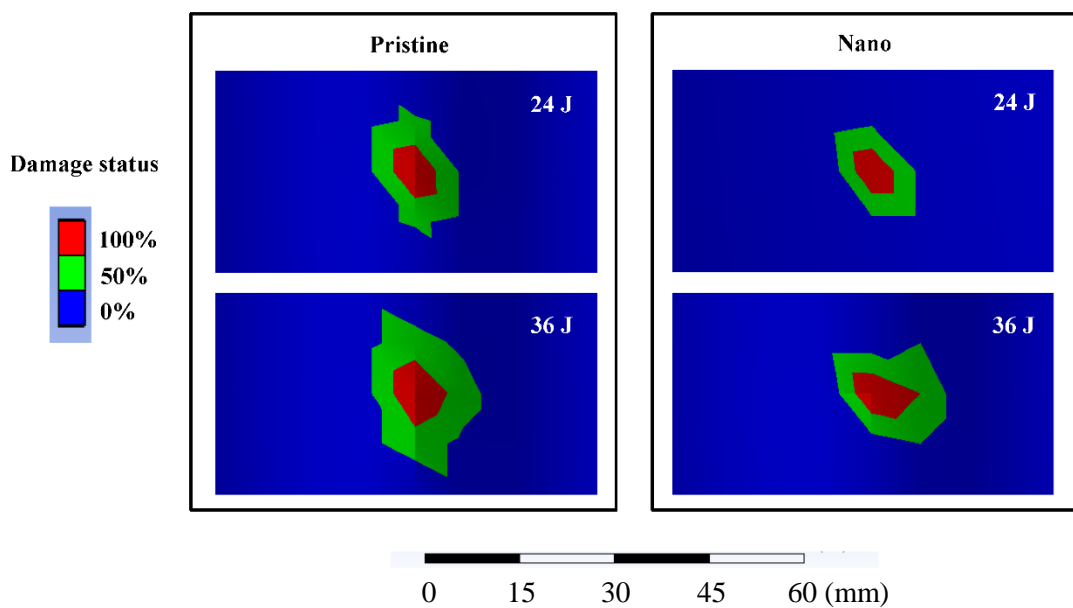

Figure 5.5 Results obtained in the cohesive element model. Area damaged after the energy impact at 24 J and 36 J for the pristine and nano composites.

The results obtained using the finite element model simulations are illustrated in Figure 5.5. The legend scale on the left refers to the level of damage in the composite specimen, where the strong blue colour (0%) represents the undamaged area of the composite and the red colour (100%) represents the severely damaged area of the composite. The green colour in between (50%) corresponds to damage states, which are in between the above two, the non-damaged and the severely damaged states, where the composite specimens are partially damaged. From the simulations, it can be clearly appreciated that nano composites are less damaged than the pristine panels for the two cases investigated (24 and 36 J). Therefore, it can be concluded that according to the finite element modelling and experiments, the incorporation of polycaprolactone nanofibers reduces the delaminated area by about 35% for the two energy levels at 24 and 36 J. This can be attributed to the good adhesion between polycaprolactone nanofibers and epoxy resin and the formation of heterogeneous separated phases on the composite interfaces, which increases the energy dissipation [21]. Additionally, the figure also shows that the most severe damage in the composite is located in the impacted zones (red area).

The experimental results show that the area damaged as result of the 24 J impact is 0.000170 and 0.000125 m^2 for the pristine and nano composites, respectively [16], and our numerical simulations confirm that the damaged area decreases from 0.000175 to 0.000126 m^2 as a result of the incorporation of polycaprolactone nanofibers. The same trend of reduction of the delaminated area is found for an impact with 36 J energy, where the area damaged in the composite laminates decreased by around 28% due to the reinforcement with polycaprolactone nanofibers. Therefore, the results obtained experimentally and numerically confirm that the composites reinforced with polycaprolactone nanofibers are less susceptible to impact damage than pristine panels.

Similar results have been reported previously in other works. For example, Ref. [22] reported that the addition of nylon nanofibers to the interfaces of carbon fibre epoxy composites significantly increased the threshold impact force (the force to

cause initiation of impact damage) up to 60%. Additionally, the same study shows that the impact damage area decreases considerably due to the interleaving with nylon nanofibers. Other works, such as [23], indicated that the incorporation of a mixture of polycaprolactone and nylon nanofibers into the composite ply interfaces could decrease the impact damage area by up to 59.3% in glass fibre epoxy composites. Other authors, such as [24, 25], suggest that the interleaving with other electrospun nanofibers -polyvinylidene fluoride and polyacrylonitrile nanofibres- is not a good choice for toughening epoxy and improving the impact damage resistance of glass fibre/epoxy laminates.

In conclusion, it can be said that the interleaving with polycaprolactone nanofibers decreases the impact damage area in glass fibre epoxy composites quite significantly by more than 30%. This can be attributed to the higher dissipation of energy during the impact of the nano modified composites with respect to the pristine samples. This discovery is of the utmost importance for structures made of composite materials (e.g., aircrafts or wind turbines), where the impacts caused by bird strikers or hailstorms are a main concern.

5.6 Conclusions

The impact resistance of materials is very important in a lot of industries, including aircraft design and production. In the last years, various kinds of polymeric nanofibers have been used for enhancing the impact response of composite laminates such as polysulfone, polyvinylidene fluoride, polyvinyl alcohol, phenoxy, and nylon. In this regard, polycaprolactone nanofibers are also attracting important attention because of its beneficial properties as high compatibility and strong adhesion with epoxy resin. The aim of this research is to investigate the effect of polycaprolactone nanofibers on the impact resistance of glass fiber epoxy composites. The performed experimental and numerical investigations suggest that the incorporation of polycaprolactone nanofibers into the interlaminar regions of composite glass fiber

epoxy composites increases the impact resistance and reduced the area damaged by impacts.

The numerical investigation offered in this research is validated with available experimental data and reveal that the incorporation of polycaprolactone nanofibers reduce a 30 % the delamination damaged caused by low-velocity impacts in glass fibre epoxy layered composites. Thus, polycaprolactone nanofibers can be used to develop composite materials with improved impact resistance which can be a used for an important number of applications, including aircrafts and wind turbines.

This work presents solid progress toward the practical applications of composites reinforced with polycaprolactone nanofibers as per example reduction of the impact damage caused by impacts. This is important from the view point of using such materials as part of any structural elements that experience impact, as the interleaving with polycaprolactone nanofibers is potentially capable the damage of such impacts.

References

[1]   M. Fotouhi, H. Saghafi, T. Brugo, G. Minak, C. Fragassa, A. Zucchelli, M. Ahmadi, Effect of PVDF nanofibers on the fracture behaviour of composite laminates for high-speed woodworking machines, J Mech Eng Sci., 231 (2016) 31-43.

[2]   H. Saghafi, T. Brugo, G. Minak, A. Zucchelli, The effect of PVDF nanofibers on mode-I fracture toughness of composite materials, Compos Part B: Eng., 72 (2015) 2013-6.

[3]   H. Saghafi, R. Palazzetti, A. Zucchelli, G. Minak, Influence of electrospun nanofibers on the interlaminar properties of unidirectional epoxy resin/glass fiber composite laminates. J. Reinf. Plast. Compos., 34 (2015) 907–914.

[4] R. Palazzetti, Flexural behavior of carbon and glass fiber composite laminates reinforced with nylon 6,6 electrospun nanofibers. J. Compos. Mater. 2015, 49, 3407–3413.

[5] B. Beylergil, M. Tanoglu, E. Aktas, Enhancement of interlaminar fracture toughness of carbon fiber-epoxy composites using polyamide-6,6 electrospun nanofibers, J. Appl. Polym. Sci., 10 (2017) 45244.

[6] G.W. Beckermann, K.L. Pickering, Mode I and mode II interlaminar fracture toughness of composite laminates interleaved with electrospun nanofiber veils, Compos. Part A, 72 (2015) 11–21.

[7] K. Molnar, E. Kostakova, L. Meszaros, The effect of needleless electrospun nanofibrous interleaves on mechanical properties of carbon fabrics/epoxy laminates, Express Polym Lett., 8 (2014) 62–72.

[8] C.V. Manh, H.J. Choi, Enhancement of interlaminar fracture toughness of carbon fiber/epoxy composites using silk fibroin electrospun nanofibers, Polym Plast Technol Eng., 55 (2016) 1048–1056.

[9] P. Akangah and K. Shivakumar, Impact damage resistance and tolerance of polymer nanofiber interleaved composite laminates. In Proceedings of the 53rd ASME Structures, Structural Dynamics and Materials Conference, Honolulu, HI, USA, 23–26 April 2012.

[10] R. Rafiee, R.M. Moghadam, Simulation of impact and post-impact behaviour of carbon nanotube reinforced polymer using multi-scale finite element modelling, J Comput Mater Sci., 63 (2012) 261-8.

[11] G. Li, P. Li, C. Zhang, Y. Yu, H. Liu, S. Zhang, X Jia, X Yang, Z Xue, S. Ryu, Inhomogeneous toughening of carbon fiber/epoxy composite using electrospun polysulfone nanofibrous membranes by in situ phase separation, Comp Sci Technol., 68 (3) 987-994.

[12] K. Magniez, C. Lavigne, B. Fox, The effects of molecular weight and polymorphism on the fracture and thermo-mechanical properties of a carbon-

fibre composite modified by electrospun poly (vinylidene fluoride) membranes, Polym., 51 (2010) 2585-2596.

[13] Y. Shao, T. Yashiro, K. Okubo, and T. Fujii, Effect of cellulose nano fiber (CNF) on fatigue performance of carbon fibre fabric composites, Composites Part A, 76 (2015) 244-254.

[14] K. Magniez, T. Chaffraix, B. Fox, Toughening of a carbon-fibre epoxy composite using electrospun poly (hydroxyether of bisphenol a) nanofibrous membranes through inverse phase separation and inter-domain etherification, Materials, 4 (2011) 1967-1984.

[15] T.M. Brugo, G. Minak, A. Zucchelli, H. Saghafi, M. Fotouhi, An investigation on the fatigue based delamination of woven carbon-epoxy composite laminates reinforced with polyamide nanofibers, Proc Eng., 109 (2015) 65-72.

[16] H. Saghafi, T. Brugo, G. Minak, A. Zucchelli, Improvement the impact damage resistance of composite materials by interleaving Polycaprolactone nanofibers, Eng Solid Mech., 3 (2015) 21-26.

[17] L.V. Schueren, B. Schoenmaker, O.I. Kalaoglu, K. Clerk, An alternative solvent system for the steady state electrospinning of polycaprolactone, Eur. Polym. J., 47 (2011) 1256–1263.

[18] G. Minak, D. Ghelli, Design of a drop-weight machine for composite materials impact testing. In the proceedings of the 5th International congress of Croatian society of mechanics, Split, Croatia, 21-23 September 2006.

[19] G. Alfano, M.A Crisfield, Finite element interface models for the delamination analysis of laminated composites: Mechanical and computational issues. Int. J. Numer. Methods Eng., 50 (2001) 1701–1736.

[20] H.M. Deuschle, A. Puck, Application of the Puck failure theory for fibre-reinforced composites under three-dimensional stress: Comparison with experimental results, J. Compos. Mater., 47 (2012) 827-846.

[21]   J. Zhang, T. Yang, T. Lin, C.H. Wang, Phase morphology of nanofiber interlayers: Critical factor for toughening carbon/epoxy composites, Compos. Sci. Technol., 72 (2012) 256–262.

[22]   P. Akangah, S. Lingaiah, K. Shivakumar, Effect of nylon-66 nano-fiber interleaving on impact damage resistance of epoxy/carbon fiber composite laminates, Compos. Struct., 92 (2010) 1432–1439.

[23]   H. Saghafi, Mechanical behaviour of flat and curved laminates interleaved by electrospun nanofibers, Ph.D. Thesis, University of Bologne, Bologne, Italy, 2013.

[24]   H. Saghafi, R. Palazzetti, A. Zucchelli and G. Minak, Impact response of glass/epoxy laminate interleaved with nanofibrous mats, Eng. Solid Mech., 1 (2013) 85–90.

[25]   H. Saghafi, R. Palazzetti, G. Minak, A. Zucchelli, Effect of PAN nanofiber interleaving on impact damage resistance of GFRP laminates. In the proceedings of the 6th International Conference on Nanomaterials- Research and Application, Brno, Czech Republic, 5–7 November 2014.

Chapter 6

Self-powered pressure sensor based on the triboelectric effect and its analysis using dynamic mechanical analysis

Since 2012 there has been a rapid rise in the development of triboelectric nanogenerators due to their potential applications in the field of energy harvesting and self-powered sensors for vibrations, accelerations, touches, pressures and other mechanical motions. This study suggests a novel triboelectric nanogenerator based on the interaction between polyvinylidene fluoride and polyvinyl pyrrolidone submicron fibers. Polyvinylpyrrolidone is introduced as a new material for the TENG because of its tendency of losing electrons easily, while polyvinylidene fluoride is selected for its strong-electron attracting ability. Electrospinning is suggested as a fabrication method for the nanofibers due to its simplicity, versatility and low-cost. Furthermore, the chapter explores the possibility to use this triboelectric nanogenerator as a self-powered pressure sensor. For this purpose, the nanogenerator is subjected to dynamic mechanic analysis which produces controlled pressure forces applied with a certain frequency. This is the first work to suggest the use of dynamic mechanical analyzer to study the relation between the applied mechanical stimulus and the electric responses of the triboelectric nanogenerator. Eventually the sensitivity of the nanogenerator to different pressures is analysed. A directly proportional relationship is found between the pressure applied and the resultant voltage and current amplitudes. The developed nanogenerator reacts to pressure in real time and as a sensor it exhibits a very high sensitivity and low experimental error for repeated measurements. The main contributions of this study are the development of a novel nanogenerator based on the triboelectric effect between polyvinylidene fluoride and polyvinylpyrrolidone electrospun fibers and the investigation for its potential use as a self-power pressure sensor. Eventually, the paper

127

explores the advantages of dynamic mechanical analyser for pressure analysis.

6.1 Introduction

Pressure sensors are required in thousands of everyday applications as touchscreens, touchpads, microphones and medical devices. According to their mechanism to convert the mechanical energy into electricity can be generally divided into the following categories: piezoelectric [1-2], capacitive [3], optical [4] and resistive sensors [5]. Among these approaches, the sensors based on the piezoelectric effect have attracted the most attention because they are self-powered and do not need a battery or an external power supply to power the sensor. Therefore, they can be used as sustainable sensors able to work independently without any external power supply which results in important cost-savings. However, the fabrication of piezoelectric sensors is rather complicated and requires time-consuming and cost processing steps as annealing (a heat treatment to increase the crystallinity of the sensing material) and electrical poling (the application of a high electrostatic field at elevated temperature to align the dipoles). Hence, it is highly desired to find alternative ways to fabricate self-powered pressure sensors using a low-cost technology.

In the last years, triboelectric nanogenerators (TENGs) has been widely reported for their potential applications in the field of energy harvesting [6-10] and self-powered active sensors for touches [11], vibrations [12], accelerations [13], velocities [14], wind speeds [15] and environmental changes [16-17]. More importantly, TENGs can also be utilized as self-powered pressure sensors with the advantages of easy fabrication and low-cost processing technology. For example, the authors from [18] reported a TENG which can detect pressures in the range from 0 to 10 KPa with exceptional pressure sensitivity. Other works as [19] reported TENGs which can detect pressures at high pressure regimes (>10 kPa). Currently, most of the reported TENGs have been tested using a mechanical lineal motor [20], shaker [21], or vibration platform [22] which provides limited information about the

characteristics of the mechanical stimulus. In this regard, we believe that it is necessary to investigate alternative techniques to analyze the characteristics of the mechanical stimulus which can be used to have a better understanding of the nature of the electric responses and its relationship with the mechanical input.

In this chapter, we introduce a novel triboelectric nanogenerator based on polyvinylidene fluoride (PVDF) and polyvinylpyrrolidone (PVP) electrospun fibers and test its application as self-powered pressure sensor. For that purpose, the technique of dynamic mechanical analyzer (DMA) is used to analyze the mechanical stimulus applied to the triboelectric nanogenerator and the TENG electric responses are measured with the aim to assess the sensitivity of the resultant electric signals to changes in the pressure applied. The main advantages of dynamic mechanical analyzer are threefold: First, it provides the mechanical stimulus applied to the TENG in real-time as per example the magnitude of the pressures applied in the time domain. Second, it can be used to analyze of the relation between the mechanical input and the TENG electrical responses (e.g. the relationship between the deformation and the electric responses). Finally, it can evaluate the TENG performance under different environmental conditions as temperature and humidity. As per the authors' knowledge, this study presents the first attempt to use dynamic mechanical analyzer to analyze the behavior of a TENG as pressure sensor. This is beneficial as it can be used to understand more precisely the nature of the TENG electric responses. The experimental results indicated that the developed pressure sensor has a very high sensitivity and reproducibility. Actually, very few publications have reported the pressure sensitivity of TENGs [18-19] and it can be concluded that the developed sensor is more sensitive than most reported triboelectric sensors in the 0-2000 Pa detection range.

Previous publications have reported that the ability of the materials to lose or gain electrons during the triboelectrification plays an essential role in the performance of TENGs [23-25]. Logically, the further away the materials are separated in the triboelectric series, more electrons are exchanged which results in an increase of the triboelectric effect and higher electric outputs. In the design of the

triboelectric nanogenerator, PVDF and PVP fibers are selected because both materials are further away from each other in the triboelectric series, which is expected to enhance the performance of the TENG. To date PVDF fibers have been widely utilized to build TENGs [26-30] due to their strong tendency to attract electrons. This is due to the large composition of fluorine in PVDF that has the highest electronegativity among all the elements and the large active surface of the nanofibers. In this paper, we suggest PVP fibers as the other triboelectric mat to design the TENG due to their strong ability to lose electrons and large contact surface. To the best of our knowledge, only a few works [27, 31] have explored the potential of PVP fibers as positive triboelectric material.

It is also well known that the performance of the TENG is largely dependent on the contact area between the frictional materials [32]. Therefore, there has been much effort to prepare triboelectric mats with large contact active surface. For example, [33-34] used patterned films and nanoparticles in the TENGs to increase contact area between the frictional mats. In this study, we utilized nanofibers to design the TENG due to their higher specific area and very high roughness, which is expected to increase the generation of triboelectric charges. For this purpose, a simple method is suggested to fabricate fibers using the technique of electrospinning. This process has the advantages of cost effective mass production, scalability and simplicity of the design and fabrication from a wide variety of triboelectric nanofibers as per example nylon [35], polystyrene [36] or poly(methyl methacrylate) [37] to mention just a few. Furthermore, the very rough surface of the fibers fabricated via electrospinning can be used to improve the performance of the triboelectric nanogenerators. Although some authors have reported triboelectric nanogenerators fabricated via electrospinning [38-39], it is important to highlight the advantages of this fabrication method and the simplicity of this process for preparation of triboelectric nanogenerators at large scale using a low-cost production technology.

The rest of the paper is organized as follows: Section 2 describes the preparation of the polymer fibers using the electrospinning technique. Section 3 and 4 are dedicated to the characterization of the produced polymer fibers. Section 5

explains the fabrication process for the triboelectric nanogenerator using the fibers. The DMA experiments carried out to assess the sensitivity of the TENG to pressures are presented in Section 6. Section 7 presents and discusses the experimental results in detail. Eventually some conclusions are offered in section 8.

6.2 Preparation of the PVDF and PVP fibers

This section explains the procedure used to prepare the fibers used in the triboelectric nanogenerator. The submicron fibers were produced using the technique of electrospinning due to its low cost, scalability, and simplicity for the fabrication of a wide variety of triboelectric mats. Furthermore, the large surface area and rough surface of the fibers produced via electrospinning can generate higher density of triboelectric charges through the triboelectric effect, resulting in larger electric outputs [27]. Thus, an increment of the thickness of the electrospun membranes (e.g. by using a large collection time in the electrospinning process), it is expected to increase the TENG electric responses up to a certain point. Fig. 6.1 illustrates a schematic description of the electrospinning process used to prepare the nanofibers for the TENG.
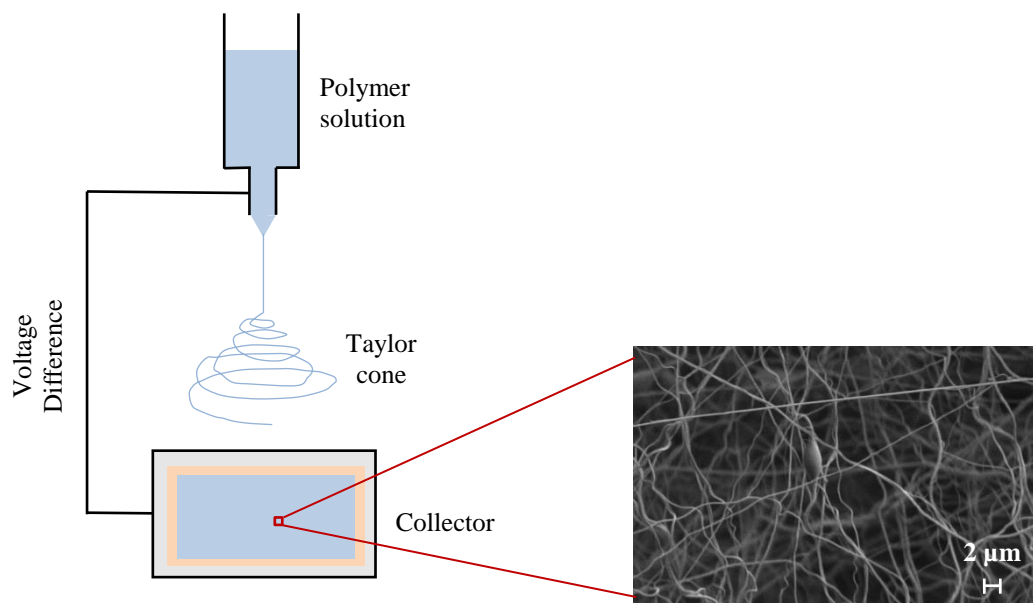

Figure 6.1 Schematic diagram of the electrospinning process. The inset shows a SEM image of the electrospun fibers.

For preparing the PVDF fibers, polyvinylidene fluoride pellets with a molecular weight of 275,000 g mol-1, N, N- dimethylformamide (DMF) and acetone solvents were used as received. Initially, a chemical solution was prepared by dissolving 2g PVDF pellets in 10 ml solvent mixture of N, N- dimethylformamide and acetone (4/6). After, the chemical solution was heated on a hot plate at 70 °C while being actively stirred to speed up the dissolution process. Finally, the homogeneous solution was inserted into a plastic syringe to be spun using the following operation conditions: A high voltage of 15 kV, a spinning distance of 15 cm and a feed rate of 1 ml/h. During the electrospinning, the equipment used (Nanon-01A) is equipped with a 21 G steel needle (inner diameter = 0.8 mm) and a static collector. As a result, membranes of PVDF submicron fibers with a thickness of approximately 2 mm are obtained.

Regarding the preparation of PVP fibers, PVP (MW= 360,000 g mol-1, Sigma Aldrich) powder was used as polymer and ethanol was used as solvent. Firstly, a chemical solution was prepared by dissolving the PVP powder in a solution of ethanol at a concentration of 10% w/v. Secondly, the chemical solution is transferred to a 5 ml plastic syringe to be spun using the following conditions: applied voltage 18 kV, feed rate 0.5 ml/h, spinning distance 12 cm, 21-gauge needle and static collector. Finally, membranes of PVP submicron fibers with a thickness of around 1 mm are prepared.

The thickness of the membranes of nanofibers plays a critical role on the performance of the nanogenerator. This behaviour is investigated by N. Cui et al. [47], where it is reported that the generation of triboelectric charges is dependent on the thickness and porosity of the nanostructured membranes. From the results of this paper, it can be clearly observed that membranes with higher thickness increases the generation of triboelectric charges up to a saturation value. This is the reason why we have used membranes with a thickness of a few milimeters instead of ultra-thin membranes of nanofibers in the microscale.

6.3 Characterization of PVDF and PVP fibres

The aim of this section is to analyze the morphology of the fibers used in the triboelectric nanogenerator. As stated above, the performance of a TENG is affected by the contact area between the frictional materials. Additionally, the internal spaces of the triboelectric layers (e.g. porosity) also affect positively the output performance of the TENG [40]. It should be said that, there has been much effort to prepare triboelectric mats with large active surface area and porosity [18-20]. One of the possible methods to prepare mats with high active surface area and porosity is to use ultra-thin fibers in the TENG.

(a)   (b)

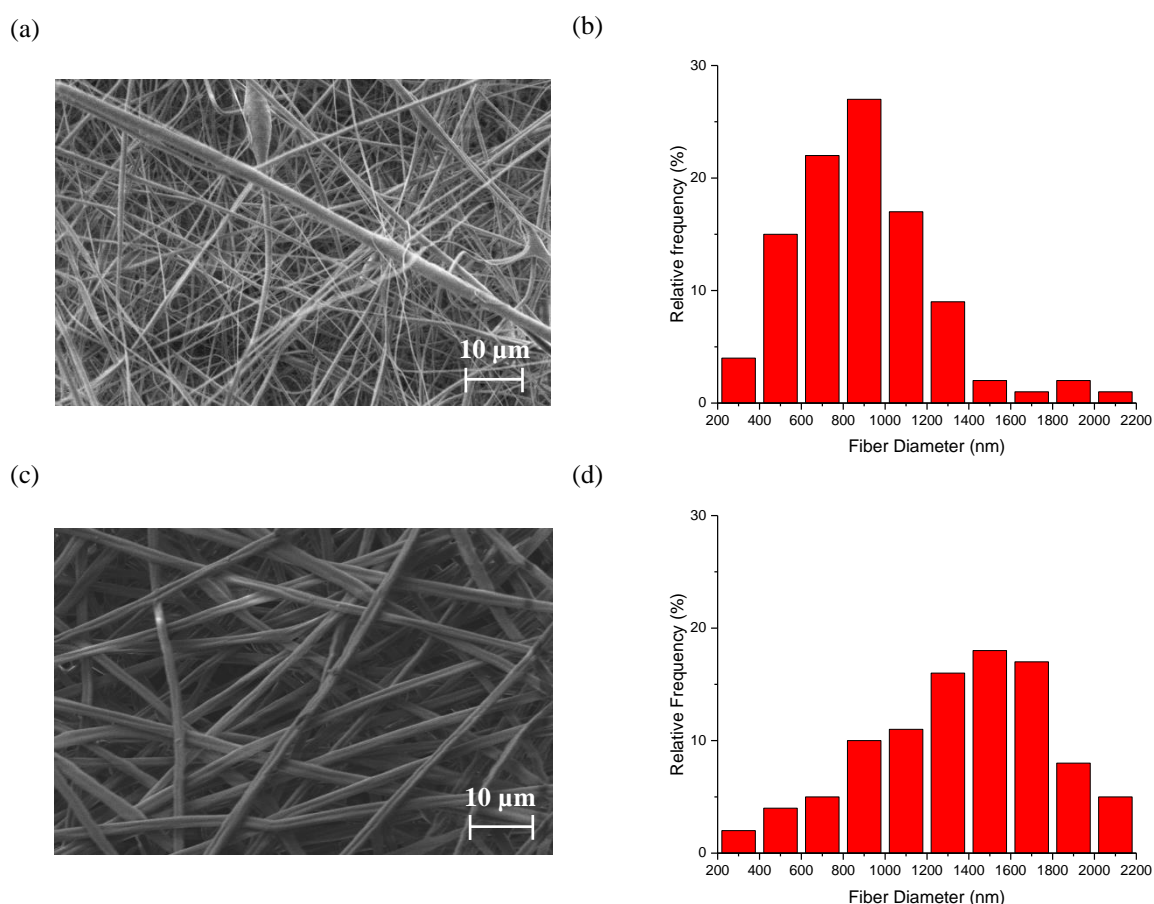(c)   (d)

Figure 6.2 Analysis of the morphology for the fibers used in the triboelectric nanogenerator: (a) SEM image of electrospun PVDF fibers, (b) fiber diameter distribution of PVDF fibers, (c) SEM image of electrospun PVP fibers and (d) fiber diameter distribution of PVP fibers. The SEM images were obtained using EVO MA15 scanning electron microscope at an accelerating voltage of 5 kV and probe intensity of 291 pA.

The morphology of the fibers was characterized using a scanning electron microscope (SEM) images. From the SEM images, the diameters of 100 fibers were measured by using the software J 1.45s. Then, the fiber diameter distribution is calculated by counting the number of fibers who possess diameters in the range selected. The analysis of the morphology for the fibers used in the TENG is presented in Fig. 6.2.

The SEM image of the PVDF submicron fibers is given in Fig. 6.2 (a) and the fiber diameter distribution is presented in Fig. 6.2 (b). The SEM image shows good quality submicron fibers with different sizes distributed randomly in the membrane. The submicron fibers are separated from each other and have a smooth surface with a few bead defects. The fiber diameter histogram shows a normal distribution which is skewed to the right thus indicating that the diameter of the spun fibers is not uniform. The histogram shows that the fibers diameter is somewhere between 800 and 1000 nm with a probability of about 28 %. The average diameter of the PVDF nanofibers was 1100 nm with a standard deviation of 370 nm.

The SEM image of PVP fibers is given in Fig. 6.2 (c) and the histogram of fiber diameter distribution is displayed in Fig. 6.2 (d). The fibers obtained are distributed in random directions without beads and other defects as indicated in SEM image. The histogram shows a normal distribution with fiber diameters between 200 and 2200 nm. The fiber diameter distribution is skewed to the left indicating that the fibers diameter is between 1400 and 1600 nm with a probability of about 17%. The average fiber diameter was 1400 ± 470 nm, indicating that PVP fibers are thicker than PVDF fibers. The wide distribution of diameters in both membranes of spun fibers (200 to 2200 nm) is explained by the Taylor cone formed during the electrospinning. As illustrated in Fig. 6.1, the polymer jet is only stable close to the tip of needle and after that, it becomes unstable changing in periodic directions.

6.4 Analysis of the crystalline phase in PVDF

PVDF is ascribed to the piezoelectric effect when there is betha crystalline phase and the ferroelectric domains of β-phase are well aligned [41]. However, PVDF is also attributed to the triboelectric effect due to their strong-electron attracting ability [26-30]. This behavior is attributed to the high percentage of fluorine in PVDF that has the highest electronegativity among all the elements which results in a strong tendency to gain negative charges when in contact with almost any other material and the large active surface area of the fibers. In this section, we investigate if the nature of the electrical signal detected from PVDF nanofibers is due to the piezoelectric effect, the triboelectric effect or a combination of both.
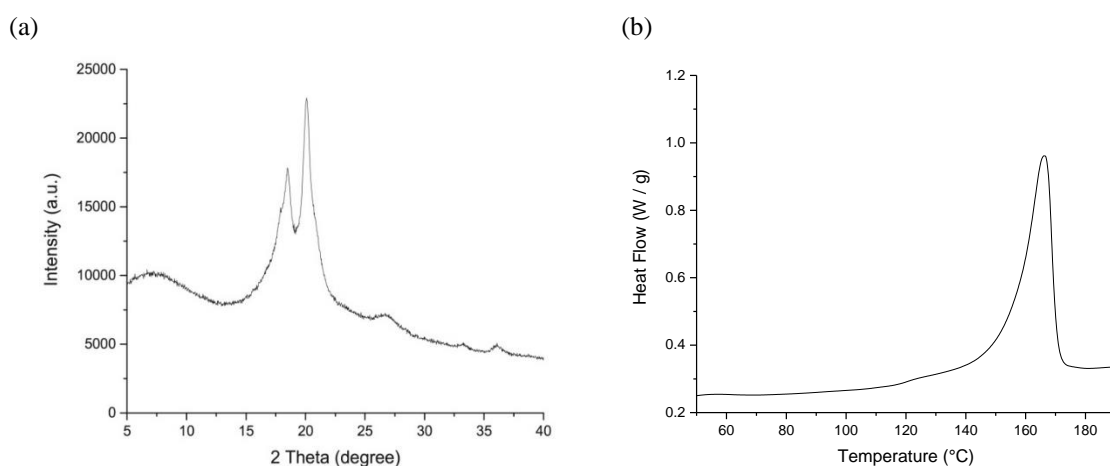
(a) (b)

Figure 6.3 Identification of the crystalline phase in PVDF fibers: (a) XRD pattern obtained on a PANalytical X-ray diffractometer with Cu radiation of 1.54 A° in reflection mode using samples scanned in the 2θ range of 5° to 40° with a step size of 0.05°. (b) DSC curve obtained using Q200 differential scanning calorimeter from TA instruments using samples heated in a temperature range from 30 to 200 °C at the heating rate of 10 °C/min.

It is well known that the PVDF piezoelectric properties depend on the crystalline phase. The α crystalline phase is non-polar due to the antiparallel packing of the dipoles and in this phase PVDF exhibits no piezoelectric properties. However, the β crystalline phase is polar and, in this phase, PVDF can exhibit a strong piezoelectric behavior when the ferroelectric domains of the β-phase are well aligned (e.g. by the application of high electric field at elevated temperature). To find out if

the electric response of the PVDF nanofibers is due to the piezoelectric effect X-ray diffraction (XRD) and differential scanning calorimetry (DSC) were carried out to identify the crystalline phase of the polyvinyl fluoride fibers. The results for the analysis of the crystalline phase are shown in Fig. 6.3.

Fig. 6.3 (a) shows the XRD spectra of the PVDF fibers. The intense peaks at 2θ = 18.53°and 20.08° correspond to the (0 2 0) and (0 1 0) planes of the alpha crystalline phase. Furthermore, the spectra shows other two small peaks around 27° and 36° associated with (0 2 1) and (2 0 0) planes of the phase α. As reported in [42], the diffraction peaks for α and γ phase are almost coincident in the XRD spectra and therefore, there has been some confusion between both crystalline phases. For this reason, DSC is used as complementary technique to assure that alpha is the crystalline phase of PVDF nanofibers. This technique allows to clearly distinguish between the α phase (the polymer melts in the range from 167 to 172 °C) and the γ phase (the melting point is about 179 to 180 °C) [42]. The DSC results for the PVDF nanofibers are shown in Fig. 6.3 (b). The DSC curve shows an endothermal peak at 167.1 °C confirming that the crystalline phase of the PVDF is the non-piezoelectric α-phase. In conclusion, the XRD and DSC results indicate that the crystalline phase of PVDF is the non-piezoelectric alpha phase. Thus, the influence of piezoelectricity on the electric output of the PVDF fibers is negligible and the electric signal detected from the PVDF fibers is only due to the triboelectric effect.

6.5 Fabrication of the TENG

This section describes the process used to fabricate the triboelectric nanogenerator using the technique of electrospinning [43]. This method was chosen because of its simplicity, versatility and low-cost. Furthermore, the rougher surface of the fibers produced via electrospinning increases the effective contact area improving the output performance of the triboelectric nanogenerator [38].

The assembly process of the triboelectric nanogenerator is depicted in Fig. 6.4. Firstly, membranes of polyvinyl fluoride and polyvinyl pyrrolidone were electrospun on copper films as shown in Fig. 6.4 (a). The role of the copper films is to collect the submicron fibers during the electrospinning and act as electrodes for the triboelectric nanogenerator. PVDF and PVP fibers served as the sensor frictional mats due to strong tendency to gain and lose electrons. Secondly, the membranes of interconnected PVDF and PVP fibers are face to each other to assemble the triboelectric nanogenerator (Fig. 6.4 (b)). Finally, the nanogenerator is sealed with polyethylene terephthalate film which acts as protection layer for the nanofibers and avoids changes in the electric responses due to humidity variations. This is also important to prevent the deliquescence of PVP nanofibers. Fig. 6.4 (c) displays a digital photograph of the nanogenerator with the small size of 40 x 40 x 3.5 mm and a low weight of 4.93 g. Fig. 6.4 (b) illustrates the structural design of the triboelectric nanogenerator. The nanogenerator consist of two sections: (i) PVDF electrospun fibers deposited on copper electrode form the top section and (ii) PVP submicron fibers adhered on copper electrode form the bottom section. As it can be appreciated, the polyvinylidene fluoride fibers are located at the top side of the nanogenerator, while the PVP fibers are placed at the bottom side. These materials are chosen for their high tendency to gain and lose triboelectric charges respectively.
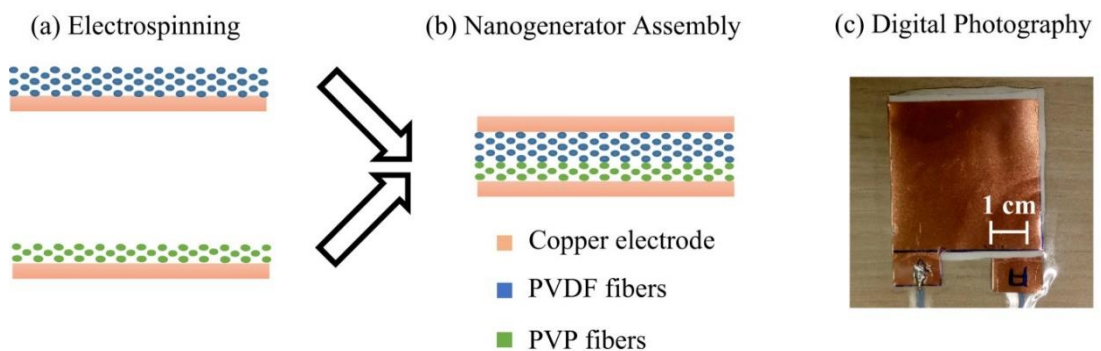

Figure 6.4 Schematic illustration of the fabrication process for the triboelectric nanogenerator: (a) Preparation of the PVDF and PVP fibers via electrospinning. (b) Structure of the fully assembled triboelectric nanogenerator (c) Digital photographic of the as-fabricated TENG.

6.6 Working principle of the TENG

The electricity generation process of the triboelectric nanogenerator is schematically described in Fig. 6.5. The working mechanism is based on the coupling effect between the triboelectrification and electrostic induction. It is worth to note that the operating principle of the TENG is self-powered. But as in most practical occasions the oscilloscope and multimeter used to measure the sensor electric signals require an external power supply.
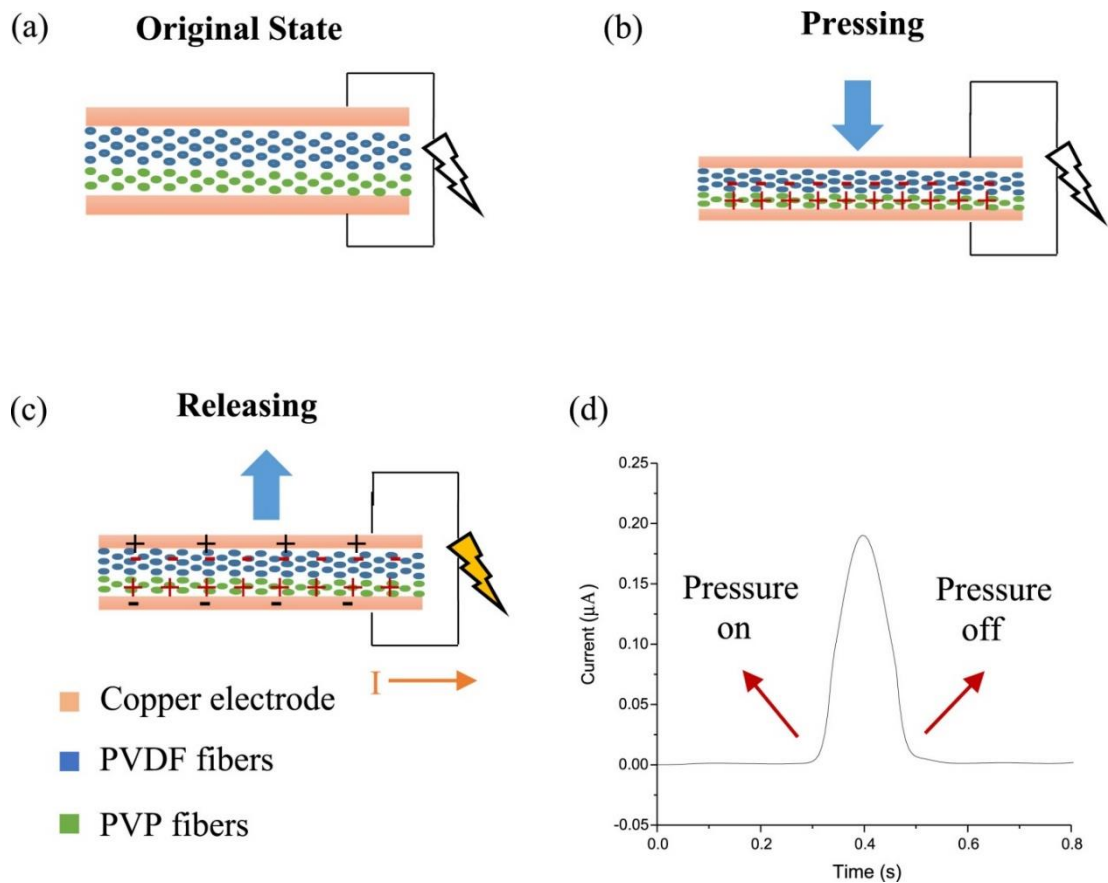

Figure 6.5 Simplified description of the generation of electricity [44-45]: (a) the original position of the nanogenerator. (b) Under a pressure, the fibers of PVDF and PVP are brought into contact which results in the generation of charges with opposite signs. (c) Once the pressure is withdrawn, the charges of PVDF and PVP are separated which results in a strong potential difference which drives the electrons from the bottom to the top electrode. (d) The variation of current in time domain due to one contact-separation caused by one finger tap.

In the original state, there is no generation of triboelectric charges and no electric potential difference between the two electrodes as indicated in Fig. 6.5 (a). When a pressure is applied to the top of the nanogenerator, the PVDF and PVP submicron fibers are brought into contact with each other, which results in the generation of triboelectric charges with opposite signs as illustrated in Fig. 6.5 (b). Due to the strong electron-attracting ability of PVDF, electrons are injected from the PVP into the PVDF fibers, leaving negative charges on the PVDF fibers and positive charges on PVP fibers. As the pressure is released, the contacting surfaces will revert to their original positions which results in the separation of the positive and the negative charges. At this stage, the PVP and the PVDF fibers are oppositely charged and the subsequent separation of charges induces a dipolar moment and strong electrical potential difference between the electrodes which causes electrons flow through external loads from the bottom electrode to the top electrode producing an electrical signal as indicated in Fig. 6.5 (c). Finally, the generation of triboelectric charges stops, and the electrons flow back producing an opposite sign electrical signal. Thus, the triboelectric nanogenerator reverts to its original state. Fig. 6.5 (d) shows the variation of current as a function of the time due to one contact-separation caused by a finger pressure.

6.7 Dynamic Mechanical Analysis

Dynamic mechanical analysis (DMA; Q800; TA Instruments) is used to evaluate the effect of the pressure on the electrical responses of the triboelectric nanogenerator. For this aim, ten different pressures in the range between 200 Pa and 2000 Pa are subjected to the nanogenerator using dynamic mechanical analysis. Simultaneously, the voltage and current output signals of the device caused by the different pressures are measured using a Tektronix 2012B commercial oscilloscope and Agilent 34410A digit multimeter. The main idea is to find out if the amplitude of the electric responses of the nanogenerator are dependent on the pressure applied, which is necessary to demonstrate the potential of the novel TENG as self-powered pressure sensor.

A schematic description of the experimental set-up is shown in Fig. 6.6. The pressures are applied on the top side of the TENG in a direction perpendicular to the device as shown in the figure. The pressures are generated by a constant force perpendicular to the nanogenerator mounted in DMA equipment and applied on a circular area of 50.24 cm^2. During the test, the pressure applied was varied in the range from 200 to 2000 Pa with increments of 200 Pa. Each pressure application was repeated five times to assess the reproducibility of the electric responses for repeated applications of the same pressure. The electric outputs are shown in the results section where the effect of the pressure applied on the electric response of the nanogenerator is analyzed. From this test, the voltage and current generated by the various pressures are investigated.
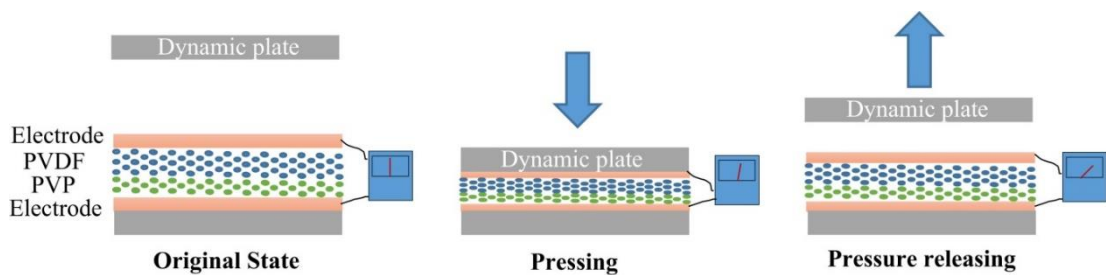

Figure 6.6 A schematic diagram of the experimental set-up to measure the electric output of the nanogenerator to pressures applied through dynamic mechanical analyzer (DMA).

As stated above, the use of the Dynamic mechanical analyzer (DMA; Q800; TA Instruments) is suggested to supply periodically applied pressures to the nanogenerator. The main benefit of using this instrument is that the mechanical stimulus applied on the nanogenerator can be monitored and record in real time. Furthermore, although this characteristic was not used in this study, this technique can also evaluate the performance of TENGs under different environmental conditions as temperature and humidity which is not possible based on conventional techniques. This can be potentially used to have a deeper understanding of the nature of the TENG electric responses.

6.8 Results and discussion

This section presents all the results obtained from the experiment described in Section 6.7. As mentioned in section above, dynamic mechanical analysis was conducted in order to evaluate the ability of the developed triboelectric nanogenerator to measure pressures. The idea is to evaluate the sensitivity of the resultant electricity signals to changes of the applied pressure with the aim to investigate the effect of the pressure on the electric output of the TENG.

Fig. 6.7 (a) shows the time history of the pressures applied to the nanogenerator in the range from 200 Pa to 2000 Pa. The pressure varied with an increment of 200 Pa and each pressure was applied for five cycles. Fig. 6.7 (b) shows the corresponding electric response of the TENG measured in terms of current. The results indicate that the current output increased from 0.4569 ± 0.0003 µA to 1.3939 ± 0.0016 µA as the pressure increased from 200 Pa to 2000 Pa. Fig. 6.7 (c) shows the electric responses of the TENG measured in terms of voltage. It can be seen that the voltage output goes up from 5.36 ± 0.09 to 13.24 ± 0.09 V when the pressure changes between 200 Pa and 2000 Pa. It can be concluded from these results, that the performance of the TENG is strongly affected by the magnitude of the pressure applied, producing a higher voltage and current output when the nanogenerator is subjected to a higher pressure. The device exhibited a peak-to-peak voltage and maximum current output of 13.24 V and 1.3939 µA, respectively under a mechanical compression of 2 kPa. The increase of the electric output with the increase of the pressure is related to the increment of effective contact between the frictional materials under a stronger pressure. At a small pressure, the rough surfaces of electrospun fibers prevent full contact between the fibers of PVDF and PVP. Thus, small areas of PVDF fibers are in contact with PVP fibers which results in a very few amounts of triboelectric charges generated and minimum electric outputs. When a stronger pressure is applied, the deformation of the device increases producing larger contact area between the PVDF and PVP fibers and consequently, more charges are generated what results in higher voltage and current outputs.
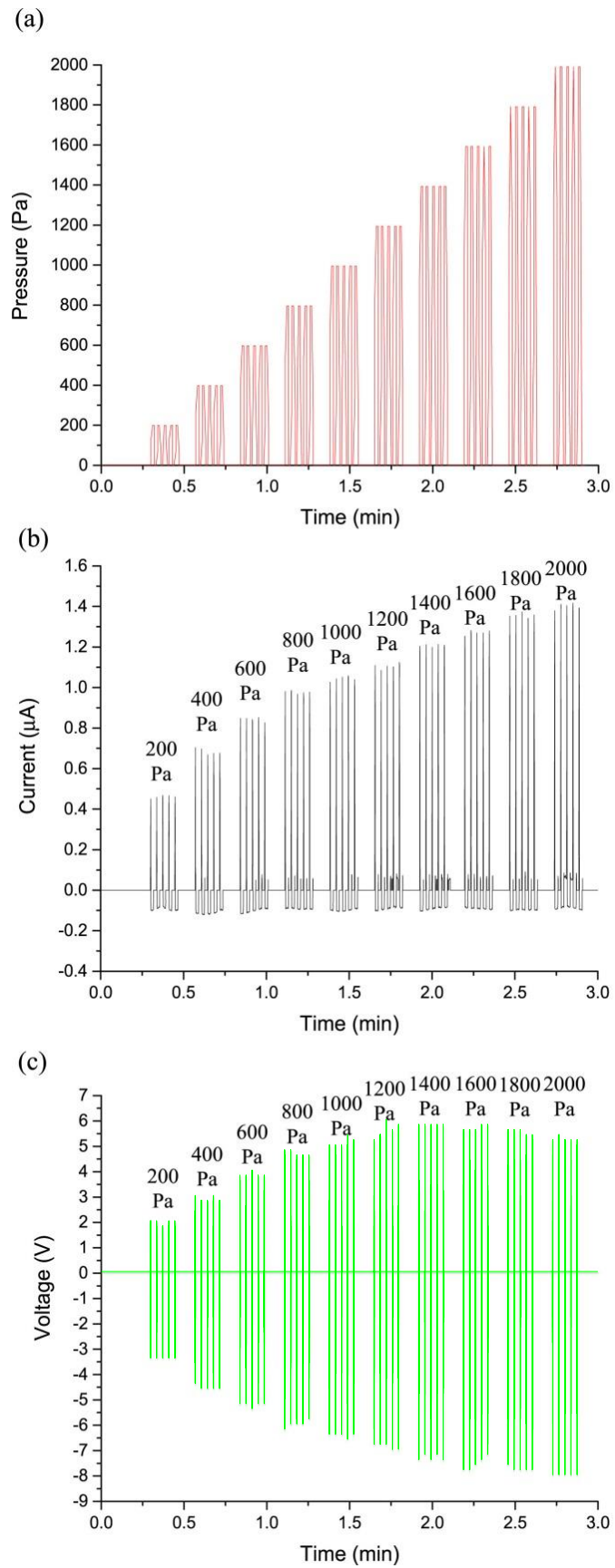
Figure 6.7 Influence of pressures on the triboelectric nanogenerator. (a) Pressures applied through DMA equipment. (b) Current output measured using a digital multimeter and (c) Voltage responses measured using a commercial oscilloscope.

Fig. 6.8 (a) shows the maximum values of the current output as a function of the pressures. The results given are the average maximum current output and the corresponding standard deviations for the five cycles performed for each pressure. From Fig. 6.8 (a) it can be appreciated that the relationship between the pressure and the maximum current can be interpolated with two straight lines one in the region from 200 to 800 Pa and another one between 800 and 2000 Pa. It is noticed that the bi-linear approximation between electric output and the pressing forces exhibits excellent linearity ($R^2 \simeq 0.99$) for the two regions. The pressure sensitivity is 0.94 nA/Pa for the low-amplitude pressure region from 200 to 800 Pa and it decreases to 0.37 nA/Pa for the pressure amplitude above 800 Pa.

Fig. 6.8 (b) shows the average voltage amplitude and the corresponding standard deviations for five repetitions as a function of the pressures. The results display that the output voltage increases at higher pressure and finally saturates at 13.2 V, when the pressure is 1600 Pa. This can be explained by the fact that higher pressure results in more contact area and hence increase the amount of triboelectric charges of the TENG. As a result, higher output voltage is obtained until the triboelectric nanogenerator saturates at 1600 Pa and 13.2 V. It can be observed that the relationship between the pressure and the average voltage exhibits three distinct regions. When pressures are below 800 Pa, the relationship voltage-pressure is nearly linear ($R^2 = 0.996$) and the pressure sensitivity is 8.8 mV/Pa. In the region between 800 Pa and 1400 Pa, the pressure sensitivity decreases up to 3.9 mV/Pa and the relation between the generated voltage and the pressure is still very close to linear ($R^2 = 0.989$). In the region beyond 1600 Pa, the TENG reaches a saturation point. On the basis of these results, it can be concluded that the TENG exhibits a very sensitive response to applied pressures in the range from 200 to 1600 Pa.

Currently the electric response of the developed triboelectric nanogenerator to different pressures in the range from 200 to 2000 Pa was tested. The results obtained in Fig. 6.8 (a) and (b) reveal that the triboelectric nanogenerator is more sensitivity to pressures in the low-pressure region. This is in good agreement with previous results.

For example, the triboelectric sensor published in [18] shows a pressure sensitivity of 44 mV/Pa for pressures below 150 Pa. However, the sensitivity decreases to 0.5 mV/Pa at higher pressures. The developed triboelectric nanogenerator shows a pressure sensitivity of 8.8 mV/Pa for pressures below 800 Pa while the sensitivity decreases to 3.9 mV/Pa for pressures in the range from 800 to 1600 Pa. Thus, it can be concluded that the triboelectric nanogenerator has a very high sensitivity in this range of pressures. It can also be observed that the current-pressure and the voltage-pressure relationships show a different bilinear trend. This can be explained by the fact that voltage and current are different characteristics. As mentioned in [46], the current is dependent of the capacitance (C) and voltage (V) of the TENG while the voltage is dependent of the density of triboelectric charges (θ), the separation distance (d) and the vacuum permittivity (ε_o). We believe that these fundamental basics can explain the differences between the current-pressure and voltage-pressure relationships. In any case, further research is needed to fully understand the differences between both relationships.
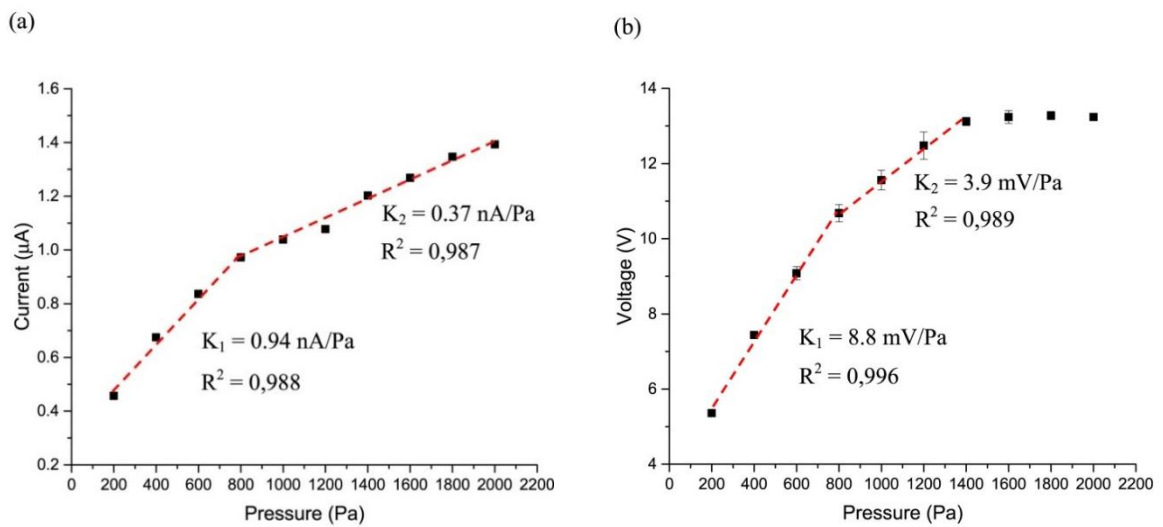

Figure 6.8 Influence of pressures on the triboelectric nanogenerator. (a) current and (b) voltage output as a function of the pressures in the range from 200 to 2000 Pa.

Furthermore, the reproducibility of the experiments is tested to determinate the stability of the electric responses for repeated applications of the same pressure. This experiment is carried out to to find out if the electrospun fibers can withstand the pressure without being damaged which will ensure the experiment stability and

reproducibility. In order to estimate the error which is due to variations in the measurement each pressure was repeated ten times. Then the mean electric values, standard deviations and coefficient of variations over the ten realizations for each of the maximum current outputs and peak-to-peak voltages were calculated.

Table 6.1 shows the mean values, the standard deviations and coefficient of variation for the voltage and the current outputs as a function of the pressure. It shows the average voltage and current measured for each of the pressures. It can be observed that the electric outputs are affected by the pressure applied in the same way as demonstrated in figure 6.8. In addition, the standard deviations for the ten measurements of voltage and current are less than 0.3 V and 0.02 µA respectively and the average coefficients of variation are 1.8 % and 1.7 % respectively. Therefore, these results indicate that the miniscule changes in the voltages and current outputs can be considered within the range of the experimental error.

Pressure (Pa)	Mean Voltage (V)	S.D. Voltage (V)	C.V. Voltage (%)	Mean Current (µA)	S.D. Current (µA)	C.V. Current (%)
200	5.3	0.1	2.5	0.44	0.02	4.71
400	7,5	0.1	1.3	0.68	0.01	1.65
600	9.2	0.2	2.7	0.84	0.01	1.55
800	10.6	0.2	2.3	0.98	0.01	0.72
1000	11.5	0.2	1.8	1.06	0.02	1.67
1200	12.4	0.3	2.2	1.11	0,02	1.79
1400	13.1	0.1	1.1	1.19	0.02	1.80
1600	13.1	0.2	1.6	1.27	0.01	0.96
1800	13.1	0.2	1.6	1.36	0.01	1.05
2000	13.2	0.1	0.9	1.41	0.02	1.22

Table 6.1 Operational stability of TENG after ten repetitions for each pressure. Average value, standard deviation, and coefficient of variation (in percent) for voltage and current.

In conclusion, it can be said that the electric outputs of the developed TENG are very stable and there is almost no change in the electric response of the nanogenerator under repeated applications of the same pressure. This indicates that the electrospun fibers of the nanogenerator are robust and not damaged due to the

repeated application of the pressures, and therefore, the developed triboelectric nanogenerator can be used as a pressure sensor.
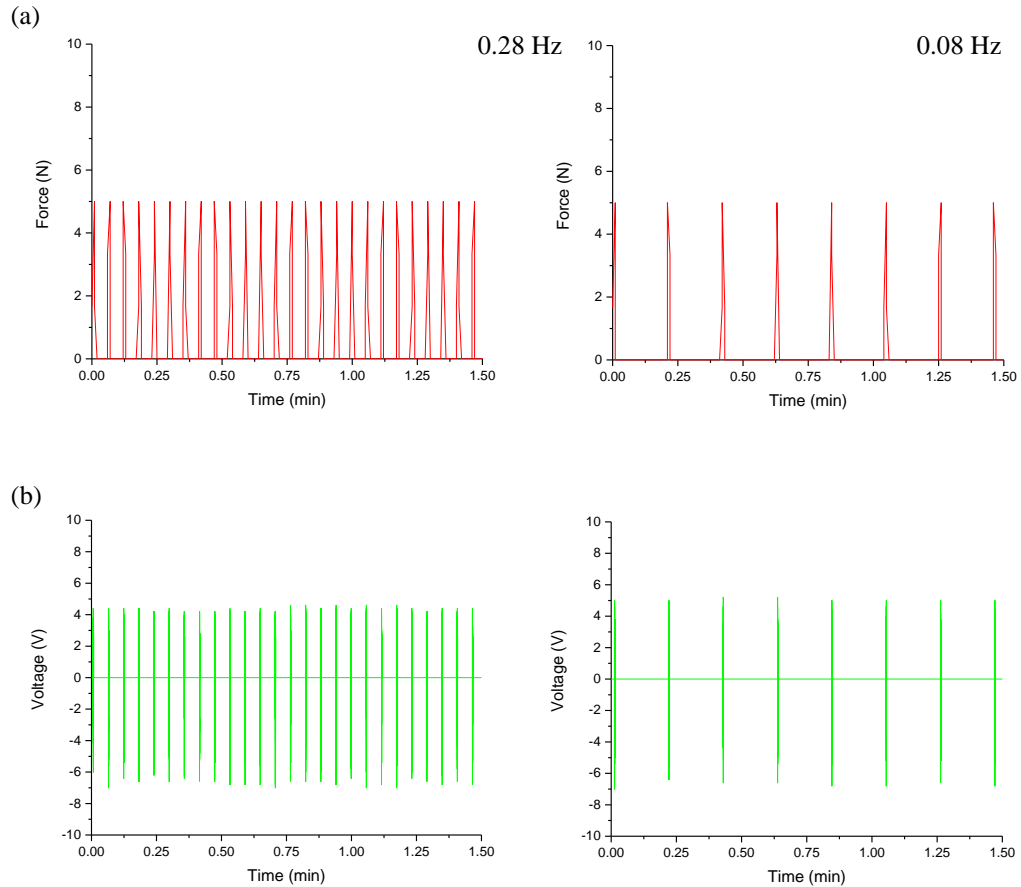
(a)

(b)

Figure 6.9 Influence of pressing frequency on the electric output of the TENG. (a) 5N pressing forces applied using DMA at a given frequency of 0.28 Hz and 0.08 Hz. (b) Voltage responses measured using a commercial oscilloscope.

The effect of the frequency on the electric response of the nanogenerator was also investigated using the technique of dynamic mechanical analysis. In this experiment, the pressing force is kept constant at 5 N while the frequency of the pressure force was changed from 0.08 Hz to 0.28 Hz. Figure 6.9 (a) shows the 5 N periodic forces applied on the TENG through the technique of dynamic mechanical analysis at two difference frequencies 0.08 Hz=4.8rpm and 0.28 Hz=16.8rpm. Figure 6.9(b) reveals the voltage responses of the nanogenerator under the two pressing frequencies. It can be appreciated from the figures that the current responses contain the same frequency as the mechanical stimulus. Therefore, it can be concluded that

the electric responses of the developed nanogenerator contains the same frequencies than the applied mechanical stimulus.

6.9 Conclusions

In summary, this research introduces a novel triboelectric nanogenerator prepared by PVDF and PVP fibers and tests its application as self-powered sensor, which detects and follows the pressure changes in real time.

An electrospinning method is used to fabricate the membranes of submicron fibers used in the TENG. This method was chosen because it is one of most economic, versatile and simple ways to prepare nanofibers. Additionally, electrospinning is a scalable industrial process and thus makes a promising alternative for fabrication of such devices on larger scale using a low-cost technology.

This study also establishes the working mechanism of the developed TENG and more precisely that it is associated to the triboelectric effect between the two materials used, rather than the piezoelectric properties of PVDF. The results from this study confirm the lack of piezoelectricity in the electric output produced by the TENG, which is concluded from the alpha crystalline structure of PVDF nanofibers. It is thus confirmed that the application of the developed device as a transducer is due to the triboelectric effect between PVDF and PVP fibres, caused by their strong ability exchange electrons which is enhanced by their large contact surface.

The effect of mechanical stimulus on the TENG electric output was analyzed through using dynamic mechanical analysis. This is the first study to suggest DMA for the purpose. It is the authors' opinion that this method can be beneficial because it can analyze the characteristics of mechanical stimulus applied to the TENG in real time (e.g. the magnitude of the pressure in the time domain) which can be used to

enhance our understanding about the electric responses of the TENG. The DMA results show a direct relationship between the mechanical stimulus applied to the TENG and the electric responses, which demonstrates the sensitivity of the device. The self-powered pressure sensor shows a very high sensitivity of 8.8 mV/Pa in the low-pressure region (< 800 Pa) while the sensitivity decreases to 3.9 mV/Pa at higher pressures. There are currently rather few publications which report the pressure sensitivity of TENGs [17], but this sensitivity is higher than the sensitivity of most reported triboelectric sensors.

Finally, the reproducibility of the electric output of the nanogenerator under the same pressure is demonstrated. The results show that the output of the fabricated TENG was very stable and the electric response of the TENG exhibits almost no change for repeated applications of the same pressure. This is a very important property for the potential applications of the developed TENG as a self-powered pressure sensor.

In our view, we believe this work will serve as an excellent initial step toward the development of a potential TENG which can be used as self-powered sensor when dynamical pressures are applied. At the same time, this work demonstrates the potential applications of TENGs for pressure monitoring with advantages of being self-powered, environmentally friendly, maintenance-free, easy fabrication and low-cost as compared to conventional sensors.

References

[1]   S. Joshi, G.M. Hedge, M.M. Nayak, K. Rajanna, A novel piezoelectric thin film impact sensor: Application in non-destructive material discrimination, Sens Actuators A Phys. 199 (2013) 272-282.

[2]   S. Hannah, D. Uttamchandani, H. Gleskova, Response of P(VDF-TrFE) Sensor to Force and Temperature, IEEE Conference on Ph.D. Research in Microelectronics and Electronics (PRIME), (2015) 369-372.

[3]   C. Metzger et al., Flexible-foam-based capacitive sensor arrays for object detection at low cost, Appl. Phys. Lett. 92 (2008) 013506.

[4]   J.S. Heo, J.H. Chung, J.J. Lee, Tactile sensor arrays using fiber Bragg grating sensors, Sens. Actuators A Phys. 126 (2006) 312-327.

[5]   H. Zhang, E. So, Hybrid resistive tactile sensing. IEEE Trans. Syst. Man Cybern. Part B, 32 (2002) 57-65.

[6]   W. Yang, J. Chen, G. Zhu, J. Yang, P. Bai, Y. Su, Q. Jing, X. Cao, Z. L. Wang, Harvesting Energy from the Natural Vibration of Human Walking, ACS Nano, 7 (2013) 11317-11324

[7]   W. Yang, J. Chen, Q. Jing, J. Yang, X. Wen, Y. Su, G. Zhu, P. Bai, Z. L. Wang, 3D Stack Integrated Triboelectric Nanogenerator for Harvesting Vibration Energy, Adv Funct Mater. 24 (2014) 4090-4096.

[8]   Y. Su, X. Wen, G. Zhu, J. Yang, J. Chen, P. Bai, Z. Wu, Y. Jiang, Z. L. Wang, Hybrid triboelectric nanogenerator for harvesting water wave energy and as a self-powered distress signal emitter, Nano Energy, 9 (2014) 186-195.

[9]   T.C. Hou, Y. Yang, H. Zhang, J. Chen, L.J. Chen, Z.L. Wang, Triboelectric nanogenerator built inside shoe insole for harvesting walking energy, Nano Energy, 2 (2013) 856-862.

[10]   H. Zhang, Y. Yang, Y. Su, J. Chen, K. Adams, S. Lee, C. Hu, Z. L. Wang, Triboelectric nanogenerator for harvesting vibration energy in full space and as self-powered acceleration sensor, Adv Funct Mater, 24 (2014) 1401-1407.

[11]   Y. Yang, H.L. Zhang, Z.H. Lin, Y.S. Zhou, Q.S. Jing, Y.J. Su, J. Yang, J. Chen, C.G. Hu, Z.L. Wang, Human Skin Based Triboelectric Nanogenerators for Harvesting Biomechanical Energy as Self-Powered Active Tactile Sensor System, ACS Nano, 7 (2013) 9213-9222.

[12] Q. Liang, Z. Zhanga, X. Yan, Y. Gu, Y, Zhao, G. Zhang, S. Lu, Q. Liao, Y. Zhang, Functional triboelectric generator as self-powered vibration sensor with contact mode and non-contact mode, Nano Energy, 14 (2015) 209-216.

[13] C. Xiang, C. Liu, C. Hao, Z. Wang, Z. Wang, L. Che, X. Zhou, A self-powered acceleration sensor with flexible materials based on triboelectric effect, Nano Energy 31 (2017) 469-477.

[14] Q. Jing, G. Zhu, W. Wu, P. Bai, Y. Xie, R.P.S. Han, Z.L. Wang, Self-powered triboelectric velocity sensor for dual-mode sensing of rectified linear and rotary motions, Nano Energy, 10 (2014) 305-312.

[15] Y. Xi, H. Guo, Y. Zi, X. Li, J. Wang, J. Deng, S. Li, C. Hu, X. Cao, Z.L. Wang, Multifunctional TENG for Blue Energy Scavenging and Self-Powered Wind-Speed Sensor, Adv. Energy Mater., 7 (2017) 1602397.

[16] Y. Su, G. Xie, S. Wang, H. Tai, Q. Zhang, H. Du, H. Zhang, X. Du, Y. Jiang, Novel high-performance self-powered humidity detection enabled by triboelectric effect, Sens Actuators B Chem., 251 (2017) 144-152.

[17] Z.H. Lin, G. Zhu, Y.S. Zhou, Y. Yang, P. Bai, J. Chen, Z.L. Wang, A self-powered triboelectric nanosensor for mercury ion detection, Angew. Chem. Int. Ed., 52 (2013) 5065-5069.

[18] G. Zhu, W.Q. Yang, T. Zhang, Q. Jing, J. Chen, Y.S. Zhou, P. Bai, Z.L. Wang, Self-Powered, Ultrasensitive, Flexible Tactile Sensors Based on Contact Electrification, Nano Lett. 14 (2014) 3208-3213.

[19] M.F. Lin, J. Xiong, J. Wang, k. Parida, P.S. Lee, Core-shell nanofiber mats for tactile pressure sensor and nanogenerator applications, Nano Energy, 44 (2018) 248-255.

[20] K.Y. Lee, H.J. Yoon, T. Jiang, X. Wen, W. Seung, S.W. Kim, Z.L. Wang, Fully Packaged Self-Powered Triboelectric Pressure Sensor Using Hemispheres-Array, Adv. Energy Mater., 6 (2016) 1502566.

[21] S. Wang, S. Niu, J. Yang, L. Lin, Z.L. Wang, Quantitative measurements of vibration amplitude using a contact-mode freestanding triboelectric nanogenerator, ACS Nano, 8 (2014) 12004-12013.

[22] Q. Liang, Z. Zhanga, X. Yan, Y. Gu, Y. Zhao, G. Zhang, S. Lu, Q. Lia, Y. Zhang, Functional triboelectric generator as self-powered vibration sensor with contact mode and non-contact mode, Nano Energy, 14 (2015) 209-216.

[23] F.R. Fan, Z.Q. Tian, Z.L. Wang, Flexible triboelectric generator!, Nano Energy, 1 (2012) 328-334.

[24] X.S Zhang, J. Brugger, B. Kim, Nano Energy, A silk-fibroin-based transparent triboelectric generator suitable for autonomous sensor network, Nano Energy, 20 (2016) 37-47.

[25] W. Li, J. Sun, M. Chen, Nano Energy, Triboelectric nanogenerator using nano-Ag ink as electrode material, Nano Energy, 3 (2014) 95-101.

[26] Y. Zheng, L. Cheng, M. Yuan, Z. Wang, L. Zhang, Y. Qin, T. Jing, An electrospun nanowire-based triboelectric nanogenerator and its application in a fully self-powered UV detector, Nanoscale, 6 (2014) 7842-7846.

[27] B.U. Ye, B.J. Kim, J. Ryu, J.Y. Lee, J.M. Baik, K. Hong, Electrospun ion gel nanofibers for flexible triboelectric nanogenerator: electrochemical effect on output power, Nanoscale, 7 (2015) 16189-16194.

[28] Y. Hao, Y. Bin, H. Tao, W. Cheng, W. Hongzhi, Z. Meifang, Preparation and Optimization of Polyvinylidene Fluoride (PVDF) Triboelectric Nanogenerator via Electrospinning, 15th IEEE International Conference on Nanotechnology, (2015) 1485-1488.

[29] B. Yu, H. Yu, H. Wang, Q. Zhang, M. Zhu, High-power triboelectric nanogenerator prepared from electrospun mats with spongy parenchyma-like structure, Nano Energy 34 (2017) 69-75.

[30] B. Zhang, L. Zhang, W. Deng, L. Jin, F. Chun, H. Pan, B. Gu, H. Zhang, Z. Lv, W. Yang, Z.L. Wang, Self-Powered Acceleration Sensor Based on Liquid Metal Triboelectric Nanogenerator for Vibration Monitoring, ACS Nano, 11 (2017) 7440-7446.

[31] C. Garcia, I. Trendafilova, R. Guzman, J. Sanchez, Triboelectric Nanogenerator as self-powered impact sensor, MATEC Web Conf., 148 (2018) 14005.

[32] C. Xiang, C. Liu, C. Hao, Z. Wang, L. Che, X. Zhou, A self-powered acceleration sensor with flexible materials based on triboelectric effect, Nano Energy, 31 (2017) 469-477.

[33] L. Dhakar, S. Gudla, X. Shan, Z. Wang, F.E.H Tay, C.H. Heng, C. Lee, Large scale triboelectric nanogenerator and self-powered pressure sensor array using low cost roll-to-roll UV embossing, Sci. Rep. 6 (2016) 22253.

[34] A. Yu, L. Chen, X. Chen, A. Zhang, F. Fan, Y. Zhan, Z. L. Wang, Triboelectric sensor as self-powered signal reader for scanning probe surface topography imaging, Nanotechnology, 26 (2015) 165501.

[35] C. Garcia, J. Wilson, I. Trendafilova, L. Yang, Vibratory behaviour of glass fibre reinforced polymer (GFRP) interleaved with nylon nanofibers, Compos. Struc. 176 (2017) 923-932.

[36] J. Lin, B. Ding, J. Yu, Y. Hsieh, ACS Appl Mater Interfaces, Direct Fabrication of Highly Nanoporous Polystyrene Fibers via Electrospinning, 2 (2010) 521-528.

[37] S. Piperno, L. Lozzi, R. Rastelli, M. Passacantando, S. Santucci, PMMA nanofibers production by electrospinning, Appl. Surf. Sci., 252 (2006) 5583-5586.

[38] F. Zhang, B. Li, J. Zheng, C. Xu, Facile fabrication of micro-nano structured triboelectric nanogenerator with high electric output, Nanoscale Res. Lett., 10 (2015) 298.

[39]   T. Huang, M. Lu, H. Yu, Q. Zhang, H. Wang, M. Zhu, Enhanced Power Output of a Triboelectric Nanogenerator Composed of Electrospun Nanofiber Mats Doped with Graphene Oxide, Sci. Rep. 5 (2015) 13942.

[40]   M. Lai, B. Du, H. Guo, Y. Xi, H. Yang, C. Hu, J. Wang, Z.L. Wang, Enhancing the Output Charge Density of TENG via Building Longitudinal Paths of Electrostatic Charges in the Contact Layers, ACS Appl. Mater. Interfaces, 10 (2018) 2158-2165.

[41]   M. Zaccaria, D. Fabiani, A. Zucchelli, J. Belcari, O. Bocchi, T. Cramer, B. Fraboni, Electret Behaviour of Electrospun PVDF-based fibers, IEEE Conference on Electrical Insulation and Dielectric Phenomena (CEIDP) (2016) 137-140.

[42]   P. Martins, A.C. Lopes, S. Lanceros-Mendez, Electroactive phases of poly(vinylidene fluoride): Determination, processing and applications, Prog. Polym. Sci. 39 (2014) 683-706.

[43]   C.J. Angammana, S.H. Jayaram, Fundamental of electrospinning and processing technologies, Part Sci Technol, 34 (2016) 72-82.

[44]   S. Wang, L. Lin, Z.L. Wang, Triboelectric nanogenerators as self-powered active sensors, Nano Energy, 11 (2015) 436-462.

[45]   Z.L. Wang, L. Lin, J. Chen, S. Niu, Y. Zi, Triboelectric nanogenerators, Green energy and technology (2016) 23-46.

[46]   Y. Wang, Y. Yang, Z.L. Wang, Triboelectric nanogenerators as flexible power sources, npj Flexible Electronics, 1 (2017) 10.

[47]   N. Cui, L. Gu, Y. Lei, J. Liu, Y. Qin, X. Ma, Y. Hao, and Z.L. Wang, Dynamic behaviour of the triboelectric charges and structural optimization of the friction layer for a triboelectric nanogenerator, ACS Nano, 10 (2016) 6131-6138.

Chapter 7

Application of a triboelectric nanogenerator as self-powered impact sensor

Recently, triboelectric nanogenerators (TENGs) are generating considerable interest due to their important applications as energy harvesters and self-powered active sensors for pressures, vibrations and other mechanical motions. However, there is still little research among the research community on their potential applications of TENGs as active self-powered impact sensors. In this chapter, we report the development of a novel triboelectric nanogenerator, which can be used for detection and evaluation of small energy impacts. For the purpose, the TENG electric outputs generated by the impact of a free-falling ball dropped from different heights are recorded. The idea is to verify if the electric responses of the nanogenerator are influenced by the magnitude of the impact. The experimental results indicate that the voltage and current outputs increase linearly under stronger energy impacts. Moreover, the electric responses of the triboelectric nanogenerator show a very high sensitivity (14 V/J) and reproducibility. The main achievement of this chapter is the development of novel triboelectric nanogenerator composed of polyvinylidene fluoride nanofibers and a thin film of polypropylene, which can be successfully used for real-time detection of small energy impacts.

7.1 Introduction

An impact sensor plays a critical role in vehicle safety, fast medical assistance of elderlies and structural health monitoring. For example, in the event of a car crash an impact sensor detect the collision to release an air-bag for the protection of the

passengers. In the case of falls in the elderly, an impact sensor can be used to inform about the accident and provide a fast-medical assistance. Other practical examples could be detection of impacts in hail storms, where impacts are responsible for a considerable number of accidents in aircrafts, wind turbines and other civil infrastructures. Therefore, the sensing of impacts is the vital importance as impacts can seriously affect the health and safety of humans.

Recently, various approaches have been developed and applied for detection and measurement of impacts in environment as for example piezoelectric sensors [1, 2], capacitive sensors [3], optical sensors [4], acoustic sensors [5] and vibration sensors [6]. However, most of these technologies require an external power supply or battery to sense the impact which is a disadvantage of the non self-powered operation which leads to limited life-time and increased maintenance cost. Therefore, an environmentally friendly self-powered technology is very much desired for the detection of impacts.

In the last five years, triboelectric nanogenerators (TENGs) are gaining a lot of popularity within the scientific community, which results in a considerable amount of literature on demonstrating the potential of triboelectric nanogenerators as self-powered active sensors for vibrations [7, 8], accelerations [9, 10], touches [11, 12], pressures [13-15], magnetic fields [16, 17], and environmental changes [18, 19]. However, until now, there are almost no works to report about the potential of triboelectric nanogenerators for detection and evaluation of impacts [10]. Therefore, it is urgently needed to investigate the potential applications of triboelectric nanogenerators for detection and measurement of impacts.

The working principle of triboelectric nanogenerators is based on the contact electrification and electrostatic induction [20, 21]. The contact electrification occurs when two materials with different electron affinities are brought into contact with each other, which induce positive and negative charges in the surfaces of the contacted mats. The amount of charge transferred between the two materials is related to the area of the materials in contact and their differences in electron

affinities [22]. The electrostatic induction takes places when the two materials with opposite and equivalent triboelectric charges are separated, which result in a dipolar moment and a strong potential difference.

In the present chapter, we report a novel triboelectric nanogenerator prepared by a membrane of polyvinylidene fluoride (PVDF) nanofibers and an ultra-thin layer of polypropylene (PP). The triboelectric nanogenerator is designed with PVDF due to its strong tendency to gain triboelectric charges from almost any other mats [23]. This behaviour is attributed to the large amount of fluorine in PVDF that has the highest electronegativity among all the elements [24]. As a result, the surfaces of PVDF and polypropylene become negative and positive charged after the contact, respectively. The design of the TENG was based on nanofibers because it is one of the practical ways to increase the effective contact area between the triboelectric materials, which is beneficial to increase the generation of triboelectric charges of the TENG [25]. To the best of our knowledge, this is the first work to report a triboelectric nanogenerator based on the combination of these triboelectric mats.

Furthermore, the chapter demonstrates the potential applications of the developed TENG as self-powered impact sensor. For that purpose, the triboelectric sensor is impacted at various energies using a free-falling ball dropped from five different heights. The idea is to study if the electric responses of the nanogenerator are affected and how by the magnitude of the impacts. The experimental results indicate that the electric responses of the triboelectric nanogenerator are influenced by the energy of the impacts, therefore higher electric outputs are found under stronger energy impacts. Furthermore, the voltage and current outputs show a very high sensitivity, linearity and reproducibility, which demonstrate the potential of the TENG as self-powered impact sensors.

The rest of the chapter is structured as follows: Section 2 describes the preparation of the triboelectric nanofibers by electrospinning. Section 3 explains the fabrication of the triboelectric nanogenerator. Section 4 presents the working mechanism of the triboelectric nanogenerator. Section 5 introduces the drop ball

impact test used to investigate the effect of impacts on the TENG electric responses. Section 6 presents and discusses the results obtained in the drop ball impact test. Our conclusions are drawn in the final section.

7.2 Fabrication of the triboelectric nanogenerator

The fabrication process of the triboelectric nanogenerator is schematically shown in Fig. 7.1 and can be divided into three main steps: preparation of the top and the bottom sections of the TENG and assembly of the nanogenerator. Initially, a 2 mm thin film of PVDF nanofibers is deposited on a copper foil via electrospinning to form the TENG top section. After that, an ultra-thin film of polypropylene with a thickness of 25 µm is attached with copper foil using double side copper tape to form the TENG bottom section. Lastly, the two prepared sections are placed face to face and sealed with polyethylene terephthalate film to form the triboelectric nanogenerator. The dimensions and weight of the developed triboelectric nanogenerator are 5.5 x 5.5 x 0.3 cm and 6.75 g, respectively. The small size and weight of the device are beneficial for the practical applications of the sensor.

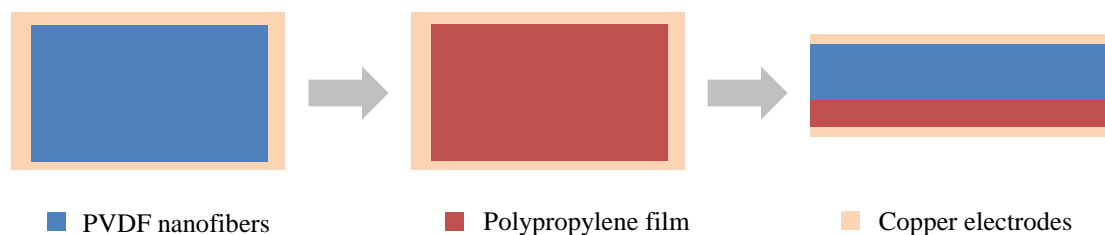■ PVDF nanofibers   ■ Polypropylene film   ■ Copper electrodes

Figure 7.1 Fabrication process of the triboelectric nanogenerator: (i) Preparation of the top section. (ii) Preparation of the bottom section and (iii) structure of the nanogenerator.

The triboelectric nanogenerator has a multi layered structure with two main sections as detailed in Fig. 7.1. The lower section is made of a film of polypropylene adhered to copper foil to act as one of the triboelectric materials. In the upper section, nanofibers of polyvinyl fluoride are deposited on copper foil and this serves as the other oppositely charged triboelectric material. The roles of PVDF nanofibers and

polypropylene film is to act as frictional materials while the copper foils serve as electrodes for the nanogenerator owing to the low cost and the high electrical conductivity of the copper.

From a fabrication point of view, this procedure is simple, low-cost and can be easily scaled-up for large scale production, which is desired for the practical applications of the device.

7.3 Preparation and characterization of PVDF nanofibers

This paragraph describes the preparation of the PVDF fibres used for the fabrication of the triboelectric nanogenerator, which is used here as an impact sensor. As was mentioned above the TENG and the current sensor are prepared using PVDF and PP nanofibers

The film of PVDF nanofibers is prepared using the technique of electrospinning because is a simple and economic way to prepare triboelectric mats with large surface area [26]. The preparation of the nanofibers can be summarized as follows: First, the polymer solution for electrospinning is prepared by dissolving 2g of PVDF pellets (MW=275,000 gmol-1) in 10 ml solvent mixture of N,N-dimethylformamide (DMF) and acetone (40/60). Second, the polymer solution is inserted into a plastic syringe to be spun in a commercial electrospinning machine (Nanon-01A) using the following processing parameters: applied voltage of 15 kV, needle tip-collector distance of 15 cm, feed rate of 1 ml/h, 21G steel needle and a static collector. As a result, a 2 mm thin layer of interconnected PVDF nanofibers is deposited on the surface of a copper electrode.

The design of the sensor was based on nanofibers because it is one of the practical ways to increase the effective contact area between the frictional materials, which is beneficial to enhance the generation of triboelectric charges [25]. Fig. 7.2

(a) shows a scanning electron microscopy image of the PVDF nanofibers prepared by electrospinning. From the image, it can be clearly appreciated a dense population of interconnected fibres of PVDF, which will result in a very large surface area. The nanofibers are distributed randomly in the membrane and show a few bead defects, which can be associated to the nature of the polymer solution and the high voltages used during the electrospinning [27].

Fig. 7.2 (b) displays the fibre diameter distribution of the nanofibers. The preparation of the fiber diameter histogram can be summarized as follow: Initially, the diameters of 100 nanofibers are measured from the SEM image using the software Image J. After, the numbers of fibers which correspond to a certain diameter range (e.g. 800-1000 nm) are counted. The histogram reveals that the diameter of the fibers is not uniform and varies between 200 and 2000 nm. The wide distribution of diameters in the fibers is attributed to the nature of the electrospinning process. From the histogram, it can be deducted that the diameter of the fibers varies between 800 and 1000 nm with a probability of about 18%. As a result, the average fibre diameter of the nanostructures is 1087 nm with a standard deviation of 419 nm.
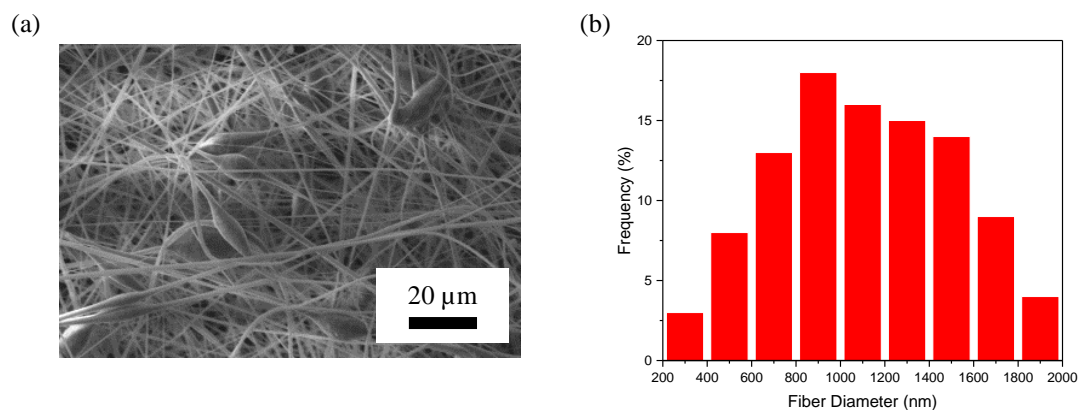

Figure 7.2 Preparation of nanofibers via electrospinning: (a) SEM image of PVDF nanofibers and (b) fibre diameter distribution of PVDF fibers.

7.4 Operating principle of the triboelectric nanogenerator

Fig. 7.3 illustrates the working principle of the triboelectric nanogenerator, which is based on the contact-separation mode reported by Wang's group [28, 29]. The electric responses of the TENG are generated due to the conjunction between contact electrification and electrostatic induction of two materials with different electron affinities [30, 31].
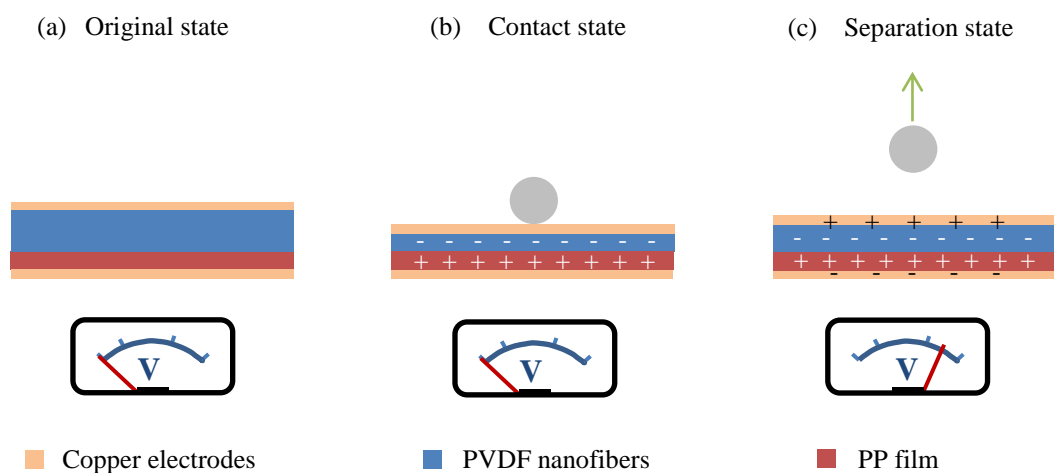

Figure 7.3 Operating principle of the triboelectric nanogenerator: (a) The original state of the TENG prior to the ball impact. (b) The state of the TENG during the ball impact and (c) the state of the TENG after the impact.

At the original position (Fig. 7.3 (a)), there is not friction between the film of PVDF nanofibers and polypropylene, which results in non-electric response. When the ball hits the sensor, the TENG configuration changes from the original to the contact state as shown in Fig. 7.3 (b). Since PVDF has a higher electronegative behaviour than polypropylene, the electrons are transferred from polypropylene to PVDF. Therefore, net negative charges are generated on the PVDF surface and equal amount positive ones in the polypropylene film. When the ball rebounds, the device changes from the contact to the separation state as described in Fig. 7.3 (c). In this configuration, the opposite triboelectric charges are separated, and a potential drop is generated between the two electrodes. As a result, there is transference of electrons between the bottom electrode and the upper one through the external circuit. Finally,

the triboelectric charges disappear, and the electrons flow back producing a reversed electrical signal to reach the electrostatic equilibrium.

7.5 Experimental testing of the triboelectric nanogenerator

The aim of this section is to describe the experiment used to evaluate the response of the manufactured sensor to impacts. To carry out this investigation, a drop ball impact test is used to find out if the electric responses of the nanogenerator are influenced by the impacts of a free-falling ball. The main goal of this experimental study is to verify that the voltage and current outputs of the triboelectric nanogenerator are affected by the energy of the impacts.
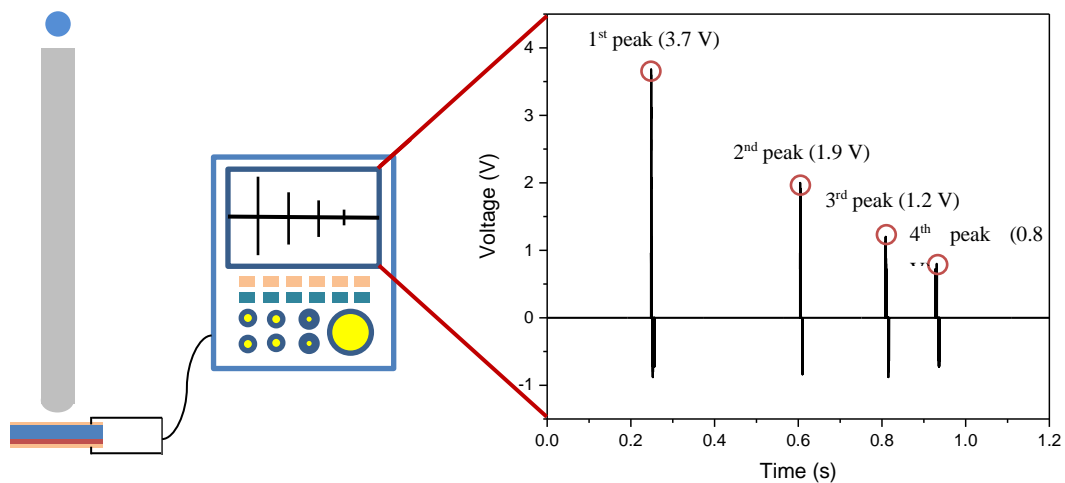

Figure 7.4 Experimental testing of the triboelectric nanogenerator: Schematic description of the experimental setup. The inset of the figure shows the electric outputs of the triboelectric nanogenerator due to the ball impact.

Fig. 7.4 shows a schematic representation of the experimental setup. From the figure, it can be appreciated that the experiment utilizes a simple setup which consist of an impact ball, a plastic tube and a triboelectric nanogenerator connected to an apparatus to measure the electric responses. In the experimental test, a 21 g glass ball with a diameter of 2 cm is dropped on the top surface of the triboelectric sensor. The

idea is to drop a glass ball from five different heights ranging from 20 to 100 cm (with a drop height interval of 20 cm) by using plastic tubes of different lengths and record the voltage and current responses of the triboelectric nanogenerator as result of the impacts by using a Tektronix 2012B commercial oscilloscope and Agilent 34410A digit multimeter. The main goal of the experiment is determinate if the amplitude of TENG electric signals is affected by the height of the ball impact.

Our experimental method was inspired by [32] and represents a simple and low-cost procedure to analyse the impact sensitivities of TENGs. The experimental procedure can be divided into the following three steps: First, a 0.02 m diameter glass ball with a weight of 0.021 Kg is dropped from five different heights of 0.2, 0.4, 0.6, 0.8 and 1 m which correspond to five different impact energies. Second, the plastic tube holds on a heavy metallic base which is used as a fall guide for the glass ball to have a direct impact on the triboelectric nanogenerator. Finally, the voltage and current responses of the triboelectric sensor are measured in order to analyse if the amplitude of the sensor electric outputs is affected by the energy of the impact. It is also important to mention that the energy of the impacts for the different impact balls is calculated using equation (11):

$$E = mgh \qquad (11)$$

where *m* represents the mass of the glass ball, *g* is the acceleration due to the gravity and *h* indicates the impact height. For the sake of simplicity, the drag forces caused by the air resistance during the ball drop and the side walls of the plastic tube are neglected.

The ball is dropped from five different heights of 0.2, 0.4, 0.6, 0.8 and 1 m respectively. Table 7.1 presents the energy of the impacts calculated theoretically for the particular drop heights. From the table, it can be clearly observed that the energy of the impacts increases when the balls are dropped from greater heights. Therefore, it can be observed that the energy of the impacts varies between 0.040 J and 0.202 J as the drop height increases from 0.2 m and 1.0 m, which demonstrates that the

developed sensor can be used for detection and measurement of very small energy impacts in the range of millijoules.

Drop Height (m)	Energy (J)
0.2	0.040
0.4	0.081
0.6	0.121
0.8	0.162
1.0	0.202

Table 7.1 The energy of the impacts calculated theoretically as a function of the drop height.

Fig. 7.4 also includes the variations of voltage caused by the impact of a free-falling ball dropped at 1 m drop height. From the graphic, it can be clearly seen four peaks which are associated to the multiple collisions of the impact ball. The largest peak is the first peak, which correspond to the highest impact energy of the ball falling on the TENG. The amplitude of the subsequent peaks decreases proportionally for the following bounces due the reduction of the impact energies. The figure also shows the time interval between the ball bounces, where it can be observed a lower time-intervals for the lower impact energies. For the sake of simplicity, the experimental results presented in the results and discussion section only show the first peak attributed to the first bounce of the ball.

7.6 Results and Discussion

This section shows and discusses the experimental results obtained from the drop ball impact test. Initially, the effect of the energy of the impacts on the electric outputs of the nanogenerator is analysed. After, the repeatability of the voltage and current responses of the TENG for five repetitions of the same energy impact is discussed.

7.6.1 Effect of the impact height on the TENG voltage output

As stated in the previous section, the triboelectric nanogenerator is subjected to various energy impacts using a drop ball impact test and the voltage outputs of the TENG are measured using a commercial oscilloscope. The aim of the experiment is to analyse if the TENG voltage outputs are affected by the energy of the impacts.

Fig. 7.5 (a) shows the voltage outputs of the triboelectric nanogenerator when the ball was dropped from five different heights of 0.2, 0.4, 0.6, 0.8 and 1 m respectively. The graph shows that when the ball was dropped from greater heights, the amplitude of the TENG voltage responses increases. Therefore, it can be clearly seen that the peak-to-peak voltage increases from 2.4 to 4.7 V as the drop height increased from 0.2 to 1 m. This trend is in good agreement with other works. For example, the authors of [33] analysed the effect of controlled height impact balls on the voltage outputs of a TENG based on PVDF nanofibers and a mercury droplet. The results reveal that the electric responses of the TENG increased from 1.3 to 10.4 V as the impact height is raised between 0.1 and 1 m. Other works as [34] obtained similar results using a triboelectric nanogenerator composed of nanofibers of polyvinylidene fluoride and polyvinylpyrrolidone. To the best of our knowledge, [33, 34] are the only two works that have investigated the effect of ball impacts in the voltage responses of triboelectric nanogenerators.

Fig. 7.5 (b) displays the peak-to-peak voltages of the triboelectric nanogenerator as a function of the impact energy. The graph includes the average peak-to-peak voltage and corresponding standard deviations for five repetitions of each energy impact. The results show that the peak-to-peak voltage responses increase gradually under higher energy impacts in the measurement range 0.040-0.2 J. This behaviour can be explained by the fact that the voltage outputs of a TENG are strongly affected by the contact surface between the frictional mats [35, 36]. Therefore, higher energy impacts lead to a more intimate contact between the

frictional mats, which results in higher electric outputs. From the results, it can also be seen a strong linear correlation for the relationship between voltage and energy with a high Pearson coefficient of 0.997. Furthermore, the sensitivity of the TENG is calculated using the slope of the interpolated straight line and a very high sensitivity of 14 V/J is found on the detection range 0.040-0.200 J.
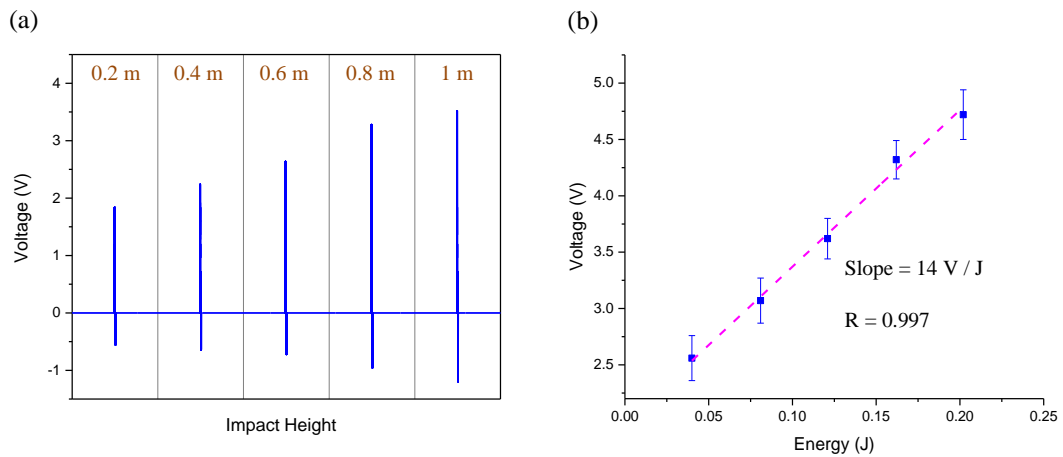

Figure 7.5 Influence of the impacts on the voltage responses of the new TENG: (a) Voltage outputs as a function of the time for the different ball impacts. (b) Voltage amplitudes as a function of the impact energy.

On the basis of these results, it can be said that the TENG voltage responses are influenced by the energy of the impacts and increase proportionally in the range between 0.040 and 0.200 J. Furthermore, the straight lines used to interpolate the voltage responses show a very high sensitivity and linearity of 14 V/J and 0.997, respectively. These characteristics are the utmost importance as sensors with very high impact sensitivity and strong linear response are always preferred.

7.6.2 Effect of the impact height on the TENG current output

As mentioned in Section 7.5, a free-falling ball is used to impact the developed TENG at different energy impacts and the current signals of the nanogenerator are measured using a digital multimeter. The main purpose is to investigate if the current electric signals of the TENG are dependent on the energy of the impacts.
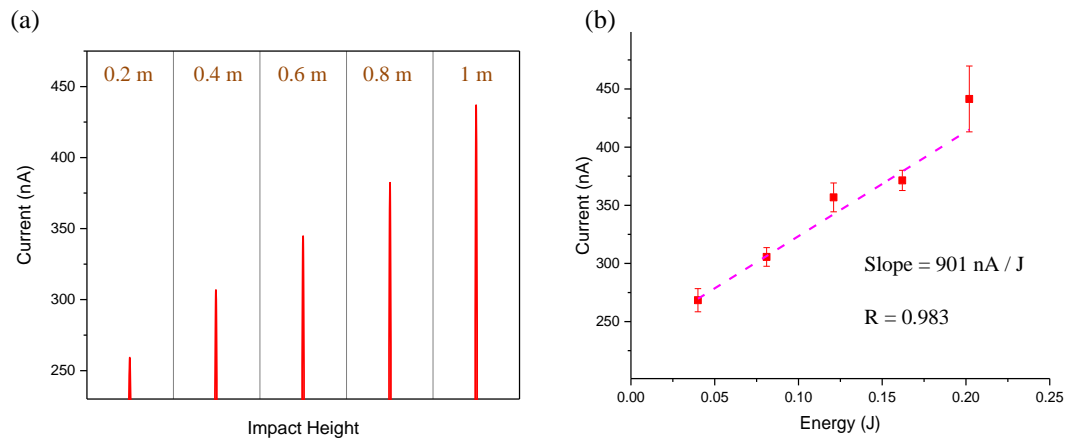
Figure 7.6 Effect of the impacts on the current outputs of the fabricated triboelectric nanogenerator: (a) Current responses for impacts at various drop heights of 0.2, 0.4, 0.6, 0.8 and 1 m. (b) Current amplitudes as a function of the impact energy.

Fig. 7.6 (a) shows the current responses of the developed triboelectric nanogenerator when the free-falling ball was dropped from various heights at 0.2, 0.4, 0.6, 0.8 and 1 m. For the sake of simplicity, the electrical outputs of the five different energy impacts are shown in the same graphic. The results show that the TENG current outputs increase significantly when height of the impact is increased. The increase of the current output as the drop impact height increases can be explained by the fact that the deformation of the TENG increases for higher energy impacts. When the TENG is impacted at smaller energies, the deformation of the sensor is smaller, which decreases the contact between the frictional mats and the generation of electricity. When the ball hits the TENG at higher energies, a stronger deformation is caused, which results in a larger contact between the frictional mats and higher current responses.

Fig. 7.6 (b) shows the current amplitudes of the triboelectric nanogenerator as a function of the energy of the impacts. The results given are the average value and corresponding standard deviation for five repetitions of the same energy impact. From the graphic, it can be appreciated that the current responses are strongly affected by energy of the impacts and the amplitude of the current responses increase from 268 to 441 nA as the energy of the impact changes between 0.040 and 0.200 J.

The results reveal that the relation between the energy of the impacts and the TENG current responses is linear and has a high Pearson coefficient of 0.983. Furthermore, the sensitivity of the triboelectric nanogenerator is calculated using the slope of the straight line and a very high impact sensitivity of 901 nA/J is found.

In general, it can be concluded that the current outputs of the nanogenerator are strongly influenced by the energy of the impacts and increase linearly under stronger energy impacts. Furthermore, the current-energy relationship shows a very high sensitivity of 901 nA/J for the measurement range between 0.040 and 0.200 J. As a result, these results indicate the good performance of triboelectric nanogenerators for detection and evaluation small energy impacts.

7.6.1 Repeatability of the TENG voltage/current outputs

This section of the chapter investigates the repeatability of the TENG electric outputs for five repetitions of the same energy impact. The idea is to verify if the triboelectric nanogenerator produce similar electrical responses when the testing conditions remain constant. For this study, the drop ball impact test explained in Section 7.5 is used to verify the stability of the TENG electric responses for five repetitions of the same impact.

Table 7.2 summarizes the average voltage and current outputs for five repetitions of the same impact. From the results, it can be clearly seen that the electric responses are influenced for the energy of the impacts and increase gradually for the impacts at higher energies. Furthermore, the table also includes the standard deviations and coefficient of variations for the five impact repetitions. The standard deviations for the voltage outputs vary between 0.17 V and 0.20 V, while the current standard deviations are increased from 6.4 nA to 28.3 nA. The coefficients of variations are small and vary in the range 2.4 - 7.9 % for the voltage and current outputs. In our view, the variations of the voltage and current responses could be

attributed to the drag forces between the ball and the side walls of the plastic tube, which vary randomly for each experiment.

Energy (J)	Voltage (V)	S.D. Voltage (V)	C.V. Voltage (%)	Mean Current (nA)	S.D. Current (nA)	C.V. Current (%)
0.040	2.56	0.20	3.70	268.4	9.9	7.97
0.081	3.07	0.20	2.62	305.6	8.0	6.54
0.121	3.62	0.18	3.50	356.8	12.4	4.97
0.162	4.32	0.17	2.40	371.4	28.3	4.00
0.202	4.72	0.22	6.41	441.4	6.4	4.64

Table 7.2 Repeatability of the electric outputs for five repetitions of the same impact

In conclusion, it can be said that the electric responses of the nanogenerator shows a good repeatability with minimum changes in the voltage and current outputs after repeated applications of the same impact. Therefore, it can be concluded that the electric responses of the developed triboelectric nanogenerator are stable and can be potentially used for the quantification of small energy impacts.

7.7 Conclusions

In summary, this chapter presents a novel triboelectric nanogenerator composed of a thin film polypropylene and a membrane of PVDF nanofibers which can be used as self-powered sensor for detection of small energy impacts in real time.

The films of electrospun nanofibers used in the nanogenerator are prepared via electrospinning because it is one of the practical ways to increase the performance of the TENG. Therefore, it can be concluded that the developed triboelectric nanogenerator is prepared by a simple fabrication method, which does not require expensive mats or high cost technologies. Furthermore, this procedure can be easily upgraded for large scale mass production, with the advantages of low-cost production.

Furthermore, the chapter investigates the practical applications of the TENG as self-powered sensor for detection of small energy impacts. For this purpose, a simple experimental test using a free-falling ball is used to analyse the effect of the energy of the impacts on the electric responses of the triboelectric nanogenerator. The experimental results reveal that the voltage and current outputs increase proportionally under higher energy impacts. Therefore, it can be observed a strong linear relationship between the electric outputs and the energy of impacts. Furthermore, the voltage and current outputs show a very high impact sensitivity of 14 V/J and 901 nA/J in the entire measurement range.

Finally, the repeatability of the electric responses of the triboelectric nanogenerator for five repetitions of the same energy impact is considered. The results show that the voltage and current outputs of the developed triboelectric nanogenerator shows minimum changes for repeated applications of the same impact. Therefore, it can be concluded that the electric responses of the triboelectric nanogenerator shows a good repeatability, which is essential for the practical applications of the TENG as self-powered impact sensor.

In conclusion, the experimental results prove that the developed nanogenerator can be used for detection of small energy impacts with the advantages of self-powered operation, maintenance-free and simple fabrication. Therefore, we are of the opinion that these results are an excellent initial step toward the development of self-powered impact sensors for multiple applications including vehicle safety, structural health monitoring and urgent medical attention of elderies.

References

[1]   M.S. Salmanpour, Z.S. Khodaei, M.H. Ferri Aliabadi, Impact damage localisation with piezoelectric sensors under operation and environmental conditions, Sensors, 17 (2017) 1178.

[2]   A. Dixit, S. Bhalla, Prognosis of fatigue and impact induced damage in concrete using embedded piezo-transducers, Sens. Actuator A-Phys., 274 (2018) 116-131.

[3]   S. Phan, Z.F. Queck, P. Shah, D. Shin, Z. Ahmed, O. Khatib, M. Cutkosky, Capacitive skin sensors for robot impact monitoring, in: Proceedings to the 24th International Conference on Intelligent Robots and Systems, 25-30 September; San Francisco, CA, USA, 2011, pp. 2992-2997.

[4]   D. Liang, B. Culshaw, Fibre optic silicon impact sensor for application to smart skins, Electron. Lett., 29 (1993) 529-530.

[5]   M. Eaton, M. Pearson, K. Holford, C. Featherston, R. Pullin, Detection and location of impact damage using acoustic emission, in: Proceedings to the 2nd International Conference on Advanced Composite Materials and Technologies for Aerospace Applications, June 11-13; Wrexham, UK, 2012, pp. 29-33.

[6]   R. Ouckama, D.J. Pearsall, Evaluation of a flexible force sensor for measurement of helmet foam impact performance, J. Biomech., 44 (2011) 904-909.

[7]   Q. Liang, Z. Zhanga, Xiaoqin Y., Y. Gu, Y. Zhao, G. Zhang, S. Lu, Q. Liao, Y. Zhang, Functional triboelectric generator as self-powered vibration sensor with contact mode and non-contact mode, Nano Energy, 14 (2015) 209-216.

[8]   S. Wang, S. Niu, J. Yang, L. Lin, Z.L. Wang, Quantitative measurements of vibration amplitude using a contact-mode freestanding triboelectric nanogenerator, ACS Nano, 8 (2014) 12004-12013.

[9]   C. Xiang, C. Liu, C. Hao, Z. Wang, L. Che, X. Zhou, A self-powered acceleration sensor with flexible materials based on triboelectric effect, Nano Energy, 31 (2014) 469-477.

[10] K. Dai, X. Wang, F. Yi, C. Jiang, R. Li, Z. You, Triboelectric nanogenerators as self-powered acceleration under high-g impact, Nano Energy, 45 (2018) 84-93.

[11] G. Zhu, W.Q. Yang, T. Zhang, Q. Jing, J. Chen, Y.S. Zhou, P. Bai, Z.L. Wang, Self-powered, ultrasensitive, flexible tactile sensors based on contact electrification, Nano Lett., 14 (2014) 3208-3213.

[12] T. Li, J. Zou, F. Xing, M. Zhang, X. Cao, N. Wang, Z.L. Wang, From dual-mode triboelectric nanogenerator to smart tactile sensor: A multiplexing design, ACS Nano, 11 (2017) 3950-3956.

[13] L. Dhakar, S. Gudla, X. Shan, Z. Wang, F.E.H. Tay, C.H. Heng, C. Lee, Large scale triboelectric nanogenerator and self-powered pressure sensor array using low cost roll-to-roll UV embossing, Sci. Rep., 6 (2016) 22253.

[14] K. Parida, V. Bhavanasi, V. Kumar, R. Bendi, P.S. Lee, Self-powered pressure sensor for ultra-wide range pressure detection, Nano Res., 10 (2017) 3557-3570.

[15] K.Y. Lee, H.J. Yoon, T. Jiang, X. Wen, W. Seung, S.W. Kim, Z.L. Wang, Fully packaged self-powered triboelectric pressure sensor using hemispheres-array, Adv. Energy Mater., 6 (2016) 1502566.

[16] Y. Yang, L. Lin, Y. Zhang, Q. Jing, T.C. Hou, Z.L. Wang, Self-powered magnetic sensor based on a triboelectric nanogenerator, ACS Nano, 6 (2012) 10378-10383.

[17] S. Qi, H. Guo, J. Chen, J. Fu, C. Hu, M. Yu, Z.L. Wang, Magnetorheological elastomers enabled high-sensitive self-powered tribo-sensor for magnetic field detection, Nanoscale, 10 (2018) 4745-4752.

[18] Y. Su, G. Xie, S. Wang, H. Tai, Q. Zhang, H. Du, H. Zhang, X. Du, Y. Jiang, Novel high-performance self-powered humidity detection enabled by triboelectric effect, Sens. Actuator B-Chem., 251 (2017) 144-152.

[19]   Z.H. Lin, G. Zhu, Y.S. Zhou, Y. Yang, P. Bai, J. Chen, Z.L. Wang, A self-powered triboelectric nanosensor for mercury ion detection, Angew. Chem. Int. Ed., 52 (2013) 5065-5069.

[20]   A. Yu, L. Chen, X. Chen, A. Zhang, F. Fan, Y. Zhan, Z.L. Wang, Triboelectric sensor as self-powered signal reader for scanning probe surface topography imaging, Nanotechnology, 26 (2015) 165501.

[21]   W. Song, B. Gan, T. Jiang, Y. Zhang, A. Yu, H. Yuan, N. Chen, C. Sun, Z.L. Wang, Nanopillar arrayed triboelectric nanogenerator as a self-powered sensitive sensor for a sleep monitoring system, ACS Nano, 10 (2016) 8097-8103.

[22]   W. Li, J. Sun, M. Chen, Triboelectric nanogenerator using nano-Ag ink as electrode material, Nano Energy, 3 (2014) 95-101.

[23]   Y. Hao, Y. Bin, H. Tao, W. Cheng, W. Hongzhi, Z. Meifang, Preparation and optimization of polyvinylidene fluoride (PVDF) triboelectric nanogenerator via electrospinning, in: Proceedings to the 15th International Conference on Nanotechnology, July 27-30; Rome, Italy, 2015, pp. 1485-1488.

[24]   C. Garcia, I. Trendafilova, R. Guzman de Villoria, J. Sanchez del Rio, Self-powered pressure sensor based on the triboelectric effect and its analysis using dynamic mechanical analysis, Nano Energy, 50 (2018) 401-409.

[25]   Y. Zheng, L. Zheng, M. Yuan, Z. Wang, L. Zhang, Y. Qin, T. Jing, An electrospun nanowire-based triboelectric nanogenerator and its application in a fully self-powered UV detector, Nanoscale, 6 (2014) 7842.

[26]   F. Zhang, B. Li, J. Zheng, C. Xu, Facile fabrication of micro-nano structured triboelectric nanogenerator with high electric output, Nanoscale Res. Lett., 10 (2015) 298.

[27]   J.M. Deitzel, J. Kleinmeyer, D. Harris, N.C. Beck Tan, The effect of processing variables on the morphology of electrospun nanofibers and textiles, Polymer, 42 (2001) 261-272.

[28]   Z.L. Wang, Triboelectric nanogenerators as new energy technology and self-powered sensors – Principles, problems and perspectives, Faraday Discuss., 176 (2014) 447-458.

[29]   S. Niu, S. Wang, L. Lin, Y. Liu, Y.S. Zhou, Y. Hu, Z.L. Wang, Theoretical study of contact-mode triboelectric nanogenerators as an effective power source, Energy Environ. Sci., 6 (2013) 3576.

[30]   Y. Xi, H. Guo, Y. Zi, X. Li, J. Wang, J. Deng, S. Li, C. Hu, X. Cao, Z.L. Wang, Multifunctional TENG for blue energy scavenging and self-powered wind-speed sensor, Adv. Energy Mater., 7 (2017) 1602397.

[31]   Y. Su, G. Zhu, W. Yang, J. Yang, J. Chen, Q. Jing, Z. Wu, Y. Jiang, Z.L. Wang, Triboelectric sensor for self-powered tracking of object motion inside tubing, ACS Nano, 8 (2014) 3843-3850.

[32]   S. Joshi, G.M. Hedge, M.M. Nayak, K. Rajanna, A novel piezoelectric thin film impact sensor: Application in non-destructive material discrimination, Sens. Actuator A-Phys., 199 (2013) 272-282.

[33]   B. Zhang, L. Zhang, W. Deng, L. Jin, F. Chun, H. Pan, B. Gu, H. Zhang, Z. Lv, W. Yang, Z.L. Wang, Self-powered acceleration sensor based on liquid metal triboelectric nanogenerator for vibration monitoring, ACS Nano, 11 (2017) 7440-7446.

[34]   C. Garcia, I. Trendafilova, R. Guzman de Villoria, J. Sanchez del Rio, Triboelectric nanogenerator as self-powered impact sensor, in: Proceedings to the International Conference on Engineering Vibration, 4-7 September; Sofia, Bulgaria, 2017, MATEC Web. Conf., 2018, 148, 14005.

[35]   T. Huang, M. Lu, H. Yu, Q. Zhang, H. Wang, M. Zhu, Enhanced power output of a triboelectric nanogenerator composed of electrospun nanofiber mats doped with graphene oxide, Sci. Rep., 5 (2015) 13942.

[36]   Y.S. Choi, Q. Jing, A. Datta, C. Boughey, S. Kar-Narayan, A triboelectric generator based on self-poled Nylon-11 nanowires fabricated by gas-flow assisted template wetting, Energy Environ. Sci., 10 (2017) 2180.

Chapter 8

Detection and measurement of impacts in composite structures using a self-powered triboelectric sensor

Composite structures as e.g. aircrafts, wind turbines or racing cars are frequently subjected to numerous impacts. For example, aircrafts may collide with hailstones and being damaged due to the impact of hailstones. These impacts harm the integrity of the composite laminates used in their structures which results in delamination and other failures which are usually very difficult to detect by visual inspections. Hence, the detection and quantification of impacts is of vital importance for monitoring the health state of composite structures. Recently, triboelectric sensors have been demonstrated to detect touches, pressures, vibrations and other mechanical motions with the advantages of being self-powered, maintenance-free and easy to fabricate. However, there is no research focusing on the potential of triboelectric sensors to detect impacts in a wide energy range. In this paper, a self-powered triboelectric triboelectric sensor is developed to measure impacts at high energy in structures made of composite materials. This could be particularly beneficial for the detection of bird strikes, hailstones and other high energy impacts in aircraft composite structures. For that purpose, composite plates are subjected to various energy impacts using a drop weight impact machine and the electric responses provided by the developed triboelectric sensor are measured in terms of voltage and current. The idea is to evaluate the sensitivity of the electrical signals provided by the sensor to changes in the impact energy. The results prove that the generated electric responses are affected by the energy of the impact and their amplitude increases linearly with the impact energy. The voltage and current sensor responses demonstrate a very good impact sensitivity of 160 mV/J and a strong linear relationship to the impact energy (R = 0.999) in a wide energy range from 2 to 30 J. This work suggests a novel

approach to measure the magnitude of the impacts in composite structures using the newly developed triboelectric sensor. The findings of this work demonstrate that the developed triboelectric sensor meets the urgent needs for monitoring high energy impacts for aeronautic and civil composite structures.

8.1 Introduction

Structures made of composite materials as aircrafts, wind turbines or bridges are frequently subjected to impacts. For example, composite structures like e.g. wind turbines can be seriously affected by the impact of hailstones. These impacts damage the integrity of the composite materials used in the structures which results in a significant loss of their structural integrity and stiffness. Furthermore, the delamination caused is almost impossible to detect by visual inspections and requires sophisticated inspection methods for its detection such as ultrasounds [1], infrared thermography [2], shearography [3], radiography [4] or rigorous mathematical tools [5]. Hence, impact sensors are vital to detect and quantify impacts as well as assess their location.

An impact sensor is a crucial component for vehicle safety [6], structural health monitoring [7], impact monitoring [8], and emergency locations of persons in distress [9]. According to its working mechanism, an impact sensor can be generally classified into piezoelectric [10, 11], capacitive [12], optical [13] and resistive types [14]. Among these, the sensors based on the piezoelectric effect have attracted considerable attention because they do not require external power supply or battery to power the sensor. However, the fabrication procedure is rather expensive and requires additional processing steps as annealing (a thermal treatment to increase the crystallinity of the material) and electrical poling (the application of a high electrostatic field at elevated temperature to align the dipoles) [15]. Thus, it is necessary to explore new approaches to develop sensors that does not rely on

external power supply and can be produced using a low-cost and easy fabrication procedure.

Very recently, triboelectric sensors (TES) have attracted much research interest as a simple, sustainable, and cost-efficient technology can be used to develop self-powered sensors for pressures [16-18], vibrations [19, 20], accelerations [21, 22], velocities [23-24], magnetic fields [25, 26], gases [27, 28], object motions [29], and surface topographies [30]. However, there are only a few papers to analyse the potential of triboelectric sensors for impact energy detection. For example, [31] reported a triboelectric sensor which can detect the impacts applied between a little ball and the sensor in the energy range from 20 to 210 millijoules (mJ). The authors from [32] reported a self-powered triboelectric sensor which can detect the energy impacts below 105 mJ applied on a fixed table using a free-falling ball. One of the limitations in the above-mentioned studies is that they only evaluate a small range of energies between 10 and 210 mJ, which is far from the energy of the impacts in practical applications (e.g. automobile crash, bird-strikes or hailstorms). In this regard, it is necessary to investigate the capabilities of self-powered triboelectric sensors for detection of impacts at higher energies and wider detection ranges.

In this chapter, we present a new class of self-powered triboelectric sensor prepared using polyvinyl fluoride (PVDF) and polyvinyl pyrrolidone (PVP) nanofibers, which can detect impacts in a wide energy range from 2 to 30 J. PVDF nanofibers are chosen as one of the frictional mats due to their strong tendency to attract electrons from other materials. This behaviour is attributed to the large composition of fluorine in PVDF that has the highest electronegativity among all the elements [33]. On the other hand, PVP nanofibers are selected as the other frictional mat due to their strong ability to donate electrons [34]. Furthermore, the rough and porous surfaces of the nanofibers extend the contact area between the frictional materials which results in an increment of the triboelectric effect [35]. The technique of electrospinning was used to prepare both layers of nanofibers due to its low cost, versatility and simplicity for the fabrication of nanofibers using a wide variety of triboelectric mats [36].

The main aim of this chapter is to investigate the ability of the developed triboelectric sensor to detect and quantify mechanical impacts applied to composite structures. For this purpose, composite plates are subjected to various impacts in the energy range from 2 to 30 J using a drop weight impact machine. Then, the electric responses of the triboelectric sensor adhered to the composites are measured in the form of voltage and current. The idea is to study the changes in the resultant electrical signals due to the variations in the impact energy. As was already mentioned, the experimental results confirm the dependence of the sensor electric responses on the impact magnitude. The measured voltage and current both demonstrate a strong linear relationship ($R^2 = 0.99$) with the energy and the force of the impact. In addition, the sensor outputs show a very high sensitivity of 160 mV/J in a wide measurement range of energies from 2 to 30 J. Finally, the chapter compares the performance of the developed triboelectric sensor with a commercial one.

This chapter suggests a new approach to detect and measure a wide range of energy impacts in composite structures using a self-powered triboelectric sensor. The findings of this work demonstrate that triboelectric sensors can be used for real-time detection of impacts in composite structures as aircrafts, wind turbines or bridges. The main application of the triboelectric sensors is to monitor high energy impacts in composite structures. This could be practically used for the detection of bird strikes, hailstones and other high energy impacts in aircrafts and civil structures. Alternatively, the amount of damage generated because of these impacts is proportional to the amount of energy involved in the impact. Therefore, the amplitude of the electric responses of the energy sensor could be also used to estimate the health state of the composite structures.

The rest of the paper is organized as follows: Section 2 explains the fabrication process of the newly developed triboelectric sensor. The next paragraph, Section 3 introduces the experiment used to study the capability of the triboelectric sensor to detect and quantify impacts in composite structures. The analysis of the experimental

results is presented and discussed in section 4. Some conclusions are drawn in the final section 5.

8.2 Fabrication of Triboelectric Sensor

This section details the fabrication of the triboelectric sensor. It is divided into two subsections. The first subsection gives a brief overview of the electrospinning procedure used to prepare the triboelectric nanofibers, while section 8.2.2 explains the design and the assembly process of the triboelectric sensor.

8.2.1 Preparation of triboelectric nanofibers

This section describes the production process used to prepare the nanofibers which served as frictional layers in the triboelectric sensor. The sensor is prepared by layers of PVDF and PVP which are made of nanofibers. The nanofibers are prepared via electrospinning because it is a simple and economic way of preparing a wide variety of polymer nanofibers [37]. Moreover, the large active surface of the electrospun nanofibers can efficiently generate triboelectric charges [38], which enhance the output performance of the triboelectric sensor.

In the preparation of PVDF fibres, polyvinylidene fluoride pellets with a molecular weight of 275,000 g mol-1, dimethylformamide (DMF) and acetone from Sigma-Aldrich were used. To prepare the solution for electrospinning, PVDF pellets were dissolved in a solvent mixture of DMF and acetone (40/60) at 20% w/v. After, the homogenous solution was placed to a plastic syringe to be spun in Nanon-01A using the following operational conditions: a high voltage of 15 kV, a spinning distance of 15 cm, a feed rate of 1 ml/h, a 21 G steel needle and a static collector. Finally, a dense array of randomly distributed PVDF nanofibers with an average diameter of 953 ± 360 nm was obtained as shown in Fig. 8.1 (a). From the figure, it

can also be observed a few beads which are attributed to the nature of the polymer solution.

For preparing the PVP fibres, polyvinyl pyrrolidone powder and ethanol were provided by Sigma-Aldrich. The polymer solution was prepared by dissolving 1 g PVP powder (MW = 360,000 g mol-1) in 10 ml of ethanol. The obtained homogenous solution was then spun using the following conditions: applied voltage of 18 kV, feed rate of 0.5 ml/h, spinning distance of 12 cm, a 21G steel needle and a static collector. As result, good quality PVP nanofibers with an average diameter of 1545 ± 349 and random orientations are obtained, and they are shown in Fig. 8.1 (b).
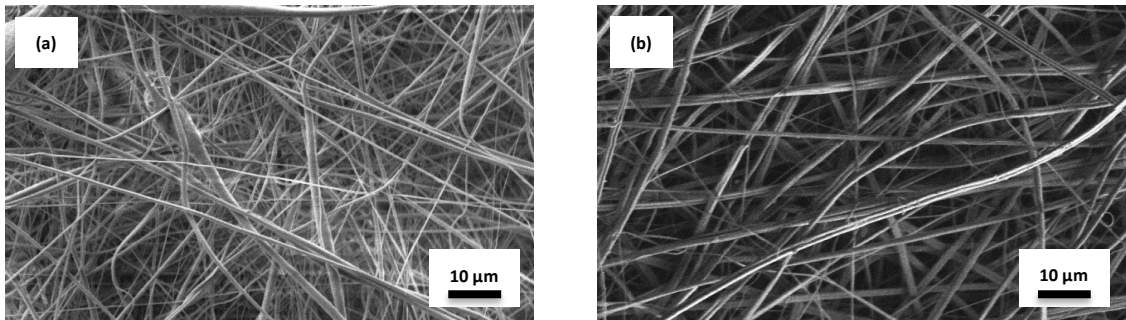
Figure 8.1 Scanning electron images of the nanofibers prepared by electrospinning: (a) SEM image of the PVDF nanofibers. (b) SEM image of the PVP nanofibers.

8.2.2 Design and assembly of triboelectric sensor

The structural design of the triboelectric sensor consists of two layers of polymer nanofibers and copper electrodes as displayed in Fig 8.2. The role of the copper films is to act as electrodes for the triboelectric sensor, while the PVDF and PVP nanofibers served as the frictional mats. PVDF is selected as one of the frictional mats due to its strong ability to charge negatively (attract electrons) when in contact with almost any other materials [39]. In contrast, PVP is chosen as the other frictional material due to its strong tendency to charge positively (lose electrons) [34]. Therefore, the contact between the layers of PVDF and PVP nanofibers

generates charges as a result of the triboelectric effect. The abilities of PVDF and PVP and other common triboelectric materials to produce negative and positive triboelectric charges respectively, are given in the triboelectric series.

Figure 8.2 Structure of the developed triboelectric sensor.

It also important to mention that the nanofibers used in the triboelectric sensor are very rough with the aim to increase the area of contact between the frictional materials and enhances the electric responses [40]. To verify the effect of the contact surface, the electric responses of a triboelectric sensor with smooth and rough frictional surfaces are compared. Fig. 8.3 shows the electric responses of two triboelectric sensors prepared by frictional materials with smooth and rough nanostructured surfaces. The voltage amplitude of the triboelectric sensors with smooth and rough frictional mats is 0.78 V and 4.44 V, respectively, under the same mechanical impact. As a result, the electric responses of the nanostructured sensor with rough surfaces are six times larger due to the higher contact surface of the nanofibers. This confirms that the use of rough nanostructured surfaces is an excellent method for improving the performance of the triboelectric sensor. These results are in very good agreement with previous studies [40, 41]. For example, F.R. Fan et al. [40] fabricated triboelectric sensors using frictional materials with different types of micropatterned arrays: film, lines, cubes and pyramids. The results show that the sensors patterned with geometric features (lines, cubes and pyramids) show from five to ten times larger electric responses than the film patterned sensor. Other studies as [41] compared the electric responses of identical triboelectric devices prepared with nanofibers and flat films. The results demonstrate that the electric responses of the device with nanofibers are seven times higher as compared the flat films.
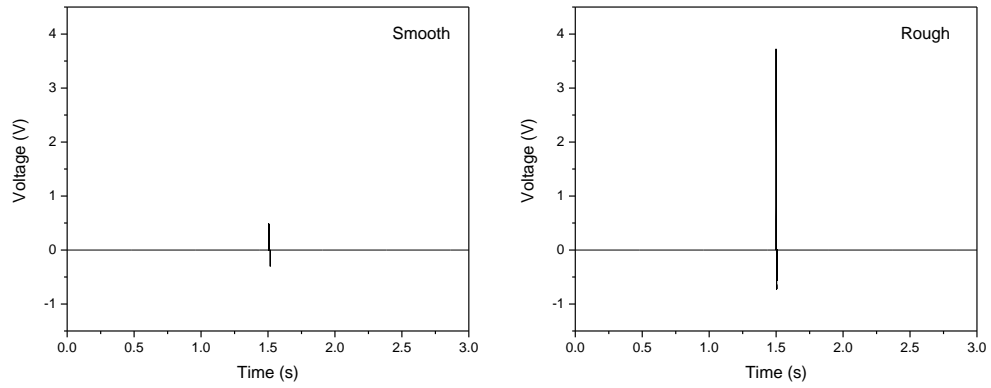
Figure 8.3 Effect of the contact surface on the electric responses of the triboelectric sensor: Voltage outputs of triboelectric sensors prepared using frictional materials with smooth and rough nanostructured surfaces.

The assembly process of the triboelectric sensor is detailed in Fig. 8.4 and can be divided into four steps. First, a layer of PVP nanofibers with a thickness of approximately 1 mm was spun on copper foil to form the bottom part of the sensor as shown in Fig. 8.4 (a). Secondly, a 2 mm layer of PVDF nanofibers was deposited on copper foil to form the top part of the sensor. A detailed description of the electrospinning procedure used to prepare the layers of PVDF and PVP nanofibers can be found in Section 8.2.1. Thirdly, the top and bottom part of the sensor are stacked to assemble the sensor as illustrated in Fig. 8.4 (b). The copper films are located at the top and bottom side of sensor while the layers of nanofibers are placed in between the electrodes. Finally, the sensor is sealed with polyethylene terephthalate film which avoids changes in the sensor electric responses due to environmental changes (humidity, rainy days) and ensure the stable performance of the device. Fig. 8.4 (c) shows a digital photograph of the triboelectric sensor as fabricated with the dimensions of 40 x 40 x 5 mm and a low weight of 5 g.
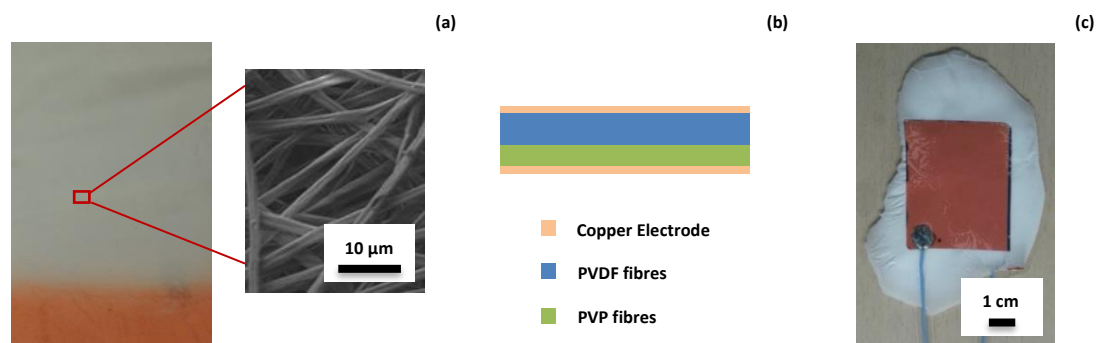

Figure 8.4 Fabrication process of the self-powered impact sensor: (a) Preparation of the bottom part of the sensor. (b) Assembly of the triboelectric sensor. (c) Photography of the fully assembled sensor.

In conclusion, it can be said that the fabrication process of the sensor is very simple and does not require sophisticated processing steps or equipments, which results in important cost-savings. Moreover, the electrospinning procedure is scalable and can be easily upgraded for large-scale production.

8.3 Detection of impacts in composite structures using the triboelectric sensor

This section explains the working principle of the developed triboelectric sensor and the experiment used to assess its capability to detect and quantify various energy impacts.

8.3.1 Working principle of the triboelectric sensor

The electric outputs of the triboelectric sensor are generated from the coupling effect of contact electrification and electrostatic induction [42-44]. Fig. 8.5 shows the working mechanism of the self-powered impact sensor, which is due to the contact-separation principle demonstrated by Wang's group [45-47]. At the original state (Fig. 8.5 (a)), the triboelectric sensor is at rest and no charge is generated, which result in no electric potential difference between the two electrodes. When the composite plates are impacted, the sensor changes from the original state to the contact state as shown in Fig. 8.5 (b). Therefore, the layers of PVDF and PVP nanofibers rub with each other which generate net negative charges on the surface of the PVDF fibers and net positive charges on the PVP fibers. This is attributed to the strong ability of PVDF and PVP nanofibers to gain and lose electrons, respectively. When the impact is released, the triboelectric sensor moves from the contact to the separation states as illustrated in Fig. 8.5 (c), (d) and (e). At this stage, the triboelectric sensor is bent downwards due to the inertia of the impact and the opposite triboelectric charges from PVDF and PVP nanofibers are separated.

Consequently, a strong potential difference between the top and bottom electrodes is generated in the triboelectric sensor. It is important to note that the potential difference is proportional to the relative distance between the positive and negative charges (electromagnetic induction effect) as can be seen in Fig. 8.5 (c) and (d). Finally, the generation of triboelectric charges stops, and the device reverts back to its initial state. This operational mechanism is an innovative alternative to the other conventional sensor working principles due to its independence on external power supply unit, sustainability and low-cost (maintenance-free).
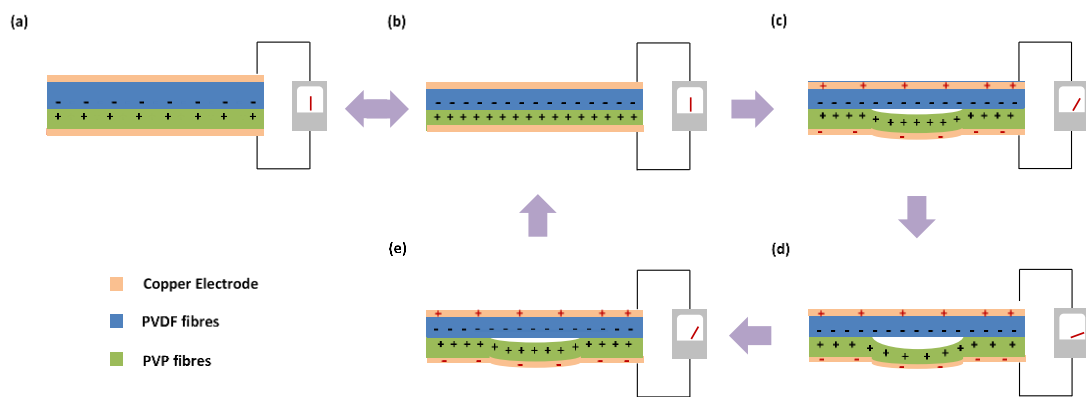

Figure 8.5 Working mechanism of the self-powered impact sensor: (a) The original state of the sensor. (b) The contact state of the sensor. (c-e) Various separation states of the triboelectric sensor. The polymer nanofibers are not illustrated in the figure for the purpose of simplification.

8.3.2 Detection of impacts using the triboelectric sensor

This paragraph shows that the energy of the impacts can be detected and measured using the developed triboelectric sensor. For the purpose, composite plates are subjected to controlled energy impacts using a drop weight impact machine (Instron CEAST 9350) and the sensor electric responses are measured in form of voltage and current using a commercial oscilloscope and digital multimeter respectively. Fig. 8.6 (a) shows a schematic representation of the experiment. The sensors are adhered to the composite plates using a strong adhesive and the sensor adhered to the composite plate is strongly fixed to the impact machine using the clamping fixture of the impact machine (see fig. 8.6 (b)). The idea of the suggested experiment is to investigate the

effect of the energy of the impacts on the electric responses of the developed triboelectric sensor.

Fig. 8.6 (b) shows a digital photo of the used experimental setup. From the image, it can be seen that carbon fibre reinforced square composite plates (CFRP) with the dimensions of (12 x 12 x 0.7) cm are clamped around the four edges and a controlled energy impact is applied in the centre of the specimen using the striker of the impact machine. The energy of the impacts was varied in a wide range of energies between 2 and 30 joules with small energy increments of 1 J. Finally, the electric responses which the triboelectric sensor produces as a result of the impacts are measured in terms of voltage and current using a commercial oscilloscope (Tektronix 2012B) and a digital multimeter (Agilent 34410A) as illustrated in Fig. 8.6 (c). The main purpose of the experiment is to evaluate the effect of the energy of the impacts on the amplitude of the resultant voltage and current electrical signals. This experiment is a simple and rapid way to evaluate the sensitivity of the developed triboelectric sensor for detection of impacts and quantification.
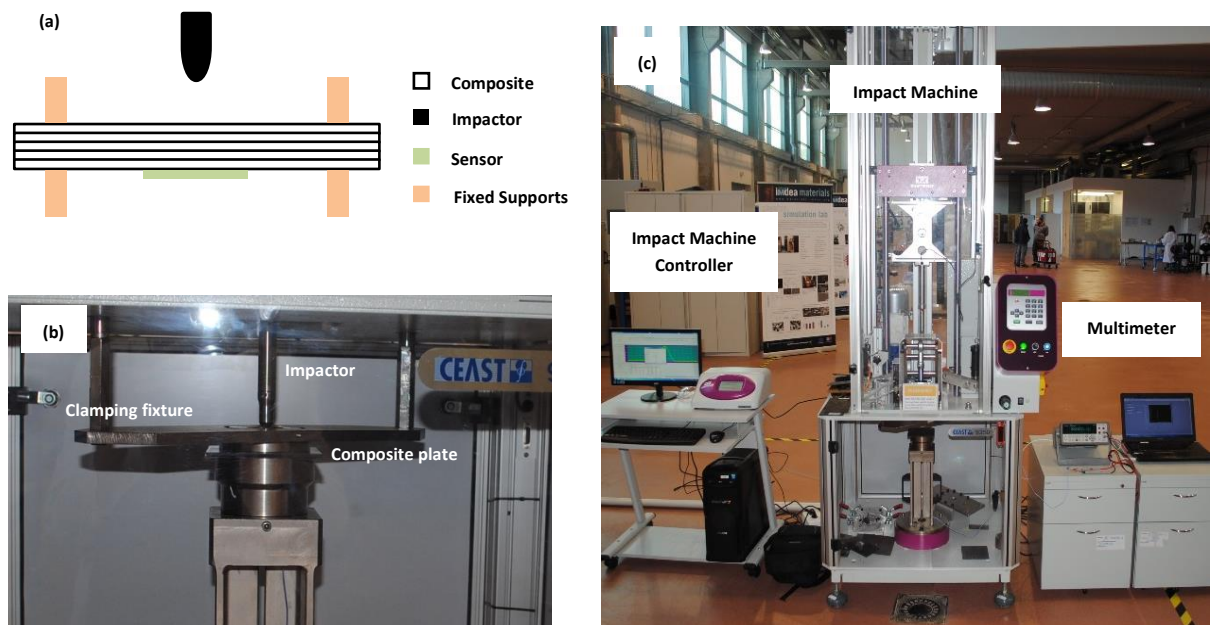

Figure 8.6 Description of the experiment used to evaluate the capability of the triboelectric sensor to detect impacts in composite plates: (a) Schematic description of the experimental setup. For the sake of clarity, a transversal view of the experimental setup is given. (b) Digital photography of the experimental setup. (c) The magnitude of the impacts is controlled using the drop-weight impact machine controller and the electric responses of the triboelectric sensor as result of the impacts are measured using a digit multimeter/ commercial oscilloscope.

8.4 Results and Discussion

This section is divided into three parts. The first section 8.4.1 studies the electric response of the sensor to various energy impacts in the range 2-30 J. In the next section 8.4.2 the effect of the impact force on the measured voltage and current responses is analysed. Finally, in the last section 8.4.3, the performance of the triboelectric sensor is compared to the performance of a commercial one.

8.4.1 Effect of the impact energy on the sensor electrical responses

The experimental procedure described in section 8.3 is used to supply various energy impacts to the composite plates tested. The energy of the impacts is varied from 2 to 30 J and the electric responses of the sensor are measured in terms of voltage and current using a commercial oscilloscope and digit multimeter respectively. The aim of this experiment is to find out how the energy of the impacts influences the electric responses of the sensor.

Fig. 8.7 (a) shows the voltage outputs of the sensor when the composite plates are impacted using energies from 2 to 30 J. From the figure, it can be appreciated that the energy of the impacts is increased with small increments of 1 J. As a result, the sensor voltage amplitudes increase gradually from 1.1 to 5.6 V with the increase of the impact energy from 2 to 30 J. This behavior can be attributed to the stronger friction between the PVDF and PVP polymer nanofibers when the composite plates are impacted at higher energy, which results in larger electric responses. In other words, the voltage outputs of the triboelectric sensor can be defined as:

$$V = \frac{\sigma d}{\varepsilon_0} \qquad (12)$$

where σ represents the density of triboelectric charges, d is associated to the distance between the layers of polymer nanofibers and ε_0 is the vacuum permittivity. In our

triboelectric sensor, the increment of the voltage outputs is attributed to the change in σ and d which results from the increase of the triboelectric charges due to the stronger friction and the higher separation distance between the polymer nanofibers. These experimental results are in good agreement with previous works [31, 32] where it was observed that the voltage responses of triboelectric sensors are directly proportional to the energy of the impact for a small range of energies between 0.02 and 0.2 J, although these results are for much smaller energies. A similar behaviour is reported by [21], where a self-powered acceleration sensor is developed for the purposes of monitoring various high acceleration impacts for military equipment and automobiles. The results of this work revealed that the electric responses of a PDMS-based triboelectric sensor increase linearly with the acceleration of the impacts in a wide measurement range up to 1.8 x 104 g.

Fig. 8.7 (b) also shows the maximum current responses of the triboelectric sensor when the composite specimens are subjected to impacts in the same energy range. From the figure, it can be clearly seen that the current amplitude increases directly and proportionally with energy of impact. From the figure, it can be also observed that the maximum current amplitude raises from 144 to 546 nA as the impact energy increases from 2 to 30 J. As indicated in [43], the current of a triboelectric sensor can be defined as:

$$I = C\frac{\partial V}{\partial t} + V\frac{\partial C}{\partial t} \qquad (13)$$

Where C is the capacitance of the triboelectric sensor and V is the voltage between the two electrodes. When the composite specimens are subjected to higher energy impacts, the voltage increases, which explains the gradual increase in the current of the triboelectric sensor when the impact energies increase from 2 to 30 J. It is also important to note that the figure shows a positive curve instead of two peaks for each energy impact. This is attributed to the following two reasons: (1) The current output signal generated by the triboelectric sensor is rectified, which results in two positive peaks for the contact and separation states and (2) the duration of the impacts is a very short time (0,003 seconds) and therefore, the two positive current peaks from the rectified signal are overlapping.
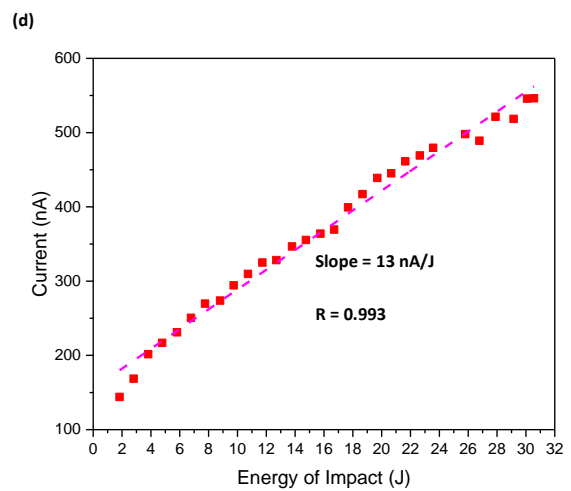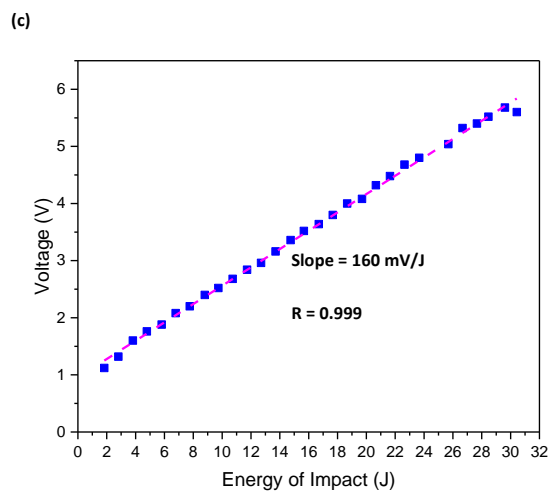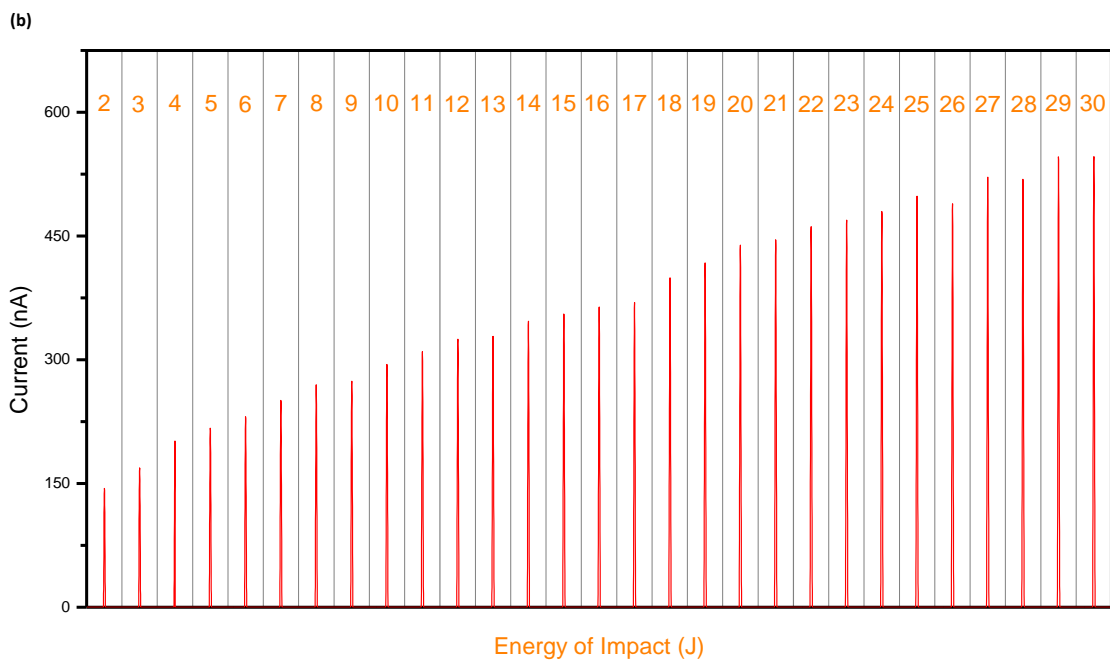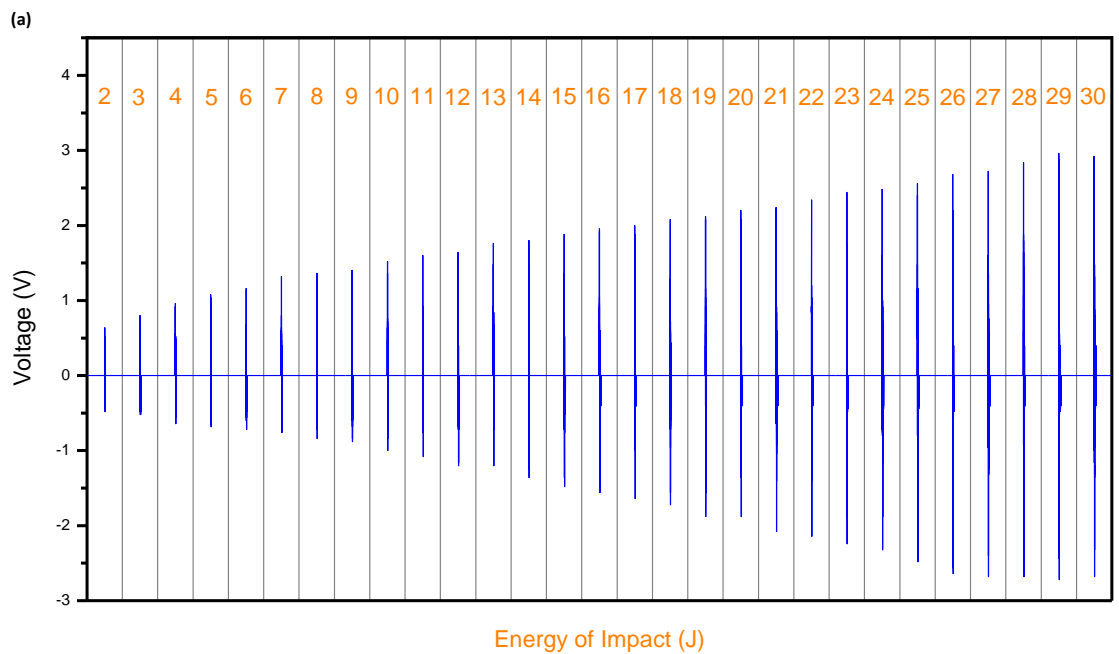
Figure 8.7 Effect of the impact energy on the electric responses of the triboelectric sensor: (a) Voltage and (b) current outputs when the composite plates are impacted using controlled impact energy from 2 to 30 J. (b) Voltage and current outputs of the sensor as a function of the energy of the impact.

Figure 8.7 (c) and (d) display the relations between the energy of the impacts and the obtained maximum current/voltage amplitudes. The graphics show a strong positive linear dependence with the energy of the impacts. The corresponding Pearson coefficients for the energy-voltage and energy-current curves are 0.999 and 0.993 respectively. Thus, very good linear relations between the impact energy and the corresponding voltage and current values can be concluded from our results for the tested energy range (between 2 and 30 J). These linear relationships are ideal as the sensor is used to measure the energy of the impact from the measured voltage/current.

The sensitivity represents the change in output of the sensor per one joule unit change. The sensitivity is also one of the most important parameters of a sensor and it can be calculated using the slope of the straight lines shown in Fig. 8.7 (c) and (d). According to our results, the voltage and current outputs show very high impact sensitivities of 160 mV/J and 13nA/J for a wide energy range from 2 to 30 J as can be seen from Fig. 8.7 (c) and (d). Accordingly, it can be concluded that the developed sensor features very high sensitivities of both the voltage and the current to changes in the impact energy, which demonstrates the capability of the sensor to measure the impact energy. It should be also mentioned that these sensitivities are higher than the reported by other authors in other research works [21, 33].

It is also important to mention that for high impact energies (> 26 J), a few small deviations can be seen among the data points on Fig 8.7 (c). and (d). Some possible explanations for these small deviations could be the high energies utilized during the impacts or small dimensional differences of the composite plates impacted.

The results presented above confirm the direct linear proportionality between the applied impact energy and the resultant voltage and current outputs. Thus, it can be concluded that the developed sensor can be used to detect impacts and quantify the energy of the applied impacts as well. Furthermore, the produced electric current

and voltage signals demonstrate a very high impact sensitivity in a wide detection range, which demonstrates the high performance of the sensor for detection of impacts.

8.4.2 Effect of the impact force on the sensor electric responses

In this section, we study the effect of the impact force on the voltage and current responses of the triboelectric sensor. As stated above, the composite plates were impacted using energies from 2 to 30 J with a step of 1J. For each energy impact, the drop weight impact machine (Instron CEAST 9350) provides the impact force by means of a sensor incorporated at the tip of the drop-weight impactor (see Fig. 8.6 (b)). With the aim to verify whether the electric response depends on the impact force, the same composite plates together with the sensor attached (see Fig. 8.6 (a)) are impacted using different impact forces which vary between 2000 and 14500 N and the electric outputs are measured as detailed in Section 8.3.

Fig. 8.8 (a) and (b) show the voltage and current amplitudes as a function of the impact forces applied. It can be clearly seen that the sensor electric responses are affected by the magnitude of the force, and the amplitude of the voltage and the current increase with the increase of the impact force. Therefore, the voltage and current vary from 1.1 to 5.6 V and 144 to 546 nA, respectively, when the impact forces increase from 2000 to 14500 N. As stated above, the increments of the sensor electric responses can be attributed to the higher friction between the PVDF and PVP nanofibers.

A strong linear relationship between the impact force and the electric voltage/current output with a high sensitivity are desired for the quantification of the impact force. From the results given in Fig. 8.8 (a) and (b), it can be observed that a strong linear relationship between the impact force and the electric current and voltage as the data points for both cases can be interpolated using a straight line with

a Pearson coefficient of 0.99. Furthermore, the electric voltage and current demonstrate sensitivities of 0.4 mV/N and 0.03 nA/N, respectively, for a very wide range of impact forces between 2000 and 15000 N. Therefore, the fabricated triboelectric sensor is capable to transform the impact force into electric current and voltage, with sensitivity higher than the sensitivity of other conventional sensors [48].
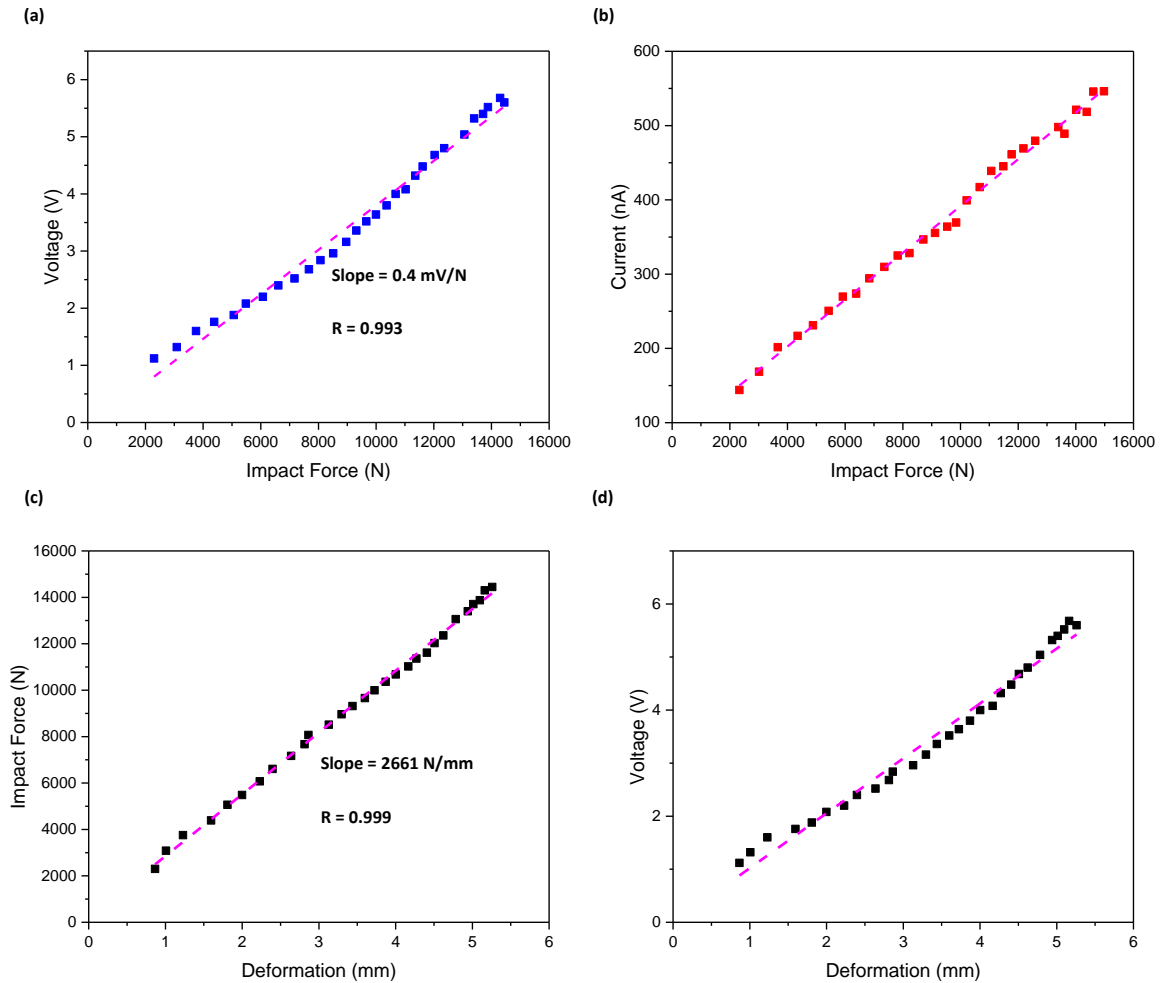

Figure 8.8 Effect of the impact forces on the electric responses of the triboelectric sensor: (b) Voltage and (c) current output of the sensor as a function of the impact force. (c) Deformation of the composite plates as a function of the impact force. (d) Voltage outputs of the composite plates as a function of the deformation.

The strong linear relationship between the impact force/energy and the sensor's electric response can be explained using the theory of small deformations [49] and the basics of contact mode TENGs [44]. According to the theory of small

deformations [49], the deformation of the composite laminates increases linearly with the energy of the impacts, when the deformation of the composite plates is much smaller than the relevant dimensions of the specimens. This behaviour can be assumed for our composite plates as the deformation of the specimens due to the impacts are very small as a result of the thickness and the high stiffness of the carbon composite plates. Therefore, it can be assumed that the deformation of the triboelectric sensors adhered to the composites increases linearly with the energy of the impacts. The small deformations and critical deformation of the sensors adhered to the composite plates can be calculated using the theory of small deformations, which is extracted from the materials mechanics theory [49]. As suggested by the theory of contact mode TENGs [44], the voltage outputs of the sensor are strongly influenced by the density of triboelectric charges and separation of triboelectric materials (see equation 12). As the deformation of the sensor increases linearly with the impact force, the generated triboelectric charges and separation of the frictional layers are linearly proportional to the sensor deformation, then it can be concluded that the generated voltage will be hence linearly proportional to the applied impact force.

The developed triboelectric sensor maintains linearity at full scale because the relationship between deformation displacement and impact force is linear in the whole measurement range. Figure 8.8 (c) shows the force-displacement curve in whole experimental measurement range. From the figure, it can be observed that there is a strong linear relationship between the impact force and the deformation with a high coefficient of Pearson of 0.999. Therefore, it can be said that the electric responses of the sensor show linearity at the full scale because the deformation of the composite is linear. We have also analysed the effect of the deformation of the triboelectric sensor on the sensor electric responses. For the purpose, the voltage outputs as a function of the deformation are plotted on Fig. 8.8 (d). The results show that there is a linear relationship (R= 0.991) between the deformation and the voltage outputs. As the deformation of the sensors is increased linearly, the generation of triboelectric charges and separation of the frictional materials is increased proportionally, which results in a linear increment of the sensor electric responses at the full scale.
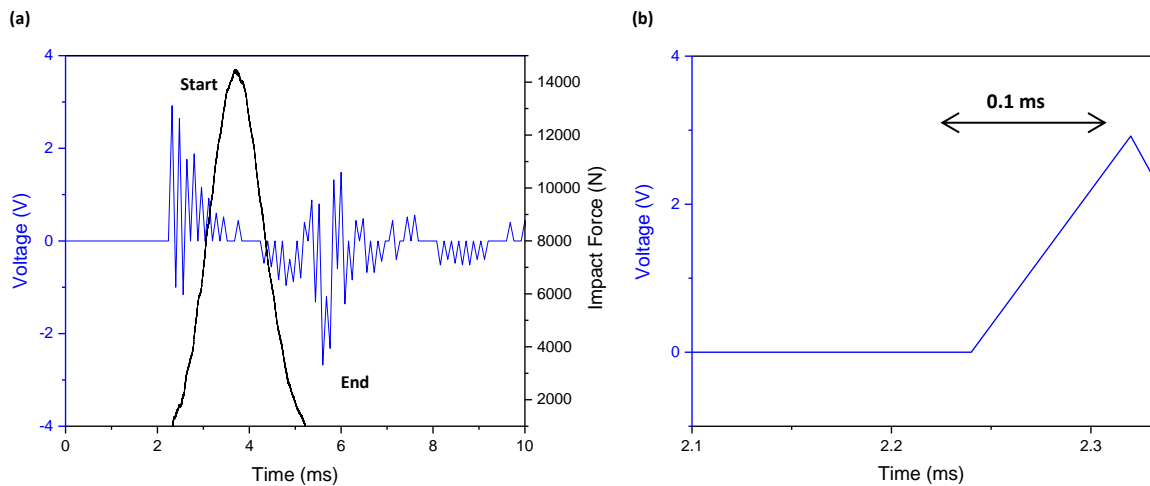
Figure 8.9 Effect of the impact forces on the electric responses of the triboelectric sensor: (a) Output voltage of the triboelectric sensor under an impact force of 14500 N. (b) Response time of the triboelectric sensor by enlarging the voltage output signal.

Fig. 8.9 (a) shows the impact force history (in black) together with the voltage response of the sensor (in blue) when the composite plates are subjected to an impact force of 14500 N. The largest positive and negative peaks in the figure indicate the start and end of the impact, respectively and are associated with the direction in which the electrons flow through the external circuit. From there it can be assumed that the triboelectric sensor could be also used to estimate the duration of the impact (0.003 s) which is the time between the two highest peaks of the voltage history. These results show the potential of this triboelectric sensor for detection and monitoring of impacts in real time. The multiple voltage peaks observed during the impact (see Fig. 8.9 (a)) are attributed to multiple contact-separations of the layers of polymer triboelectric nanofibers caused by the impact. Furthermore, it should be also mentioned that the largest positive and negative peaks of the voltage signal show a minimum separation with the start and end of the impact force, which demonstrates that the sensor can be used to measure impacts in real time. Fig. 8.9 (b) shows the amplified voltage signal for the 14500 N force impact. From the figure, it can be seen that the response time of the sensor is very fast (0.0001 s), which is defined as the time between zero to the maximum voltage.

In conclusion, it can be said that the sensor's electric response (in terms of voltage and current) are both linearly proportional to the impact forces and both the current and the voltage are characterized by high sensitivity for a rather wide detection range of the impact force. Furthermore, it should be also mentioned that the response of the developed sensor is very fast and shows a negligible delay to the application of the impact energy.

8.4.3 Comparison between triboelectric sensor and commercial sensor

The present section aims to compare the performance of the developed triboelectric impact sensor with a piezoelectric commercial sensor which is used for measuring impact force/energy. This is done by comparing the sensitivity, the Pearson coefficient (strength of the linear relationship between the impact force and the corresponding electric voltage), and the response time for both the developed triboelectric impact sensor and the piezoelectric sensor. For the purpose, both sensors, the developed one and the piezoelectric one were subjected to the same experiment as presented in section 8.3, which was used to determine their sensitivity, linearity and response time. The commercial sensor used in the impact tests is kindly provided by the company Measurement Specialities. The sensor is composed of a flexible polyvinylidene fluoride film which is often used for touch, vibration and impact sensing. As a result of the impacts, a voltage output with a large amplitude up to 50 V is created when the film moves back and forth.

Fig. 8.10 (a) shows the voltage output of the piezoelectric comercial sensor, when the same composite plate with the piezoelectric sensor attached to it (see Fig. 8.6 (a)) is subjected to an impact force of 14500 N. The voltage output signal shows positive and negative peaks, which can be observed during and after the impact, with the highest peaks being referred to the start and the end of the impact, respectively. Additionally, the time interval between the highest positive and negative peaks is 0.003 s, which can be associated to the duration of the impact. Figure 8.10 (b) shows the response time of the commercial sensor, which is defined as the time interval between zero and the maximum voltage response, which is the time taken by the

sensor to reach the maximum voltage corresponding to the applied impact force. From the figure, it can be seen that the response time of the commercial sensor to an impact of 14500 N is 0.0003 s. Similar results found for the fabricated triboelectric sensor where the response time is 0.0001 s for the same mechanical impact as displayed in Fig. 8.10 (b). Therefore, it can be concluded that the response time of both sensors to impact, the new triboelectric sensor and the piezoelectric one, are rather short (less than one 0.001 s), which means it takes both sensors a very short time to respond to the applied impact.
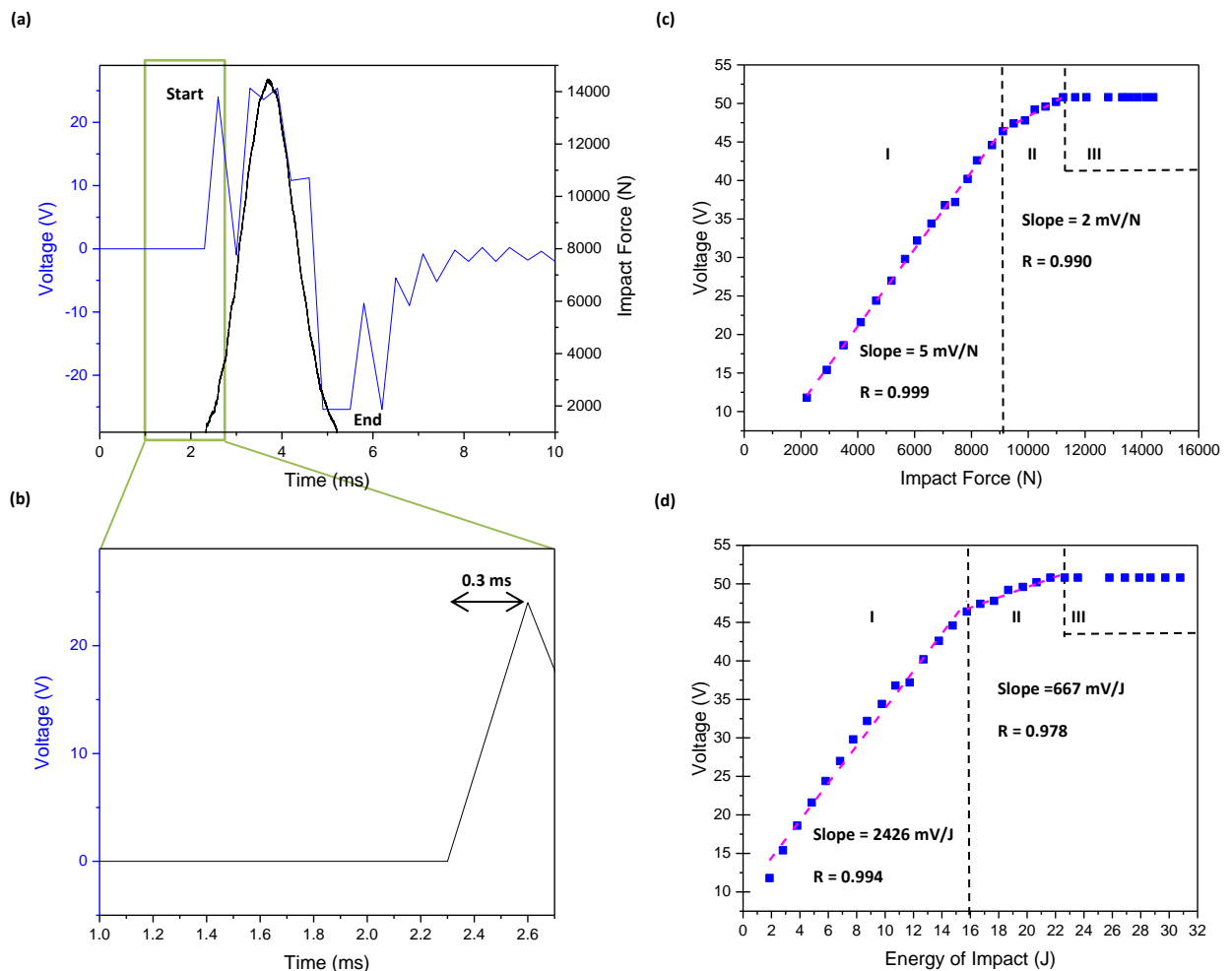

Figure 8.10 Performance of the commercial sensor: (a) Output voltage of the piezoelectric sensor under an impact force of 14500 N. (b) The response time of the commercial sensor by enlarging the output voltage signal. Voltage outputs as a function of the impact forces (c) and energy of the impact (d).

Fig. 8.10 (c) and (d) illustrate the voltage outputs of the piezoelectric sensor, when the composite plates with the sensor attached are impacted using different forces/energies, which vary in the range between 2000 and 14500 N (2 -30 J). The figures show that the peak-to-peak voltage increase together with the raise of the impact force /energy and finally saturate at 50.8 V, at an impact force of 11200 N (22 J). These results indicate that the relation between the impact energy/force and voltage is linear for the regions I and II and nonlinear over the whole measurement range.

On the other hand, our results showed that the developed triboelectric sensor has a nearly perfect linear relationship between the impact energy/force and the electric sensor responses over the whole measurement range. From the results given in Section 8.4.1 and 8.4.2, it can be observed a strong linear relationship between the impact force-voltage and impact energy-voltage relationships, which are both characterised by a Pearson coefficient of 0.99 in the detection range (2-30 J and 2000-14500 N). This means that the developed sensor can be used to quantify the energy/force of the impacts by measuring the resulting voltage in a wider force/energy range than the commercial piezoelectric sensor.

The sensitivity of the voltage outputs measured by piezoelectric sensor are calculated in the same way as this was done with the developed triboelectric sensor using the slope of the corresponding straight lines shown in Fig. 8.10 (c) and (d). Fig. 8.10 (c) exhibits three distinct regions. In the first region when the impact forces are below 9500 N, it is noticed that the sensor shows a very high impact sensitivity of 5 mV/N. In the second region, between 9500 to 11200 N, the impact sensitivity decreases to 2 mV/N. In the region above 11200 N, the output voltage saturates at 50.8 V and the piezoelectric sensor reachs a limit point after which it can no longer register changes in the applied impact force. As can be seen from Fig. 8.10 (d), the sensitivity of the commercial sensor is 2426 mV/J in the low impact energy region, below 16 J while the sensitivity is 667 mV/J in the higher impact energy region from 16 to 22 J. In conclusion, it can be said that the commercial piezoelectric sensor shows very high impact sensitivity in the low energy/forces region.

The electric responses generated by the triboelectric sensor are approximately ten times smaller as compared to the piezoelectric commercial sensor. In our view, this is not a limitation because the electric responses of the triboelectric sensor can be increased significantly by the incorporation of a separator between the layers of polymeric nanofibers [50, 51]. For example, T.C. Hou et al. [50] proved that the electric outputs of a triboelectric nanogenerator can be increased around 700% by adding a 3 mm spacer between the frictional layers. Similar results were found on [51] where the output voltage raises from 13 to 160 V, when the spacer distance increases from 0.5 to 6.5 mm. Additionally, this hypothesis is also verified by equation 12, where it can be appreciated that the output voltage will increase with increasing the distance between the layers of nanofibers (e.g. by adding a spacer in the triboelectric sensor).

Finally, the measurement range from the developed triboelectric sensor and commercial sensor is compared. As can be seen in Fig. 8.10 (c) and (d), the commercial sensor shows a smaller detection range from 2 to 22 J as compared to the triboelectric sensor (2 - 30 J). This characteristic is the utmost importance as impact sensors are required to measure in a wide detection range.

Characteristic	Units	Triboelectric Sensor	Commercial Sensor
Response time	s	0.0001	0.0003
Linearity	dimensionless	0.999	0.978 - 0.994
Sensitivity	mV/J	160	667 - 2426
Detection Range	J	2-30	2-22

Table 8.1 A comparison of the triboelectric and commercial sensor characteristics for impact energy detection.

In summary, this section compares the performance of the triboelectric sensor with a standard commercial sensor. For that purpose, the response time, linearity, sensitivity and detection range of the developed triboelectric sensor and commercial sensor are compared as can be seen in Table 8.1. The results reveal that the response

times of the developed and triboelectric sensor are very fast (less than 1 ms). From the table, it can be observed that the developed triboelectric sensor shows smaller impact sensitivity respect to the commercial sensor. However, the sensitivity of the triboelectric sensor is constant over the whole detection range while the sensitivity for the piezoelectric commercial sensor varies for the different regions (see Fig. 8.10 (d)). Finally, the triboelectric sensor shows a higher linear response and wider measurement range as compared to the commercial sensor. These findings can be used to demonstrate that a triboelectric sensor can be used to detect and measure impacts with a similar performance than a commercial sensor.
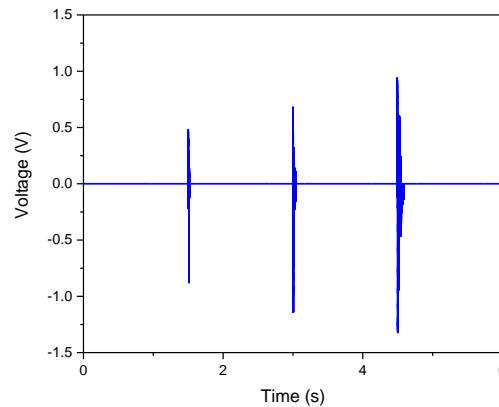

Figure 8.11 Voltage outputs of the triboelectric sensor for three different hailstone impacts.

Additionally, we demonstrate the practical application of the triboelectric sensor for real-time detection and measurement of hailstone impacts in composite structures. As shown in the video S1 in the supplementary information of [52], the electric signal of the triboelectric sensor generated at the moment of the hailstone impact collisions, which verifies that the sensor can measures impacts in real-time. Fig. 8.11 shows the voltage outputs for three different hailstone impacts. According to the voltage-energy relationship showed in Fig. 8.7 (c), the energy of the three hailstone impacts are about 2.5 J, 5.4 J and 8.1 J. The results from the drop weight impact and hailstone tests demonstrates the commercial applications of the triboelectric sensor for monitorization of impacts in aircrafts, wind turbines and other structures made of composite materials.

8.5 Conclusions

In this chapter, we have demonstrated for the first time that a triboelectric sensor can be successfully used to detect and measure impacts in structures made of composite materials. The findings of this study indicate that the developed triboelectric sensor shows good sensitivity to impacts in a wide range of energies and impact forces between 2-30 J and 2000-14500 N, respectively. Moreover, it was shown that the voltage and current outputs show a strong linear relationship with the energy of the impacts (R=0.99). It has been also demonstrated that the current and the voltage outputs show a very fast response to the impacts. This is very important as it indicates that the developed sensor can be used to measure impacts in real time with a negligible delay.

From a fabrication point of view, the preparation of the triboelectric sensor is very simple and does not require sophisticated processing steps. Moreover, this procedure can be easily upgraded for large-scale production. From an innovation point of view, the triboelectric sensor is a potential alternative to other conventional impact sensors due to their independence of an external power supply unit and lower cost due to the cheap materials used and easy fabrication. From a technical point of view, the sensor shows very high sensitivity and linearity in a wide detection range which is comparable to other commercial sensors.

In conclusion, our work has proved for the first time an innovative approach to detect and measure the magnitude of the impacts in composites structures. The present findings demonstrate that the developed triboelectric sensors can be successfully utilized for real-time detection and measurement of the energy and/or the force of impacts in structures made of composite mats. This can have important applications for monitoring of impacts in composite structures as aircrafts, wind turbines or bridges.

References

[1]   N.K. Ravikiran, A. Venkataramanaiah, M.R. Bhat, C.R.L. Murthy, Detection and evaluation of impact damage in CFRP laminates using ultrasound C-Scan and IR thermography, in: Proceedings of National Seminar on Non-Destructive Evaluation, December 2006.

[2]   Y. Li, G. Tian, Z. Yang, W. Zhang, W. Luo, Detection capability evaluation of low velocity impact damage in composites using ultrasonic infrared termography, Chin. J. Sci. Instrum. 37 (2016) 1124-1130.

[3]   Y.Y. Hung, Shearography for non-destructive evaluation of composite structures, Opt. Laser Eng. 24 (1996) 161-182.

[4]   D. Vavrik, J. Jakubek, I. Jandejsek, I. Kumpova, J. Zemlicka, X-ray radiography and tomography study of a delamination in a CFRP and honeycomb structures, in: Proceedings of 5th Conference on Industrial Computed Tomography (iCT), 2014, pp. 63-66.

[5]   D. Garcia, I. Trendafilova, A multivariate data analysis approach towards vibration analysis and vibration-based damage assessment: Application for delamination detection in a composite beam, J. Sound Vib. 333 (2014) 7036-7050.

[6]   D. Toomey, E. Winkel, R. Krishnaswami, Evaluation of air-bag electronic sensing system collision performance through laboratory simulation, in: Proceedings of SAE World Congress and Exhibition, April 2015.

[7]   Y. Choi, S.H. Abbas, J.R. Lee, Aircraft integrated structural health monitoring using lasers, piezoelectricity, and fiber optics, Measurement, 125 (2018) 294-302.

[8]   M.S. Salmanpour, Z.S. Khodaei, M.H.F. Aliabadi, Impact damage localisation with piezoelectric sensors under operational and environmental conditions, Sensors, 17 (2017) 1178.

[9]   S. Rihana, J. Mondalak, Wearable fall detection system, in: Proceedings of 3rd Middle East Conference on Biomedical Engineering (MECBME), October 2016.

[10]   S. Joshi, G.M. Hedge, M.M. Nayak, K. Rajanna, A novel piezoelectric thin film impact sensor: Application in non-destructive material discrimination, Sens. Actuators A Phys. 199 (2013) 272-282.

[11]   A. Dixit, S. Bhalla, Prognosis of fatigue and impact induced damage in concrete using embedded piezo-transducers, Sens. Actuators A Phys. 274 (2018) 116-131.

[12]   S. Phan, Z.F. Queck, P. Shah, D. Shin, Z. Ahmed, O. Khatib, M. Cutkosky, Capacitive skin sensors for robot impact monitoring, in: Proceedings of International Conference on Intelligent Robots and Systems, September 2011, pp. 2992-2997.

[13]   D. Liang, B. Culshaw, Fibre optic silicon impact sensor for application to smart skins, Electron. Lett. 29 (1993) 529-530.

[14]   R. Ouckama, D.J. Pearsall, Evaluation of a flexible force sensor for measurement of helmet foam impact performance, J. Biomech. 44 (2011) 904-909.

[15]   K. Parida, V. Bhavanasi, V. Kumar, R. Bendi, P.S. Lee, Self-powered pressure sensor for ultra-wide range pressure detection, Nano Res. 10 (2017) 3557-3570.

[16]   C. Garcia, I. Trendafilova, R. Guzman de Villoria, J. Sanchez del Rio, Self-powered pressure sensor based on the triboelectric effect and its analysis using dynamic analysis, Nano Energy, 50 (2018) 401-409.

[17]   K.Y. Lee, H.J. Yoon, T. Jiang, X. Wen, W. Seung, S.W. Kim, Z.L. Wang, Fully packaged self-powered triboelectric pressure sensor using hemispheres-array, Adv. Energy Mater. 6 (2016) 1502566.

[18] M.F. Lin, J. Xiong, J. Wang, K. Parida, P.S. Lee, Core-Shell nanofiber mats for tactile pressure sensor and nanogenerator applications, Nano Energy, 44 (2018) 248-255.

[19] Q. Liang, Z. Zhanga, X. Yan, Y. Gu, Y. Zhao, G. Zhang, S. Lu, Q. Liao, Y. Zhang, Functional triboelectric generator as self-powered vibration sensor with contact mode and non-contact mode, Nano Energy, 14 (2015) 209-216.

[20] S. Wang, S. Niu, J. Yang, L. Lin, Z.L. Wang, Quantitative measurements of vibration amplitude using a contact-mode freestanding triboelectric nanogenerator, ACS Nano, 8 (2014) 12004-12013.

[21] K. Dai, X. Wang, F. Yi, C. Jiang, R. Li, Z. You, Triboelectric nanogenerators as self-powered acceleration sensor under high-g impact, Nano Energy, 45 (2018) 84-93.

[22] C. Xiang, C. Liu, C. Hao, Z. Wang, L. Che, X. Zhou, A self-powered acceleration sensor with flexible materials based on the triboelectric effect, Nano Energy, 31 (2017) 469-477.

[23] Q. Jing, G. Zhu, W. Wu, P. Bai, Y. Xie, R.P.S. Han, Z.L. Wang, Self-powered triboelectric velocity sensor for dual-mode sensing of rectified linear and rotatory motions, Nano Energy, 10 (2014) 305-312.

[24] Y. Xi, H. Guo, Y. Zi, X. Li, J. Wang, J. Deng, S. Li, C. Hu, X. Cao, Z.L. Wang, Multifunctional TENG for blue energy scavenging and self-powered wind-speed sensor, Adv. Energy Mat. 7 (2017) 1602397.

[25] Y. Yang, L. Lin, Y. Zhang, Q. Jing, T.C. Hou, Z.L. Wang, Self-powered magnetic sensor based on a triboelectric nanogenerator, ACS Nano, 6 (2012) 10378-10383.

[26] S. Qi, H. Guo, J. Chen, J. Fu, C. Hu, M. Yu, Z.L. Wang, Magnetorheological elastomers enabled high-sensitive self-powered tribo-sensor for magnetic field detection, Nanoscale, 10 (2018) 4745.

[27] Y. Su, G. Xie, S. Wang, H. Tai, Q. Zhang, H. Du, H. Zhang, X. Du, Y. Jiang, Novel high-performance self-powered humidity detection enabled by triboelectric effect, Sens. Actuators B Chem. 251 (2017) 144-152.

[28] S. Cui, Y. Zheng, T. Zhang, D. Wang, F, Zhou, W. Liu, Self-powered ammonia nanosensor based on the integration of the gas sensor and triboelectric nanogenerator, Nano Energy, 49 (2018) 31-39.

[29] Y. Su, G. Zhu, W. Yang, J. Yang, J. Chen, Q. Jing, Z. Wu, Y. Jiang, Z.L. Wang, Triboelectric sensor for self-powered tracking of object motion inside tubing, ACS Nano, 8 (2014) 3843-3850.

[30] A. Yu, L. Chen, X. Chen, A. Zhang, F. Fan, Y. Zhan, Z.L. Wang, Triboelectric sensor as self-powered signal reader for scanning probe surface topography imaging, Nanotechnology, 26 (2015) 165501.

[31] C. Garcia, I. Trendafilova, R. Guzman de Villoria, J. Sanchez del Rio, Triboelectric nanogenerator as self-powered impact sensor, in: Proceedings of International Conference on Engineering Vibration (ICoEV), September 2017, 148 (2018) 14005.

[32] B. Zhang, L. Zhang, W. Deng, L. Jin, F. Chun, H. Pan, B. Gu, H. Zhang, Z. Lv, W. Yang, Z.L. Wang, Self-powered acceleration sensor based on liquid metal triboelectric nanogenerator for vibration monitoring, ACS Nano, 11 (2017) 7440-7446.

[33] G. Zhu, W.Q. Yang, T. Zhang, Q. Jing, J. Chen, Y.S. Zhou, P. Bai, Z.L. Wang, Self-powered, ultrasensitive, flexible tactile sensors based on contact electrification, Nano Lett. 14 (2014) 3208-3213.

[34] Y. Hao, Y. Bin, H. Tao, W. Cheng, W. Hongzhi, Z. Meifang, Preparation and optimization of polyvinylidene fluoride (PVDF) triboelectric nanogenerator via electrospinning, in: Proceedings of the 15th IEEE International Conference on Nanotechnology, July 2015, pp. 1485-1488.

[35] F. Zhang, B. Li, J. Zheng, C. Xu, Facile fabrication of micro-nano structured triboelectric nanogenerator with high electric output, Nanoscale Res. Lett. 10 (2015) 298.

[36] Y. Zheng, L. Cheng, M. Yuan, Z. Wang, L. Zhang, Y. Qin, T. Jing, An electrospun nanowire-based triboelectric nanogenerator and its application in a fully self-powered UV detector, Nanoscale, 6 (2014) 7842.

[37] B. Yu, H. Yu, H. Wang, Q. Zhang, M. Zhu, High-power triboelectric nanogenerator prepared from electrospun mats with spongy parenchyma-like structure, Nano Energy, 34 (2017) 69-75.

[38] T. Huang, M. Lu, H. Yu, Q. Zhang, H. Wang, M. Zhu, Enhanced power output of a triboelectric nanogenerator composed of electrospun nanofiber mats doped with graphene oxide, Sci. Rep. 5 (2015) 13942.

[39] N. Cui, L. Gu, Y. Lei, J. Liu, Y. Qin, X. Ma, Y. Hao, Z.L. Wang, Dynamic behaviour of the triboelectric charges and structural optimization of the friction layer for a triboelectric nanogenerator, ACS Nano, 10 (2016) 6131-6138.

[40] F.R. Fan, L. Lin, G. Zhu, W. Wu, R. Zhang, Z.L. Wang, Transparent triboelectric nanogenerators and self-powered pressure sensors based on micropatterned plastic films, Nano Lett. 12 (2012) 3109-3114.

[41] B.U. Ye, B.J. Kim, J. Ryu, J.Y. Lee, J.M. Baik, K. Hong, Electrospun ion gel nanofibers for flexible triboelectric nanogenerator: electrochemical effect on output power, Nanoscale, 7 (2015) 16189-16194.

[42] W. Song, B. Gan, T. Jiang, Y. Zhang, A. Yu, H. Yuan, N. Chen, C. Sun, Z.L. Wang, Nanopillar arrayed triboelectric nanogenerator as self-powered sensitive sensor for a sleep monitoring system, ACS Nano, 10 (2016) 8097-81103.

[43]   S.Y. Shin, B. Saravanakumar, A. Ramadoss, S.J. Kim, Fabrication of PDMS-based triboelectric nanogenerator for self-sustained power source application, Int. J. Energy Res. 40 (2015) 3.

[44]   Y. Wang, Y. Yang, Z.L. Wang, Triboelectric nanogenerators as flexible power sources, NPJ Flex. Electron. 1 (2017) 10.

[45]   S. Niu, S. Wang, L. Lin, Y. Liu, Y.S. Zhou, Y. Hu, Z.L. Wang, Theoretical study of contact-mode triboelectric nanogenerators as an effective power source, Energy Environ. Sci. 6 (2013) 3576.

[46]   Z.L. Wang, Triboelectric nanogenerators as new energy technology and self-powered sensors – Principles, problems and perspectives, Faraday Discuss. 176 (2014) 447.

[47]   Z.L. Wang, L. Lin, J. Chen, S. Niu, Y. Zi, Triboelectric nanogenerators, Green Energy Technol. (2016) 23-47.

[48]   Z.H. Zhang, J.W. Kan, X.C. Yu, S.Y. Wang, J.J. Ma, Z.X. Cao, Sensitivity enhancement of piezoelectric force sensors by using multiple piezoelectric effects, AIP Adv., 6 (2016) 075320.

[49]   A.F. Bower, Applied Mechanics of Solids, Taylor and Francis Group, CRC Press, 2011.

[50]   T.C. Hou, Y. Yang, H. Zhang, J. Chen, L.J. Chen, Z.L. Wang, Triboelectric nanogenerator built inside shoe insole for harvesting walking energy, Nano Energy, 2 (2013) 856-862.

[51]   W. Li, J. Sun, M. Chen, Triboelectric nanogenerator using nano-Ag ink as electrode material, Nano Energy, 3 (2014) 95-101.

[52]   C. Garcia, I. Trendafilova, J. Sanchez del Rio, Detection and measurement of impacts in composite structures using a self-powered triboelectric sensor, Nano Energy, 56 (2019) 443-453.

Chapter 9

A new self-powered triboelectric nanostructured sensor for impact monitoring through measuring the impact velocity.

Impacts and collisions are quite frequent for a number of crucial and important structures, including aircrafts, wind turbines, bridges and other composites structures. Some examples are the collisions between birds and aircrafts or the impacts with hailstones. Hence, the detection and the measurement of impacts is of critical importance for monitoring the integrity of a structure. This chapter suggests a novel triboelectric nanostructured sensor and investigates its potential for monitoring impact velocities. The main idea is to monitor the impacts applied to composite plates. For the purpose an experiment is designed where composite plates are subjected to different impacts and the impact velocity is measured by adhering the prepared sensor to the plates. This study demonstrates the possibility for measuring the impact velocity through the newly developed sensor. Our results show that the sensor electric response increases with the increase of the impact velocity. Additionally, the produced voltage and current outputs show a linear directly proportional relationship to the measured impact velocity, which facilitates greatly the estimation of the impact velocity from the measured electric response. Furthermore, it should be noted that the suggested sensor demonstrates quite high sensitivity for a wide measurement range of impact velocities between 1.27 and 3.21 m/s. This research extends the application of triboelectric sensors for the purposes of impact monitoring, by measuring the impact velocity, through the development and the preparation of a novel triboelectric nanostructured sensor made of polyvinyl(fluoride) nanofibers and a film of polypropylene.

9.1 Introduction

Impacts are frequent in airplanes, wind turbines, bridges and other civil composite structures. For example, the operational state of wind turbines can be seriously affected due to the impact of hailstones. The integrity of aircraft composite structures can be seriously damaged because of the collisions with birds. Therefore, impacts are responsible for a big part of accidents in aerospace and civil structures affecting the working and health state of aircrafts, bridges and other structures made of composite laminates. Consequently, the detection and quantification of impacts is of critical importance for the health assessment of composite structures.

It is well known that impact sensors are very important for the detection and the correct quantification of impacts. Impact sensors are usually classified according to their working mechanism as piezoelectric [1, 2], resistive [3], triboelectric [4, 5], capacitive [6], and optical types [7]. Among them, the sensors operating based on the triboelectric effect are attracting considerable attention among the research community. The main advantage of triboelectric sensors is that they are self-powered and do not require an external power supply or battery. Furthermore, the materials used in triboelectric sensors as for example teflon, PVC or aluminium are cheap and commonly available in our daily life, which results in important cost-savings.

In the last years, several papers have investigated the applications of triboelectric sensors as self-powered active sensors for pressures [8-11], touches [12, 13], vibrations [14, 15], accelerations [16-18], dynamic motions [19, 20], and velocities [21-23]. For example, in ref. [21], the potential of a triboelectric sensor for measurement of velocities in the range between 100 and 500 rpm is investigated. The results showed that the voltage sensor responses increase from 17 V to 31 V as the rotational velocity changes from 100 to 500 rpm. Other studies as refs. [22, 23] suggest that triboelectric sensors can be successfully used as self-powered wind speed sensors. However, there are no previous studies to report about the potential of triboelectric sensors for detection and measurement of impact velocities in composite structures.

In this chapter, we design a novel triboelectric sensor using the combination of two cost-effective polymers named polyvinylidene fluoride (PVDF) and polypropylene (PP). In the design of the sensor, polyvinyl fluoride nanofibers are selected as negative triboelectric material because of their strong electron attracting ability [24-26]. In contrast, a film of polypropylene is used as positive triboelectric mat due to its low-cost and lower electron affinity as compared to PVDF. To the best of our knowledge, this is the first attempt to develop a triboelectric sensor based on the interaction between polyvinylidene fluoride (PVDF) nanofibers and a film of polypropylene (PP).

The aim of this chapter is to demonstrate the potential of the developed triboelectric sensor for monitoring impacts in composite structures like e.g. aircrafts. For this study, composite plates equipped with a triboelectric sensor are subjected to various impacts using a drop-weight impact machine with velocities ranging from 1.27 to 3.21 m/s. Then, the sensor electric responses are measured in form of voltage and current using a commercial oscilloscope and digital multimeter respectively. The idea is to investigate if the amplitude of the voltage and current signals is affected by the velocity of the impacts. The results show that the sensor electric outputs increase with the increase of the impact velocities applied to the composite plates. According to our results, a strong linear relation between the velocity of the impacts and the sensor electric outputs was observed. Additionally, the voltage and current outputs show very high impact sensitivity for a wide detection range between 1.27 and 3.21 m/s.

The main contributions of this chapter can be summarised as follows: First, this chapter suggests a new class of triboelectric sensors based on the interaction between a film of polypropylene and polyvinylidene fluoride nanofibers. Second, this work demonstrates for the first time the applications of triboelectric sensors for monitoring impacts in composite structures through measuring the velocity of the impacts. This is very important as impacts can harm the integrity of the composite structures through delamination and other fault mechanisms. The findings of this chapter can be

potentially used to demonstrate the potential applications of triboelectric sensors for impact velocity monitoring in composite structures, such as aircrafts or wind turbines.

The rest of the chapter is organised as follows: Section 2 describes the design and fabrication process of the triboelectric sensor. Section 3 shows a brief overview of the working mechanism of the triboelectric sensor. Section 4 explains the methodology used to study the potential applications of the sensor for impact assessment in composite structures. Section 5 presents, analyses and discusses the experimental results obtained during the experiment. The last section offers some conclusions.

9.2 Preparation of the triboelectric sensor

The triboelectric sensor used for this study was fabricated using polyvinylidene fluoride nanofibers and a film of polypropylene. The aim of this section is to explain the structural design and fabrication process of the triboelectric sensor.

9.2.1 Design of the sensor

The structure of the triboelectric sensor is schematically illustrated in Fig. 9.1 and can be divided into two sections: The top plate of the sensor consists of polyvinylidene fluoride nanofibers deposited on copper foil and the bottom plate of the sensor is based on a polypropylene film adhered to copper foil. The role of the copper foils is to act as electrodes for the sensor while the PVDF and PP serve as triboelectric frictional mats. In the design of the sensor, polyvinylidene fluoride nanofibers are purposely chosen according to the triboelectric series because they can easily gain electrons from the polypropylene film as detailed in table 9.1. This behaviour can be explained by the large composition percentage of fluorine in PVDF

and the large effective contact area of the nanofibers, which results in a strong ability to gain electrons (negative charges) from other triboelectric mats [9].
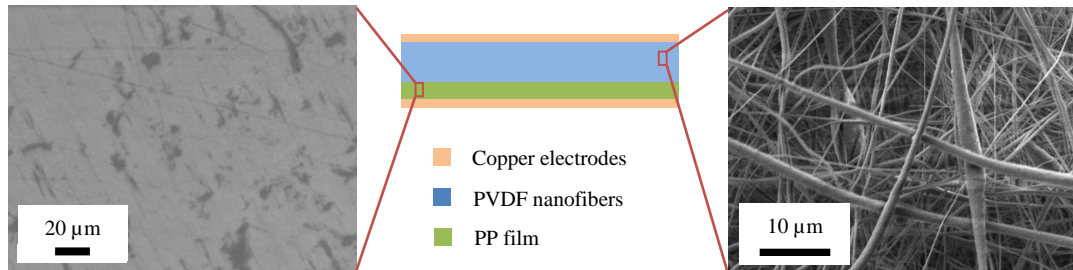

Figure 9.1 Schematic description of the sensor structure: The left inset of the figure shows a SEM image of the polypropylene film, while the right inset shows a SEM image of the polyvinyl fluoride nanofibers.

Table 9.1: List of triboelectric materials in accordance with their tendency of easy gaining electrons (negative) to losing electrons (positive). The materials at the top of the table possess a stronger ability to gain electrons and become negatively charged as compared to the materials at the bottom of the table.

A scanning electron microscope (SEM) image of the polypropylene film is depicted at left-hand side of Fig. 9.1. The image shows a few scratches uniformly distributed on the surface of polypropylene, which are beneficial to increase the contact surface of the frictional layer. Another more detailed SEM image of the PVDF nanofibers is shown at the right-hand side of Fig. 9.1. From the image, a dense array of PVDF nanofibers with random orientations can be appreciated. The average

diameter of the nanofibers was measured to be about 800 ± 350 nm. Furthermore, it can be observed that the nanofibers contain a few beads which can be attributed to the nature of the polymer solution used in the electrospinning.
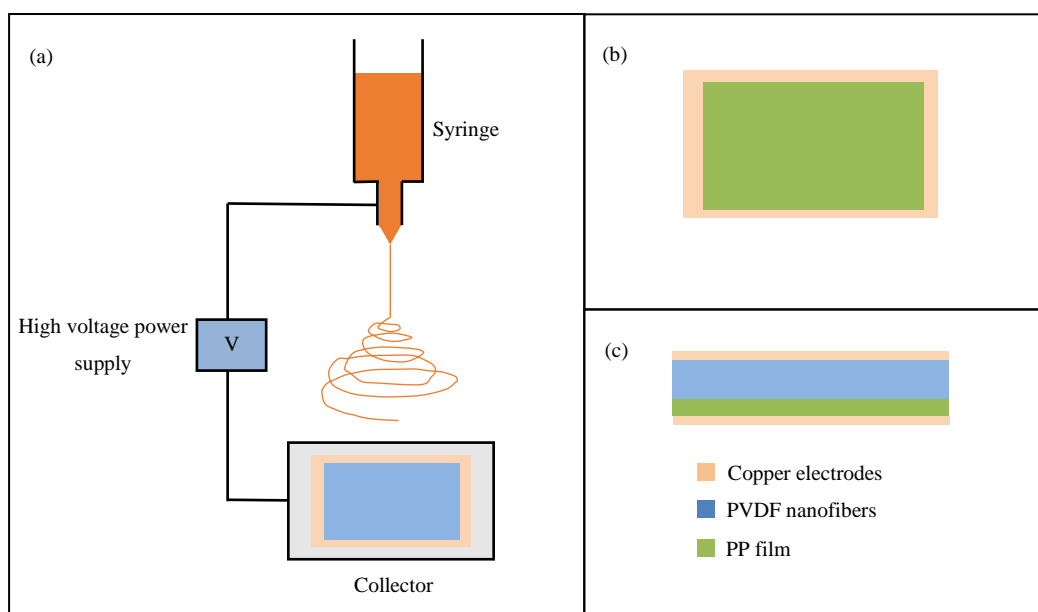
9.2.2 Fabrication of the sensor

Figure 9.2 Schematic diagram of the sensor fabrication process: (a) Preparation of the sensor top plate. (b) Preparation of the sensor bottom plate and (c) final assembly of the triboelectric sensor.

The fabrication process of the triboelectric sensor is depicted in Fig. 9.2. First, a membrane of interconnected PVDF nanofibers (2 mm) is electrospun on copper foil to form the top plate of the sensor as shown in Fig. 9.2 (a). To prepare the solution for electrospinning, 2 g PVDF pellets are dissolved into 10 ml solvent mixture of N,N-dimethylformamide and acetone (4/6). Then, the chemical solution is electrospun by a Nanon-01A electrospinning unit using the following operational conditions: voltage applied 15 kV, spinning distance 15 cm, feed rate of 1 ml/h, 21-gauge needle and static collector. It is important to mention that the nanofibers are deposited on a copper foil which acts as collector for them during the electrospinning. Secondly, a thin polypropylene film (25 µm) is adhered to copper foil by a double-sided adhesive copper tape to form the bottom plate of the sensor as

detailed in Fig. 9.2 (b). Finally, the top and bottom plate are assembled to produce the triboelectric sensor (fig. 9.2 (c)). The sensor is sealed with polyethylene terephthalate film which acts as a protection layer. The dimensions and the weight of the fabricated triboelectric sensor are 55 x 55 mm and 6.75 g, respectively.

In summary, the fabrication process of the sensor is very simple and does not require expensive materials or technologies, which makes the process cheap and easy to perform [27, 28]. Moreover, the process can be easily upgraded for large-scale production, which suggests a promising method for fabrication of such sensors on an industrial scale using a low-cost technology.

9.3 Working mechanism of the triboelectric sensor

The working principle of the triboelectric sensor is schematically depicted in Fig. 9.3. The mechanism is based on the combination of contact electrification and electrostatic induction [29, 30]. In the initial state, there is no friction between the polypropylene and the polyvinyl fluoride nanofibers. As a result, there is no generation of triboelectric charges which results in non electric output as shown in Fig. 9.3 (a). When the composites are impacted, the triboelectric sensor is deformed as result of the impact. Therefore, PVDF and PP rub against each other which induce negative charges on the surface of the PVDF and positive charges on the surface of the PP (Fig. 9.3 (b)). When the impact stops, the sensor tends to revert back to its original state. As a result, the positive and negative charges are separated which result in a potential difference between the two electrodes as detailed in Fig. 9.3 (c). Therefore, the sensor electric responses are generated by the contact and separation of two triboelectric layers with opposite polarity. Finally, the triboelectric charges disappear, and the sensor returns to the initial state.

This is a self-powered mechanism and thus the triboelectric sensor does not require an external power supply, which is completely different from other conventional sensors [31].

(b)   Contact state   (c)   Separation state

0.0 V   0.0 V   2.3 V

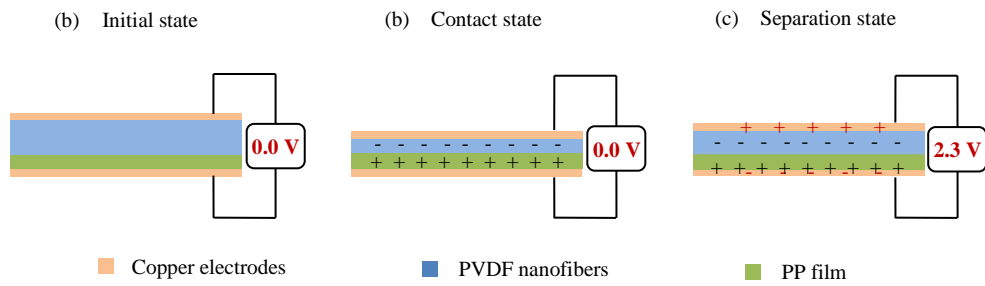■ Copper electrodes   ■ PVDF nanofibers   ■ PP film

Figure 9.3 Working mechanism of the triboelectric sensor: (a) The state of the sensor before the impact. (b) The state of the sensor during the impact and (c) the state of the sensor after the impact.

9.4 Description of the experiment

The main objective of the experiments is to verify that the sensor electric responses are affected by the velocity of the impacts. This is important as we are aiming to expand the applications of triboelectric sensors for measurement of impact velocities in composite structures, such as airplanes, wind turbines and bridges.

A schematic diagram of the experimental setup is shown in Fig. 9.4 (a). Initially, the composite plates are impacted with controlled impact velocities using a drop-weight impact machine (Instron CEAST 9350). It is important to mention that the velocity of the impacts is varied in the range between 1.27 and 3.21 m/s with small increments of ~ 0.2 m/s. Subsequently, the sensor electric responses in form of voltage and current are measured using a commercial oscilloscope (Tektronix 2012 B) and a digital multimeter (Agilent 34410A). The purpose of the experiment is to verify that the sensor electric responses are dependent on the velocity of the impact.

Fig. 9.4 shows a description of the experimental procedure which can be divided into four steps. First, the triboelectric sensor is adhered to the bottom clamp of the impact machine as shown in Fig. 9.4 (b). Secondly, a carbon plate with length of 0.12 m, width of 0.12 m and a thickness of 0.07 m is adhered to the triboelectric sensor (Fig. 9.4 (c)). Thirdly, the composite plate is clamped around the four edges

and a controlled velocity impact is applied to the centre of the plate using the impactor of the drop-weight machine (Fig. 9.4 (d)). Finally, the sensor electric response is obtained as shown in Fig. 9.4 (e). The figure 9.4 (e) shows the history of the voltage changes during the impact. From the figure, it can be observed that the voltage goes through a positive and a negative peak which are associated to the start and the end of the impact respectively. Thus, the time interval between both peaks (0.003 s) can be defined as the duration of the impact.
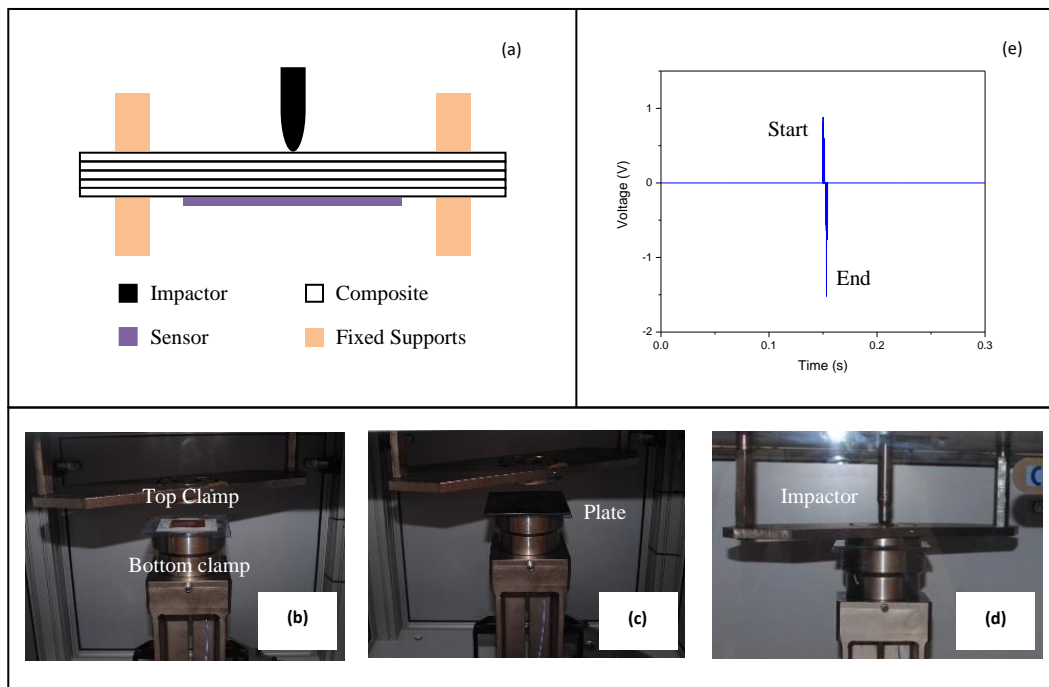

Figure 9.4 Methodology used to investigate the applications of the sensor for impact velocity monitoring: (a) Schematic description of the experimental setup (transversal view). Description of the experimental procedure: (b) The triboelectric sensor is adhered to the bottom clamp of the impact machine. (c) A composite plate is adhered to the sensor. (d) The composite plate is clamped around the four edges and a controlled impact is applied. (e) The sensor electric responses are measured.

9.5 Results and Discussion

This section presents the results obtained from the experiment detailed in Section 9.4. Initially, the effect of the impact velocities on sensor electric responses is

investigated. Lastly, the voltage and current outputs obtained with the developed triboelectric sensor and a piezoelectric commercial sensor are compared.

9.5.1 Effect of impact velocity on voltage output

As mentioned in Section 9.4, composite plates were subjected to various impact velocities using a drop weight machine and the voltage responses of the triboelectric sensor were measured using a commercial oscilloscope. The idea is to investigate if the sensor voltage outputs are influenced by the velocity of the impacts.
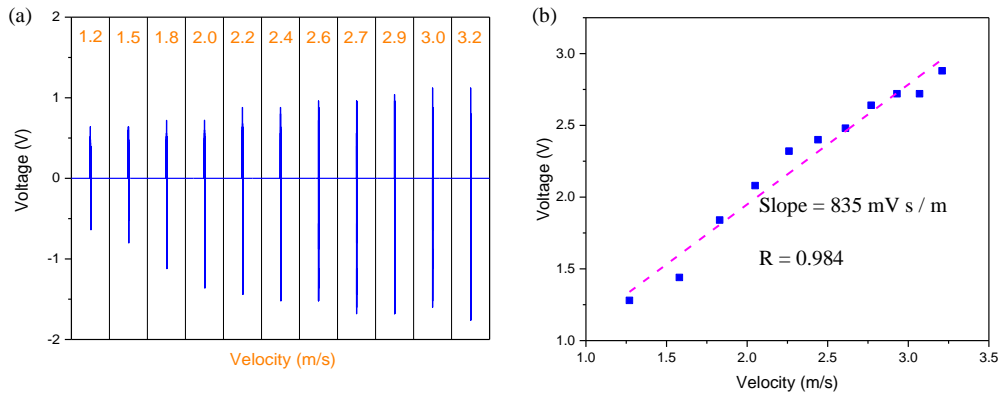

Figure 9.5 Effect of the impact velocity on the electric outputs of the triboelectric sensor: (a) Voltage responses for various impact velocities in the range between 1.27 and 3.21 m/s. (b) Voltage amplitudes as a function of the impact velocity.

Fig. 9.5 (a) displays the voltage outputs of the triboelectric sensor when the composite plates are impacted at various impact velocities ranging from 1.27 to 3.21 m/s. It is noticed that higher impact velocities increase the voltage sensor outputs, which reach up to 2.88 V under the impact velocity of 3.21 m/s. As indicated in refs. [32, 33], the voltage output of a triboelectric sensor can be calculated as:

$$V = \frac{\sigma d}{\varepsilon_0} \qquad (14)$$

Where σ is the density of triboelectric charges, d is the distance between the frictional layers and ε_0 is the vacuum permittivity. In our triboelectric sensor, the

distance between the frictional layers is constant because there is no separator between the layers. Therefore, the voltage changes are only due to the changes of triboelectric charges (σ) caused by the strong friction between the layers of the sensor.

Fig. 9.5 (b) shows that the voltage amplitudes of the sensor as a function of the impact velocity. From the figure, it can be observed that the voltage responses are influenced by the impact velocities and the amplitude of the voltage outputs increases from 1.28 to 2.88 V as the impact velocity increases from 1.27 to 3.21 m/s. Additionally, the results show a strong linear relationship between the impact velocities and the voltage outputs with a Pearson coefficient of 0.984. Furthermore, the velocity-voltage relationship exhibits a very high sensitivity of 835 mV per unit velocity of m/s in a wide measurement range between 1.27 and 3.21 m/s. This is important as sensors with high sensitivity, linearity and wide detection range are always preferred for practical reasons and applications of the sensor.

To the best of our knowledge, only one study so far has investigated the potential of triboelectric sensors to measure impact velocities. As detailed in ref. [34], a triboelectric sensor composed of a mixture of polyvinylidene fluoride and polyvinyl pyrrolidone is used to detect the impacts applied by a free-falling ball at four impact velocities in the range from 1.4 to 4.4 m/s. The results show that the voltage responses increase from 3.8 V to 23.44 V, when the velocity of the impacts increases from 1.4 to 4.4 m/s. The same behaviour is observed for the current sensor, for which it can be clearly seen that the voltage outputs increase between 1,28 V and 2,88 V as the velocity of the impacts increase from 1,2 m/s to 3,2 m/s. The higher amplitude of the electric responses in ref. [34] can be explained by the following three reasons: 1st) The impacts are applied directly on the surface of the sensor instead of a composite plate, which causes a strong increment of the sensor electric responses. 2nd) The different material nature and nanostructured surface of the coupling triboelectric materials used in the sensor, which affects the generation of triboelectric charges and 3rd) the different measurement conditions used in the oscilloscope to measure the electrical signal.

A major limitation of the above study [34] is the small energy of the impacts (less than 0.225 J), which is far from the energy of impacts in real case scenarios as per example bird strikes or hailstone impacts. In this study, the energy of the impacts is much higher and varies between 2 and 12 J as the impact velocity increases from 1.27 to 3.21 m/s as shown in Figure 9.6. From the figure, it can be observed that the relationship between the energy and the velocity of the impacts is approximately linear for this range of low velocity impacts. Therefore, it can be seen that the energy of the impact increases proportionally under higher impact velocities.
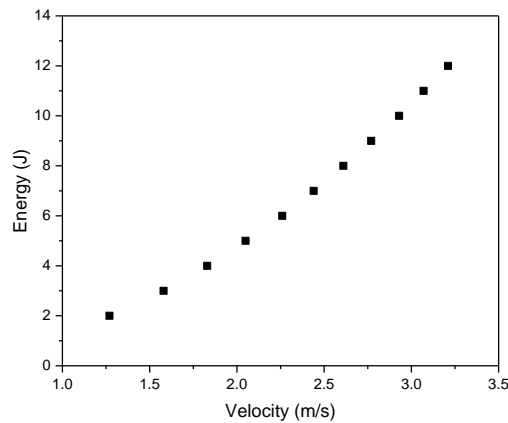

Figure 9.6: Energy of the impacts as a function of the impact velocity.

On the basis of the above results, it can be concluded that the voltage output depends on the velocity of the impacts and it increase linearly with the velocity for the measured range between 1.27 and 3.21 m/s. Furthermore, the relationship between the impact velocities and the voltage outputs show a high sensitivity for this measurement range. This demonstrates that the developed triboelectric sensor can be potentially used for impact velocity measurement.

9.5.2 Effect of impact velocity on current output

As was explained above, a drop weight impact machine is used to subject composite specimens to controlled velocity impacts and the corresponding current responses of the triboelectric sensor are acquired using a digital multimeter. The idea is to check if the current electric output is affected by the velocity of the impact.

Fig. 9.7 (a) shows the current responses of the triboelectric sensor when the composite specimens are subjected to various impact velocities in the range from 1.27 to 3.21 m/s. The graphic shows that the current electric outputs are affected by the velocity of the impacts and the current sensor responses increases from 111 to 530 nA as the impact velocity changes between 1.27 and 3.21 m/s. The current responses of a triboelectric sensor can be expressed as [35, 36]:

$$I = C\frac{\partial V}{\partial t} + V\frac{\partial C}{\partial t} \qquad (15)$$

Where C represents the capacitance of the sensor and V is the potential drop across the electrodes. As a result, the changes of current can be explained by the changes in the potential across the top and bottom electrodes.
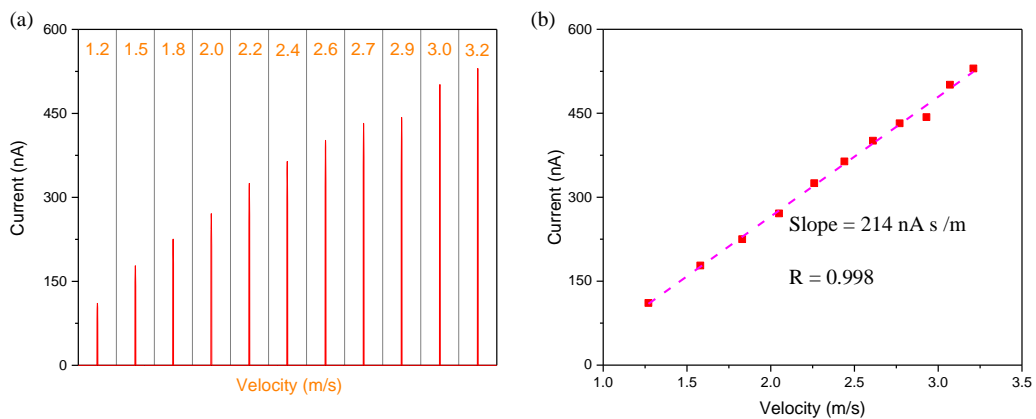
Figure 9.7 Effect of the impact velocity on the triboelectric sensor electric responses: (a) Current outputs for various impact velocities in the range between 1.27 and 3.21 m/s. (b) Current amplitudes as a function of the impact velocity.

Fig. 9.7 (b) displays the current amplitudes of the sensor as a function of the impact velocity. From the figure 9.7 (b), it can be clearly seen that the current outputs are strongly affected by the impact velocity and the amplitude of the current

electric outputs increase with the impact velocity, as the velocity changes from 1.27 to 3.21 m/s. The experimental data points can be interpolated with a straight line which possess a strong linear behaviour (R = 0.998). Moreover, the current sensor responses are characterized by a very high sensitivity of 214 nA s / m in the large velocity measurement range investigated (between 1.27 and 3.21 m/s). This is of utmost importance from a technical point of view, because sensors with high sensitivity, linearity and a wide working range are preferred from practical considerations.

In general, it can be said that the current sensor responses are affected by the velocity of the impacts and the current responses increase linearly with the impact velocity applied to the composite plates. Furthermore, the relationship between the impact velocities and the voltage outputs show a high sensitivity for a wide detection range between 1.27 and 3.21 m/s. These results are important and can be said to expand the applications of triboelectric sensors for detection and quantification of impact velocities in composite structures.

9.5.3 Comparison between the developed triboelectric sensor and a piezoelectric commercial sensor

As explained in Section 9.4, composite plates were subjected to different velocity impacts by using a drop weight impact machine and the sensor electric outputs are measured and compared to those of a piezoelectric commercial sensor. The main goal of the experiment is to compare the sensitivity, linearity and response time of the fabricated triboelectric sensor to a commercial piezoelectric sensor.

Fig. 9.8 (a) and (b) show the voltage and current outputs of the piezoelectric commercial sensor as functions of the impact velocity. The plots show that the sensor electric responses depend on the impact velocity and increase proportionally with the increase of the impact velocities. It can be seen that there is a strong linear relationship between the impact velocities and the sensor electric outputs with a

Pearson coefficient of R= 0.998 and 0.986 for the voltage and current outputs, respectively. Furthermore, the commercial piezoelectric sensor shows very high sensitivities of 13778 V and 1350 nA per unit velocity of m/s for the considered velocity range from 1.27 to 3.21 m/s.
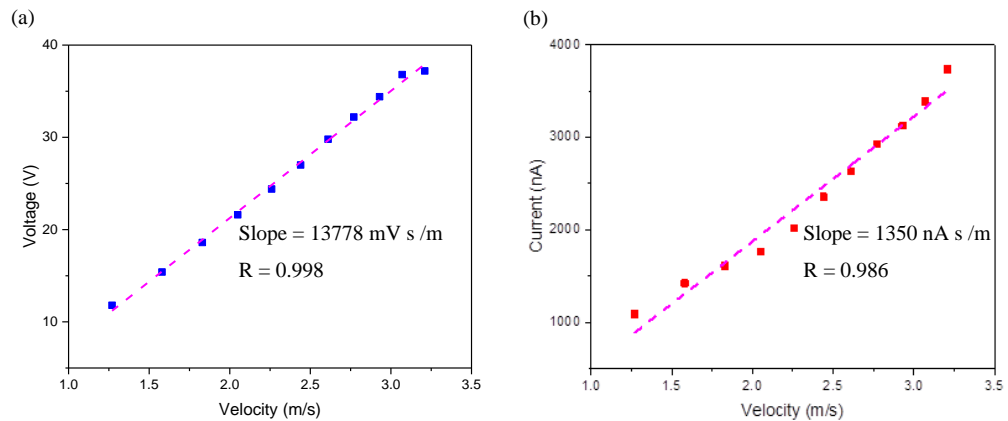

Figure 9.8 Effect of the impact velocity on the piezoelectric commercial sensor responses: (a) Voltage and (b) current output as a function of the impact velocity.

The response time of a sensor can be defined as the time required for reaching the maximum voltage output which is calculated as the time interval between zero and the maximum voltage response. Figures 9.9 (a) and 9.9 (b) display the response times of the triboelectric and the commercial sensor for an impact velocity of 3.21 m/s. The figures show that the response time of the triboelectric sensor is 0.0001 s, while the response time of the commercial sensor increases up to 0.0011 s. Therefore, the response of the developed sensor to impact is very fast, even faster as compared to a commercial sensor, which is critical for the real time detection of impacts in composite structures.

The sensitivity, linearity and response times of the triboelectric and commercial piezoelectric sensor are presented in Table 9.2. From the table, it can be seen that the sensitivity of the commercial sensor is higher as compared to the sensitivity of the triboelectric sensor. This can be explained by the fact that the amplitude of the electric outputs of the triboelectric sensor is relatively small (see figures 9.5, 9.6 and 9.7). Although amplitudes of the electric responses of the

triboelectric sensor are small, we believe that the sensor electric outputs can be considerably increased by separating the frictional layers of the triboelectric sensor using a spacer [37, 38]. On the other hand, it can be seen also that the response of the developed triboelectric sensor is eleven times faster as compared to the piezoelectric commercial sensor. In this respect, it can be said that the developed triboelectric sensor with a response time of 0.0001 s outwits the commercial piezoelectric sensor which shows a response time of 0.0011 s. The response time is a very important factor for a sensor as it shows how fast the response can be detected after the excitation (the impact in this case) is applied. Furthermore, a high linearity of the current/velocity and voltage/velocity relationships is found for the newly developed triboelectric sensor which is very much the same to the one of the commercial piezoelectric sensor (R varies between 0.984 and 0.998).
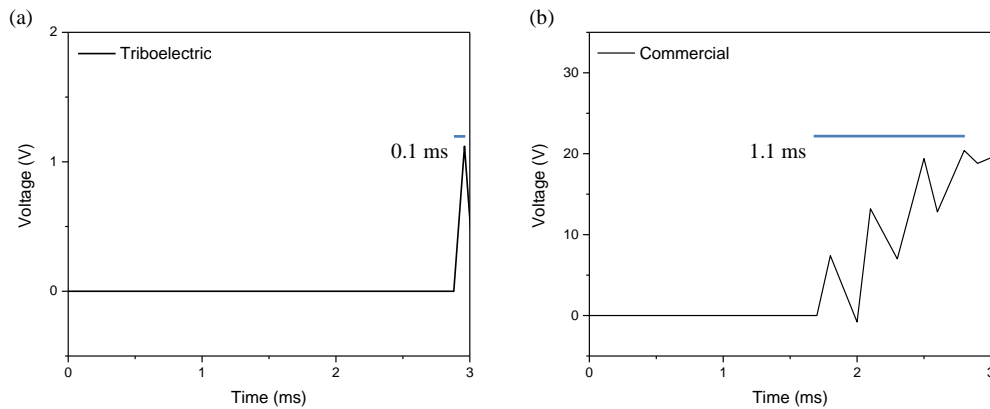
Figure 9.9 Analysis of the response time for a velocity impact of 3.21 m/s: (c) Response time of triboelectric and (d) commercial sensor.

Characteristic	Units	Triboelectric	Commercial
Sensitivity	nA s / m	214	1350
	mV s / m	835	13778
Linearity	Dimensionless	0.998	0.986
		0.984	0.998
Response time	s	0.0001	0.0011

Table 9.2 The table compares the sensitivity, linearity and response time of the triboelectric and piezoelectric commercial sensor.

In summary, this section compares the sensitivity, the linearity of the input-output relationships and the response time of the suggested triboelectric sensor and commercial piezoelectric sensor. The results demonstrate that the newly developed triboelectric sensor shows a good impact sensitivity and faster response time as compared to the commercial one. Moreover, a strong linear relationship of the voltage-velocity and current-velocity relations can be observed for the developed triboelectric sensor in a large measurement range between 1.27 and 3.21 m/s. These sensor characteristics can be used to demonstrate the outstanding performance of the developed triboelectric sensor for impact detection and velocity measurement in composite structures, such as aircrafts or wind turbines.

9.6 Conclusions

The detection and quantification of impacts is of vital importance for monitoring the health state of composite structures such as aircrafts or wind turbines. The main achievement of this chapter is to demonstrate for the first time that triboelectric sensors can be potentially used for measuring impact velocities in composite structures.

Initially, a new class of triboelectric sensors based on polyvinyl fluoride nanofibers and a thin film of polypropylene is developed. The sensor is self-powered and does not require an external power supply, so this is an energy saving and environmentally friendly sensor. The fabrication process of the sensor is very simple and does not require expensive materials or equipment's, which brings down the manufacturing cost of the sensor. Additionally, the fabrication process can be easily developed for large-scale production, which offers a promising alternative for producing such sensors on an industrial scale using a low-cost technology.

Furthermore, the chapter demonstrates the applications of the suggested sensor as self-powered impact sensor. The results show that the voltage and the current outputs increase proportionally with the impact velocities and a good linear

relationship between the impact velocity and the sensor electric outputs (voltage and current) is found. Furthermore, it can be observed very high impact sensitivity in a wide velocity range between 1.27 and 3.21 m/s. It is also demonstrated the responses of the sensor to impacts are very fast (with a very short response time of ~ 0.0001 s), which indicates that the impacts are detected in real time.

In our view, this chapter presents a solid progress toward the practical applications and implementation of triboelectric sensors as self-powered impact sensors. The findings of this study demonstrate that triboelectric sensors can be potentially used for the measurement of impact velocities in composite structures, which can have important applications for monitoring of impacts in aircrafts, bridges and other composite structures.

References

[1]   S. Joshi, G.M. Hedge, M.M. Nayak and K. Rajanna, A novel piezoelectric thin film impact sensor: Application in non-destructive material discrimination, Sens. Actuator A-Phys., 199 (2013) 272-282.

[2]   A. Dixit and S. Bhalla, Prognosis of fatigue and impact induced damage in concrete using embedded piezo-transducers, Sens. Actuator A-Phys., 274 (2018) 116-131.

[3]   R. Ouckama and D.J. Pearsall, Evaluation of a flexible force sensor for measurement of helmet foam impact performance, J. Biomech., 44 (2011) 904-909.

[4]   Z.H. Lin, G. Zhu, Y.S. Zhou, Y. Yang, P. Bai, J. Chen and Z.L. Wang, A self-powered triboelectric nanosensor for mercury ion detection, Angew. Chem. Int. Ed., 52 (2013) 5065-5069.

[5]   Y. Su, G. Xie, S. Wang, H. Tai, Q. Zhang, H. Du, H. Zhang, X. Du and Y. Jiang, Novel high-performance self-powered humidity detection enabled by triboelectric effect, Sens. Actuator B-Chem., 251 (2017) 144-152.

[6]   S. Phan, Z.F. Queck, P. Shah, D. Shin, Z. Ahmed, O. Khatib and M. Cutkosky, Capacitive skin sensors for robot impact monitoring, in Proccedings of International Conference on Intelligent Robots and Systems, September 2011, pp. 2992-2997.

[7]   D. Liang and B. Culshaw, Fibre optic silicon impact sensor for application to smart skins, Electron. Lett., 29 (1993) 529-530.

[8]   L. Dhakar, S. Gudla, X. Shan, Z. Wang, F.E.H. Tay, C.H. Heng and C. Lee, Large scale triboelectric nanogenerator and self-powered pressure sensor array using low cost roll-to-roll UV embossing, Sci. Rep., 6 (2016) 22253.

[9]   C. Garcia, I. Trendafilova, R. Guzman de Villoria and J. Sanchez del Rio, Self-powered pressure sensor based on the triboelectric effect and its analysis using dynamic mechanical analysis, Nano Energy, 50 (2018) 401-409.

[10]   K. Parida, V. Bhavanasi, V. Kumar, R. Bendi and P.S. Lee, Self-powered pressure sensor for ultra-wide range pressure detection, Nano Res., 10 (2017) 3557-3570.

[11]   K.Y. Lee, H.J. Yoon, T. Jiang, X. Wen, W. Seung, S.W. Kim and Z.L. Wang, Fully packaged self-powered triboelectric pressure sensor using hemispheres-array, Adv. Energy Mater., 6 (2016) 1502566.

[12]   G. Zhu, W.Q. Yang, T. Zhang, Q. Jing, J. Chen, Y.S. Zhou, P. Bai and Z.L. Wang, Self-powered, ultrasensitive, flexible tactile sensors based on contact electrification, Nano Lett., 14 (2014) 3208-3213.

[13]   T. Li, J. Zou, F. Xing, M. Zhang, X. Cao, N. Wang and Z.L. Wang, From dual-mode triboelectric nanogenerator to smart tactile sensor: A multiplexing design, ACS Nano, 11 (2017) 3950-3956.

[14]   Q. Liang, Z. Zhanga, Xiaoqin Y., Y. Gu, Y. Zhao, G. Zhang, S. Lu, Q. Liao and Y. Zhang, Functional triboelectric generator as self-powered vibration sensor with contact mode and non-contact mode, Nano Energy, 14 (2015) 209-216.

[15]   S. Wang, S. Niu, J. Yang, L. Lin and Z.L. Wang, Quantitative measurements of vibration amplitude using a contact-mode freestanding triboelectric nanogenerator, ACS Nano, 8 (2014) 12004-12013.

[16]   C. Xiang, C. Liu, C. Hao, Z. Wang, L. Che and X. Zhou, A self-powered acceleration sensor with flexible materials based on triboelectric effect, Nano Energy, 31 (2017) 469-477.

[17]   K. Dai, X. Wang, F. Yi, C. Jiang, R. Li and Z. You, Triboelectric nanogenerators as self-powered acceleration under high-g impact, Nano Energy, 45 (2018) 84-93.

[18]   B. Zhang, L. Zhang, W. Deng, L. Jin, F. Chun, H. Pan, B. Gu, H. Zhang, Z. Lv, W. Yang and Z.L. Wang, Self-powered acceleration sensor based on liquid metal triboelectric nanogenerator for vibration monitoring, ACS Nano, 11, (2017) 7440-7446.

[19]   L. Jin, J. Tao, R. Bao, L. Sun and C. Pan, Self-powered real-time movement monitoring sensor using triboelectric nanogenerator technology, Sci. Rep., 7 (2017) 10521.

[20]   Y. Su, G. Zhu, W. Yang, J. Yang, J. Chen, Q. Jing, Z. Wu, Y. Jiang and Z.L. Wang, Triboelectric sensor for self-powered tracking of object motion inside tubing, ACS Nano, 8 (2014) 3843-3850.

[21]   Q. Jing, G. Zhu, W. Wu, P. Bai, Y. Xie, R.P.S. Han and Z.L. Wang, Self-powered triboelectric velocity sensor for dual-mode sensing of rectified linear and rotary motions, Nano Energy, 10 (2014) 305-312.

[22]   Y. Xi, H. Guo, Y. Zi, X. Li, J. Wang, J. Deng, S. Li, C. Hu, X. Cao and Z.L. Wang, Multifunctional TENG for blue energy scavenging and self-powered wind-speed sensor, Adv. Energy Mater., 7 (2017) 1602397.

[23]   H. Yong, J. Chung, D. Choi, D. Jung, M. Cho, S. Lee, Highly reliable wind-rolling triboelectric nanogenerator operation in a wide wind speed range, Sci. Rep., 6 (2016) 33977.

[24]   B. Yu, H. Yu, H. Wang, Q. Zhang and M. Zhu, High-power triboelectric nanogenerator prepared from electrospun mats with spongy parenchyma-like structure, Nano Energy, 34 (2017) 69-75.

[25]   P.K. Sarkar, S. Maji, G.S. Kumar, K.C. Sahoo, D. Mandal and S. Acharya, Triboelectric generator composed of bulk poly(vinylidene fluoride) and polyethylene polymers for mechanical energy conversion, RSC Adv., 6 (2016) 910-917.

[26]   T. Huang, M. Lu, H. Yu, Q. Zhang, H. Wang and M. Zhu, Enhanced power output of a triboelectric nanogenerator composed of electrospun nanofiber mats doped with graphene oxide, Sci. Rep., 5 (2015) 13942.

[27]   F. Zhang, B. Li, J. Zheng and C. Xu, Facile fabrication of micro-nano structured triboelectric nanogenerator with high electric output, Nanoscale Res. Lett., 10 (2015) 298.

[28]   Y. Zheng, L. Zheng, M. Yuan, Z. Wang, L. Zhang, Y. Qin and T. Jing, An electrospun nanowire-based triboelectric nanogenerator and its application in a fully self-powered UV detector, Nanoscale, 6 (2014) 7842.

[29]   S. Qi, H. Guo, J. Chen, J. Fu, C. Hu, M. Yu and Z.L. Wang, Magnetorheological elastomers enabled high-sensitive self-powered tribo-sensor for magnetic field detection, Nanoscale, 10 (2018) 4745-4752.

[30]   A. Yu, L. Chen, X. Chen, A. Zhang, F. Fan, Y. Zhan and Z.L. Wang, Triboelectric sensor as self-powered signal reader for scanning probe surface topography imaging, Nanotechnology, 26 (2015) 165501.

[31]   S. Cui, Y. Zheng, T. Zhang, D. Wang, F. Zhou and W. Liu, Self-powered ammonia nanosensor based on the integration of the gas sensor and triboelectric nanogenerator, Nano Energy, 49 (2018) 31-39.

[32]   W. Song, B. Gan, T. Jiang, Y. Zhang, A. Yu, H. Yuan, N. Chen, C. Sun and Z.L. Wang, Nanopillar arrayed triboelectric nanogenerator as a self-powered

sensitive sensor for a sleep monitoring system, ACS Nano, 10 (2016) 8097-8103.

[33] S.Y. Shin, B. Saravanakumar, A. Ramadoss and S.J. Kim, Fabrication of PDMS-based triboelectric nanogenerator for self-sustained power source application, Int. J. Energy Res., 40 (2015) 3.

[34] C. Garcia, I. Trendafilova, R. Guzman de Villoria, J. Sanchez del Rio, Triboelectric nanogenerator as self-powered impact sensor, in Proceedings of the International Conference on Engineering Vibration, September 2017, 148 (2018) 14005.

[35] F.R. Fan, L. Lin, G. Zhu, W. Wu, R. Zhang and Z.L. Wang, Transparent triboelectric nanogenerators and self-powered pressure sensors based on micropatterned plastic films, Nano Lett., 12 (2012) 3109-3114.

[36] F.R. Fan, Z.Q. Tian and Z.L. Wang, Flexible triboelectric generator!, Nano Energy, 1 (2012) 328-334.

[37] T.C. Hou, Y. Yang, H. Zhang, J. Chen, L.J. Chen and Z.L. Wang, Triboelectric nanogenerator built inside shoe insole for harvesting walking energy, Nano Energy, 2 (2013) 856-862.

[38] W. Li, J. Sun, M. Chen, Triboelectric nanogenerator using nano-Ag ink as electrode material, Nano Energy, 3 (2014) 95-101.

Chapter 10

Conclusions and Future Work

10.1 Conclusions

This thesis is made of two main parts which are both related to nanofibers and composites, but they consider different aspects of the application of the nanofibers. In the first part of the present thesis, the use of electrospun nanofibers as reinforcement for glass fibre epoxy composites is considered. The effect of nanofibers on the structure made of composite laminate is minimal as the weight and the size of the nanofibers are miniscule, and therefore, they will not affect neither the weight nor the shape of the structure. However, the mechanical and dynamical properties of the composites can be significantly improved due to the incorporation of nanofibers. The major conclusions and contributions of the first part of the thesis are presented below:

i. The thesis investigates the effect of nylon nanofibers on the natural frequencies and damping of glass fibre epoxy composites. These characteristics are rather important for the purposes of designing structures as most structures vibrate while being in use. Our research found that the natural frequencies of the nanomodified laminates are not influenced by the incorporation of nylon nanofibers. The frequencies underwent very small changes, which can be considered within the range of the experimental and measurement error. Thus, in terms of natural frequencies the vibratory behaviour of the nanomodified specimens is the same as the behaviour of the pristine ones. On the other hand, the damping ratio considerably increased due to the reinforcement with nylon nanofibers and a considerable increment of 36% is reported. This can be potentially used for the purposes of reduction of the vibration amplitudes, which limit the propagation of cracks and other irreversible damages.

ii.   The authors succeeded to demonstrate that a finite element model based on transient analysis is able to give adequate simulation of the vibratory properties of pristine and nylon nanomodified composites. The authors are one the opinion that such a model is rather flexible, and its simplicity makes it easy to use for predicting the dynamic behaviour of other nanomodified materials.

iii.   The main weak point of the composite laminates is their poor interlaminar strength, which can result in delamination. One of the techniques to prevent the delamination is the incorporation of electrospun nanofibers in the interlaminar regions of the composite laminates. The experimental results from the present thesis indicated that the interlaminar shear strength of the glass fibre epoxy composites increases quite substantially from 50.2 MPa to 63.81 MPa due to the incorporation of nylon nanofibers. Therefore, nylon nanomodified glass fibre epoxy composites are less susceptible to delamination than pristine specimens. This is of great important for the industry as composite laminates reinforced with nylon nanofibers could be used to prevent the delamination failures in aircrafts, wind turbines and other civil structures.

iv.   A three-dimensional finite element model is developed to simulate the delamination behaviour of pristine and nylon nanomodified composites. The numerical results are in good agreement with the experimental ones and confirm that the interlaminar shear strength of the pristine and nylon nanomodified composites increases quite notably from 51.5 MPa to 63.1 MPa. Thus, our simulations demonstrate that the interleaving with nanofibers can be used for the purposes of delamination prevention and restriction.

v.   Higher impact resistance (e.g. bird strikes or hailstones) is of critical importance for the health of the composite laminates used in aircrafts, wind turbines and other civil structures. The numerical investigation offered in this research is validated with available experimental data and reveal that the addition of polycaprolactone nanofibers in glass fibre epoxy composites increase substantially the impact resistance of glass fibre epoxy layered

composites. Thus, polycaprolactone nanofibers can be used to develop composite materials with improved impact resistance, which can be used for the prevention and reduction of the damage caused by impacts in aircrafts and wind turbines.

In the second part of the thesis the use of nanofibers for the production and application of triboelectric nanogenerators as self-powered active sensors is considered. This research first of all offers two novels triboelectric nanogenerators made of electrospun nanofibers from different materials. By combining these particular materials and by the use of nanofibers we have tried to increase the electric response generated by different stimuli, via pressure and impact. As compared to traditional sensors, triboelectric nanogenerators are self-powered and do not require an external power supply or battery to sense the mechanical stimulus. Furthermore, they are environmentally friendly, low-cost and maintenance-free. In the present thesis, the potential of triboelectric nanogenerators as self-powered sensors for pressures and impacts is demonstrated. The main outcomes of the second part of this study are summarized below:

vi. In the present thesis, we develop a new class of triboelectric nanogenerator composed of polyvinyl fluoride (PVDF) and polyvinyl pyrrolidone (PVP) nanofibers and demonstrate its application as self-powered pressure sensor, which measure dynamic pressures in real-time.

The effect of the pressures on the electric responses of the nanogenerator is analysed using the technique of dynamical mechanical analysis. In our view, this method is beneficial because it can analyse the characteristics of the mechanical stimulus in real time (e.g. pressures applied to the nanogenerator), which can be used to enhance our understanding about the electric responses of the nanogenerator. The findings of this study indicate that the developed triboelectric nanogenerator shows a high sensitivity to pressures in a wide measurement range between 200 Pa and 2000 Pa. Moreover, it was shown that the current outputs show an excellent linear

relationship with the pressure applied, which is important for the practical applications of the device.

In summary, our results prove that the developed triboelectric nanogenerator can be used as self-powered sensor to measure dynamic pressures in real time. This demonstrates the potential of TENGs for monitoring of pressures with the advantages of being self-powered, maintenance-free and environmental-friendly.

vii. The chapter seven of this study presents a novel triboelectric nanogenerator composed of a thin film polypropylene and membrane of PVDF nanofibers and. The films of electrospun nanofibers used in the nanogenerator are prepared via electrospinning because it is one of the practical ways to increase the performance of the TENG. Therefore, it can be concluded that the developed triboelectric nanogenerator is prepared by a simple fabrication method, which does not require expensive mats or high cost technologies.

Furthermore, the seven chapter also investigates the practical applications of the TENG as self-powered sensor for detection of small energy impacts in real time. The experimental results reveal that the voltage and current outputs increase proportionally under higher energy impacts. Therefore, it can be said that the developed nanogenerator can be used for detection of small energy impacts with the advantages of self-powered operation, maintenance-free and simple fabrication. This can be used in multitude of practical applications as per example vehicle safety, structural health monitoring or urgent medical attention of elderlies.

viii. Aircrafts, wind turbines and other composite structures are frequently subjected to impacts or collisions. In this thesis, we have demonstrated for the first time that a triboelectric nanostructured sensor can be successfully used to detect and measure impacts in structures made of composite materials. The findings of this study indicate that the developed triboelectric sensor shows

good sensitivity to impacts in a wide range of energies and impact forces between 2-30 J and 2000-14500 N, respectively.

From a fabrication point of view, the preparation of the triboelectric sensor is very simple and does not require sophisticated processing steps. Moreover, this procedure can be easily upgraded for large-scale production. From an innovation point of view, the triboelectric sensor is a potential alternative to other conventional impact sensors due to their independence of an external power supply unit and lower cost due to the cheap materials used and easy fabrication. From a technical point of view, the sensor shows very high sensitivity and linearity in a wide detection range which is comparable to other commercial sensors.

In conclusion, chapter 8 has suggested and validated for the first time an innovative approach to detect and measure the magnitude of the impacts in composites structures. The present findings demonstrate that the developed triboelectric sensors can be successfully utilized for real-time detection and measurement of the energy and/or the force of impacts in structures made of composite mats. This can have important applications for monitoring of impacts in composite structures as aircrafts, wind turbines or bridges.

ix. The detection and quantification of impacts is of vital importance for monitoring the health state of composite structures such as aircrafts or wind turbines. In the nine chapter of the present thesis, we demonstrate for the first time that the developed triboelectric nanogenerator can be potentially used for measuring impact velocities in composite structures. The results show that the voltage and the current outputs increase proportionally with the impact velocities and a good linear relationship between the impact velocity and the sensor electric outputs (voltage and current) is found. Furthermore, it is also demonstrated the responses of the sensor to impacts are very fast (with a very short response time of ~ 0.1 ms), which indicates that the impacts are detected in real time. The findings of this study present solid progress toward the practical applications demonstrate that triboelectric sensors can be

potentially used for the measurement of impact velocities in composite structures, which can have important applications for monitoring of impacts in aircrafts, bridges and other composite structures.

10.2 Recommendations and Future Work

The first part of this thesis investigated the use of electrospun nanofibers as means to improve the mechanic and dynamic properties of composite laminates. Despite the fact that the research on this topic started more than ten years ago and a solid knowledge on the topic has been built since them. There are several research gaps in the literature that still need to be addressed and some of them are indicated below.

i. The research on the vibratory properties of composite laminates reinforced with electrospun nanofibers is still at its beginning and only a few papers have investigated how nylon and polycaprolactone nanofibers are able to enhance the vibratory response of the laminates [1-3]. In this regard, we believe that it is necessary to demonstrate that other type of nanofibers can be used to reduce the amplitude of the composite vibrations. This could be potentially used to develop composite structures with smaller amplitude vibrations, which will have important applications for structures in which vibrations are a source of problems.

ii. The enhanced delamination response of composite laminates interleaved with electrospun nanofibers have been widely reported in the literature [4-6]. However, there are still some issues that still need to be discussed as per example the development of an optimum strategy to fabricate the composite reinforced with nanofibers or the effect of nanofibers on the fatigue behaviour of composite laminates. Additionally, the author of this thesis considers that it is necessary additional research to fully understand the reinforcement mechanism of the nanomodified laminates,

iii. Research on the impact response of nanomodified composites is still far to be completed. Therefore, we recommend investigating the effect of the nanolayer thickness, morphology and number of nanofibers in the impact response of the laminates. Furthermore, it is interesting to study how the reinforcement effect of the nanofibers is affected by the location of the nanofibers in the laminate.

In the second part of the thesis, we have analysed the use of electrospun nanofibers for the development of self-powered triboelectric sensors for pressures and impacts. Since the invention of the first triboelectric sensor in 2012, a large number of research works has been published on this research topic [7-10]. However, there are still many issues that need to be investigated; some of them are indicated below.

iv. The performance of a triboelectric sensor is strongly affected by the electron affinity of the frictional materials [11, 12]. Interestingly, the vast majority of the research till date has almost exclusively focused on materials with strong ability to capture electrons as polytetrafluoroethylene (PTFE). However, there are very little research works to explore the use of new triboelectric materials with higher ability to donate electrons as nylon. This can be explained by the fact that the majority of materials with strong tendency to give electrons are natural biological materials (e.g. human skin or cotton) which are difficult to use in practical devices. In this regard, it is necessary to develop new materials which can be easily integrated in electronic devices and possess high ability to donate electrons.

v. The electric responses of a triboelectric sensor are strongly influenced by the area superficial of the frictional materials [13, 14]. As a result, an increment of the contact area of the frictional materials is an effective way to increase the electric response of the devices. Thus, it would be interesting to study how the morphology and porosity of the nanofibers is essentially correlated with the output performance of the triboelectric sensor.

vi. The periodic contact and separations between the frictional materials of the triboelectric sensor are of critical importance for enhancing the generation of electricity. Therefore, triboelectric sensors with different structural designs as the arch-shaped structure [15], spring-assisted structure [16] or other advanced designs [17-19] have been designed with the aim to maximize the generation of electricity. In the author's opinion, there is a need to develop triboelectric sensors with new structural designs which can enhance the performance of the triboelectric sensor.

For the future, the author of this thesis would like to continue this research in with focus on two major directions: First, the development of composite laminates with improved mechanical properties (e.g. higher resistance to impacts or low susceptibility to the initiation and propagation of delamination failures). Second, the development of new triboelectric sensors with improved sensing characteristics (e.g. high sensitivity, large measurement range or fast response time) and minimum fabrication costs. In the author's opinion, the integration of triboelectric nanofibers into composite laminates is one of the major challenges for the industry and can give a significant impulse to their commercialization with the development of new composite structures with improved mechanical properties and new self-sensing abilities.

References

[1] C. Garcia, J. Wilson, I. Trendafilova and L. Yang, Vibratory behaviour of glass reinforced polymer (GFRP) interleaved with nylon nanofibers, Compos Struct., 176 (2017) 923-923.

[2] C. Garcia, I. Trendafilova and A. Zucchelli, The effect of polycaprolactone nanofibers on the dynamic and impact behaviour of glass fibre reinforced polymer composites, Compos Sci., 2 (2018) 43.

[3]   R. Palazzetti, A. Zucchelli and I. Trendafilova, The self-reinforcing effect of Nylon 6,6 nano-fibres on CFRP laminates subjected to low velocity impact, J Compos Struct., 106 (2013) 661-72.

[4]   M. Di Filippo, S. Alessi, G. Pitarresi, M. Sabatino, A. Zucchelli, C. Dispenza, Hydrothermal aging of carbon reinforced epoxy laminates with nanofibrous mats as toughening interlayers, Polym Degrad Stab., 126 (2016) 188-95.

[5]   R. Palazzetti, A. Zucchelli, C. Gualandi, M. Focarete, I. Donati, G. Minak, and S. Ramakrishna, Influence of electrospun Nylon 6,6 nanofibrous mats on the interlaminar properties of Gr-epoxy composite laminates, Compos Struct., 94 (2012) 571-9.

[6]   W. Doris, L. Lin, P. McGrail, T. Peijs, and P. Hogg, Improved fracture toughness of carbon fibre/epoxy composite laminates using dissolvable thermoplastic fibers, Compos Part A, 41 (2010) 759-767.

[7]   H. Askari, E. Asadi, Z. Saadatnia, A. Khajepour, M.B. Khamesee, and J. Zu, A flexible tube-based triboelectric-electromagnetic sensor for knee rehabilitation assessment, Sens Actuators A, 279 (2018) 694-704.

[8]   X. Cui, C. Zhang, W. Liu, Y. Zhang, J. Zhang, J. Zhang, X. Li, L. Geng, and X. Wang, Pulse sensor based on single-electrode triboelectric nanogenerator, Sens Actuators A, 280 (2018) 326-331.

[9]   J. Zhu, X. Hou, X. Niu, X. Guo, J. Zhang, J. He, T. Guo, X. Chou, C. Xue, and W. Zhang, The d-arched piezoelectric-triboelectric hybrid nanogenerator as a self-powered vibration sensor, Sens Actuators A, 263 (2017) 317-325.

[10]   W. Liu, C. Zhang, H. Lin, W. Qu, X. Li, X. Wang, Texture and sliding motion sensation with a triboelectric-nanogenerator transducer, Sens Actuators A, 256 (2017) 89-94.

[11]   P. Bai, G. Zhu, Y.S. Zhou, S. Wang, J. Ma, G. Zhang, Z.L. Wang, Dipole-moment-induced effect on contact electrification for triboelectric nanogenerators, Nano Res., 7 (2014) 990-997.

[12]   A.F. Diaz, R.M. Felix-Navarro, A semi-quantitative triboelectric series for polymeric materials: The influence of chemical structure and properties, J. Electrostat., 62 (2004) 277-290.

[13]   S.H. Shin, Y.H. Kwon, Y.H. Kim, J.Y. Jung, M.H. Lee, and J. Nah, Triboelectric charging sequence induced by surface functionalization as a method to fabricate high performance triboelectric generators, ACS Nano, 9 (2015) 4621-4627.

[14]   C. Jeong, K. Baek, S. Niu, T. Nam, Y. Hur, D. Park, G.T. Hwang, M. Byun, Z.L. Wang, Y.S. Jung, Topographically-designed triboelectric nanogenerator via block copolymer self-assembly, Nano Lett., 14 (2014) 7031-7038.

[15]   S.H. Wang, L. Lin and Z.L. Wang, Nanoscale triboelectric-effect-enabled energy conversion for sustainably powering portable electronics, Nano Lett., 12 (2012) 6339-6346.

[16]   G. Zhu, Z.H. Lin, Q.S. Jing, P. Bai, C.F. Pan, Y. Yang, Y.S. Zhou, Z.L. Wang, Toward large-scale energy harvesting by a nanoparticle-enhanced triboelectric nanogenerator, Nano Lett., 13 (2013) 847-853.

[17]   P. Bai, G. Zhu, Z.H. Lin, Q.S. Jing, J. Chen, G. Zhang, J. Ma, and Z.L. Wang, Integrated multi-layered triboelectric nanogenerator for harvesting biomech-anical energy from human motions, ACS Nano, 7 (2013) 3713-3719.

[18]   S.H. Wang, L. Lin, Y.N. Xie, Q.S. Jing, S.M. Niu, Z.L. Wang, Sliding-triboelectric nanogenerators based on in-plane charge-separation mechanism, Nano Lett., 13 (2013) 2226-2233.

[19]   J. Chun, J.W. Kim, W.S. Jung, C.Y. Kang, S.W. Kim, Z.L. Wang, J.M. Baik, Mesoporous pores impregnated with Au nanoparticles as effective dielectrics for enhancing triboelectric nanogenerator performance in harsh environments, Energy Environ Sci., 8 (2015) 3006-3012.